REMARKS/ARGUMENTS

Reconsideration of this application is requested. Claims 1-3, 6-11 and 13-15 are in the case.

I. ELECTION/RESTRICTIONS

The election of Group II is hereby affirmed. Claims 4 and 5 have been cancelled without prejudice to pursuing that subject matter in a separate divisional application.

II. THE 35 U.S.C. §112, SECOND PARAGRAPH, REJECTION

Claims 1-3 and 8-15 stand rejected under 35 U.S.C. §112, second paragraph, as allegedly indefinite for the reasons detailed on page 3 of the Action. That rejection is respectfully traversed.

In response, and without conceding to the merit of the rejection, claim 1 has been amended to specify that when the amino groups Y^1 and Y^2 are tertiary amino, they are selected from -1-piperazinyl and 4-alkyl-1-piperazinyl. Basis for this amendment appears on page 4, lines 15-16 of the originally filed application. No new matter is entered.

In addition, claim 1 has been amended to incorporate the dosage range of between 400mg/day and 700mg/day. Basis appears in original claim 12 which has been cancelled without prejudice.

Withdrawal of the outstanding 35 U.S.C. §112, second paragraph, rejection is now believed to be in order. Such action is respectfully requested.

III. THE ANTICIPATION REJECTIONS

Claims 1-3, 6-9, 11, 12 and 15 stand rejected under 35 U.S.C. §102(b) as allegedly anticipated by Lunardi *et al.* (Neurology, Vol. 48 (6), 1997, pages 1714-1717, PTO-892). Claims 1-3, 6-9, 11-13 stand rejected under 35 U.S.C. §102(b) as allegedly anticipated by WO 00/61231 to Bountra *et al.* Those rejections are respectfully traversed.

The invention as claimed in claim 1 is directed to a method of treating a patient in need of therapy for multiple sclerosis. The method comprises administering to that patient a therapeutically effective dose between 400mg/day and 700mg/day of a compound of formula I wherein R^1, R^2, R^3, R^4 and R^5 are independently selected from the group consisting of hydrogen, trihaloalkyl and halo substituents; X^1, X^2 and X^3 are independently selected from the group consisting of CH, CCH_2F, CCF_3, CO alkyl and CCH_3, and nitrogen atoms, with at two of X^1, X^2 and X^3 being nitrogen, alkyl being preferably ethyl, ethyl or propyl; and Y^1 and Y^2 are independently selected from the group consisting of hydrogen and primary, secondary and tertiary amino groups wherein the tertiary amino groups are selected from -1-piperazinyl and 4-alkyl-1-piperazinyl.

Lunardi specifies a maximum dose of 400 mg/day (see abstract and Table on page 1715). None of the patients with multiple sclerosis were given this dose (see page 1715, column 1, lines 1 to 5 where these patients are identified as numbered 16 to 20 in the table). The maximum dose given to multiple sclerosis patients was 125mg/day. Thus, Lunardi does not constitute an anticipatory disclosure, inherently or otherwise of the presently claimed treatment. Withdrawal of the anticipation rejection is respectfully requested.

Bountra likewise contains no disclosure of the invention as claimed. Bountra proposes that sodium channel antagonists may be used to treat neuronal apoptosis. This is irrelevant to multiple sclerosis (MS), as it is well evidenced in the art that this mechanism is not significant in that disease.

The role of apoptosis in the aetiology of MS appears equivocal and unproven. In a recent paper from Cedric Raine's group, (Cannella et al. Multiple sclerosis: Death receptor expression and oligodendrocyte apoptosis in established lesions. J. Neuroimmunology. 2007,188: 128-137 – copy attached), the authors conclude that "death of oligodendrocytes by apoptosis was an infrequent event in all human CNS samples examined".

In another study (Goertsches et al. Detection of apoptotic cells in cerebrospinal fluid of patients suffering from neurological disease. J. Neuroimmunology. 2007, 188:175-180 – copy attached), the authors conclude that "No apoptotic processes were detected by either analytical method in CSF of clinically distinct diseases, amongst others multiple sclerosis".

In a further study, (Singh et al, Resveratrol Ameliorates Experimental Allergic Encephalomyelitis (EAE) Primarily via Induction of apoptosis in T cells involving activation of AhR and ER. Mol Pharmacol. 2007. Sep 14; PubMed – copy attached), the authors demonstrate that resveratrol exhibited anti-inflammatory and anti-oxidant properties and decreased clinical symptoms and inflammatory responses in EAE. Mice treated with resveratrol had significant apoptosis in spinal cord and high levels of apoptosis in activated T-cells. Thus, the positive effect in EAE was attributed to a pro-apoptotic drug effect on T-cells.

G Ramsaransing et al: B Med Journal p1113 (22nd April 2000 – copy attached) disclose that use of the sodium channel blocker carbamazepine **makes multiple sclerosis worse**.

From the above papers, the scientific argument presented in Bountra's Summary of Invention and Claims for the use of compounds which inhibit apoptosis in the treatment of relapse and EDSS in MS appears unfounded and not credible.

Regarding the dosage range as now claimed, Smith and Meldrum, 1995 (Cerebral protective effect of lamotrigine after focal ischemia in rats, Stroke:26,117-122 – copy attached) show that lamotrigine is only neuroprotective in models of focal ischemia over a narrow dose range. In fact, only a dose of 20mg/kg significantly reduced neurological scores. One of ordinary skill in the art would not have had any reasonable expectation from this, and the papers cited above, that the presently claimed dose would be efficacious.

Based on the above, it is clear that the invention as now claimed is not anticipated by Lunardi et al. or Bountra et al. Reconsideration and withdrawal of the outstanding anticipation rejections are accordingly respectfully requested.

IV. THE OBVIOUSNESS REJECTION

Claims 10, 14 and 15 stand rejected under 35 U.S.C. §103(a) as allegedly unpatentable over Bountra et al. That rejection is respectfully traversed.

For the reasons outlined above, Bountra does not render the present invention obvious. Bountra provides no credible guidance on how to dose and what to dose. A

person of ordinary skill in the art might easily have selected carbamazepine, as did Ramsaransing et al, and then dose at 900mg with serious detrimental effect.

The present inventors have discovered how to significantly impact the very serious disease, multiple sclerosis. The prior art patent is merely an invitation to carry out a search which would be more likely to fail than succeed.

Based on the above, it is clear that one of ordinary skill would not have been motivated to arrive at the invention as now claimed based on Bountra. Absent any such motivation, a *prima facie* case of obviousness has not been generated in this case. Reconsideration and withdrawal of the outstanding obviousness rejection are accordingly respectfully requested.

Favorable action on this application is awaited.

Respectfully submitted,

NIXON & VANDERHYE P.C.

By: _____
Leonard C. Mitchard
Reg. No. 29,009

LCM:lff
901 North Glebe Road, 11th Floor
Arlington, VA 22203-1808
Telephone: (703) 816-4000
Facsimile: (703) 816-4100
Attachments: Canella, B., et al, pp. 128-137; Wallace, M.S., et al, pp. 227-233; Smith, S.E., et al, pp. 117-122; Garthwaite, G., et al, pp. 1219-1230; Goertsches, R., et al, pp. 175-180; Pitt, D., et al, pp. 1113-1120; Singh, N.P., et al, pp. 1508-1521, and Wiard, R.P., et al, pp. 466-472

ELSEVIER

Journal of Neuroimmunology 188 (2007) 128–137

Journal of
Neuroimmunology

www.elsevier.com/locate/jneuroim

Multiple sclerosis: Death receptor expression and oligodendrocyte apoptosis in established lesions

Barbara Cannella *, Stefanie Gaupp, Kakuri M. Omari, Cedric S. Raine

Department of Pathology, Neurology and Neuroscience, Albert Einstein College of Medicine, 1300 Morris Park Ave., Bronx, NY 10461, United States

Received 26 February 2007; received in revised form 14 May 2007; accepted 23 May 2007

Abstract

To determine whether TNF and TRAIL death receptors (DR), and decoy receptors (DcR), play a role in oligodendrocyte depletion in the lesions of chronic multiple sclerosis (MS), we investigated the presence and functionality of these molecules on oligodendrocytes in MS and non-MS brain tissue and on human oligodendrocytes in vitro. For this, we performed immunocytochemistry, Western blotting, TUNEL and FACS analysis for the presence of DR and apoptosis in sections of fresh frozen CNS tissue from cases of chronic MS, other neurologic diseases and normals, and in fetal human oligodendrocytes in vitro. The results showed that although oligodendrocytes demonstrated both DR and DcR, particularly in vitro, there was no predilection of the phenomenon for MS and apoptosis of oligodendrocytes, common in cultures after ligation with TRAIL, was negligible in CNS tissue in situ. Thus, death of oligodendrocytes by apoptosis was an infrequent event in all human CNS samples examined. We postulate that while oligodendrocyte apoptosis might prevail during the initial stages of MS, from our findings other mechanisms probably account for their loss in the established lesion and decoy receptors may play a protective role in oligodendrocyte survival.

Keywords: TRAIL; Oligodendrocytes; Cell death

1. Introduction

While it is well recognized that the pathogenesis of the inflammatory demyelinating lesion in multiple sclerosis (MS) is complex and possibly heterogeneic, there is consensus that initiating events have an immunologic, perhaps autoimmune, basis (Frohman et al., 2006). In support of this are numerous studies showing that the course of MS can be beneficially altered by a number of anti-inflammatory or immune-modulating therapies (Frohman et al., 2006; Noseworthy et al., 2005), many of which act on the pro-inflammatory cytokine profile to down-regulate inflammation. At the level of CNS pathology in MS, a major unresolved issue relates to the fate of the myelinating cell, the oligodendrocyte, during the evolution of the lesion. In the established lesion, total depletion of oligodendrocytes is common (Prineas and McDonald, 1997; Raine, 1997), but whether they die by classic apoptosis or a cytotoxic mechanism (necrosis), remains a question. Since patterns of oligodendrocyte death have been used to determine lesion type and/or stages in MS (Lucchinetti et al., 2000, 1996), clarification of this issue might have considerable pathogenetic import. One cytokine frequently implicated in lesion growth in MS is tumor necrosis factor (TNF), a proinflammatory molecule linked to oligodendrocyte injury and death (D'Souza et al., 1996; Jurewicz et al., 2005; Selmaj and Raine, 1988).

The TNF family of cytokines and their receptors (TNFR), are well known to play critical roles in immune regulation and inflammation and have important functions in cell death mechanisms in all tissues. Some members of the TNFR family of homologous transmembrane proteins bear an intracellular death domain and are able to mediate apoptosis directly. The death receptors (DR), TNF-R1 (DR1), and Fas (DR2), are well-characterized members of the group and have been studied previously in MS (Bonetti and Raine, 1997; Dowling et al., 1996; D'Souza et al., 1996). DR3 is preferentially expressed by lymphocytes and is induced after T-cell activation (Bodmer

* Corresponding author. Department of Pathology, F140, Albert Einstein College of Medicine, 1300 Morris Park Avenue, Bronx, NY 10461-1602, United States. Tel.: +1 718 430 2499; fax: +1 718 430 3710.
E-mail address: cannella@aecom.yu.edu (B. Cannella).

0165-5728/$ - see front matter © 2007 Elsevier B.V. All rights reserved.
doi:10.1016/j.jneuroim.2007.05.018

et al., 1997). DR4 and DR5 (TRAIL-R1 and TRAIL-R2), are two of five cloned receptors of the TNF-related apoptosis-inducing ligand, TRAIL (Pan et al., 1997; Sheridan et al., 1997; Walczak et al., 1997; Wiley et al., 1995). Two other receptors of TRAIL-DcR1 and DcR2 (TRAIL-R3 and TRAIL-R4), are thought to be protective and to act as decoy receptors (Degli-Esposti et al., 1997a,b). TRAIL and its receptors are constitutively expressed in a variety of normal tissues and tumor cells (Pan et al., 1997; Schneider et al., 1997; Wiley et al., 1995). More recent studies have shown TRAIL and its receptors in human brain tissue (Dorr et al., 2002; Frank et al., 1999; Nakamura et al., 2000). DR6, one of the newer members of the DR family, is widely expressed in human tissues (Pan et al., 1998). RT-PCR data indicate that DR6 is abundant in normal human CNS (Harrison et al., 2000).

Since the receptors DR3–DR6; DcR1 and DcR2, and TRAIL ligand have not been examined in MS, the present study was undertaken to investigate these molecules in chronic lesions and whether expression was related to ongoing disease and oligodendrocyte pathology. To investigate possible functional implications of DR, human fetal oligodendrocytes were grown in vitro, exposed to TRAIL, and apoptosis measured by the TUNEL technique for DNA fragmentation.

2. Materials and methods

2.1. Tissue samples

All tissues used in this study came from a brain bank maintained in this laboratory and the tissue was collected with appropriate approval from an institutional IRB. Cryostat sections from OCT-embedded blocks from 10 cases of MS displaying chronic active and chronic silent lesions, 5 cases of other neurologic diseases (OND), one each, amyotropic lateral sclerosis, olivopontocerebellar degeneration, and stroke, and 2 Alzheimer's, and CNS tissue from 4 normal cases, were used in this study (see Table 1). For neuropathology, sections were stained with hematoxylin and eosin, and Luxol fast blue for myelin. For Western blotting, tissue was stored as fresh frozen slices until needed.

With regard to lesion staging, chronic active MS lesions display a sharp edge, perivascular cuffs of infiltrating cells, lipid-laden macrophages, hypertrophic astrocytes, some degenerating axons and ongoing demyelination. At the lesion margin, an increased number of oligodendrocytes and some remyelination may be seen. The demyelinated lesion center is usually hypocellular, containing naked axons embedded in a matrix of scarring (fibrous) astrocytes, lipid-laden macrophages, a few infiltrating leukocytes, and virtually no oligodendrocytes. Chronic silent lesions are defined by sharply demarcated, gliotic, chronically demyelinated, hypocellular areas of white matter lacking inflammatory activity, with variable degrees of axonal loss and severe depletion of oligodendrocytes.

2.2. Immunocytochemistry

Frozen sections were processed as previously described (Cannella and Raine, 2004), and incubated overnight at 4 °C with primary antibodies against the following: mouse anti-TRAIL (R&D, Minneapolis, MN); polyclonal goat anti-DR4/TRAIL-R1 (R&D); polyclonal goat anti-DR5/TRAIL-R2, anti-TRAIL-R3/DcR1 (Alexis Corp., Lausen, Switzerland), and TRAIL-R4/DcR2 (R&D); mouse anti-DR3 (Biolegend, San Diego, CA), and polyclonal rabbit anti-DR6 (Alexis Corp). For phenotypic controls, mAbs were used against: CD68 (Dako Corp., Carpinteria, CA), CNPase (Sigma, St. Louis, MO), GFAP-Alexa 488 (Molecular Probes, Eugene, OR), and CD45 (Dako), for the staining of microglia, oligodendrocytes, astrocytes and leukocytes, respectively. Secondary biotinylated antibodies were

Table 1
Clinical summary of case studied

Patient #	Diagnosis	Gender/ age	Disease duration (yr)	Cause of death	PMI (h)
1	PPMS	F/31	8	Resp. failure	3
2	PPMS	F/32	3	Bronchopneum.	8
3	PPMS	F/37	17	Resp. failure	6
4	SPMS	F/38	11	Bronchopneum.	8
5	SPMS	M/46	15	Cardiac arrest	8
6	SPMS	F/59	35	Bronchopneum.	8
7	SPMS	F/56	21	Cardiac arrest	2
8	SPMS	F/55	20	Sepsis	6
9	SPMS	F/49	15	Bronchopneum	8
10	SPMS	M/60	16	Bronchopneum	9
11	Stroke	F/80	12 h	Stroke	5
12	ALS	F/49	5	Bronchopneum.	8
13	OPCD	M/31	4	Bronchopneum.	4
14	Alzheimer's	F/73	n/a	Cardiac arrest	5
15	Alzheimer's	M/68	n/a	Pneumonia	7
16	Normal	F/84	n/a	Pulmonary embolus	8
17	Normal	M/62	n/a	Cardiac arrest	6
18	Normal	F/88	n/a	Cardiac arrest	7.5
19	Normal	M/72	n/a	Cardiac arrest	9

applied for 1 h at room temperature followed by the avidin–biotin–horseradish peroxidase complex (ABC) reagent (Vector Labs., Burlingame, CA), for another 1 h. The chromogen used was 3,3′diaminobenzidine (DAB). In addition to the above immunoperoxidase staining, double-label immunofluorescence was used to confirm the identity of positive cells, using anti-mouse IgG-Cy2 (Jackson Immunoresearch, West Grove, PA), with the phenotypic monoclonal antibodies and anti-rabbit IgG-Alexa 568 and anti-goat IgG-Alexa 568 (Molecular Probes), with the polyclonal receptor antibodies. Negative controls consisted of omission of primary antibodies and were performed to exclude non-specific staining. Immunoreactivity was scored in a blinded fashion by two observers on a scale from 0 to 4+, as reported previously (Cannella and Raine, 1995).

2.3. Western blots

Freshly thawed samples of human white matter were processed as described previously (Cannella and Raine, 2004). Immunodetection for DR was performed by overnight incubation at 4 °C with primary antibody and as a standard, anti-tubulin antibody (Sigma, St. Louis, MO). Blots were incubated with horseradish peroxidase-labeled secondary Ab (Southern Biotechnology), for 1 h and then washed and developed with an ECL kit (Amersham, Piscataway, NJ). The bands were quantitated by scanning densitometry and expressed as a ratio over the standard to correct for protein loading.

2.4. TUNEL

To investigate the degree and localization of apoptosis in vivo and in vitro, the terminal deoxynucleotidyl transferase (TdT)-mediated deoxyuridine triphosphate nick-end labeling (TUNEL) technique was applied to frozen sections of MS, OND and normal CNS tissue, according to the manufacturer's instructions (R&D). Immunohistochemistry was performed to characterize cell phenotype. Sections were post-fixed with a formaldehyde reagent — BD Cytofix/Cytoperm (Becton Dickinson Biosciences Pharmingen, San Diego, CA), for 15 min, washed and incubated with the labeling reaction mixture for 60 min at 37 °C. For negative control purposes, TdT enzyme was omitted from the reaction mixture. As a positive control, sections were treated with nuclease which produced staining of all nuclei. Cell phenotype (oligodendrocyte and infiltrating cells), was visualized using horseradish peroxidase with DAB as substrate, and the TUNEL reaction with streptavidin-alkaline phosphotase and neofuchsin as substrate. The number of apoptotic cells was quantitated by counting TUNEL-positive cells per 40× field (approximately 200 fields), and reported as the number of positive cells per mm^2. Statistical significance was determined using the Student's *t*-test.

2.5. Cell culture

Human oligodendrocytes were isolated from spinal cords of electively-aborted fetuses, obtained from the Einstein Human Fetal Tissue Repository (New York, NY), in accordance with approved Internal Review Board protocols. Primary cultures were established from 18–22 week gestation fetal spinal cords, as described previously (Omari et al., 2005). Oligodendrocyte cultures were maintained in N2B3 medium alone, or supplemented with 10 ng/ml PDGF-AA (Sigma), and media was replenished every other day. In initial experiments, cells were exposed to doses of 10, 100 and 1000 ng/ml of TRAIL. The optimal dose was determined to be 100 ng/ml. Since cyclohexamide has been shown by others to be necessary for increasing TRAIL activity (Li et al., 2003; Matysiak et al., 2002), it was added to the cells before TRAIL treatment and simultaneously with TRAIL to determine the best method of treatment. It was found that pre-treatment was no more effective and in all further experiments, it was added simultaneously with TRAIL. The optimal time of exposure to TRAIL was then determined by exposing the cells for two different timepoints: 6 h and 16 h. The shorter time period was found to be better. After 5 days in vitro, duplicate cultures were treated for 6 h with 100 ng/ml SuperKillerTrail (Alexis) alone, or in combination with cyclohexamide (5 μg/ml, Sigma), to investigate the role of TRAIL receptors on oligodendrocytes. Cells maintained in N2B3 media alone served as negative controls. Experiments were repeated 4–5 times.

2.6. FACS analysis

For fluorescence microscopy of cultured cells and FACS analysis, cells were stained in a manner similar to the above-described procedures with CNPase and visualized with secondary antibodies directly conjugated to Alexa568, and TUNEL-positive cells were visualized with Streptavidin-Alexa488. For FACS analysis, cells were trypsinized and analyzed at 2×10^5 cells on a FACScan flow cytometer (Becton Dickinson, Sunnyvale, CA), with the use of software WINMD12.8 (Trotter). Negative controls omitting primary antibodies were run in parallel. FACS analysis was repeated 3 times.

3. Results

3.1. Death receptors in CNS tissue

The results of the immunocytochemical analysis are summarized in Table 2, which shows average levels of selected TNFR death receptors, decoy receptors and the ligand, TRAIL, in CNS tissue from active and silent MS lesions, OND and normal cases. Reactivity for DR varied among microglia, astrocytes, oligodendrocytes and infiltrating cells, and in some cases, the same molecule was expressed by several cell types.

DR3 reactivity was seen at moderate levels on astrocytes, and at low levels on microglia and perivascular macrophages (Fig. 1A). Chronic active MS lesions showed DR3 on inflammatory cells in perivascular cuffs and on astrocytes (Fig. 1B). In chronic silent lesions, DR3 was seen at low levels on all cell types (Table 2). However, Western blots failed to show any quantitative differences between groups (Fig. 2). Immunoreactivity for DR4 was found at low levels on microglia and infiltrating cells (Fig. 1C), and at similar levels on

Table 2
TNF and TRAIL receptor expression in human CNS tissue

	DR3	DR4 (TRAIL-R1)	DR5 (TRAIL-R2)	DR6	DcR1 (TRAIL-R3)	DcR2 (TRAIL-R4)	TRAIL
Active MS $n=4$			+OL		±OL		±OL
		±M	+M	±M	+M	++M	
	+A	+A		±A		±A	
	+INF	+INF	+INF	+INF	+INF	+INF	+INF
Silent MS $n=5$	±OL		+OL		+OL		±OL
	±M	±M		++M		++M	+M
	±A	±A	±A		±A		
OND $n=2$			+OL		++OL		±OL
	±M	±M		+M		+M	
					±A		
Normal $n=4$			±OL		++OL		±OL
		±M		±M		±M	
	+A	±A					

Scored on a 0 to 4 scale based on extent and degree of immunoreactivity. OL = oligodendrocyte, A = astrocyte, M = microglia, INF = infiltrating cells.

astrocytes in silent lesions and normal CNS. In active lesions, DR4 expression was higher on astrocytes. Western blots showed differences in expression between cases within the same group, e.g. chronic active MS and normal CNS, rendering conclusions on quantitative differences between MS and normal CNS difficult. DR5 was seen consistently on oligodendrocytes in all cases (Table 2; Fig. 1D), with higher levels in MS and OND, compared to constitutive levels in normal brain tissue. In active lesions, DR5 was also seen on microglia and infiltrating cells (Fig. 1E), and in silent lesions, on astrocytes at low levels. In grey matter, DR5 immunoreactivity was seen on neurons. Western blotting showed an increase in DR5 expression in chronic silent lesions compared to other groups (Fig. 2). DR6 was expressed on microglia in all groups (Table 2; Fig. 1F), with up-regulation in active and silent lesions. Astrocytes and inflammatory cells also showed low-level reactivity in active MS lesions.

3.2. Decoy receptors in CNS tissue

The decoy receptor, DcR1 (TRAIL-R3), was found constitutively at moderately high levels on oligodendrocytes in normals and OND, and at lower levels in MS (Fig. 3A). In chronic active lesions, it was also expressed by microglia and infiltrating cells and in silent lesions and OND, by astrocytes at low levels (Fig. 3B).Double-labeling for DcR1 and DR5 showed colocalization on cell bodies with the phenotype of oligodendrocytes as well as on astrocytes and their processes (Fig. 3C). Neuronal positivity for DcR1 was seen in grey matter. Western blots showed no significant differences in levels between the groups. DcR2 (TRAIL-R4), occurred almost exclusively on microglia (Table 2), higher in MS and lower in normals.

3.3. TRAIL in CNS tissue

Low level expression of TRAIL ligand was found on oligodendrocytes in all cases, with some reactivity on microglia in silent lesions and perivascular infiltrating cells in active lesions (Table 2). Interestingly, TRAIL levels were higher in established MS lesions and lower in normals and OND. Western blotting revealed an increase in TRAIL in MS and OND compared to barely detectable levels in normals.

3.4. Quantitation of apoptosis in situ

Chronic active lesions ($n=4$), showed the highest levels of apoptosis (mean, 2.8 ± 0.7 cells/mm^2 — Fig. 4), due primarily to TUNEL-positive infiltrating cells in perivascular cuffs that were also CD45+ (Fig. 5A). Silent lesions ($n=5$), showed lower levels of apoptosis (mean, 0.8 ± 0.4 cells/mm^2 — Fig. 4), related to decreased inflammatory activity. The degree of apoptosis observed in CNS tissue from 5 cases of OND and 4 normals, was negligible (mean, 0.2 ± 0.15 and 0.1 ± 0.07 cells/mm^2, respectively — Fig. 4). The difference in the levels of TUNEL-positive cells was found to be statistically significant between that seen in chronic active MS and OND ($p=0.02$), and between chronic silent MS and OND ($p=0.002$), using the t-test. In general, there was minimal apoptosis in parenchymal cells in CNS tissue from all groups. Occasionally, an apoptotic oligodendrocyte was seen around an active MS lesion, but this was infrequent (Fig. 5A). Thus, although oligodendrocytes showed expression of DR5 (Fig. 1D), apoptotic oligodendrocytes in chronic lesions were rare. The latter may have been related to the protective effect of DcR1 on the same cell type (Fig. 3A and C), see above. The negligible levels of oligodendrocyte apoptosis in normals and OND may have been a reflection of the higher levels of DcR1 on oligodendrocytes (Table 2).

3.5. DR on oligodendrocytes in vitro

Oligodendrocyte cultures were established from human fetal spinal cord and the cells analyzed for DR in vitro. Immunocytochemistry revealed expression of DR3, DR4, DR5, DR6, as

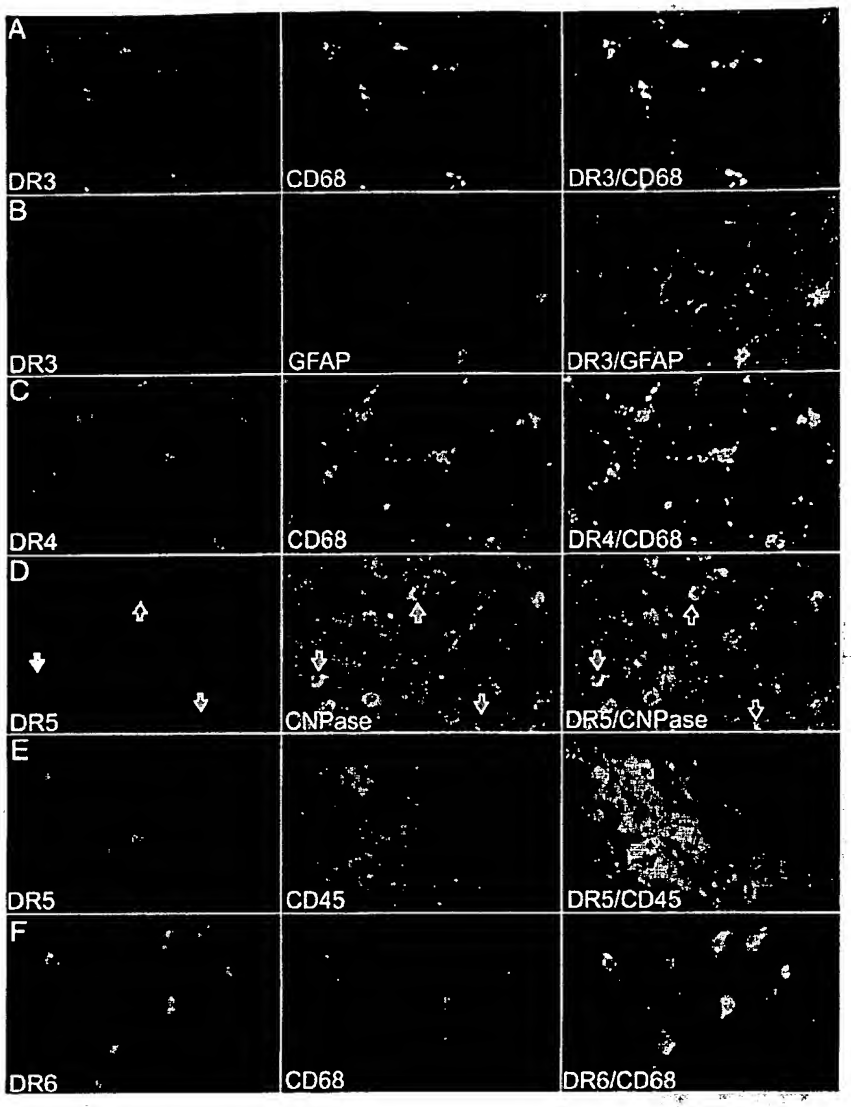

Fig. 1. Double immunofluorescence confirms the phenotype of cells immunoreactive for DR around MS lesions. All figures 400×. (A–B) DR3 positivity seen on CD68+ microglia and on GFAP+ astrocytes. Note the DR3+ inflammatory cells in the upper left corner in (B). (C) DR4+ cells were identified in a chronic active MS lesion to be microglia shown in the merged image on the right. (D) DR5+ cells were CNPase+ oligodendrocytes (arrows). (E) Active MS lesion showed DR5 reactivity also in perivascular inflammatory cells (CD45+). (F) DR6 reactivity was predominantly microglial as verified by colocalization with CD68 in the merged image to the right.

well as the decoy receptors, DcR1 and DcR2 (Fig. 6). The findings were somewhat different from adult CNS tissue in situ where DR4 and DR6 were not observed on oligodendrocytes. Widespread oligodendrocyte reactivity for DR in vitro was probably a combination of developmental and tissue culture-related phenomena.

3.6. Treatment of oligodendrocytes with TRAIL in vitro

To examine whether TRAIL receptors on oligodendrocytes were functional, human fetal oligodendrocyte cultures were treated with TRAIL then examined for evidence of apoptosis. Morphologic assessment revealed TUNEL-positive, CNPase-positive cells (Fig. 5B). Process-bearing, differentiated CNPase+ cells undergoing apoptosis were rare compared to rounded-up apoptotic CNPase+ cells. Treatment with TRAIL alone increased the number of apoptotic cells over baseline levels, as did treatment with cyclohexamide alone. TRAIL and cyclohexamide combined appeared to have an additive effect (see Fig. 5B).

To quantitate the effect of TRAIL on oligodendrocyte apoptosis, cultures were analyzed by FACS. The results showed

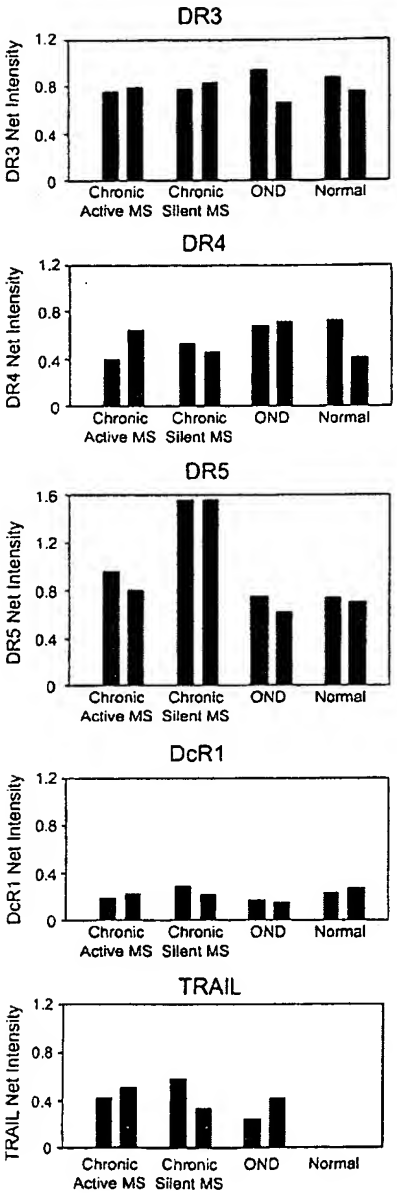

Fig. 2. Western blots (upper horizontal panel in each figure), show immunoreactivity for DR in white matter from chronic active and chronic silent MS lesions, other neurological diseases (OND), and normal subjects ($n=2$ for each group). Densitometric analysis (histograms) of blots suggests up-regulation of DR5 protein levels in chronic silent MS lesions. DR3, DR4 and DcR1 showed no differences among the groups. Levels of the ligand, TRAIL, were increased in MS and OND compared to normal CNS, where it was barely detectable.

that treatment with TRAIL increased the percentage of CNPase+ TUNEL+ cells from a baseline level of 27% (no treatment), to 48% (Fig. 7). Cyclohexamide alone had a minor effect (29%), and combined with TRAIL, this increased to 50%.

4. Discussion

In the present study, we examined MS and non-MS CNS tissue for a novel group of DR known to be involved in apoptosis (DR3, 4, 5 and 6). Having determined their presence in CNS tissue in situ, we then tested TRAIL DR functionally on oligodendrocytes in vitro. Finally, we investigated and quantitated classical apoptosis in situ by DNA fragmentation. With different MS lesion types plus control CNS tissue, our findings have failed to support a significant role for apoptosis in the loss of oligodendrocytes from the established MS lesion, both active and silent. Expression of DR proved to be a constitutive property and a common feature in CNS tissue from all groups. However, while the incidence of apoptosis, as assessed by TUNEL staining, was greatest in MS, this was found to involve CD45+ infiltrating cells, not parenchymal cells. Furthermore, there was no overt difference in expression of DR between MS and controls although shifts in expression towards microglia occurred in MS and OND. Astrocytes and microglia were the main cells showing DR, except for DR5 which displayed a predilection for oligodendrocytes. Quantitatively, westerns showed higher levels of DR5 in chronic silent MS lesions. Westerns also showed up-regulation of TRAIL in MS and OND, indicating that this was not MS-specific.

Although observed herein but not a focus of the present study, neuronal TRAIL DR and DcR expression has been extensively studied. One study reported TRAIL induction of apoptosis in human brain slices (Nitsch et al., 2000), a second examined TRAIL ligand/receptors in brain tissue obtained from individuals with epilepsy (Dorr et al., 2002), and a third reported TRAIL-related neuronal death in a mouse model of MS (Aktas et al., 2005). There are no reports analyzing DR in MS tissue. While similarities between the present study and that of Dorr et al. (2002), were seen in DR4 and DR5, the DcR1 and DcR2 patterns were somewhat different with oligodendrocytes and neurons being the main cells expressing DcR1 in this study [versus neurons only (Dorr et al., 2002)], and microglia here showing DcR2 [versus oligodendrocytes and neurons (Dorr et al., 2002)]. In addition, the latter authors were unable to find TRAIL in human CNS. To what extent these differences may have been related to the source of the CNS tissue tested and antibodies used, remains to be seen. These differences notwithstanding, it is interesting from our work that regardless of condition (MS, OND, normal), one decoy receptor (DcR1), was preferentially expressed by oligodendrocytes, while the other (DcR2), was prominent on microglia. Considering that both microglia and oligodendrocytes also expressed different TRAIL DR (DR4 and DR5, respectively), this may indicate that the relative ratio of the respective death versus decoy receptor expression on these two cell types may be a determining factor in their survival. Furthermore, it would appear that different cell types may be protected by different receptors, a more efficient system biologically.

Examination of human fetal oligodendrocytes in culture showed both presence and functionality of DR following ligation with TRAIL. Previous studies using adult human oligodendrocytes (Matysiak et al., 2002), came to similar conclusions and went on to show that DR4 was the receptor responsible for apoptosis. These studies in vitro appear to support a role for DR in

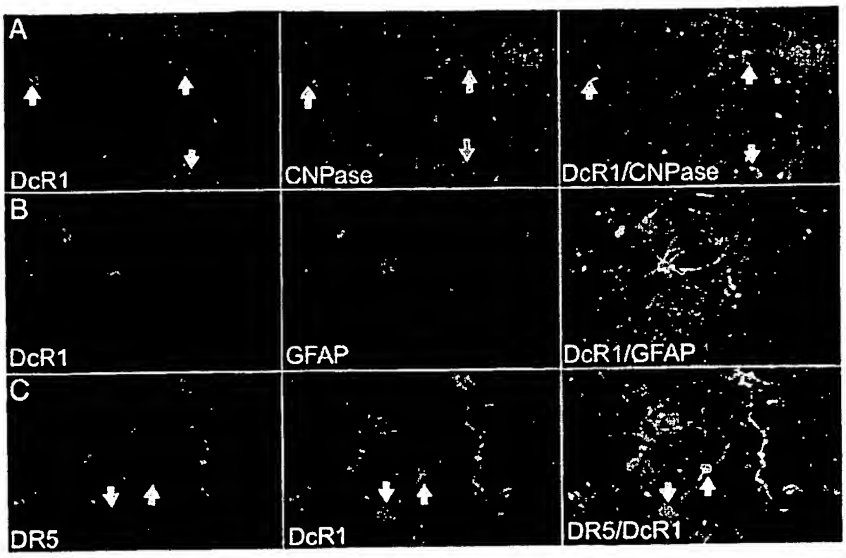

Fig. 3. (A) Oligodendrocyte immunoreactivity for DcR1 at the edge of a chronic active MS lesion was confirmed by colocalization with CNPase (arrows). (B) Astrocytes were also positive for DcR1, shown here by double-staining with GFAP. (C) Colocalization of DR5 (TRAIL-R2) and DcR1 (TRAIL-R3) on oligodendrocytes (arrows), and astrocytes.

oligodendrocyte death, an observation not supported by our parallel studies of CNS tissue in situ. Whether this reflects in vitro/in vivo differences or non-apoptotic functions of DR, as proposed previously (Wajant, 2003), are possibilities.

Oligodendrocyte depletion in MS and its association with apoptosis has been the subject of many studies, some claiming apoptosis not to be prominent (Bonetti and Raine, 1997; D'Souza et al., 1996), and others claiming it to be a significant mechanism (Barnett and Prineas, 2004; Dowling et al., 1996; Lucchinetti et al., 1996). However, considerable uncertainty as to the fate of oligodendrocytes in MS still exists due in some part to the fact that the criteria for apoptosis differ among studies (Barnett and Prineas, 2004; Lucchinetti et al., 2000). More recently, the distinction between the different classical death pathways has become less clear (Jaattela and Tschopp, 2003). This may be a contributing factor to differences of opinion between investigators examining oligodendrocyte death processes in MS. Given that oligodendrocyte apoptosis was a rare event in this study on established MS lesions, one has to reconcile the findings with how and when depletion of this cell type occurs in MS. Major oligodendrocyte loss is almost certainly an early event of short duration occurring during the initial acute stages, and the window of opportunity for its detection is probably very narrow. Unfortunately, the chances of obtaining autopsy tissue containing the earliest lesions, are slim since this stage has been proposed to last for a few hours only (Barnett et al., 2006). Since the course of MS evolves over several decades and chronic lesions are known to continue to expand during the relapsing–remitting phase, the same mechanism of oligodendroglial cell death may or may not prevail. However, not to be excluded is that oligodendrocyte apoptosis occurring at an exceedingly low rate may still be the cause of oligodendrocyte depletion in MS. Although ample evidence of apoptotic infiltrating cells was consistently found in chronic active lesions, oligodendrocytes were only rarely TUNEL-positive. These results are not in accord with previous work (Dowling et al., 1996; Lucchinetti et al., 1996), which depicted an abundance of DNA fragmentation in oligodendrocytes along the borders of chronic active lesions. Whether these discrepancies relate to the use of differently processed material remains a possibility.

Taken in concert, we have documented for the first time, the widespread expression of DR in MS and non-MS CNS tissue. The same DR were tested on human oligodendrocytes in vitro and were shown to be effective in inducing apoptosis after TRAIL ligation. The incidence of expression of DR in situ failed to correlate with the low degree of apoptosis observed.

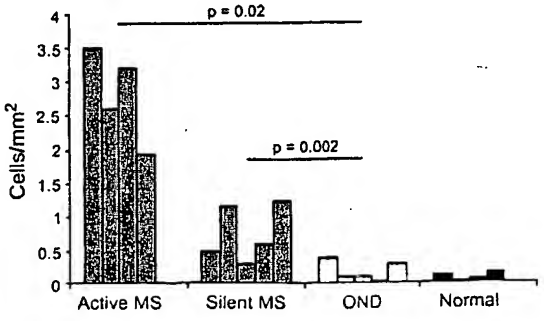

Fig. 4. This histogram illustrates the average number of TUNEL positive cells per square millimeter in the CNS of MS (chronic active, $n=4$; chronic silent, $n=5$), OND ($n=5$) and normal cases ($n=4$). Levels of TUNEL-positive cells were significantly different between those seen in active MS and OND ($p=0.02$), and between silent MS and OND ($p=0.002$), using the Student's t-test.

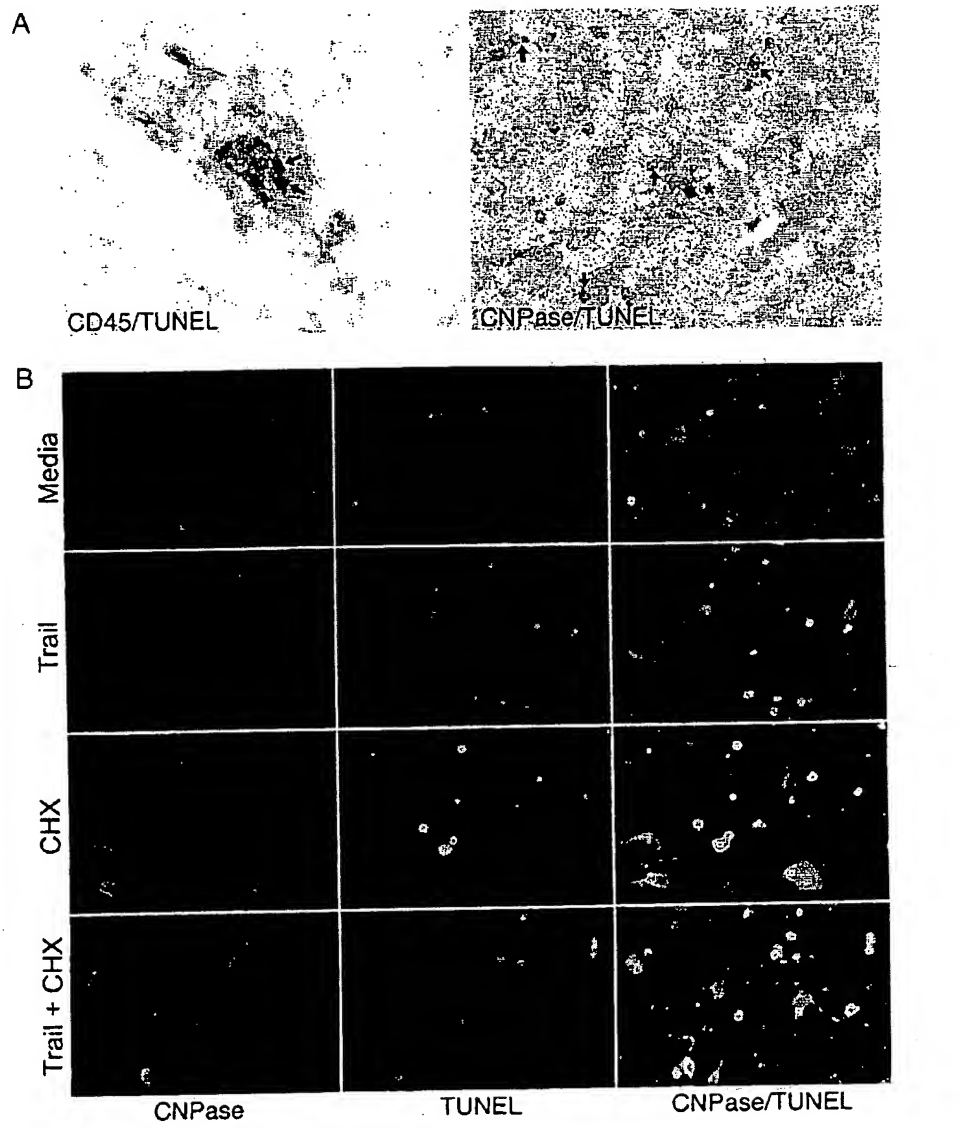

Fig. 5. (A) Representative fields showing, on the left, two apoptotic (red), CD45+ inflammatory cells (arrows), in a perivascular cuff around a vessel with a collapsed lumen in an active MS lesion. On the right, a rare TUNEL-positive red oligodendrocyte (asterisk), is seen among the numerous healthy (CNPase+) oligodendrocytes (arrows). (B) Treatment with TRAIL induces apoptosis of oligodendrocyte in vitro. Morphologic assessment revealed that treatment with TRAIL alone (second row), increased the number of apoptotic cells over control (media), baseline levels (first row), as did treatment with cyclohexamide alone (third row). TRAIL and cyclohexamide combined (below), appeared to have an additive effect.

Whether this indicated a lack of receptor activation, blockade of downstream signaling, or the protective effect of simultaneously expressed decoy receptors, provides subjects for future investigation. Nevertheless, the presence of DR and DcR expression within the CNS supports the existence of innate mechanisms operative during development and disease which influence cell fate. These pathways may play more of a role in the elimination of infiltrating cells (shown here in active MS lesions), rather than the death/survival of parenchymal cells, at least during the chronic stages of this devastating disease.

Acknowledgements

We thank Vina Cruz for assistance with Western blotting; Dr. B. Poulos of the Einstein Tissue Repository, for human fetal CNS tissue; M. Pakingan for technical assistance; and P. Cobban-Bond for administrative support. Dr. C. Petito, University of Miami

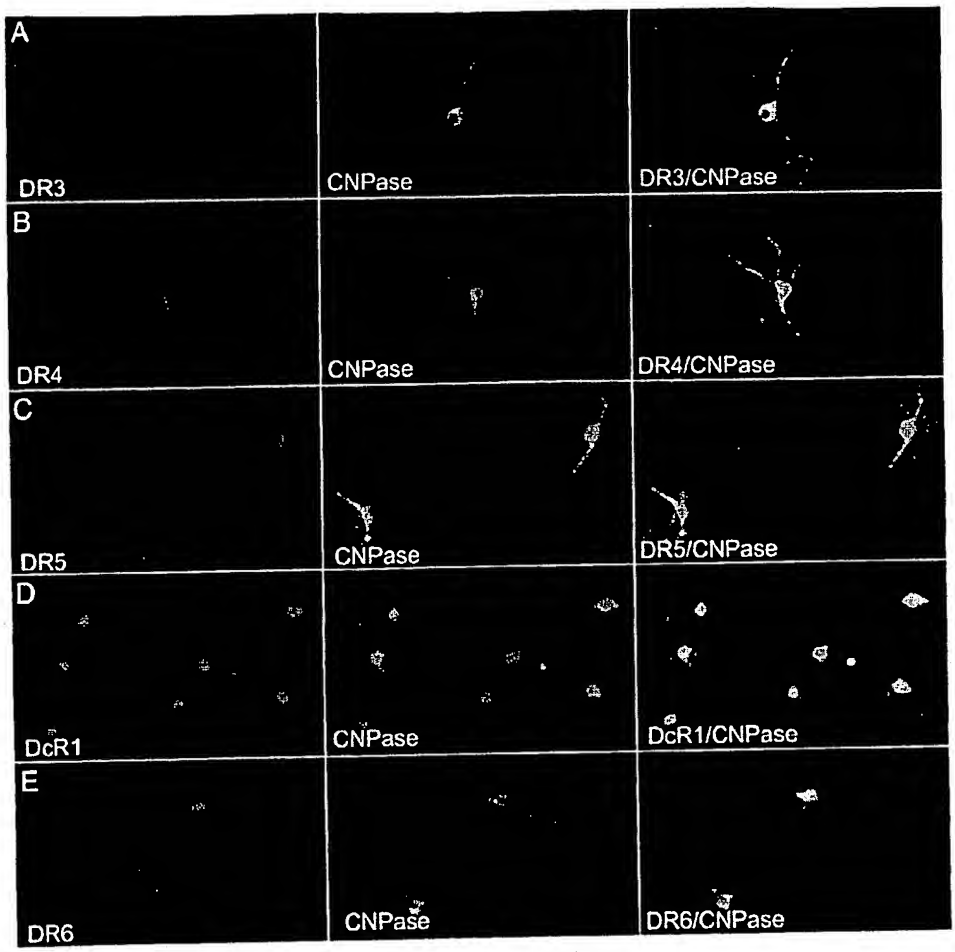

Fig. 6. Human fetal oligodendrocytes show surface expression of DR in vitro. In A–E, mature CNPase-positive oligodendrocytes show double-staining for DR3 (A), DR4 (B), DR5 (C), DcR1 (D) and DR6 (E).

Brain Bank (HD 83284), and Dr. S. Morgello, Manhattan HIV Brain Bank (MH 59724) provided normal CNS samples.

Supported in part by USPHS grants NS 08952, NS 11920 and NS 07098; NMSS grant RG 1001-K-11; the MS Foundation; and the Wollowick Family Foundation.

References

Aktas, O., Smorodchenko, A., Brocke, S., Infante-Duarte, C., Topphoff, U.S., Vogt, J., Prozorovski, T., Meier, S., Osmanova, V., Pohl, E., Bechmann, I., Nitsch, R., Zipp, F., 2005. Neuronal damage in autoimmune neuroinflammation mediated by the death ligand TRAIL. Neuron 46, 421–432.

Barnett, M.H., Prineas, J.W., 2004. Relapsing and remitting multiple sclerosis: pathology of the newly forming lesion. Ann. Neurol. 55, 458–468.

Barnett, M.H., Henderson, A.P., Prineas, J.W., 2006. The macrophage in MS: just a scavenger after all? Pathology and pathogenesis of the acute MS lesion. Mult. Scler. 12, 121–132.

Bodmer, J.L., Burns, K., Schneider, P., Hofmann, K., Steiner, V., Thome, M., Bornand, T., Hahne, M., Schroter, M., Becker, K., Wilson, A., French, L.E., Browning, J.L., MacDonald, H.R., Tschopp, J., 1997. TRAMP, a novel apoptosis-mediating receptor with sequence homology to tumor necrosis factor receptor 1 and Fas(Apo-1/CD95). Immunity 6, 79–88.

Bonetti, B., Raine, C.S., 1997. Multiple sclerosis: oligodendrocytes display cell death-related molecules in situ but do not undergo apoptosis. Ann. Neurol. 42, 74–84.

Cannella, B., Raine, C.S., 1995. The adhesion molecule and cytokine profile of multiple sclerosis lesions. Ann. Neurol. 37, 424–435.

Cannella, B., Raine, C.S., 2004. Multiple sclerosis: cytokine receptors on oligodendrocytes predict innate regulation. Ann. Neurol. 55, 46–57.

Degli-Esposti, M.A., Dougall, W.C., Smolak, P.J., Waugh, J.Y., Smith, C.A., Goodwin, R.G., 1997a. The novel receptor TRAIL-R4 induces NF-kappaB and protects against TRAIL-mediated apoptosis, yet retains an incomplete death domain. Immunity 7, 813–820.

Degli-Esposti, M.A., Smolak, P.J., Walczak, H., Waugh, J., Huang, C.P., DuBose, R.F., Goodwin, R.G., Smith, C.A., 1997b. Cloning and characterization of TRAIL-R3, a novel member of the emerging TRAIL receptor family. J. Exp. Med. 186, 1165–1170.

Dorr, J., Bechmann, I., Waiczies, S., Aktas, O., Walczak, H., Krammer, P.H., Nitsch, R., Zipp, F., 2002. Lack of tumor necrosis factor-related apoptosis-

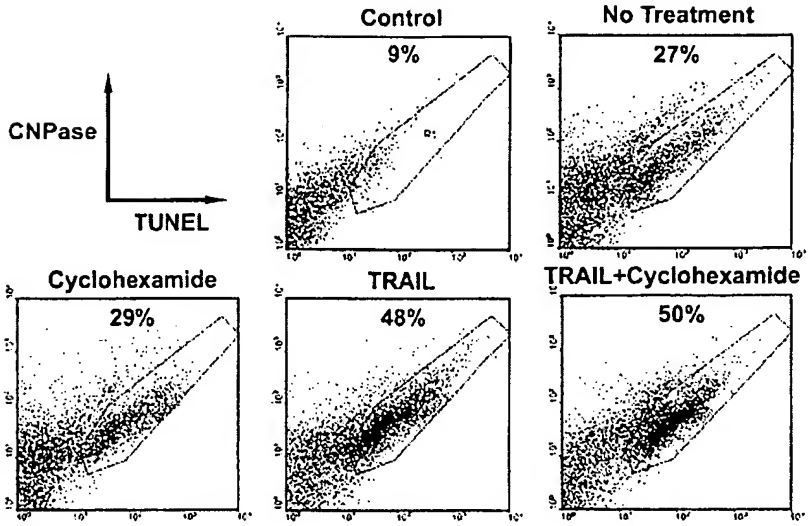

Fig. 7. FACS analysis of TRAIL-induced apoptosis in oligodendrocyte cultures. 2×10^5 cells were analyzed by two color immuno-flow cytometry. Representative plot from one of 3 experiments is shown. The panels indicate different treatments of human oligodendrocytes in vitro. The values indicate the percentages of TUNEL-positive cells.

inducing ligand but presence of its receptors in the human brain. J. Neurosci. 22 (RC209), 1–5.

Dowling, P., Shang, G., Raval, S., Menonna, J., Cook, S., Husar, W., 1996. Involvement of the CD95 (APO-1/Fas) receptor/ligand system in multiple sclerosis brain. J. Exp. Med. 184, 1513–1518.

D'Souza, S.D., Bonetti, B., Balasingam, V., Cashman, N.R., Barker, P.A., Troutt, A.B., Raine, C.S., Antel, J.P., 1996. Multiple sclerosis: Fas signaling in oligodendrocyte cell death. J. Exp. Med. 184, 2361–2370.

Frank, S., Kohler, U., Schackert, G., Schackert, H.K., 1999. Expression of TRAIL and its receptors in human brain tumors. Biochem. Biophys. Res. Commun. 257, 454–459.

Frohman, E.M., Racke, M.K., Raine, C.S., 2006. Multiple sclerosis—the plaque and its pathogenesis. N. Engl. J. Med. 354, 942–955.

Harrison, D.C., Roberts, J., Campbell, C.A., Crook, B., Davis, R., Deen, K., Meakin, J., Michalovich, D., Price, J., Stammers, M., Maycox, P.R., 2000. TR3 death receptor expression in the normal and ischaemic brain. Neuroscience 96, 147–160.

Jaattela, M., Tschopp, J., 2003. Caspase-independent cell death in T lymphocytes. Nat. Immunol. 4, 416–423.

Jurewicz, A., Matysiak, M., Tybor, K., Kilianek, L., Raine, C.S., Selmaj, K., 2005. Tumour necrosis factor-induced death of adult human oligodendrocytes is mediated by apoptosis inducing factor. Brain 128, 2675–2688.

Li, J.H., Kirkiles-Smith, N.C., McNiff, J.M., Pober, J.S., 2003. TRAIL induces apoptosis and inflammatory gene expression in human endothelial cells. J. Immunol. 171, 1526–1533.

Lucchinetti, C.F., Bruck, W., Rodriguez, M., Lassmann, H., 1996. Distinct patterns of multiple sclerosis pathology indicates heterogeneity on pathogenesis. Brain Pathol. 6, 259–274.

Lucchinetti, C., Bruck, W., Parisi, J., Scheithauer, B., Rodriguez, M., Lassmann, H., 2000. Heterogeneity of multiple sclerosis lesions: implications for the pathogenesis of demyelination. Ann. Neurol. 47, 707–717.

Matysiak, M., Jurewicz, A., Jaskolski, D., Selmaj, K., 2002. TRAIL induces death of human oligodendrocytes isolated from adult brain. Brain 125, 2469–2480.

Nakamura, M., Rieger, J., Weller, M., Kim, J., Kleihues, P., Ohgaki, H., 2000. APO2L/TRAIL expression in human brain tumors. Acta Neuropathol. (Berl) 99, 1–6.

Nitsch, R., Bechmann, I., Deisz, R.A., Haas, D., Lehmann, T.N., Wendling, U., Zipp, F., 2000. Human brain-cell death induced by tumour-necrosis-factor-related apoptosis-inducing ligand (TRAIL). Lancet 356, 827–828.

Noseworthy, J., Miller, D., Compston, A., 2005. Disease-modifying treatments in multiple sclerosis. In: Compston, A. (Ed.), McAlpines's Multiple Sclerosis. Churchill Livingstone Elsevier, Philadelphia, PA.

Omari, K.M., John, G.R., Sealfon, S.C., Raine, C.S., 2005. CXC chemokine receptors on human oligodendrocytes: implications for multiple sclerosis. Brain 128, 1003–1015.

Pan, G., O'Rourke, K., Chinnaiyan, A.M., Gentz, R., Ebner, R., Ni, J., Dixit, V.M., 1997. The receptor for the cytotoxic ligand TRAIL. Science 276, 111–113.

Pan, G., Bauer, J.H., Haridas, V., Wang, S., Liu, D., Yu, G., Vincenz, C., Aggarwal, B.B., Ni, J., Dixit, V.M., 1998. Identification and functional characterization of DR6, a novel death domain-containing TNF receptor. FEBS Lett. 431, 351–356.

Princas, J.W., McDonald, W.I., 1997. Demyelinating Diseases. In: Graham, D.I., Lantos, P.L. (Eds.), Greenfield's Neuropathology, vol. I. Arnold, London, pp. 813–896.

Raine, C.S., 1997. The neuropathology of multiple sclerosis. In: Raine, C.S., McFarland, H.F., Tourtellotte, W.W. (Eds.), Multiple Sclerosis Clinical and pathogenetic basis. Chapman & Hall Medical, London, pp. 151–171.

Schneider, P., Bodmer, J.L., Thome, M., Hofmann, K., Holler, N., Tschopp, J., 1997. Characterization of two receptors for TRAIL. FEBS Lett. 416, 329–334.

Selmaj, K.W., Raine, C.S., 1988. Tumor necrosis factor mediates myelin and oligodendrocyte damage in vitro. Ann. Neurol. 23, 339–346.

Sheridan, J.P., Marsters, S.A., Pitti, R.M., Gurney, A., Skubatch, M., Baldwin, D., Ramakrishnan, L., Gray, C.L., Baker, K., Wood, W.I., Goddard, A.D., Godowski, P., Ashkenazi, A., 1997. Control of TRAIL-induced apoptosis by a family of signaling and decoy receptors. Science 277, 818–821.

Wajant, H., 2003. Death receptors. Essays Biochem. 39, 53–71.

Walczak, H., Degli-Esposti, M.A., Johnson, R.S., Smolak, P.J., Waugh, J.Y., Boiani, N., Timour, M.S., Gerhart, M.J., Schooley, K.A., Smith, C.A., Goodwin, R.G., Rauch, C.T., 1997. TRAIL-R2: a novel apoptosis-mediating receptor for TRAIL. EMBO J. 16, 5386–5397.

Wiley, S.R., Schooley, K., Smolak, P.J., Din, W.S., Huang, C.P., Nicholl, J.K., Sutherland, G.R., Smith, T.D., Rauch, C., Smith, C.A., et al., 1995. Identification and characterization of a new member of the TNF family that induces apoptosis. Immunity 3, 673–682.

A Multicenter, Double-Blind, Randomized, Placebo-Controlled Crossover Evaluation of a Short Course of 4030W92 in Patients With Chronic Neuropathic Pain

Mark S. Wallace,* Michael Rowbotham,† Gary J. Bennett,‡ Troels S. Jensen,§ Rosemarie Pladna,‖ and Steve Quessy‖

Abstract: Several lines of evidence suggest that neuropathic pain is mediated in part by an increase in the density of voltage-sensitive sodium channels in injured axons and the dorsal root ganglion of injured axons. The purpose of this study was to examine the safety, analgesic efficacy, and tolerability of oral 4030W92 (a new novel sodium channel blocker) in a group of subjects with chronic neuropathic pain. This study used a randomized, double-blind, placebo-controlled, crossover design in 41 subjects with neuropathic pain with a prominent allodynia. Each subject received a 2-week course of 4030W92 (25 mg/day) and placebo separated by a 2-week washout period. At baseline, postdose day 1, day 7, and day 14, the following were measured: (1) spontaneous and evoked pain scores, (2) dynamic and static allodynia mapping, (3) Short Form McGill Pain Questionnaire, and (4) blood sample for 4030W92 assay. At baseline and day 14 the following were measured: (1) thermal testing in the painful area, (2) Medical Outcomes Study Short Form 36 Questionnaire, and (3) patient global satisfaction. Allodynia severity was significantly lower ($P = .046$) on treatment day 1, postdose for 4030W92 compared to placebo. However, this was not maintained on treatment day 7 or 14. The area of static allodynia was significantly smaller ($P = .03$) on treatment day 7 for 4030W92 compared to placebo. However, this was not maintained to treatment day 14. There was no significant effect of 4030W92 on any other efficacy measure. Side effects were minimal. 4030W92, at 25 mg/day, produced a nonsignificant reduction in pain without treatment limiting side effects. The maximum analgesic effect of this drug remains unknown.

Key words: Neuropathic, pain, sodium, channel, antagonists

Chronic neuropathic pain after nervous system injury is often debilitating and refractory to treatment. Neuropathic pain may display several characteristics including (1) an ongoing spontaneous pain, (2) an exaggerated pain response to a noxious stimulus (hyperalgesia), and/or (3) a pain response to a nonpainful stimulus (allodynia). Both the spontaneous and evoked pain may be mediated in part by an increase in the density of voltage-sensitive sodium channels in the injured areas of the axon and dorsal root ganglion of the injured primary afferent neuron.[10,12,15] In animal models of neuropathic pain, spontaneous and evoked pain behavior is significantly diminished after delivery of sodium channel antagonists.[7,32] Importantly, these effects occur at plasma concentrations that do not produce an afferent conduction block.[12]

Oral sodium channel antagonists, such as mexiletine and lamotrigine, have been reported to be effective in a variety of neuropathic pain syndromes including diabetic neuropathy,[11,14,24] alcoholic neuropathy,[20] peripheral nerve injury,[6] and trigeminal neuralgia.[34] However, not all studies have shown efficacy, especially when doses are low.[19,31]

4030W92 is a new sodium channel antagonist similar in structure to lamotrigine with high selectivity for use-dependent sodium channels (tetrodotoxin resistant). Preclinical studies have found efficacy of 4030W92 in inflammatory and neuropathic pain models.[8,9,26] 4030W92 was at least 5 times more potent than lamotrigine in animal pain models and exhibited a greater separation between doses that elicited analgesic effects and those that elicited behavioral effects (ataxia). The more favorable potency and safety index were considerations in selecting 4030W92 for further study in humans. In phase I studies, 4030W92 has been well tolerated with an elim-

Received August 10, 2001; Revised October 11, 2001; Accepted October 11, 2001.

From the *Department of Anesthesiology, University of California San Diego, San Diego, CA; †Departments of Neurology and Anesthesia, University of California San Francisco, UCSF Pain Clinical Research Center, San Francisco, CA; ‡Department of Neurology, MCP Hahnemann University, Philadelphia, PA; §Department of Neurology & Danish Pain Research Center, Aarhus University Hospital, Denmark; and ‖Department of Neurology and Psychiatry, Glaxo Wellcome Inc, Research Triangle Park, NC.

Funded and sponsored by Glaxo Wellcome, Research Triangle Park, NC, and London, UK.

Address reprint requests to Mark S. Wallace, MD, Department of Anesthesiology, University of California, San Diego, 9500 Gilman Drive #0924, La Jolla, CA 92093-0924.

1526-5900/2002 $35.00/0
doi:10.1054/jpai.2002.123650

ination half-life of 67 hours (unpublished observations). The purpose of the present study was to examine the safety, analgesic efficacy, and tolerability of oral 4030W92 in a group of subjects with chronic neuropathic pain.

Methods

Subjects

The study protocol (Glaxo Wellcome N2AA2003) was approved by the Institutional Review Boards of the 4 participating institutions. With informed consent, subjects with neuropathic pain of moderate to severe intensity (visual analog scale [VAS] score of 30 mm or greater) and a well-defined primary area of mechanical allodynia were recruited for the study. Subjects were required to fall within 1 of 3 diagnostic groups: (1) postherpetic neuralgia (PHN) of at least 3 months' duration, (2) complex regional pain syndrome (CRPS) type I or II of greater than 12 months' and less than 3 years' duration, or (3) definable lesion of a peripheral nerve not associated with ongoing infection. Subjects were not allowed to use tricyclic antidepressants or anticonvulsants during the study. Continued use of their rescue analgesic of choice was allowed, if the dose had been stable for at least 4 weeks.

Study Overview

A randomized, double-blind, placebo-controlled, crossover design was used. Subjects came to the research center for a total of 8 visits during a 9-week period. After the initial eligibility evaluation, subjects entered a 7-day screen during which they underwent sensory testing for mechanical allodynia and made a daily record of analgesic medication usage and pain severity. At the second visit, eligible subjects were randomized to treatment sequence (placebo-4030W92 or 4030W92-placebo) and received their first dose of study medication during a full-day study session. Subjects took one 25-mg tablet of 4030W92 or matching placebo once a day during the rest of the treatment period. Subjects were reevaluated after 7 days of treatment and again at the end of the 14-day treatment period. After a 14-day washout period, subjects entered the second treatment period. On completion of the second treatment, a second 14-day washout period ensued before the final follow-up visit.

At the day 1 visit of each treatment period, the following assessments were made before dose and 4 hours after dose: (1) spontaneous and evoked pain scores, (2) dynamic and static allodynia mapping, (3) Short Form McGill Pain Questionnaire (SF-MPQ), and (4) blood sample for 4030W92 assay. These assessments were repeated at the day 7 and day 14 visits for each treatment period. On day 1 before dose and day 14, subjects also underwent (1) thermal testing in the painful area, (2) Medical Outcomes Study Short Form 36 (SF-36) Questionnaire, and (3) patient global satisfaction. Throughout the study, patients were asked to record pain VAS and pain relief scores and rescue analgesic use in a diary each evening.

Outcome Measures: Primary

A VAS, consisting of a 100-mm line with "no pain" written at one end and the "worst imaginable pain" written at the other end, was used to assess spontaneous pain. Each evening, the subject was asked to place a mark along the line that corresponded with their pain for the entire day. The distance, in millimeters, from the no pain end to the location of the mark gave a measurement of the pain. The primary efficacy end point was the change from baseline to the end of the 2-week treatment period in pain intensity on the VAS (also referred to as the pain intensity difference [PID]).

Outcome Measures: Secondary

The following assessments were evaluated as secondary end points in this study:

1. Mean pain intensity on the VAS during the treatment period.
2. The percentage of days with "moderate" pain relief or better. Every evening during the treatment periods, subjects rated their level of pain relief for the entire day on a 6-item category scale (worse, no relief, slight relief, moderate relief, a lot of relief, and complete relief).
3. Evoked pain intensity. Allodynia severity was determined by stroking the most painfully sensitive area of the skin 3 times during a period of 5 seconds at a rate of 5 cm/s with a foam brush. Summation phenomena were determined by "bouncing" a von Frey hair (filament size #14, equal to 5.18 g of pressure) on the most painfully sensitive area of the skin 10 times. In each test, the subject indicated the amount of pain evoked on a 100-mm VAS scale.
4. Dynamic and static allodynia mapping. The area of dynamic allodynia was determined by gently stroking the skin with a 1-inch foam brush from outside the sensitive area toward the center of the sensitive area along 8 approximately evenly spaced radii while asking the subject to report when the sensation changed to become unpleasant or painful. The area of static allodynia was determined by gently pressing the skin from outside the sensitive area gradually toward the center of the sensitive area with a #14 von Frey hair until the filament curved, while asking the subject to report when the sensation changed to become unpleasant or painful. Each area of allodynia was traced on transparent paper, if small enough, and measured (in cm^2) by using a compensating polar planimeter. If the area was larger than the transparent paper size, the areas were approximated and transferred to a standard homunculus provided to each study site for estimation of area (in cm^2).
5. Thermal testing. Thermal thresholds were determined in the area of greatest pain and the corresponding spot on the unaffected side with the Thermal Sensory Analyzer (TSA) (Medoc Advanced Medical Systems, Minneapolis, MN). The thermode size was 30 × 30 mm. To prevent skin injury, temperature limits of 50°C and

0°C were used. Thresholds were calculated as the average of 4 consecutive trials. The baseline temperature was set at 32°C. For warming and cooling detection thresholds, the temperature ramp was 1°C/s. For cold and heat pain thresholds, the ramp rate was 2°C/s. Subjects also rated the painfulness of the fourth ramp on the VAS.

6. Short Form McGill Pain Questionnaire. Subjects were asked to rate the present intensity of each pain-related adjective by circling none, mild, moderate, or severe.
7. Medical Outcomes Study Short Form (SF-36). This 36-item questionnaire is summed into 8 multi-item scales measuring health concepts encompassing physical and mental health.

4030W92 assay

A mass spectrometry–based method for the determination of 4030W92 in plasma was used. The method used solid-phase extraction in 96-well microliter plate format, which had been automated by means of a custom-built Zymark robotic system. The extracts were analyzed by liquid chromatography–tandem mass spectrometry by using Turbo Ionspray and multiple reaction monitoring. The method provided a lower limit of quantification of 25 ng/mL from a 0.2-mL sample size.

Safety Monitoring

Adverse event queries were completed at each post-randomization study visit. Women of childbearing potential underwent urine pregnancy tests to document the absence of pregnancy before participation in the study, before each treatment period, on the last day of treatment, and at the final follow-up. To rule out arrhythmias or conduction defects, serial electrocardiograms were conducted at the screen visit, before and after dose on the first day of each treatment period, on the last day of each treatment period, and at the final follow-up.

Data Analysis

All data are expressed as the mean + the standard deviation. PID was compared with analysis of covariance (ANCOVA). Tests for carryover effects from one study session to the other were performed in 2 ways: (1) 2 sample *t* tests on the period differences of the baseline values and (2) ANCOVA on subject totals with the first period baseline as the covariate. Mean pain intensity, evoked pain intensity, area of allodynia, thermal thresholds, and the total score for the SF-MPQ were compared with ANCOVA. The percentage of days with moderate pain relief or better during the treatment period was compared by using the Koch nonparametric method for a two-period crossover. SF-36 scores were compared with analysis of variance. Subjects who discontinued prematurely from the study were handled in 2 ways:

1. Last observation carried forward (LOCF): the last observation before the time of discontinuation was carried forward to the end of the study period from which they discontinued. Data were only carried forward within a specific study period and not across to any subsequent study periods. If the baseline reading was worse than the last observation, then the baseline was carried forward instead.
2. Observed data: data were regarded as missing at random and no values were imputed.

For the primary end point, analysis was performed with both the LOCF approach (primary analysis) and observed data (additional sensitivity analysis). For all secondary end points, analysis was only performed with the LOCF approach.

With a difference of 6 mm and within-subject standard deviation of 9.2 mm, a total of 37 subjects were needed on the basis of a one-sample *t* test for crossover studies, for 80% power and a .05 (two-sided) significance level. On the basis of these calculations, 20 subjects per treatment sequence group were enrolled.

Table 1. Subject Demographics

CATEGORY	DEMOGRAPHICS
Age (y)	Mean, 53.4; range, 25-82
Gender (No.)	Men, 15; women, 26
Race (No.)	White, 40; black, 1
Pain syndrome	CRPS type I, 8; type II, 1; postherpetic neuralgia, 15; peripheral nerve injury, 15; other, 2
Pain duration (mo)	Mean, 50; range, 3-279
Mean screening VAS (mm)	Mean, 59.3; range, 24-96
Mean screening allodynia VAS (mm)	Mean, 47.6; range, 0-98
Mean screening area of static allodynia (cm^2)	Mean, 38.8; range, 1.4-191.9
Mean screening area of dynamic allodynia (cm^2)	Mean, 31.6; range, 0-182.3

Results

A total of 41 subjects entered the study and received at least 1 dose of study medication. Table 1 summarizes the demographics of the study cohort. Thirty of the 41 subjects had either PHN or peripheral nerve injury. Ninety percent (n = 37) completed the study and 10% (n = 4) were discontinued early from the study. Two subjects were withdrawn from the study for the following reasons: 1 subject withdrew consent, and 1 subject was lost to follow-up.

Primary Efficacy Measure

On the primary end point PID, there was no significant difference between 4030W92 and placebo ($P = .137$) (Fig 1). There was an improvement in pain scores (ie, higher positive values of PID) on 4030W92 compared with placebo, but the treatment difference was small, 4.0 mm with a 95% confidence interval of −1.4 mm to +9.4 mm (Fig 1). The crossover design was valid, because there was no evidence of a difference between the baselines at the

start of each treatment period, treatment interaction, or period effect of 4030W92 on pain scores.

Secondary Efficacy Measures

There was no significant difference between 4030W92 and placebo in mean pain intensity during the treatment period. Although mean values were higher during 4030W92 treatment, there was no significant difference ($P = .190$) between 4030W92 and placebo in the percentage of days with moderate pain relief or better (Fig 2). On most days and for both treatments, fewer than 20% of subjects experienced relief that was rated as moderate or better. Compared to placebo, rescue analgesic use was not significantly different during 4030W92 treatment.

Allodynia severity was significantly lower ($P = .046$) on treatment day 1, postdose for 4030W92 compared to placebo (Fig 3). However, this was not maintained on treatment day 7 or 14. There was a nonsignificant decrease in abnormal temporal summation with 4030W92. The area of static allodynia was significantly smaller ($P = .03$) on treatment day 7 for 4030W92 compared with placebo (Fig 4, left panel). However, this was not maintained to treatment day 14. There was no significant difference between 4030W92 and placebo in area of dynamic allodynia at any time (Fig 4, right panel).

Table 2 summarizes the baseline thermal thresholds in both affected and unaffected skin. Baseline measurements showed elevated warm and cool detection thresholds and decreased cold pain thresholds (ie, cold pain was evoked at a temperature that was warmer than normal). As reflected in higher VAS pain scores with thermal stimulation of the painful region, there was also evidence of heat and cold hyperalgesia. There was no significant difference between 4030W92 and placebo on thermal thresholds or thermally evoked pain intensity.

There was no significant difference between 4030W92 and placebo in the total score for the SF-MPQ pain descriptors at any time. On the SF-36, changes in the 8 domains during 4030W92 were not significantly different from placebo.

Adverse Events

The overall incidence of adverse events during treatment was similar for 4030W92 (63%) and placebo (61%). There were no subjects who discontinued the study because of side effects. The incidence of drug-related adverse events during treatment was higher for 4030W92 (50%) than for placebo (37%). The adverse events with a greater than 5% higher incidence on 4030W92 compared to placebo were sedation (15% vs 2%), malaise and fatigue (8% vs 2%), nausea (10% vs 5%), diarrhea (5% vs 0%), and eating problems (5% vs 0%). Skin rash was reported in 3% of subjects during 4030W92 treatment and in 0% during placebo treatment.

4030W92 plasma levels

Peak plasma levels for 4030W92 occurred on day 14. The plasma levels suggested relatively low/moderate intersubject variability. Median trough values were approximately 75% of the steady state trough values obtained on day 14 (Fig 5).

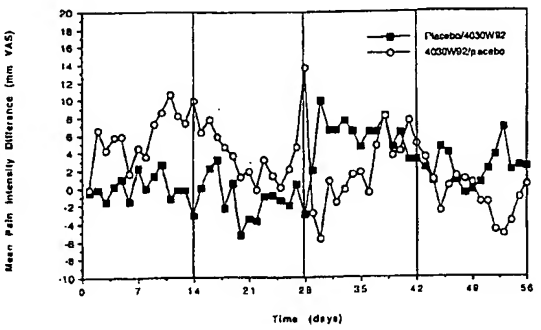

Figure 1. Line graph of mean PIDs in mm on the VAS during the 14-day treatment periods for 4030W92 and placebo. A positive number means a greater reduction in pain.

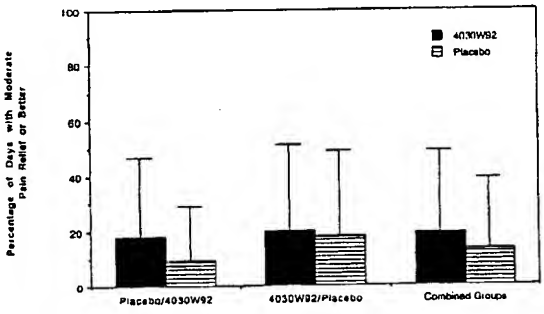

Figure 2. Bar plot of percentage of days with moderate pain relief or better during the study by treatment sequence group and by treatment.

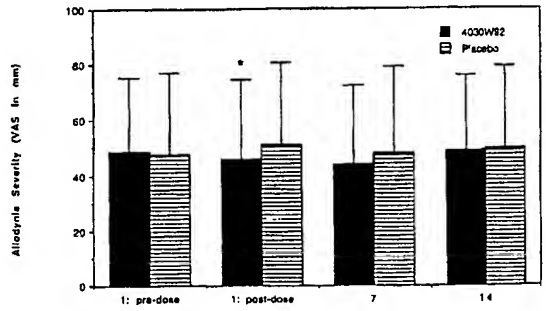

Figure 3. Bar plot of allodynia severity as measured by the VAS (in mm) pre-dose, post-dose, day 7, and day 14. *$P < .05$.

Discussion

In the present study there was no significant decrease in daily pain throughout the 14-day treatment period with 4030W92 compared to placebo. The present study did demonstrate a significant first-dose effect of 4030W92 on allodynia severity that was not maintained

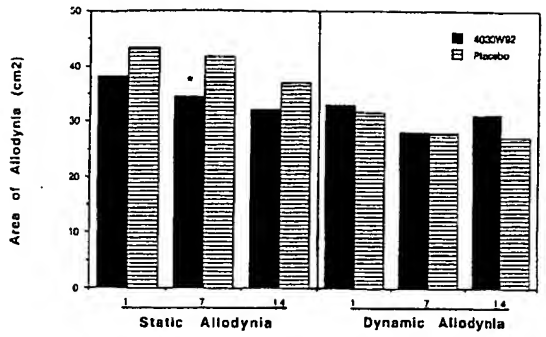

Figure 4. Bar plot of the area of static and dynamic allodynia (cm^2) 4 hours day 1 post-dose, day 7, and day 14. *$P < .05$.

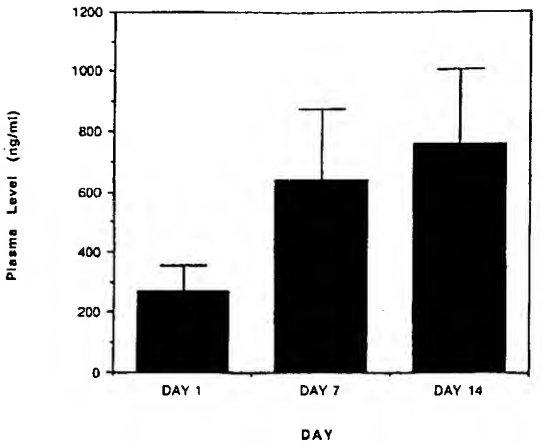

Figure 5. Bar plot of 4030W92 plasma levels at 4 hours day 1 post-dose, day 7, and day 14.

on days 7 and 14. There was also a transient early effect on the area of allodynia to static (but not dynamic) stimuli. Temporal summation to repetitive stimuli was consistently, but only slightly, reduced.

There are several possible reasons why these results failed to provide statistical significance. First, the number of patients included was relatively small; however, the power analysis outlined in the methods section suggested that the sample size was adequate. Second, given the minimal side effects observed at the dose of 25 mg/day, the changes in spontaneous and evoked pain with 4030W92 may represent threshold effects that would be of greater duration and magnitude with a larger daily dose. Positive studies involving neuropathic pain populations often use dose titration to individualize tolerability limits. Perhaps increasing the dose of 4030W92 could have shown greater efficacy with an increase in safety risk. Constraints imposed on the design of this study may not have allowed individual subjects to reach a maximum response. Third, the group of patients was heterogeneous; however, they all had the common link of mechanical allodynia, suggesting a common neuropathic pain mechanism.

Previous studies with oral and intravenous sodium channel blockers suggested dose-response relationships may be important. For example, Galer et al[16] showed that 2 mg/kg intravenous lidocaine produced less relief of neuropathic pain than 5 mg/kg. With computer-controlled infusions to target specific plasma levels, Wallace et al[27] showed increased pain reduction with higher blood levels. Studies with oral mexiletine have shown little or no pain reduction at doses of 450 to 750 mg/day but more impressive pain relief when the dose was pushed to a maximum of 1200 mg/day or the drug was given on a per kilogram basis.[6,22,24,31] For lamotrigine, a controlled study of 200 mg/day in patients with neuropathic pain produced negative results, whereas studies using 400 mg/day were successful.[14,19,34]

Table 2. Baseline Thermal Thresholds (°C ± Standard Deviation) and Thermal Elicited Pain Score (VAS in mm ± Standard Deviation)

	Unaffected	*Affected*
Warm	36.9 ± 4.4	38.6 ± 4.8
Cool	27.7 ± 3.1	25.0 ± 5.5
Hot pain	45.0 ± 3.5	45.3 ± 7.5
Cold pain	12.4 ± 9.4	15.4 ± 9.5
Hot pain VAS	47.2 ± 28.7	64.4 ± 20.7
Cold pain VAS	30.8 ± 26.3	46.0 ± 28.6

NOTE. The thermal thresholds are the temperatures at which the change was detected (from a starting temperature of 32°C).

The patients with neuropathic pain examined in this study all had mechanical allodynia. The mechanisms of the hyperalgesia and allodynia after peripheral nerve injury are not completely understood. There is abundant evidence for abnormal sodium channel accumulation on peripheral axons after nerve injury.[12,15] Anecdotally, allodynia and hyperalgesia may be dramatically reduced during intravenous lidocaine infusion in patients with chronic pain. Overall, sodium channel blockers produce only modest changes in experimental pain models that use normal human volunteers. In the intradermal capsaicin injection model, intravenous lidocaine and oral mexiletine decrease the C-fiber mediated flare response with minimal effects on the secondary hyperalgesia.[3,28] Systemic lidocaine inhibited punctate-evoked but not brush-evoked hyperalgesia in the intradermal capsaicin injection model,[18] but the opposite pattern was seen in the heat/capsaicin sensitization model.[13]

In the present study, thermal sensory testing was carried out to determine baseline small fiber function and the effects of 4030W92. Fascicular recording and compression-ischemia block have shown that low-threshold tactile sensations are subserved by large myelinated fibers (Aβ), cool sensation by small myelinated fibers (Aδ), and warmth and pain by small unmyelinated fibers (C-fibers).[21,25,33] Consistent with the diagnosis of neuropathic pain, baseline thermal testing showed an elevation of warming and cooling detection thresholds and a

slight decrease in cold pain thresholds. Heat and cold hyperalgesia was evident in the form of higher pain intensity VAS scores from noxious thermal stimulation on the painful side. We found no effect of 4030W92 on small fiber function. This is not surprising, because several studies have found no effect of intravenous lidocaine (at plasma levels up to 3 μg/mL) and mexiletine (at plasma levels up to 0.5 μg/mL) on acute sensory thresholds in both the normal and neuropathic pain states.[3,5,28,29]

Aside from the known anticonvulsant effects of lidocaine, there is evidence to indicate that central actions of sodium channel blockers are relevant to their analgesic effects. Lidocaine increased the threshold for evoking the nociceptor flexor reflex in patients with diabetic neuropathy without altering peripheral conduction and suppresses polysynaptic C-fiber evoked reflexes in animals.[5,30] Similarly, lidocaine has been shown to reduce neuronal activity in the dorsal horn of the spinal cord in rats with experimental neuropathy.[23] Two recent controlled studies have shown relief of central nervous system injury pain with sodium channel blockers. Attal et al[4] showed a reduction of spontaneous ongoing pain and of brush- and pinprick-evoked hyperalgesia after intravenous lidocaine in patients with central pain due to spinal cord injury or stroke. Andersen et al[2] found an analgesic effect of lamotrigine in poststroke pain by using a double-blind, placebo-controlled, crossover design. Therefore, it may be of interest to explore 4030W92 further in patients with central pain syndromes.

There are many subtypes of sodium channels expressed in the nervous system. Certain pain-sensitive peripheral sensory neurons express a distinct type of tetrodotoxin-insensitive sodium channel.[1] Pain relief may be significantly greater with highly subtype-selective drugs that allow for greater blockade of abnormal neuronal activity mediated by sodium channels before side effects supervene. Future studies should be directed at further identification of the subtypes of sodium channels located on pain-sensitive nerve fibers after nerve injury and their modulation by subtype-specific channel blockers. Unfortunately, all of the existing agents, including 4030W92, are not selective for this sodium channel. Because the 25-mg/day dose of 4030W92 used in the present study produced an insignificant pain reduction without treatment limiting side effects, the maximum analgesic effect of this drug remains unknown.

Acknowledgements

We thank Drusilla Noronha, statistics; Louisa Pickering, drug assay analyst; and Linda Sutherland, editing.

References

1. Akopian AN, Sivilotti L, Wood JN: A tetrodotoxin-resistant voltage-gated sodium channel expressed by sensory neurons. Nature 379:257-262, 1996

2. Andersen G, Vestergaard K, Kristensen BT, Gottrup H, Jensen TS: The analgesic efficacy of lamotrigine in central post-stroke pain, in Proceedings of the 9th World Congress on Pain. Seattle, IASP Press, 1999, p 434

3. Ando K, Wallace MS, Schulteis G, Braun J: Neurosensory finding after oral mexiletine in healthy volunteers. Reg Anesth Pain Med 25:468-474, 2000

4. Attal N, Gaude V, Brasseur L, Dupuy M, Guirimand F, Parker F, Bouhassira D: Intravenous lidocaine in central pain: A double-blind, placebo controlled, psychophysical study. Neurology 54:564-574, 2000

5. Bach FW, Jensen TS, Kastrup J, Stigsby B: The effect of intravenous lidocaine on nociceptive processing in diabetic neuropathy. Pain 40:29-34, 1990

6. Chabal C, Jacobson L, Mariano A: The use of oral mexiletine for the treatment of pain after peripheral nerve injury. Anesthesiology 76:513-517, 1992

7. Chabal C, Russell DA, Buchiel KJ: The effect of intravenous lidocaine, tocainide, and mexiletine on spontaneous active fibers originating in rat sciatic neuromas. Pain 38:333-338, 1989

8. Clayton NM, Collins SD, Sargent R, Brown T, Nobbs M, Bountra C: The effect of the novel sodium channel blocker 4030W92, in models of acute and chronic inflammatory pain. Br J Pharmacol 123:79, 1997

9. Collins SD, Clayton NM, Nobbs M, Bountra C: The effect of 4030W92, a novel sodium channel blocker on the treatment of neuropathic pain in the rat. Br J Pharmacol 123:16, 1997

10. Cummins TR, Waxman SG: Down regulation of tetrodotoxin-resistant sodium currents and upregulation of a rapidly repriming tetrodotoxin-sensitive sodium current in small spinal sensory neurons after nerve injury. Neuroscience 17:3503-3514, 1997

11. Dejgard A, Petersen P, Kastrup J: Mexiletine for treatment of chronic painful diabetic neuropathy. Lancet 1:9-11, 1988

12. Devor M, Govrin-Lippmann R, Angelsides K: Na channel immunolocalization in peripheral mammalian axons and changes following nerve injury and neuroma formation. J Neuroscii 13:1976-1992, 1993

13. Dirks J, Fabricius P, Petersen KL, Rowbotham MC, Dahl JB: The effect of systemic lidocaine on pain and secondary hyperalgesia associated with the heat/capsaicin sensitization model in healthy volunteers. Anesth Analg. In Press

14. Eisenberg E, Alon N, Ishay A, Daoud D, Yarnitsky D: Lamotrigine in the treatment of painful diabetic neuropathy. Eur J Neurol 5:167-173, 1998

15. England JD, Happel LT, Kline DG: Sodium channel accumulation in humans with painful neuromas. Neurology 47: 272-276, 1996

16. Galer BS, Harle J, Rowbotham MC: Response to intravenous lidocaine infusion predicts subsequent response to oral mexiletine: A prospective study. J Pain Symptom Manage 12:161-167, 1996

17. Galer BS, Miller KV, Rowbotham MC: Response to intravenous lidocaine infusion differs based on clinical diagnosis

and site of nervous system injury. Neurology 43:1233-1235, 1993

18. Gottrup H, Hansen PO, Arendt-Nielson L, Jensen TS: Differential effects of systemic administration ketamine and lidocaine on dynamic and static hyperalgesia induced by intradermal capsaicin in humans. Br J Anaesth 84:155-163, 2000

19. McCleane G: 200mg daily of lamotrigine has no analgesic effect in neuropathic pain: A randomized, double-blind, placebo controlled trial. Pain 83:105-107, 1999

20. Nishiyama K, Sakuta M: Mexiletine for painful alcoholic neuropathy. Intern Med 34:577-579, 1995

21. Ochoa JL, Torebjork HE: Sensations evoked by intraneural microstimulation of C nociceptor fibres in human skin nerves. J Physiol 415:583-599, 1989

22. Oskarsson P, Ljunggren JG, Lins PE: Efficacy and safety of mexiletine in the treatment of painful diabetic neuropathy: The Mexiletine Study Group. Diabetes Care 20:1594-1597, 1997

23. Sotgiu ML, Lacerenza M, Marchettini P: Effects of systemic lidocaine on dorsal horn neuron hyperactivity following chronic peripheral nerve injury in rats. Somatosens Mot Res 9:227-233, 1992

24. Stracke H, Meyer UE: Mexiletine in the treatment of diabetic neuropathy. Diabetes Care 15:1550-1555, 1992

25. Torebjork HE, Vallbo AB, Ochoa JL: Intraneural microstimulation in man: Its relation to specificity of tactile sensations. Brain 110:1509-1529, 1987

26. Trezise DJ, John VH, Xie XM: Voltage- and use-dependent inhibition of Na+ channels in rat sensory neurones by 4030W92, a new antihyperalgesic agent. Br J Pharmacol 124: 953-963, 1998

27. Wallace MS, Dyck JB, Rossi SS, Yaksh TL: Computer-controlled lidocaine infusion for the evaluation of neuropathic pain after peripheral nerve injury. Pain 66:69-77, 1996

28. Wallace MS, Laitin S, Licht D, Yaksh TL: Concentration-effect relations for intravenous lidocaine infusions in human volunteers: Effect on acute sensory thresholds and capsaicin-evoked hyperpathia. Anesthesiology 86:1262-1272, 1997

29. Wallace MS, Ridgeway B, Leung A, Yaksh TL: Concentration-effect relationship of intravenous lidocaine on the allodynia of complex regional pain syndrome types I and II. Anesthesiology 92:75-83, 2000

30. Woolf CJ, Wiesenfeld-Hallin Z: The systemic administration of local anaesthetics produces a selective depression of C-afferent fibre evoked activity in the spinal cord. Pain 23: 361-374, 1985

31. Wright JM, Oki JC, Graves L: Mexiletine in the symptomatic treatment of diabetic peripheral neuropathy. Ann Pharmacother 31:29-34, 1997

32. Xu XJ, Hao JX, Seiger A, Amer S, Lindblom U, Wiesenfeld-Hallin Z: Systemic mexiletine relieves chronic allodynia-like symptoms in rats with ischemic spinal cord injury. Anesth Analg 74:649-652, 1992

33. Yarnitsky D, Ochoa JL: Warm and cold specific somatosensory systems: Psychophysical thresholds, reaction times and peripheral conducttion velocities. Brain 114:1819-1826, 1991

34. Zakrzewska JM, Chaudhry Z, Nurmikko TJ, Patton DW, Mullens EL: Lamotrigine (lamictal) in refractory trigeminal neuralgia: Results from a double-blind placebo controlled crossover trial. Pain 73:223-230, 1997

Cerebroprotective Effect of Lamotrigine After Focal Ischemia in Rats

Stuart E. Smith, MSc, PhD; Brian S. Meldrum, MB, BChir, PhD

Background and Purpose Glutamate receptor antagonists are protective in animal models of focal cerebral ischemia. Lamotrigine (3,5-diamino-6-[2,3-dichlorophenyl]-1,2,4-triazine) is an anticonvulsant drug that blocks voltage-gated sodium channels and inhibits the ischemia-induced release of glutamate. We describe the cerebroprotective effect of lamotrigine (as the isethionate salt) after middle cerebral artery occlusion in rats.

Methods Neurological deficit and infarct volume (visualized by the lack of reduction of 2,3,5-triphenyltetrazolium chloride) 24 hours after permanent left middle cerebral artery occlusion were studied in Fischer rats (n=8 per group per dose).

Results Lamotrigine at 20 mg/kg IV over 10 minutes administered immediately after middle cerebral artery occlusion reduced total infarct volume by 31% and cortical infarct volume by 52%. Lamotrigine at 8 mg/kg IV over 10 minutes reduced cortical infarct volume by 38%. Lamotrigine at 50 mg/kg IV for 10 minutes was not cerebroprotective and induced a decrease of 29±15 mm Hg in mean arterial blood pressure ($P<.05$, n=8). The optimum dose of lamotrigine (20 mg/kg IV over 10 minutes) when administered with a 1-hour delay after middle cerebral artery occlusion reduced cortical infarct volume by 41%. Lamotrigine (20 mg/kg IV over 10 minutes) with a 2-hour delay after middle cerebral artery occlusion was ineffective. Neurological deficits after 24 hours were improved after immediate treatment with lamotrigine at 20 mg/kg IV over 10 minutes.

Conclusions The cerebroprotective effect of lamotrigine in rats is limited to a narrow dose range between 8 and 20 mg/kg. Lamotrigine or analogous compounds may be useful when given shortly after the onset of stroke. (*Stroke*. 1995;26:117-122.)

Key Words • cerebral ischemia • sodium channels • neuroprotection • glutamates • rats

The activation of excitatory amino acid receptors is thought to be involved in the development of infarction of cerebral tissue.[1,2] During focal cerebral ischemia, augmented concentrations of glutamate and aspartate (peaking at 0.5 to 2 hours after occlusion) have been detected in the extracellular space using microdialysis techniques.[3-6] Based on electrophysiological studies, postsynaptic ionotropic receptors for excitatory amino acids at which glutamate may act are classified into three main subtypes.[7] These comprise the receptors preferring *N*-methyl-D-aspartate (NMDA), kainate, and *S*-α-amino-3-hydroxy-5-methyl-4-isoxazolepropionate (AMPA). AMPA and kainate receptors are referred to as "non-NMDA receptors." Glutamate has excitotoxic effects acting via NMDA or non-NMDA receptors in vivo and in vitro.[8,9] Cerebroprotection with excitatory amino acid antagonists acting at NMDA and non-NMDA receptors has been established after focal cerebral ischemia.[2,10-19] An alternative approach is to reduce the release of glutamate during and after the ischemic insult.[20-23]

Lamotrigine (3,5-diamino-6-[2,3-dichlorophenyl]-1,2,4-triazine; Lamictal) is a novel anticonvulsant agent with efficacy in patients with partial seizures or generalized tonic clonic seizures. The time course for the anticonvulsant effect for lamotrigine in animals and in photosensitive epileptic patients is relatively long (from 1 to 24 hours) after intravenous, intraperitoneal, or oral administration. Lamotrigine is completely bioavailable after oral administration in rats and is distributed throughout the body; anticonvulsant doses of 2 to 4 mg/kg result in plasma concentrations of lamotrigine of 1 to 2 μg/mL. Lamotrigine is rapidly absorbed, and its half-life for elimination in the Wistar rat is 12 to 15 hours.[24-28]

See Editorial Comment, page 121

The mechanism of anticonvulsant action of lamotrigine is thought to involve action at voltage-sensitive sodium channels.[29-31] Lamotrigine reduces veratrine- but not K^+-induced glutamate, aspartate, and γ-aminobutyric acid release with ED_{50} values of 21 μmol/L, 21 μmol/L, and 44 μmol/L, respectively, in cerebrocortical slices from the rat in vitro.[24,25,28] Lamotrigine has no effect on the binding of a wide range of radiolabeled neurotransmitters (including dopamine D_1 and D_2; adrenergic α_1, α_2, and β; adenosine A_1 and A_2; muscarinic; or σ binding sites), but it does compete with [^{3}H]batrachotoxinin-A-20-α-benzoate (pK_i=3.5),[25,30] a ligand interacting with a sodium channel site related to activation of sodium channel fluxes, and with [^{3}H]quipazine (pK_i=5.7), a ligand interacting with 5-HT_3 recognition sites.[25]

The present study was designed to determine whether lamotrigine has cerebroprotective effects after permanent left middle cerebral artery (MCA) occlusion in rats. Preliminary data have been presented.[32-34]

Materials and Methods

Adult male Fischer F344 rats weighing 250 to 310 g were housed in groups of four to six in polyvinylchloride cages (350

Received March 7, 1994; final revision received August 11, 1994; accepted September 20, 1994.

From the Department of Neurology, Institute of Psychiatry, De Crespigny Park, Denmark Hill, UK.

Correspondence to B.S. Meldrum, Department of Neurology, Institute of Psychiatry, De Crespigny Park, Denmark Hill, SE5 8AF, UK.

mm wide×530 mm long×180 mm high) in an environment maintained at 19°C to 22°C and a relative humidity of 55±3%, respectively, with a 14-h light/10-h dark cycle (light on from 6 AM to 8 PM). Food and water were available ad libitum. Halothane was used to induce (4% in a mixture of 70% N_2O and 30% O_2) and maintain (2%) anesthesia. Each rat was allowed to breathe spontaneously, and rectal temperature was maintained at 37°C (36.5°C to 38°C) with a heating blanket. The left femoral vein was cannulated for drug administration, and the caudal (tail) artery was cannulated for the continuous monitoring of arterial blood pressure, repeated blood sampling for serial measurements of blood glucose concentration, PaO_2, $PaCO_2$, and pH levels. Arterial blood (200 μL total volume) was collected without the need for induced negative pressure from the caudal artery of the rats for immediate analysis at 15 minutes before and 15 minutes after MCA occlusion and in some experiments at 30-minute intervals thereafter. Blood gases and pH were analyzed using an IL13404 analyzer (Instrumentation Laboratories), and blood glucose level was measured with Glucostix strips (Bayer Diagnostics, Ames Division). The temperature of the exposed temporalis muscle was monitored using a thermoprobe.

All rats underwent subtemporal subperiosteal craniectomy (with intact zygoma) and exposure of the main trunk of the left MCA under 25-fold magnification of an operating stereomicroscope.[35,36] The exposed artery was electrocauterized from a point proximal to the lenticulostriate branch(es) to its junction with the inferior cerebral vein.

The rats received in a blinded fashion vehicle (0.25% wt/vol methylcellulose [Sigma Chemical Co], 400 cp, in high-performance liquid chromatography water) or lamotrigine (3.2, 8, 20, or 50 mg/kg IV over 10 minutes; 1 mL/kg; all doses refer to the isethionate salt of lamotrigine) immediately after MCA occlusion (n=8 per group per dose). In a further experiment, vehicle or lamotrigine (20 mg/kg IV over 10 minutes) was administered 1 or 2 hours after MCA occlusion (n=8). During the 10-minute infusions and the 1- or 2-hour delay, rats were lightly anesthetized with 0.5% halothane in a mixture of 70% N_2O and 30% O_2. Fifteen minutes after MCA occlusion or 5 minutes after the delayed infusion, the cannulas were removed, the anesthesia was discontinued, and the animals were allowed to recover in cages warmed with an overhead lamp (60-W bulb, 30-cm distance). Rectal temperature was measured at +1 hour after vehicle or drug infusion.

Twenty-four hours after MCA occlusion, the rats were assessed in a blinded fashion for neurological deficits based on the rating scales used by Bederson et al[37] and Germano et al.[10] The following grading scale was used: grade 0, no observable deficit; grade 1, forelimb flexion; grade 2, forelimb flexion and decreased resistance to lateral push; and grade 3, forelimb flexion, decreased resistance to lateral push, and unilateral circling in three successive trials. The animals were then decapitated, and the brain was rapidly removed (within 2 minutes), examined for proximal MCA occlusion, and then placed into a vibratome containing saline at 8°C. Ten coronal sections (1 mm thick) were cut from the frontal pole and then incubated for 30 minutes in microwells, each containing 2 mL 2% wt/vol triphenyltetrazolium chloride in saline at 37°C before storage in 0.1 mol/L phosphate-buffered (pH 7.4) 5% vol/vol formaldehyde in saline for 1 to 5 days. The sections were photographed to scale, and slides were prepared and used to estimate the left and right hemispheric and the total, cortical, and noncortical infarct areas using an IBAS image analyzer (Kontron Elektronik, GmbH). These areas were used to calculate the hemispheric and infarct volumes in cubic millimeters by use of a BASIC integration program that is based on the ends of spheres and truncated cones. Infarct volumes are expressed as mean±SD and were analyzed using Student's unpaired *t* test or Dunnett's test (SAS/STAT version 6). Neurological deficit is expressed as frequency for observed deficit and was analyzed using an unpaired rank test. Rectal and temporalis temperatures, blood pressure, glucose, and gases, and pH recorded during the experiment were analyzed using MANOVA.

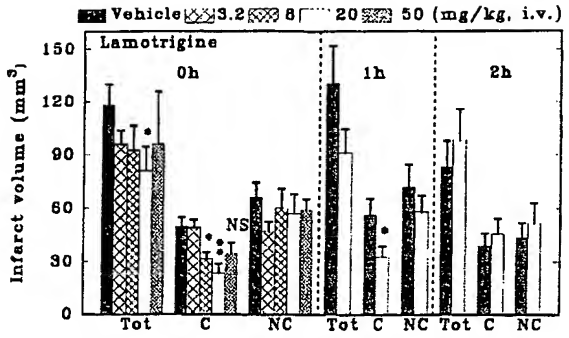

FIG 1. Bar graph showing infarct volumes 24 hours after middle cerebral artery (MCA) occlusion. Rats received 10-minute infusions of either vehicle or lamotrigine isethionate (3.2, 8, 20, or 50 mg/kg IV) immediately, or vehicle or lamotrigine isethionate (20 mg/kg IV) 1 hour or 2 hours after MCA occlusion. Values are mean±SD infarct volumes in cubic millimeters. Significant reduction in infarct volume after lamotrigine isethionate administration by Student's unpaired *t* test with the respective vehicle-treated group (n=8); * $P<.05$; ** $P<.01$. Tot indicates total; C, cortical; and NC, noncortical.

Results

There was a consistent pattern of ischemic brain damage after permanent MCA occlusion. Lesions were seen in the dorsolateral frontoparietal cortex, the caudate putamen, and the globus pallidus. The boundaries between the areas of infarction and the normal adjacent areas were sharply demarcated.

Immediate Administration of Lamotrigine

Immediate postocclusion infusion of lamotrigine (3.2 mg/kg IV over 10 minutes) did not significantly reduce the total, cortical, or noncortical infarct volumes (Fig 1). Neurological deficit was not reduced (Fig 2; vehicle score, 1.8±0.5; lamotrigine score, 1.5±0.9; $P>.05$). Immediate postocclusion infusion of lamotrigine (8 mg/kg IV over 10 minutes) reduced the cortical infarct volume by 38% (from 50±15 mm^3 in vehicle-treated to 31±11 mm^3 in lamotrigine-treated rats; $P<.05$). Total and noncortical infarct volumes were not significantly reduced (Fig 1). Neurological deficit was not reduced (Fig 2; vehicle score, 1.8±0.5; lamotrigine score, 1.6±0.5; $P>.05$).

Immediate postocclusion infusion with lamotrigine (20 mg/kg IV over 10 minutes) reduced the total infarct volume by 31% (from 118±33 mm^3 in vehicle-treated to 81±38 mm^3 in lamotrigine-treated rats; $P<.05$). Cortical infarct volume was reduced by 52% (from 50±15 mm^3 in vehicle-treated to 24±15 mm^3 in lamotrigine-treated rats; $P<.05$). Noncortical infarct volume was not significantly reduced (Fig 1). Neurological deficit was also reduced (Fig 2; vehicle score, 1.8±0.5; lamotrigine score, 0.8±0.7; $P<.05$). Temporalis temperature rose by 1°C in the lamotrigine-treated group 15 minutes after MCA occlusion ($P<.05$).

Immediate postocclusion infusion with lamotrigine (50 mg/kg IV over 10 minutes) did not significantly reduce the total, cortical, or noncortical infarct volumes (Fig 1). Neurological deficit was not reduced (Fig 2;

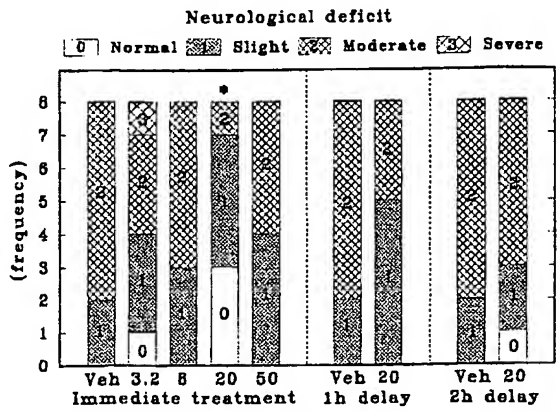

FIG 2. Stacked bar graph showing neurological scores of rats 24 hours after middle cerebral artery (MCA) occlusion. Rats received 10-minute infusions of vehicle (Veh) or lamotrigine isethionate (3.2, 8, 20, or 50 mg/kg IV) immediately, or vehicle or lamotrigine isethionate (20 mg/kg IV) 1 hour or 2 hours after MCA occlusion. Bars show the numbers of rats with observed neurological scores of 0 to 3. Significant reduction in neurological deficit by unpaired rank test; *$P<.05$.

vehicle score, 1.8±0.5; lamotrigine score, 1.5±0.5; ($P>.05$).

1-Hour Delay Before Administration of Lamotrigine

Delayed (1 hour) postocclusion infusion with lamotrigine (20 mg/kg IV over 10 minutes) reduced cortical infarct volume by 41% (from 56±25 mm^3 in vehicle-treated to 33±17 mm^3 in lamotrigine-treated rats; $P<.05$). The total and noncortical infarct volumes were not significantly reduced (Fig 1). Neurological deficit was not reduced (Fig 2; vehicle score, 1.8±0.5; lamotrigine score, 1.4±0.5; $P>.05$).

2-Hour Delay Before Administration of Lamotrigine

Delayed (2 hours) postocclusion infusion with lamotrigine (20 mg/kg IV over 10 minutes) had no effect on total, cortical, or noncortical infarct volume (Fig 1). Neurological deficit was not reduced (Fig 2; vehicle score, 1.8±0.5; lamotrigine score, 1.4±0.6; $P>.05$).

Adverse Effects

Lamotrigine (3.2 to 20 mg/kg IV over 10 minutes) induced no significant changes in blood gases, pH, or glucose levels, mean arterial blood pressure, or rectal or temporalis temperature (n=8).

Lamotrigine (50 mg/kg IV over 10 minutes) induced a reduction of 29±15 mm Hg in mean arterial blood pressure compared with vehicle-treated rats ($P<.05$; Student's unpaired t test). A regression and correlation analysis of the drop of blood pressure against infarct volume (total, cortical, or noncortical) in each rat showed no significant correlation between changes in blood pressure and infarct volume (n=8). Other physiological variables were unaffected (n=8).

On recovery from anesthesia, the animals displayed no adverse behavioral effects after the 10-minute infusion of 3.2, 8, or 20 mg/kg of lamotrigine isethionate. Severe impairment of locomotor coordination (duration, 5 to 8 hours) was observed after the 10-minute infusion of 50 mg/kg of lamotrigine.

For all groups, rectal temperatures were similar, ranging between 36.8°C and 37.5°C. Temporalis temperature was lower, ranging between 32.5°C and 33.9°C.

Discussion

Lamotrigine (20 mg/kg) reduces total and cortical infarct volume and improves neurological deficit in rats when administered immediately after MCA occlusion. After delayed (+1 hour) administration of lamotrigine (20 mg/kg), cortical infarct volume was significantly reduced. Neurological deficit was unaffected. The therapeutic time window for a cerebroprotective effect coincides with the peak increase of extracellular concentrations of glutamate and aspartate, which occurs 0.5 to 2 hours after occlusion during focal cerebral ischemia.[3-6]

Neuronal cell loss after focal injection of kainate into the striatum of the rat is thought to be mediated by the release of neuronal glutamate.[38] Lamotrigine (8 to 16 mg/kg IP) at similar doses as those used in this study protects against kainate neurotoxicity in rat striatum.[39]

Reduction of cortical infarct volume has been described with compounds with chemical structure similar to lamotrigine, which also block sodium channels and inhibit glutamate release: BW1003C87 (5-[2,3,5-trichlorophenyl]-2,4-diaminopyrimidine ethane sulphonate; 20 mg/kg IV for 5 minutes) administered immediately after permanent MCA occlusion in rats[20,21] and BW619C89 (4-amino-2-[4-methylpiperazine-1-yl]-5-[2,3,5-trichlorophenyl]pyrimidine; 5 to 30 mg/kg IV for 5 to 10 minutes.[22,23]

Other compounds with an ability to block sodium channels or to inhibit ischemia-induced glutamate release, which both reduce cortical infarct volume in models of focal cerebral ischemia in the rat, include the κ-opiate agonist CI-977 (enadoline; [5R]-[5α, 7α, 8β]-*N*-methyl-*N*-[7-(1-pyrrolidinyl)-1-oxaspiro-(4,5)-dec-8-yl]-4-benzofuranacetamide · HCl),[40,41] riluzole,[42,43] and phenytoin.[44] Basal microdialysate concentrations of glutamate are unaffected by lamotrigine,[25] BW1003C87,[20,45] or CI-977.[46]

BW1003C87 and BW619C89 are more potent inhibitors of veratrine-induced glutamate release than lamotrigine and are also cerebroprotective in rat models of transient forebrain ischemia.[23,45] Lamotrigine exhibits a bell-shaped dose-response curve for cerebroprotective effect after MCA occlusion in rats. The optimally effective dose is 20 mg/kg, which is 10-fold the anticonvulsant dose in rats (anticonvulsant ED_{50} values against maximal electroshock-induced or sound-induced seizures are 2 mg/kg).[24-26]

When administered before or during focal cerebral ischemia, lamotrigine, BW1003C87, or BW619C89 reduce the ischemia-induced release of glutamate.[21,23,34] The clinical use of BW1003C87 is limited by its ability to inhibit dihydrofolate reductase, which could lead to anemia, thrombocytopenia, and teratogenicity. Lamotrigine congeners like BW619C89, which inhibit ischemia-induced release of glutamate, may provide a novel approach for the therapy of stroke. The precise site and mechanism of the cerebroprotective effect of lamotrigine, BW1003C87, and BW619C89 have not yet been identified. Evidence suggests that an interference with sodium flux across neuronal membranes may be the basis of the anticonvulsant and cerebroprotective effects of these compounds.[28-31] A primary action and use-dependent blockade at sodium channels may result in a

number of effects: (1) inhibition of high-frequency neuronal firing rate, resulting in less glutamate release;[29,31] (2) prevention of an ischemia-induced anoxic depolarization that is characterized by an intraneuronal accumulation of sodium, calcium, and chloride ions;[8] (3) maintenance of the intracellular and extracellular sodium gradient that contributes to the outward movement of Ca^{2+} (via the Na^+/Ca^{2+} exchanger) and the inward movement of glutamate (via the Na^+-coupled glutamate transporter);[47] (4) prevention of cytotoxic edema that occurs after ischemia; and (5) inhibition of spreading depression that may be an indicator or determinant of the process of infarction.[48]

Comparable degrees of cerebroprotection are observed with representative compounds from the following classes of glutamate antagonists: competitive NMDA (D-[*E*]-4-[3-phosphonoprop-2-enyl]piperazine-2-carboxylic acid [D-CPPene]), uncompetitive NMDA (MK801), and non-NMDA antagonists (NBQX and GYKI52466) after focal cerebral ischemia in rats.[2,10-19] These compounds have minimum effective doses in animal models of stroke that are close to doses that induce adverse effects (impairment of locomotor performance, hypotension, respiratory depression). Analogues of these compounds with fewer adverse effects may be developed. Lamotrigine and BW619C89 have a greater separation between effective doses in animal models of stroke and doses that induce adverse effects.[49,50]

Adverse neurological effects were observed after intravenous administration of 50 mg/kg lamotrigine to rats in the present study; cerebroprotection was observed with 20 mg/kg IV lamotrigine, a dose that did not induce any evident adverse behavioral effects. Doses of lamotrigine above 20 mg/kg may have less cerebroprotective effect than a dose of 20 mg/kg because of the increased likelihood of hypotensive effects.

The present data confine the therapeutic time window with lamotrigine to less than 2 hours after the onset of stroke in rodents. Infarction after MCA occlusion develops more slowly in primates, suggesting that the therapeutic time window may be longer in humans.[51]

These studies suggest that compounds of this class may be useful in the treatment of stroke and related neurodegenerative disorders.

Acknowledgments

This study was supported by the Bethlem Maudsley Research Fund, the Medical Research Council of Great Britain, and the Wellcome Foundation. We thank Dr M. Leach from the Wellcome Research Centre, Beckenham, Kent, for the supply of lamotrigine and for his scientific comments on the manuscript.

References

1. Choi DW, Rothman SM. The role of glutamate neurotoxicity in hypoxic-ischemic neuronal death. *Annu Rev Neurosci*. 1991;13:171-182.
2. Meldrum BS. Protection against ischaemic neuronal damage by drugs acting on excitatory neurotransmission. *Cerebrovasc Brain Metab Rev*. 1990;2:27-57.
3. Hillered L, Hallstrom A, Segersvard S, Persson L, Ungerstedt U. Dynamics of extracellular metabolites in the striatum after middle cerebral artery occlusion in the rat, monitored by intracerebral microdialysis. *J Cereb Blood Flow Metab*. 1989;9:607-616.
4. Graham SH, Shiraishi K, Panter SS, Simon RP, Faden AI. Changes in extracellular amino acid neurotransmitters produced by focal cerebral ischaemia. *Neurosci Lett*. 1990;110:124-130.
5. Takagi K, Ginsberg MD, Globus MYT, Dietrich WD, Martinez E, Kraydieh S, Busto R. Changes in amino acid neurotransmitters and cerebral blood flow in the ischemic penumbral region following middle cerebral artery occlusion in the rat: correlation with histopathology. *J Cereb Blood Flow Metab*. 1993;13:575-585.
6. Graham SH, Chen J, Sharp FR, Simon RP. Limiting ischemic injury by inhibition of excitatory amino acid release. *J Cereb Blood Flow Metab*. 1993;13:88-97.
7. Monaghan DT, Bridges RJ, Cotman CW. The excitatory amino acid receptors: their classes, pharmacology, and distinct properties in the function of the central nervous system. *Annu Rev Pharmacol Toxicol*. 1989;29:365-402.
8. Rothman SM, Olney JW. Glutamate and the pathophysiology of hypoxic-ischemic brain damage. *Ann Neurol*. 1986;19:105-111.
9. Choi DW, Koh JY, Peters S. Pharmacology of glutamate neurotoxicity in cortical cell culture: attenuation by NMDA antagonists. *J Neurosci*. 1988;8:185-196.
10. Germano IM, Pitts LH, Meldrum BS, Bartkowski HM, Simon RP. Kynurenate inhibition of cell excitation decreases stroke size and deficit. *Ann Neurol*. 1987;22:730-734.
11. Ozyurt E, Graham DI, Woodruff GN, McCulloch J. Protective effect of the glutamate antagonist MK801 in focal cerebral ischaemia in the cat. *J Cereb Blood Flow Metab*. 1988;8:138-143.
12. Park CK, Nehls DG, Graham DI, Teasdale GM, McCulloch J. The glutamate antagonist MK801 reduces focal ischaemic brain damage in the rat. *Ann Neurol*. 1988;24:543-551.
13. Roman R, Bartkowski H, Simon RP. The specific NMDA receptor antagonist AP-7 attenuates focal ischemic brain injury. *Neurosci Lett*. 1989;104:19-24.
14. Simon RP, Shirashi K. *N*-methyl-D-aspartate antagonist reduces stroke size and regional glucose metabolism. *Ann Neurol*. 1990;27:606-611.
15. McCulloch J, Bullock R, Teasdale GM. Excitatory amino acid antagonists: opportunities for the treatment of ischaemic brain damage in man. In: Meldrum BS, ed. *Frontiers in Pharmacology and Therapeutics: Excitatory Amino Acid Antagonists*. Oxford, UK: Blackwell Scientific Publishers; 1991:287-326.
16. Gill R, Lodge D. The neuroprotective action of 2,3-dihydroxy-6-nitro-7-sulfamoyl-benzo(F)quinoxaline (NBQX) in a rat focal ischaemia model. *Brain Res*. 1992;580:35-43.
17. Buchan AM, Xue D, Huang Z, Smith KH, Lesiuk H. Delayed AMPA receptor blockade reduces cerebral infarction by focal ischemia. *Neuroreport*. 1991;2:473-476.
18. Smith SE, Meldrum BS. Cerebroprotective effects of a non–*N*-methyl-D-aspartate antagonist, GYKI 52466, after focal ischemia in the rat. *Stroke*. 1992;23:861-864.
19. Smith SE, Meldrum BS. Cerebroprotective effects of a non-*N*-methyl-D-aspartate antagonist, NBQX, after focal ischaemia in the rat. *Funct Neurol*. 1993;8:43-48.
20. Meldrum BS, Swan JH, Leach MJ, Millan MH, Gwinn R, Kadota K, Graham SH, Chen J, Simon RP. Reduction of glutamate release and protection against ischemic brain damage by BW 1003C87. *Brain Res*. 1992;593:1-6.
21. Simon RP, Chen J, Graham SH. A new strategy for ameliorating excitotoxicity in cerebral ischemia: inhibition of glutamate release by 5-(2,3,5-trichlorophenyl)-2,4-diaminopyrimidine. In: Simon RP, ed. *Fidia Research Foundation Series: Excitatory Amino Acids*. New York, NY: Thieme Medical Publishers; 1992:241-246.
22. Leach MJ, Swan JH, Eisenthal D, Dopson M, Nobbs M. BW619C89, a glutamate release inhibitor, protects against focal cerebral ischemic damage. *Stroke*. 1993;24:1063-1067.
23. Smith SE, Lekieffre D, Sowinski P, Meldrum BS. Cerebroprotective effect of BW 619C89 after focal or global cerebral ischaemia in the rat. *Neuroreport*. 1993;4:1339-1342.
24. Miller AA, Sawyer DA, Roth B. Lamotrigine. In: Meldrum BS, Porter RP, eds. *New Anticonvulsant Drugs*. London, UK: John Libbey; 1986:165-177.
25. Leach MJ, Baxter MG, Critchley MAE. Neurochemical and behavioral aspects of lamotrigine. *Epilepsia*. 1991;32(suppl 2):S4-S8.
26. Smith SE, Al-Zubaidy ZA, Chapman AG, Meldrum BS. Excitatory amino acid antagonists, lamotrigine and BW 1003C87 as anticonvulsants in the genetically epilepsy-prone rat. *Epilepsy Res*. 1993;15:101-111.
27. Meldrum BS, Leach MJ. Mechanism of action of lamotrigine. *Rev Contemp Pharmacother*. 1994;5:107-114.
28. Leach MJ, Marden CM, Miller AA. Pharmacological studies on lamotrigine, a novel potential antiepileptic drug, II: neurochemical studies on mechanism of action. *Epilepsia*. 1986;27:490-497.
29. Lang DG, Wang CM, Cooper BR. Lamotrigine, phenytoin and carbamazepine interactions on ionic currents on the sodium current

present in N4TG1 mouse neuroblastoma cells. *J Pharmacol Exp Ther*. 1993;266:829-835.
30. Cheung H, Kamp D, Harris E. An in vitro investigation of the action of lamotrigine on neuronal voltage-activated sodium channels. *Epilepsy Res*. 1992;13:107-112.
31. Lees G, Leach MJ. Studies on the mechanism of action of the novel anticonvulsant lamotrigine (Lamictal) using primary neuroglial cultures from rat cortex. *Brain Res*. 1993;612:190-199.
32. Smith SE, Meldrum BS. Cerebroprotection with lamotrigine (3,5-diamino-6-(2,3-dichlorophenyl)-1,2,4-triazine) after focal ischaemia in the rat. *J Cereb Blood Flow Metab*. 1993;13(suppl 1):S698. Abstract.
33. Smith SE, Meldrum BS. Cerebroprotective effect of lamotrigine after focal cerebral ischaemia in the rat. *Br J Pharmacol*. 1994; 111:91P. Abstract.
34. Graham JL, Smith SE, Chapman AG, Meldrum BS. Effect of lamotrigine on microdialysate amino acid concentration in the striatum after focal cerebral ischaemia in the rat. *Br J Pharmacol*. 1994;112:278P. Abstract.
35. Tamura A, Graham DI, McCulloch J, Teasdale GM. Focal cerebral ischaemia in the rat, I: description of technique and early neuropathological consequences following middle cerebral artery occlusion. *J Cereb Blood Flow Metab*. 1981;1:53-60.
36. Shigeno T, Teasdale GM, McCulloch J, Graham DI. Recirculation model following MCA occlusion in rats. *J Neurosurg*. 1985;63: 272-277.
37. Bederson JB, Pitts LH, Tsuji M, Nishimura MC, Davis RL, Bartkowski H. Rat middle cerebral artery occlusion: evaluation of the model and development of a neurologic examination. *Stroke*. 1986;17:472-476.
38. McGeer EG, McGeer PL. Some factors influencing the neurotoxicity of intrastriatal injections of kainic acid. *Neurochem Res*. 1978;3:501-517.
39. McGeer EG, Zhu SG. Lamotrigine protects against kainate but not ibotenate lesions in rat striatum. *Neurosci Lett*. 1990;112:348-351.
40. Hayward NJ, McKnight AT, Woodruff GN. Neuroprotective effect of enadoline in the acute rat model of focal ischaemia. *Br J Pharmacol*. 1993;108:91P. Abstract.
41. Kusumoto K, Mackay KB, McCulloch J. The effect of the kappa-opioid receptor agonist CI-977 in a rat model of focal cerebral ischaemia. *Brain Res*. 1992;576:147-151.
42. Rataud J, Bardot F, Blanchard JC, Laduron PM, Stutzman JM. Riluzole, a voltage sensitive Na^+ channel blocker, is a neuroprotective agent. In: Krieglstein J, Oberpichler-Schwenk H, eds. *Pharmacology of Cerebral Ischaemia*. Proc suppl. 1992;DV397. Abstract.
43. Wahl F, Allix M, Plotkine M, Boulu RG. Riluzole reduces infarct size induced by focal cerebral ischemia. In: Krieglstein J, Oberpichler-Schwenk H, eds. *Pharmacology of Cerebral Ischaemia*. 1992;167-174.
44. Boxer PA, Cordon JJ, Mann ME, Rodolosi LC, Vartanian MG, Rock DM, Taylor CP, Marcoux FW. Comparison of phenytoin with noncompetitive *N*-methyl-D-aspartate antagonists in a model of focal brain ischemia in rats. *Stroke*. 1990:21(suppl III):III-47-III-51. Abstract.
45. Lekieffre D, Meldrum BS. The pyrimidine-derivative, BW 1003C87, potently protects CA_1 neurons following transient severe forebrain ischemia in rats: a microdialysis and histological study. *Neuroscience*. 1993;56:93-99.
46. Hayward NJ, Hitchcott PK, McKnight AT, Woodruff GN. Effect of enadoline on ischemia-induced glutamate release. *Br J Pharmacol*. 1993;110:62P. Abstract.
47. Taylor CP, Geer JJ, Burke SP. Endogenous extracellular glutamate accumulation in rat neocortical cultures by reversal of the transmembrane sodium gradient. *Neurosci Lett*. 1992;145:197-200.
48. Gill R, Andine L, Hillered L, Persson L, Hagberg H. The effect of MK 801 on cortical spreading depression in the penumbral zone following focal ischaemia in the rat. *J Cereb Blood Flow Metab*. 1992;12:371-379.
49. Meldrum BS, Leach MJ, Swan J, Smith SE. Effectiveness of excitatory amino acid antagonists, lamotrigine and BW 619C89 in experimental epilepsy and stroke in rats. In: Program and abstracts of the XVth World Congress of Neurology; September 5-10, 1993; Vancouver, Canada. Abstract.
50. Meldrum BS. The role of glutamate in epilepsy and other CNS disorders. *Neurology*. 1994;44(suppl 8):S14-S23.
51. Pulsinelli WA. Pathophysiology of acute ischaemic stroke. *Lancet*. 1992;339:533-536.

Editorial Comment

There are many potential mechanisms of brain damage in focal cerebral ischemia. The rapid loss of neuronal ATP results in a loss of ionic homeostasis and a drop in membrane potential to the point where voltage-dependent *N*-methyl-D-aspartate and Na^+ channels open, causing an influx of Na^+ to initiate a new round of depolarizing events. Several studies[1,2] have examined the role of tetrodotoxin-sensitive ion channels in animal models of hypoxic-ischemic neuronal damage and concluded that Na^+ influx is an important initiating event leading to anoxic damage. A recent review on noninactivating Na^+ currents suggests that an altered state (perhaps phosphorylation) of relatively few voltage-dependent Na^+ channels could be responsible for sustained (seconds to minutes) Na^+ influx.[3] In the present study, the authors have examined lamotrigine as a potential neuroprotectant and suggest that it may have utility as a Na^+ channel blocker and glutamate release inhibitor. The current study from this laboratory is the most recent in a series of new efforts devoted to exploring modulation of Na^+ channels to prevent glutamate release. The clinical significance of targeting an earlier event in the ischemic cascade (glutamate release) would be to augment or supplement therapies that are specifically directed against glutamate receptors, since there are few existing therapeutics that can embrace both modalities.[1] Additionally, augmented therapies may help to rescue the noncortical areas that are difficult to protect in focal ischemia models.

Most ischemic glutamate release is thought to be nonvesicular in nature, arising from the reversal of the electrogenic, Na^+-dependent, Ca^{2+}-independent glutamate transporter. During ischemia, Na^+ influx and the resulting ionic imbalance will initiate reversal of the glutamate transporter, causing release of cytosolic glutamate. As mentioned previously,[3] sustained Na^+ currents are often seen to contribute to oscillations in membrane potential independent of action potentials and could initiate ischemic damage. By modulating the activity of neuronal Na^+ channels, lamotrigine may prevent excessive depolarizations and serve to limit the excitotoxic glutamate release.

Lamotrigine and the related BW619C89, while having significant therapeutic activity, should be followed by more robust compounds because the effectiveness of lamotrigine's posttreatment paradigms dwindled with elapsed time after infarct. The total lack of a protective effect at the higher dosage of 50 mg/kg could have been due to the noted hypotension or cross-reactivity at Ca^{2+} channels, and motor impairment was reminiscent of the ataxic effects of MK-801.

It will be interesting to see what beneficial effects lamotrigine may have in a multiple, postocclusion dosing regimen.

Paul G. Lysko, PhD
Giora Feuerstein, MD, *Guest Editors*
Department of Cardiovascular Pharmacology
SmithKline Beecham Pharmaceuticals
King of Prussia, Pa

References

1. Lysko PG, Webb CL, Feuerstein G. Neuroprotective effects of carvedilol, a new antihypertensive, as a Na^+ channel modulator and glutamate transport inhibitor. *Neurosci Lett.* 1994;171:77-80.
2. Lysko PG, Webb CL, Yue T-L, Gu J-L, Feuerstein G. Neuroprotective effects of tetrodotoxin as a Na^+ channel modulator and glutamate release inhibitor in cultured rat cerebellar neurons and in gerbil global brain ischemia. *Stroke.* 1994;25:2476-2482.
3. Taylor CP. Na^+ currents that fail to inactivate. *Trends Neurosci.* 1993;11:455-460.

Pergamon

PII: S0306-4522(99)00389-9

Neuroscience Vol. 94, No. 4, pp. 1219–1230, 1999

0306-4522/99 $20.00+0.00

MECHANISMS OF ISCHAEMIC DAMAGE TO CENTRAL WHITE MATTER AXONS: A QUANTITATIVE HISTOLOGICAL ANALYSIS USING RAT OPTIC NERVE

G. GARTHWAITE,*† G. BROWN,‡ A. M. BATCHELOR,* D. A. GOODWIN* and J. GARTHWAITE*

*Wolfson Institute for Biomedical Research, University College London, 1 Wakefield Street, London WC1N 1PJ, U.K.

‡The Medicine Research Centre, Glaxo Wellcome, Gunnels Wood Road, Stevenage, Hertfordshire SG1 2NY, U.K.

Abstract—The mechanism of ischaemic injury to white matter axons was studied by transiently depriving rat optic nerves *in vitro* of oxygen and glucose. Light and electron microscopic analysis showed that increasing periods of oxygen/glucose deprivation (up to 1 h) caused, after a 90-min recovery period, the appearance of increasing numbers of swollen axons whose ultrastructure indicated that they were irreversibly damaged. This conclusion was supported by experiments showing that the damage persisted after a longer recovery period (3 h). To quantify the axonal pathology, an automated morphometric method, based on measurement of the density of swollen axons, was developed. Omission of Ca^{2+} from the incubation solution during 1 h of oxygen/glucose deprivation (and for 15 min either side) completely prevented the axonopathy (assessed following 90 min recovery). Omission of Na^+ was also effective, though less so (70% protection). The classical Na^+ channel blocker, tetrodotoxin (1 μM), provided 92% protection. In view of this evidence implicating Na^+ channels in the pathogenesis of the axonal damage, the effects of three different Na^+ channel inhibitors, with known neuroprotective properties towards gray matter in *in vivo* models of cerebral ischaemia, were tested. The compounds used were lamotrigine and the structurally-related molecules, BW619C89 and BW1003C87. All three compounds protected the axons to varying degrees, the maximal efficacies (observed at 30 to 100 μM) being in the order: BW619C89 (>95% protection) > BW1003C87 (70%) > lamotrigine (50%). At a concentration affording near complete protection (100 μM), BW619C89 had no significant effect on the optic nerve compound action potential. Experiments in which BW619C89 was added at different times indicated that its effects were exerted during two distinct phases, one (accounting for about 50% protection) was during the early stage of oxygen/glucose deprivation itself and the other (also about 50%) during the first 15 min of recovery in normal incubation solution.

The results are consistent with a pathophysiological mechanism in which Na^+ entry through tetrodotoxin-sensitive Na^+ channels contributes to Na^+ loading of the axoplasm which then results in a lethal Ca^{2+} overload through reversed Na^+–Ca^{2+} exchange. The identification of BW619C89 as a compound able to prevent oxygen/glucose deprivation-induced injury to white matter axons without affecting normal nerve function opens the way to testing the importance of this pathway in white matter injury *in vivo*.

Key words: ischaemia, white matter, optic nerve, Na^+ channel, BW619C89, lamotrigine.

In the CNS, ischaemia results in damage to both neuronal cell bodies/dendrites located in the gray matter and myelinated axons in the white matter. The overwhelming majority of studies into the mechanisms of ischaemic damage have so far concentrated on neurons in the gray matter, wherein abundant evidence suggests that excessive stimulation of glutamate receptors plays an important role in the ensuing pathology.[4,31] White matter appears to be comparatively resilient to ischaemia,[29] possibly because axons have a relatively low metabolic rate and do not express glutamate receptors capable of mediating excitotoxic damage.[39] Nevertheless, axons and oligodendroglia in white matter are vulnerable in focal cerebral ischaemia[36] and there are situations where white matter is preferentially affected. One example is in lacunar infarcts,[3,13] which account for about 20% of stroke cases. Here, the degree of cognitive impairment correlates with the extent of white matter atrophy.[72] Pathological alterations in central white matter, which have been attributed to ischaemia, are recognized in the elderly,[35] specially in those exhibiting cognitive impairment.[2] In addition, spinal cord ischaemia, caused by trauma or complications associated with aortic surgery, appears to affect particularly the white matter.[9,14]

Despite the recognized importance of white matter damage occurring as a consequence of ischaemia, little is known of the underlying mechanisms. One reason for this is that the pathophysiology of white matter has been much more difficult to investigate than that of neuronal cell bodies/dendrites, for which *in vitro* tissue culture or brain slice techniques have been available for many years. Most of the relevant information on central axonal pathology has come from electrophysiological studies of the effects of transient anoxia on the subsequent ability of the isolated optic nerve to conduct action potentials, combined with measurements of the associated changes in elemental Na, K and Ca.[51,68] These investigations concluded that anoxia causes axonal depolarization and a loading of the axoplasm with Na^+ due to influx through voltage-dependent Na^+ channels; depolarization plus Na^+ loading causes the Na^+–Ca^{2+} exchanger to operate in reverse, thereby imposing a lethal axoplasmic Ca^{2+} overload.

In present experiments, we sought to determine the mechanisms by which the combined insult of oxygen and glucose deprivation (OGD) affects the viability of white matter axons. Despite probably being more pertinent to ischaemic damage than anoxia alone, this has not been attempted previously. OGD represents a harsher insult than anoxia in that axonal function is irreversibly lost more rapidly.[10] The presence or absence of glucose may also

†To whom correspondence should be addressed. Tel.: +44-171-5044186; fax: +44-171-8371347.

E-mail address: g.garthwaite@ucl.ac.uk (G. Garthwaite)

Abbreviations: ACSF, artificial cerebrospinal fluid; EGTA, ethyleneglycol-bis(aminoethyl ether)tetra-acetate; OGD, oxygen and glucose deprivation; TTX, tetrodotoxin.

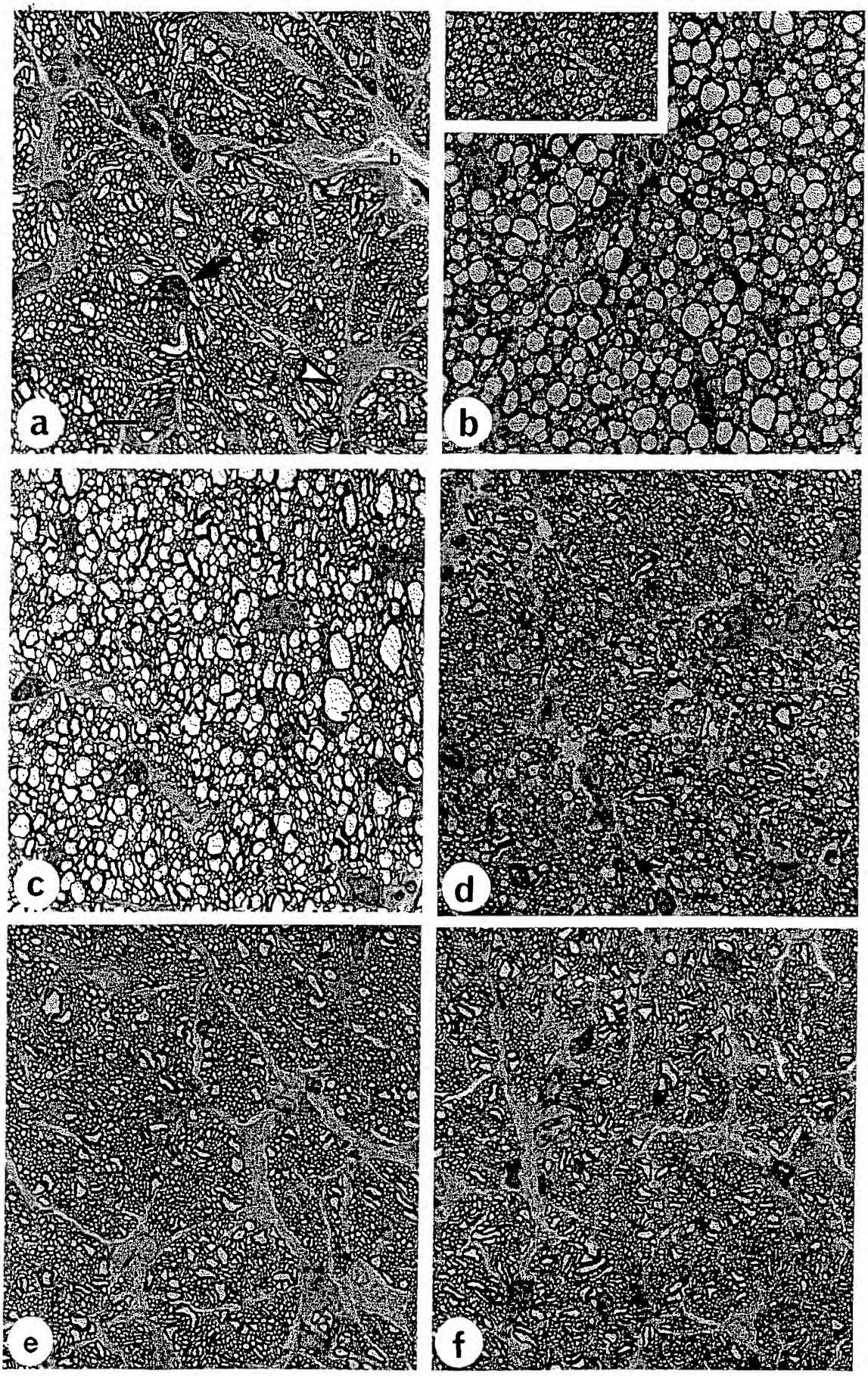

Fig. 1.

influence the pathological pathway because, with glucose present, anaerobic metabolism leads to the accumulation of lactate and, hence, to changes in pH[43] which could affect the functioning of relevant proteins.

To study the mechanism of OGD-induced white matter pathology, we have used the adult rat optic nerve maintained *in vitro*,[51] and have used quantitative morphometric analysis for assessing the integrity of the optic nerve axons, a method that is easier to perform and likely to be of broader utility than the electrophysiological techniques used previously.

EXPERIMENTAL PROCEDURES

Optic nerves

Optic nerves were excised from adult Wistar rats (weighing 240 to 280 g) after decapitation. They comprised lengths of nerve (each about 9 mm long) running from immediately behind the eyeball to just in front of the optic chiasm. The nerves were incubated in Erlenmeyer flasks (50 ml capacity) containing 20 ml of an artificial cerebrospinal fluid (ACSF) solution composed of (mM): NaCl (120) KCl (2.0), $CaCl_2$ (2.0), $NaHCO_3$ (26), KH_2PO_4 (1.18), $MgSO_4$ (1.19) and glucose (11), continuously gassed with 95% O_2/5% CO_2. The flasks were held in a shaking water bath at 37°C. For the Ca^{2+}-free medium, EGTA (1 mM) was substituted for $CaCl_2$ and for the Na^+-free medium, 120 mM choline chloride and 26 mM choline bicarbonate replaced NaCl and $NaHCO_3$, respectively.

After 1 to 2 h preincubation in ACSF, OGD was imposed on test nerves by transferring them for different periods of time into ACSF lacking glucose and gassed with 5% CO_2 in N_2. Afterwards, unless stated otherwise, the nerves were allowed a 90 min recovery period in ACSF. Modified ACSF and the test drugs were normally present from 15 min before until 15 min after OGD, except where stated. In the experiments designed to examine the importance of O_2- and glucose-reintroduction, the test compound (BW619C89) was added 2 min before the end of OGD in order to allow time for diffusion into the tissues before they were re-exposed to normal ACSF. Likewise, in certain experiments where it was desired to remove the compound during the recovery period, the final 2 min of OGD was used for washout.

Histology

Nerves were fixed for 2 h in a mixture of 4% paraformaldehyde and 2.5% glutaraldehyde in 0.1 M phosphate buffer (pH 7.4), and postfixed with 1% osmium tetroxide for 1 h. After dehydration the tissues were embedded in Durcupan resin in such a way that half of each nerve could be sectioned longitudinally and the other half transversely. Semi-thin (1 μm) sections were stained with either Toluidine Blue or Thionine for light microscopy and ultrathin sections were stained with uranyl acetate and lead citrate.

To quantify the extent of axonal pathology under the light microscope, the degree of distension of the axon profiles was measured. Morphometric measurements from cross-sections of nerves were made using the Seescan image analysis system. Glial cell bodies, glial processes and blood vessels were excluded from the analysis. Because the cross-sections of optic nerve axons are not uniformly circular, we measured their Feret diameter, which is the mean of 36 diameters measured in 5° intervals. The diameter of axons from four fields, each field covering an area of 2,500 μm^2, was measured. The fields in all cases were at the periphery of two axes drawn through the centre of the nerve, at right angles to each other; this gives representative results because, in the rat, fibres of various diameters are homogeneously distributed across the nerve.[7] In the case of oval nerves, the short and the long axes were used. In general, a count of the density of axons having an average internal diameter (i.e. myelin excluded) above 2.5 μm was used as the index of damage (see Results). The data are expressed as mean number of axons per 10^4 μm^2 (±S.E.M.) in fields from five to 39 nerves in two to 18 separate experiments. For each test condition in a given experiment, there were two to three nerves, each from a different animal. Statistical evaluation was done using Student's *t*-test; a *P*-value of less than 0.05 was considered significant.

Electrophysiology

The isolated optic nerve was installed in a three-compartment, grease-gap recording bath similar to the one used for monitoring synaptic transmission in brain slices.[17] The main body of the nerve was contained in the central chamber and the two ends passed into the side chambers through greased holes in the partitions. One end was stimulated with rectangular voltage pulses (0.05 Hz, 70 to 110 V amplitude, 50 μs width) using a bipolar twisted-wire electrode. The other end was crushed at the point where it crossed the grease seal to ensure that the action potentials recorded from this chamber (relative to the middle chamber) were monophasic. The central chamber (0.5 ml capacity) was perfused with ACSF at 2–3 ml/min and the whole chamber and the perfusate were kept at a temperature of 37 ± 0.5°C by a heated water jacket. The two side chambers were filled with ACSF but were not perfused. Compound action potentials were recorded differentially using Ag/AgCl electrodes embedded in agar, amplified (Grass P16) and sampled at 200 kHz by a digital storage oscilloscope interfaced with a personal computer. Traces shown are an average of three to five sequential responses. The area under the compound action potential[60] was calculated from just after the stimulus artefact to the end of the oscilloscope sweep. Statistical evaluation was done using Student's *t*-test.

Materials

BW619C89, BW1003C87 and lamotrigine were synthesized by the Wellcome Research Laboratories (Beckenham, U.K.). Osmium tetroxide was from Agar Scientific (Stanstead, U.K.). Tetrodotoxin was from Latoxan Laboratories (Rosans, France). Other chemicals were purchased from either Sigma–Aldrich (Poole, Dorset, U.K.) or BDH/Merck (Poole, Dorset, U.K.).

RESULTS

Light and electron microscopic observations

Rat optic nerves incubated under control conditions *in vitro* for at least 5 h showed very good preservation, in both the light (Fig. 1a) and electron microscopes (Fig. 2a). No major differences were discernible compared with nerves fixed *in situ* (see also Ref. 67).

Nerves were exposed to OGD for different periods of time (30, 45 and 60 min) followed, in each case, by 90 min of recovery in normal ACSF. This resulted in a graded axonopathy with the 60-min exposure causing the most severe effects, as judged by persisting axonal swelling. In the light microscope, axons in the treated nerves (60 min OGD plus 90 min recovery), were swollen and distended, giving a lacy and fenestrated appearance to the nerve (Fig. 1b). Ultrastructurally, most axons showed advanced pathology. In cross-sections they appeared as large holes, containing some follicular debris (Fig. 2b) and swollen degenerating mitochondria, although the myelin sheaths generally kept their periodicity. Some cell death was also observed but, due to the advanced state of this degeneration, the identification of the cells (as astrocytes or oligodendrocytes) was not possible. To further check that the axonal damage was irreversible, some nerves were given a more prolonged (3 h) recovery period and

Fig. 1. Light micrographs of incubated optic nerves. (a) Cross-section of a control nerve incubated for 6 h; arrow indicates oligodendrocyte, arrowhead indicates astrocyte, b indicates blood vessel. (b) Nerve given 1 h of OGD plus 90 min recovery shows numerous swollen axons. The inset shows a nerve which was subjected to 1 h of OGD without recovery. (c) Nerve exposed for 1 h to veratridine (20 μM) showing a pathology similar to that produced by OGD. (d) Nerve subjected to OGD in the presence of TTX (1 μM). (e) Nerve subjected to OGD in Ca^{2+}-free medium. Scale bar = 10 μm. (f) Nerve subjected to OGD in the presence of BW619C89 (30 μM).

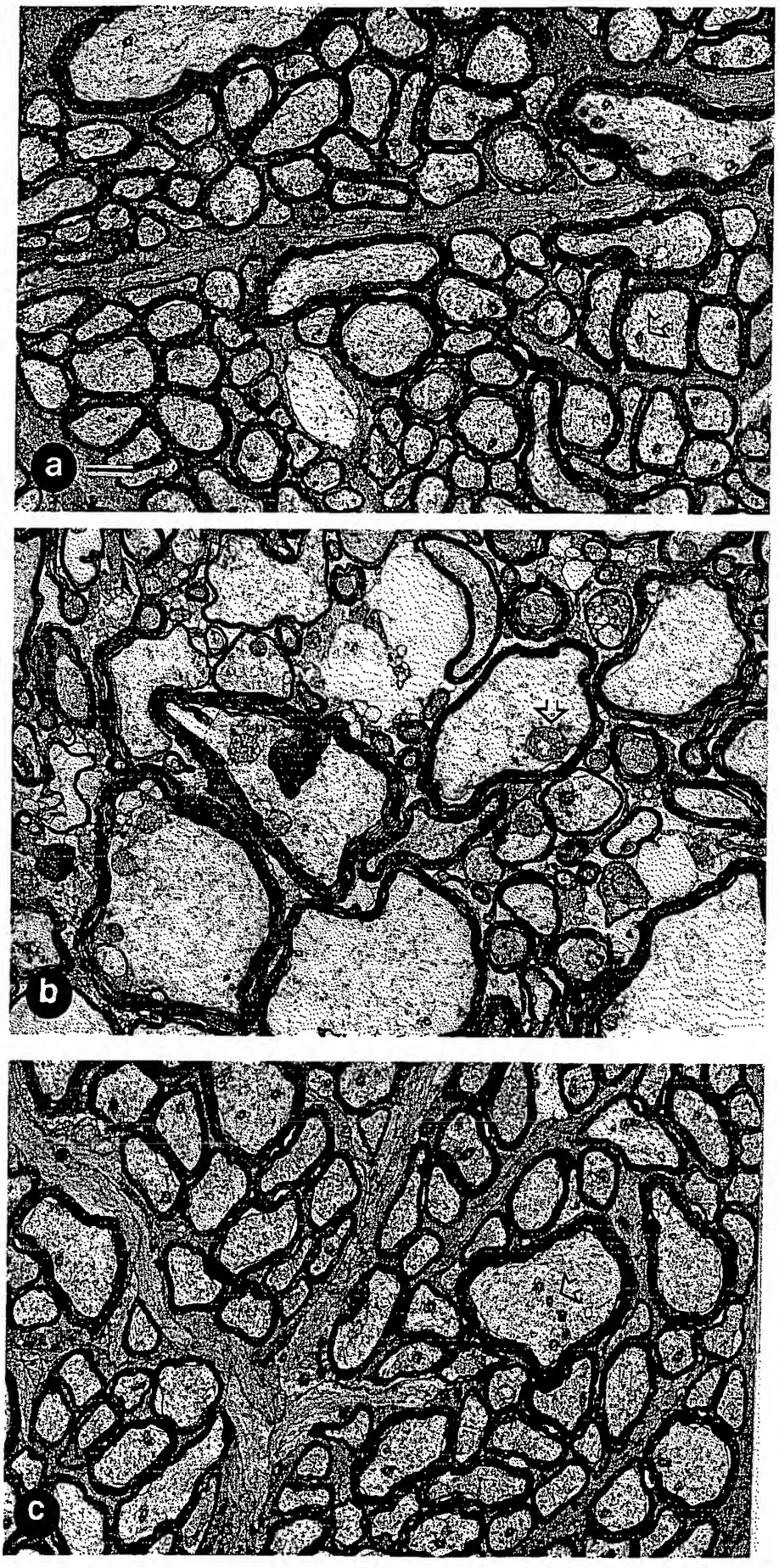
a
b
c

examined under the light microscope. The axonal swelling did not diminish but, instead, was more exaggerated ($n=4$; results not shown).

Morphometry was used to quantify the degree of damage. In control incubated optic nerves, the distribution of axonal Feret diameters (Fig. 3a), using a bin size of 0.2 μm, showed a modal peak at 0.4 to 0.6 μm, a tail towards larger diameters, and almost no fibres larger than 5 μm. In nerves subjected to 60 min OGD (plus recovery), there was a reduction in the frequency of smaller diameter axons (<1 μm) and an increased frequency of larger axons (Fig. 3a). Superficially, the extent of the shift in size did not appear as marked as might have been anticipated from the histological differences observed (Figs 1b, 2b) or from an 80% loss of viable axons incurred following 60 min of OGD.[10] Closer inspection using longitudinal sections of OGD-treated nerves, however, showed that the swelling along the axonal length (where sufficient length was contained in a section) was focal (Fig. 3c); in between the swellings, the axons tended to be dark and shrunk. This "string of pearls" appearance, contrasting with that of axons in control nerves (Fig. 3b), is found in degenerating white matter axons *in vivo*[42] and it provides an explanation for the less-than-expected shift in the distribution curves when cross-sections are studied (Fig. 3a, inset).

Based on the differences in size distributions, measurement of the density of axons having cross-sectional Feret diameter above 2.5 μm provided a simple yardstick of axonal damage. Analysis of nerves subjected to 0, 30, 45 and 60 min of OGD (plus 90 min recovery) in this way gave indices of axonopathy of 22 ± 2, 33 ± 3, 101 ± 9 and $168 \pm 7/10^4$ μm², respectively ($n=6$). Subsequently, 60 min of OGD was used routinely as this produced an advanced state of axonal degeneration and provided a wide window for quantifying protective measures.

Nerves that had been exposed to OGD (60 min) without a subsequent recovery in normal ACSF were also examined. By light microscopy, the axons appeared appreciably less damaged, the major effect being that they became more uniformly circular in shape (Fig. 1b, inset) compared with controls. Morphometry indicated no significant difference from control nerves in the numbers of axons having diameters above 2.5 μm ($26 \pm 3/10^4$ μm² compared with $21 \pm 2/10^4$ μm² in controls, $n=6$ to 7). When the criterion used for measurement was reduced (Feret diameter above 1.5 μm), there was a significant increase ($188 \pm 14/10^4$ μm²) compared with controls ($90 \pm 9/10^4$ μm², $n=7$ to 9, $P<0.001$).

Ionic mechanisms of oxygen and glucose deprivation-induced axonopathy

When nerves were exposed to OGD in the absence of Ca^{2+} in the bathing medium, the axonopathy was eliminated (Figs 1e, 4). Inclusion of nifedipine (5, 10 or 20 μM), an organic blocker of L-type Ca^{2+} channels had no effect ($n=4$ for each concentration, results not shown).

Total replacement of Na^+ with choline during OGD reduced the pathology by 73% (Fig. 4) whereas tetrodotoxin (TTX, 1 μM) was significantly more effective in that over 90% of the axonal swelling was eliminated (Figs 1d, 4). In view of these findings implicating Na^+ influx and Na^+ channels, we tested if veratridine (20 μM), an alkaloid which keeps Na^+ channels in open state, was able to induce axonopathy in the absence of OGD. The results showed that OGD-type pathology could be partially replicated (Figs 1c, 4) by incubating the nerves for 1 h in normal ACSF containing veratridine.

Two conditions that result in non-specific optic nerve depolarization and loss of the conducted action potential[26,59] were also tested. Exposure of the nerves to ouabain (1 mM), an inhibitor of the Na^+–K^+–ATPase, for 1 h (followed by 90 min recovery) had no detectable effect on the axons, as judged by light microscopy, although glial cells appeared dark and shrunken ($n=4$, results not shown). Nerves incubated with 30 or 50 mM K^+ (1 h plus 90 min recovery) appeared normal; when examined without recovery, however, intense glial swelling was observed ($n=4$, results not shown).

Effect of neuroprotective Na^+ channel inhibitors

An important objective is to identify targets for protecting white matter *in vivo* from ischaemic damage, without interfering adversely with normal function. Various drug classes (local anaesthetics, anticonvulsants, antiarrythmics, Na^+–Ca^{2+} exchange inhibitors) have previously been examined for their protective effects against anoxia-induced optic nerve malfunction.[51,68] Given evidence for the involvement of voltage-dependent Na^+ channels in OGD-induced axonopathy (above) we have tested for protective actions of three Na^+ channel inhibitors shown previously to be effective in protecting cerebral gray matter from ischaemic damage, namely the compounds BW619C89, BW1003C87 and lamotrigine.[62,65]

Inclusion of BW619C89 (100 μM) during OGD (and for 15 min either side) led to a complete protection of the axons as judged by light and electron microscopy (Figs 1f, 2c). Morphometric measurement (Fig. 5) showed that the protection was concentration-dependent, with half-maximal effects occurring at 3 μM and complete protection at 100 μM. The compound BW1003C87 also protected the axons but its efficacy was less than that of BW619C89 in that the maximum protection achieved (at 30 μM) amounted to about 65%. Lamotrigine produced significant protection but was the least efficacious since maximal protection (at 100 to 300 μM) was only 40 to 50% (Fig. 5).

To test the ability of these agents to interfere with normal nerve function, compound action potentials were recorded from the isolated optic nerves using a grease-gap recording technique. As in previous studies,[60] the response comprised three main components appearing at different latencies after the stimulus (Fig. 6). Responses were stable for at least 1–3 h after an initial settling-down period (20–30 min) and so with this method it was unnecessary to correct for changes in the extracellular resistance (cf. Ref. 56). Compounds were applied until a stable effect was achieved or for at least 20 min if no change in the compound action potential was observed. The compound BW619C89 caused a small reduction of the peak amplitude in some nerves at the highest concentration used (100 μM; Fig. 6a) although there was no significant decrease in the total area under the compound action potential (Fig. 6d). Lamotrigine had no significant

Fig. 2. Electron micrographs of adult rat optic nerves maintained *in vitro*. (a) Cross-section of nerve maintained in control conditions. (b) Nerve given 1 h of OGD followed by 90 min of recovery. (c) Nerve given OGD in the presence of BW619C89 (30 μM). Arrows indicate mitochondria. Scale bar = 1 μm.

(a)

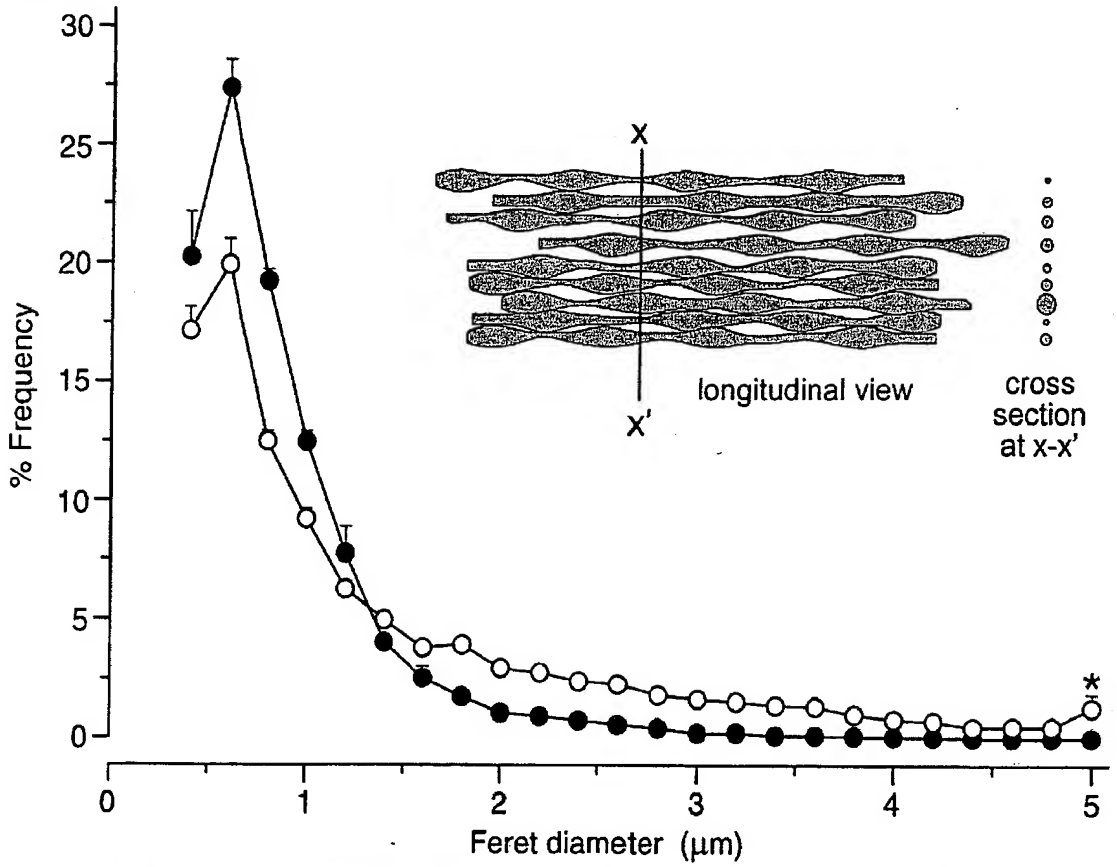
30
25
20
15
10
5
0
% Frequency
0
1
2
3
4
5
Feret diameter (μm)
*
X
X'
longitudinal view
cross
section
at x-x'

(b)

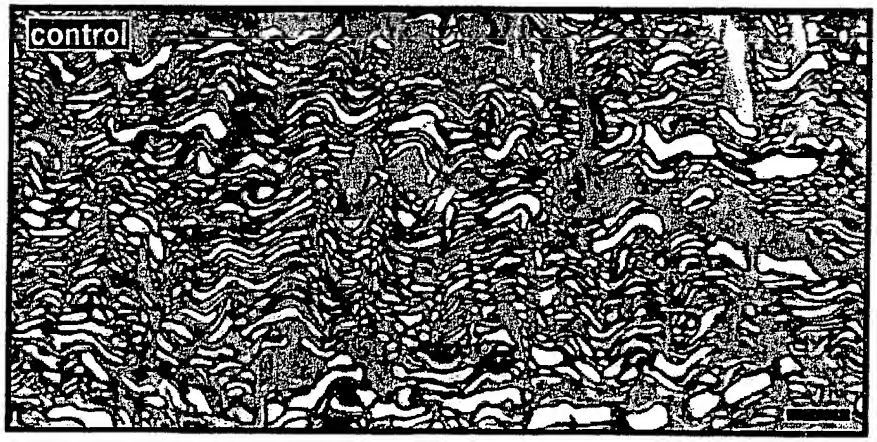
control

(c)

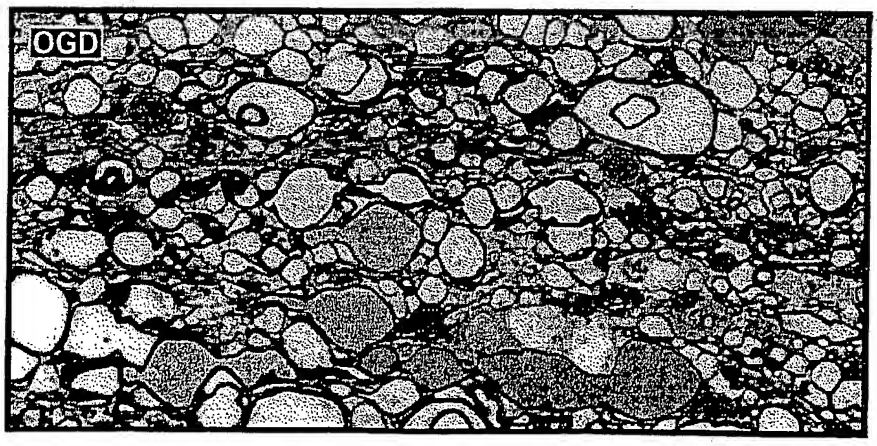
OGD

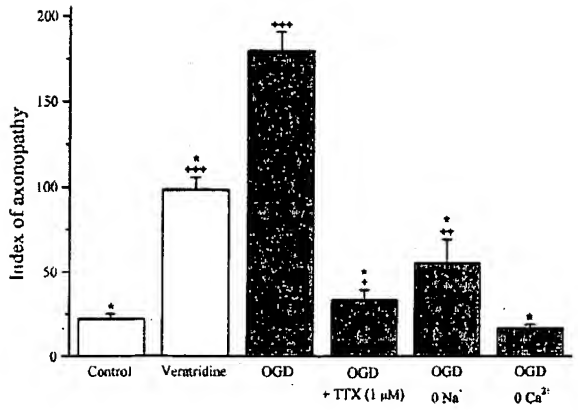

Fig. 4. Ionic mechanism of OGD-mediated axonopathy. The index of axonopathy represents the number of axons with Feret diameter above 2.5 μm/10^4 μm^2. Values are means ± S.E.M. ($n = 6$–12). *$P < 0.0001$ vs OGD; $^+P < 0.04$, $^{++}P < 0.001$, $^{+++}P < 0.0001$ vs control nerves.

effect over the concentration range tested (Fig. 6b, e). In contrast, BW1003C87 had significant inhibitory effects on the area under the compound action potential at 100 μM, but not at 30 μM, despite a reduction in the peak amplitude (Fig. 6c, f). The compound action potentials were completely abolished by 1 μM TTX.

Experiments were then conducted to identify the period during which this type of agent needs to be present in order to achieve protection. These tests used BW619C89 since it proved to be a highly efficacious compound whose effects (unlike those of TTX) are readily reversible.[71] As before, the presence of BW619C89 during OGD and for 15 min either side achieved complete protection (Fig. 7a, b; column/row B). Omission of the 15-min preincubation period with the compound did not diminish its protective effect (column/row C). About 70% of the pathology could still be prevented if BW619C89 was introduced 20 min after the induction of OGD (column/row D). Addition of BW619C89 after 30 min OGD resulted in about 50% protection (column/row E), a result that was also obtained with addition of the compound after 40 min (column/row F) or 50 min (column/row G). Interestingly, a similar level of protection (58%) was also afforded if BW619C89 was present only during the first 15 min of the recovery period (column/row H). This relatively short part of the recovery period appeared critical because if the compound was present throughout the 90 min recovery, there was no further protective effect (51 ± 7%; $n = 10$). If BW619C89 was included only during OGD, the degree of protection achieved was 62% (column/row I).

DISCUSSION

Methodological considerations

The primary method used to assess the integrity of optic nerve axons was histology combined with a quantitative morphometric analysis of the dimensions of axonal cross-sectional profiles. This is logical in view of abundant previous evidence that axonal swelling characterizes irreversible axonal pathology following metabolic inhibition.[67] That the damage was irreversible in our experiments is indicated both by the severe disruption of the axonal cytoskeleton and mitochondria and by the finding that the swelling did not subside if the nerves were given extended recovery periods. In agreement, similar periods of OGD have been shown in other studies to give irreversible loss of optic nerve axon function.[10] Morphometry proved to be a convenient and rapid method for quantifying the extent of damage. When applied to control nerves, the skewed distribution of axon diameters (Fig. 3) resembled closely that found previously by light and electron microscopy of rat optic nerves fixed *in situ*.[6,7,15,40] These previous studies reported a peak modal diameter of 0.6 to 0.7 μm (excluding myelin) based on measurement of the mean of the maximum and minimum diameters. The slightly smaller value found in our studies (about 0.5 μm) is likely to be the consequence of measuring the Feret diameter (the mean of 36 diameters): in oblong structures (like many normal optic nerve axons) this measure will inevitably be weighted towards the smaller diameters. For nerves subjected to OGD, the chosen parameter for assessing damage was a mean Feret diameter of 2.5 μm or above. This only accommodates a minority of the axon profiles in a given cross-section (14% compared with 1.6% of axons in control nerves; Fig. 3a). As discussed above (see Results), however, the proportion of axons that are damaged will be greatly underestimated using this criterion because their swelling was focal. The method would also exclude damaged axons whose Feret diameter falls below 2.5 μm but as these were not detected by direct visual inspection of the same sections (cf. nerves subjected to OGD without recovery; Fig. 1b, inset), this is not considered likely to distort the results. Hence, we conclude that the method is a reliable one for quantifying axonal injury. In support of this, we have recently developed an alternative assay based on axonal function and find essentially identical results to those reported here.[16]

Ionic requirements for oxygen and glucose deprivation-induced axonopathy and the role of Na^+ channels

Ionic substitution experiments showed that OGD-induced axonal damage could be completely prevented if the insult was imposed in the absence of extracellular Ca^{2+} and that removal of Na^+ was partially (70%) effective. A dependence on extracellular Ca^{2+} agrees with what has been found previously for injury to optic nerve axons caused just by oxygen deprivation[58] and implies (cf. Ref. 54) that irreversible axonal damage results from a Ca^{2+} overload in the axoplasm. With the anoxic optic nerve, Na^+ removal was relatively more efficacious than in our experiments with OGD, since this manoeuvre allowed 90% or more recovery of the compound action potential.[60] The less than maximal

Fig. 3. Morphometric analysis of optic nerve axonopathy. (a) The % frequency distribution of axons of different Feret diameter in control nerves (filled circles) and nerves subjected to 1 h of OGD plus 90 min recovery (open circles). The bin widths were set at 0.2 μm. Diameters less than 0.2 μm were below the resolution of the imaging apparatus and are omitted; the first data points thus correspond to diameters falling in the range of 0.2–0.4 μm. Data are the means ± S.E.M. (four nerves); the measurements were made in four fields containing a total of about 4000 axons in control nerves and roughly half that number in OGD-treated nerves. *Sum of profiles of Feret diameter ≥ 5 μm. The inset depicts how focal swellings along the length of the axons (see c) would appear in cross-section. (b) Longitudinal section from a control nerve showing axons with relatively uniform diameter. (c) Longitudinal section from a nerve subjected to 1 h of OGD and 90 min recovery. Some of the axon profiles are coloured to show the focal nature of the swellings. Scale bar (b, c) = 10 μm.

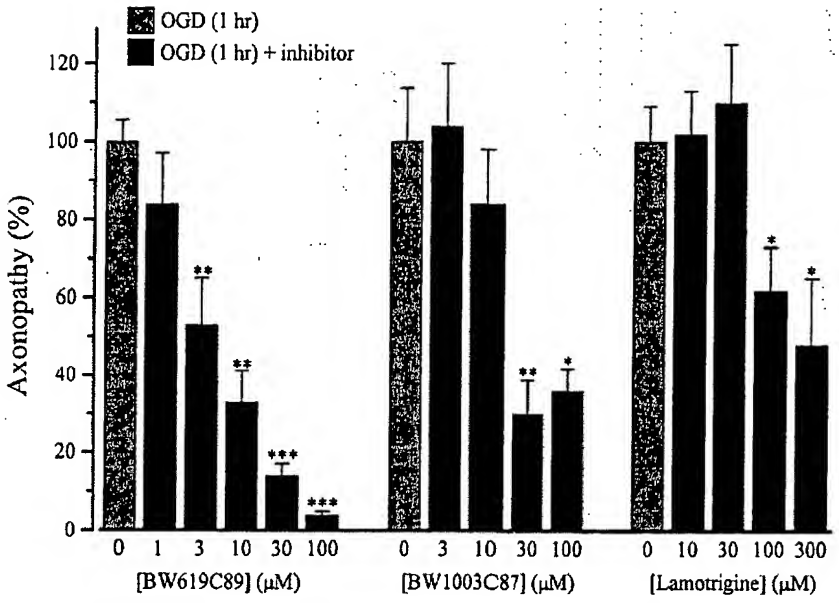

Fig. 5. Axonoprotective effects of different concentrations of Na^+ channel inhibiting compounds against OGD. Data are means ± S.E.M. of the index of axonopathy expressed relative to nerves exposed to OGD alone ($n = 3$–39). $^*P < 0.01$, $^{**}P < 0.001$, $^{***}P < 0.0001$ vs OGD.

effect seen in our experiments may be explained if incubation of the nerves in Na^+-free ACSF leads to temporary rise of the intracellular Ca^{2+} concentration, due to reversed Na^+–Ca^{2+} exchange,[41] the residue of which sums with the intracellular Ca^{2+} increase occurring through Na^+-independent pathways during OGD, to an extent sufficient to produce limited damage. The existence of a Na^+-independent Ca^{2+} influx pathway is suggested from experiments on the anoxic optic nerve[54] and it may be more significant when glucose is additionally absent (as in our experiments), since energy-dependent Ca^{2+} efflux pathways would not be operational. Hence, our findings are consistent with the mechanism of OGD-induced axonopathy being the same as that caused by anoxia,[51,68] namely that influx of Na^+ causes secondary loading of the axoplasm by Ca^{2+} through reversed operation of the Na^+–Ca^{2+} exchanger, which appears to be expressed in high density in optic nerve axons.[49] Interestingly, compression-induced injury to spinal cord axons is also Na^+-dependent but, in this case, the Na^+–H^+ exchanger appears to be more pathologically relevant than the Na^+–Ca^{2+} exchanger.[1] This

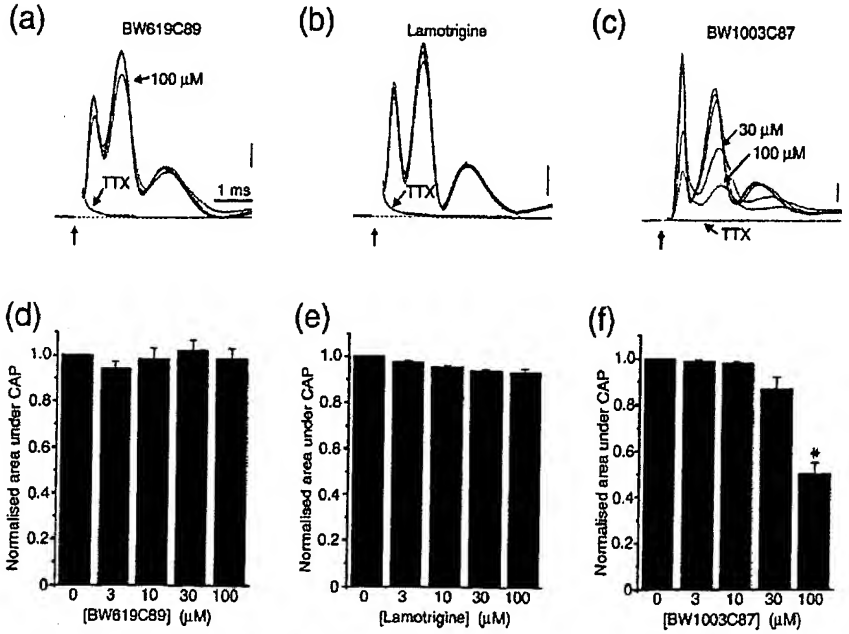

Fig. 6. Effect of Na^+ channel inhibitors on the optic nerve compound action potential. (a–c) Representative traces evoked by electrical stimulation of the nerve at the time indicated by the vertical arrow. The stimulation artifact (partially blanked for clarity) is followed by a typical three-component potential. In each set of traces are superimposed the control waveform, the waveforms in the presence of different concentrations of drug, and the waveform after perfusion of TTX (1 μM). Voltage scale bar = 1 mV; time-scale bar (a) also applies to (b) and (c). (d–f) Data (means ± S.E.M; $n = 4$) were quantified by measuring the area under the compound action potential (CAP) and expressed relative to the control area. $^*P < 0.01$.

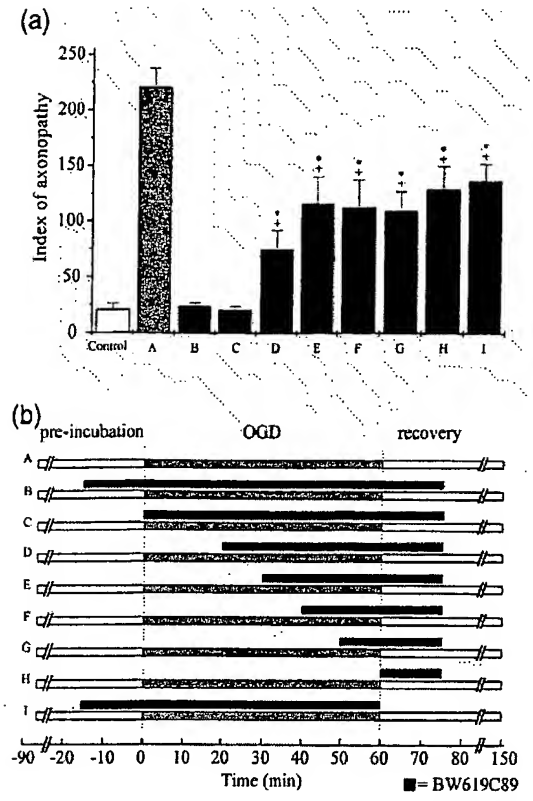

Fig. 7. Intervals during which BW619C89 confers protection to optic nerve axons subjected to OGD. The experimental conditions for each lettered data column (a) are indicated in protocol underneath (b). The values are the mean index of axonopathy ±S.E.M. (eight to 12 nerves). $^{*}P < 0.001$–0.0001 vs control; $^{+}P < 0.001$–0.0001 vs OGD.

indicates that interfering with the routes of Na^+ entry during trauma or ischaemia may provide a more generally applicable strategy for protecting white matter than targeting specific ion-transporting proteins.

In this regard, the substantial (>90%) inhibition of OGD-induced axonal damage by TTX, coupled with the partial replication of the damage (in normal ACSF) by veratridine suggests that voltage-dependent Na^+ channels are the principal conduits for pathological Na^+ entry. Likewise, TTX has been shown to confer protection to anoxic optic nerve axons[60] and to traumatized spinal cord axons *in vitro*.[1] Classical Na^+ channels become mostly inactivated during sustained depolarization, as occurs following metabolic inhibition in the optic nerve.[27] Optic nerve axons, however, express non-inactivating TTX-sensitive Na^+ channels[59] and it is these that appear to be responsible for much of the Na^+ influx (and associated Ca^{2+} influx) during anoxia.[54] It is reasonable to suppose that this population of Na^+ channels are also the operative ones during OGD. As the axons survived depolarization due to treatment with the Na^+–K^+–ATPase inhibitor, ouabain,[26] or elevated extracellular K^+,[59] indicates that energy deprivation is likely to be a necessary condition for this mechanism to translate into axonal damage.

Pharmacological intervention in oxygen and glucose deprivation-induced axonopathy

A variety of pharmacological agents have been tested for their ability to reduce axonal injury brought about by anoxia. In one study, blockers of L- and N-type voltage-gated Ca^{2+} channels were shown to offer limited protection[12] (but see Ref. 55). In the present investigation, the L-type channel blocker, nifedipine (5 to 20 μM) was unable to protect against OGD and previously neither nifedipine (5 μM) nor the related agent, nomodipine, was found to reduce anoxia-induced changes in elemental Na, K or Ca in the axoplasm.[54]

Other types of intervention tested earlier on optic nerve include local anaesthetics,[57] classical anticonvulsants (phenytoin, carbamazepine and diazepam[11]) and antiarrhythmics.[50] These different agents, which have in common the ability to block voltage-dependent Na^+ channels, were found to protect optic nerve from the effects of anoxia to differing extents. While lending support to the possibility of pharmacological intervention through Na^+ channel blockade, only one compound, at one concentration, was found to be completely efficacious without having the unwanted effect of depressing normal axonal conduction. This was the quaternary local anaesthetic, QX-314 (0.3 mM[57]). QX-314 has the important disadvantage of poor membrane permeability, which impedes its access to the intracellular compartment needed for Na^+ channel blockade.[37]

We chose to examine compounds that are lipophilic and so traverse membranes easily. These were the novel antiepileptic drug, lamotrigine, and two structurally-related molecules, BW619C89 and BW1003C87. Lamotrigine itself has previously been reported to be neuroprotective towards gray matter in animal models of focal and global ischaemia.[5,47,69] Towards OGD-induced axonopathy in optic nerve, lamotrigine was only partially effective, reducing the damage by, at most, 50%. This is similar to the degree of protection against anoxia in the optic nerve afforded by phenytoin and carbamazepine[11] but, in contrast to these drugs, lamotrigine did not affect normal axonal conduction, even at high concentrations, which is consistent with the lack of side-effects of lamotrigine in humans.[38] It should be noted, however, that the lowest concentration of lamotrigine giving significant neuroprotection in our experiments (100 μM) is appreciably higher than the cerebrospinal fluid concentration in epileptic patients (about 4 μM[8]). Neuroprotective doses of lamotrigine in animal models of global cerebral ischaemia, likewise, have usually been five- to 10-fold higher than those required for anticonvulsant effects[65] suggesting that the concentrations needed to protect white matter and gray matter are similar.

The compound BW1003C87 also has potent lamotrigine-like anticonvulsant activity in animal models[33,44] but it is relatively more effective than lamotrigine as a neuroprotectant in models of focal cerebral ischaemia, providing 50 to 60% reduction in total infarct volume[20,32] as against a maximum of 31% for lamotrigine.[47] It is also effective in models of transient global ischaemia.[18,32] Against OGD-induced optic nerve axonopathy, BW1003C87 was able to protect maximally by 70%. Unlike lamotrigine, however, BW1003C87 did affect normal axonal conduction at higher concentrations but, this was slight at the lowest concentration giving the maximal protection achievable with this compound (30 μM).

The most interesting compound to emerge from the present investigation was BW619C87. This molecule is not known to have anticonvulsant properties but it has proved effective in several laboratories in models of focal and global ischaemia, as well as of traumatic brain injury.[19,24,25,45,46,61,64] BW619C89 has also undergone early clinical trials in human stroke

patients.[34] In the optic nerve, BW619C89 was able to give complete protection against OGD without significantly affecting axonal conduction. Moreover, the experiments with BW619C89 indicated that there are two phases of the pathological process during which the compound exerts beneficial effects (Fig. 7). One is during OGD itself, specifically during the first 20 min, because addition of BW619C89 after this time gave a similar degree of protection (about 50%) to that observed when introduction of BW619C89 was delayed until the end of OGD. In other words, the protection seen when BW619C98 was added 30 min or more into OGD could be explained by its effects during a second phase occurring during the first 15 min after reinstatement of ACSF. About 50% of the protection given by BW619C89 could be accounted for by its effects during this early part of the recovery period. Other evidence pointing to the importance of mechanisms occurring post-OGD to the final pathological outcome comes from the histological finding that the axonal swelling was greatly enhanced following the recovery period compared with just after OGD (Fig. 1b). Likewise, measurements of the elemental composition of optic nerve axons subjected to anoxia indicated that severe ionic deregulation (particularly of Ca^{2+}) takes place during reoxygenation.[53] The presence of BW619C89 throughout OGD (with removal of the compound at the end of OGD) did not appear to prevent the vulnerability of the axons to "reperfusion" with oxygen- and glucose-containing ACSF, as the protection under these circumstances was only about 60%. Hence, potentially damaging processes are set in motion during OGD, despite the presence of BW619C89. Persisting ionic derangements are likely to be involved since previous work has shown that, during 60 min of anoxia, marked alterations in the contents of Na, K and Cl in axonal cytoplasm and mitochondria developed, despite the presence of TTX.[54] These would be expected to be more intense when glucose is also absent, as in our experiments. "Reperfusion" may then provide the conditions for the translation of the persisting ionic derangements into irreversible damage through, for example, mitochondrial dysfunction and free radical generation (see Ref. 53). The capacity of BW619C89 to protect the axons from this "reperfusion" damage is interesting as it implies (see below) an involvement of ion channels in this aspect of the pathological mechanism.

Mechanisms underlying pharmacological protection

In view of the protection against OGD-induced damage provided by lamotrigine, BW1003C87 and, especially, BW619C89, it is important to understand their relevant mechanism of action. The compounds were originally described as "glutamate release inhibitors" but their ability to inhibit glutamate release provoked by the Na^+ channel opener, veratrine, but not that by elevated K^+, pointed to an action on Na^+ channels, a hypothesis that was supported by early electrophysiological and binding studies (see Ref. 65). Detailed investigation of two of the compounds, lamotrigine and BW619C89, showed them to be use- and voltage-dependent inhibitors of native neuronal Na^+ channels in hippocampal neurons and of type IIA Na^+ channels (a channel subunit found abundantly in the CNS) expressed in a cell line.[70,71] The conclusion was that the drugs acted by stabilizing the inactivated state(s) of the Na^+ channel with estimated affinities of 12 μM for lamotrigine and 3 μM for BW619C89. In view of the evidence that Na^+ channels are required for anoxia- and OGD-induced axonopathy in optic nerve, it is reasonable to suppose that the protective action of the drugs is a consequence of a Na^+ channel inhibiting effect.

The question then arises as to why compounds having this action in common, exhibit markedly differing axonoprotective efficacies. One factor to be considered is the identity of the relevant Na^+ channel. As mentioned above, for anoxia-induced optic nerve damage, a non-inactivating TTX-sensitive Na^+ channel appears to be of particular importance.[59] It is not clear if this represents a distinct channel type or the functional state of a proportion of a homogenous population of channels. With respect to the latter possibility, Na^+ currents (through type IIA channels) that normally inactivate almost completely, can become persistent as a result of interactions with G-proteins[28] and hypoxia has been shown to increase persistent Na^+ currents in cardiac myocytes[23] and hippocampal neurons.[22] Regardless of its origin, the pharmacological properties of the persistent current have not been investigated and so it is possible that the differential protective efficacy of the Na^+ channel inhibitors tested may reflect differential block of the persistent Na^+ current.

The other consideration is whether activities at other channels could contribute or not. Neither lamotrigine nor BW619C89 act specifically on Na^+ channels (no relevant information on BW1003C87 is available). Inhibitory activity of both drugs, in the concentration range 10–100 μM, on N- and/or P-type Ca^{2+} channels have been reported.[30,48,66] One study has suggested that Ca^{2+} channels (of the L- and N-type) are involved in anoxic injury to optic nerve axons,[12] in contrast with a previous conclusion.[55] Hence, it cannot be discounted that Ca^{2+} channel blockade by lamotrigine and BW619C89 contributes to their axonoprotective effects in OGD, although no such actions of BW619C89 at concentrations less than 10 μM, which give more than 50% protection to axons in our experiments, have been reported. In addition, lamotrigine (100 μM) has been reported to increase a transient outward K^+ current in the hippocampus,[21] whereas BW619C89 inhibits outward K^+ currents to some extent (30% with 10 μM BW619C89 at −60 mV membrane potential[71]). Anoxia-induced loss of optic nerve axon function appears unaffected by several K^+ channel blockers, but significant restoration was recently obtained using caesium ions (5 mM), an effect that was interpreted to indicate that blockade of inward rectifier channels is axonoprotective.[52] The possibility that a component of the protection by BW619C89 against OGD could be ascribed to K^+ current inhibition will, therefore, need to be examined.

While a contribution of other possible actions of the drugs cannot be discounted, the fact that BW619C89 gives protection in concentrations known to inhibit Na^+ channel function, and does so to an extent comparable with that attained using TTX, indicates that Na^+ channel inhibition is likely to be the principal mechanism of relevance.

CONCLUSIONS

In the present study, OGD-induced axonopathy in isolated optic nerve was dependent on extracellular Ca^{2+} and Na^+, and could be inhibited most effectively by TTX and BW619C89, and to a lesser degree, by lamotrigine and BW1003C87. The findings are consistent with a mechanism in which metabolic compromise results in a loading of the

axoplasm with Na^+ through non-inactivating, voltage-dependent Na^+ channels and, subsequently, to reversed operation of the Na^+–Ca^{2+} exchanger. Moreover, it is shown through the use of the compound BW619C98 that it is possible to prevent completely OGD-induced axonal damage without compromising the ability of the axons to conduct action potentials normally. This result indicates that it should be feasible to protect white matter axons from the effects of ischaemia, without imposing serious side effects. The protective effects of Na^+ channel inhibitors *in vivo* against gray matter ischaemia has been well documented.[62,65] Much less has been done *in vivo* to explore the possible benefits of this approach for protecting white matter. Indications that the *in vitro* findings are likely to be pertinent, however, stem from experiments showing that in an *in vivo* model of spinal cord injury, local application of TTX resulted in a sparing of white matter and a reduction in associated functional deficits.[63] Since BW619C89, unlike TTX, can be safely delivered systemically and has good bioavailability, it is likely to be an important tool for testing the relevance of the present findings to white matter damage *in vivo*.

Acknowledgement—This research was supported by The Wellcome Trust.

REFERENCES

1. Agrawal S. K. and Fehlings M. G. (1996) Mechanisms of secondary injury to spinal cord axons *in vitro*: role of Na^+, Na^+–K^+–ATPase, the Na^+–H^+ exchanger, and the Na^+–Ca^{2+} exchanger. *J. Neurosci.* **16,** 545–552.
2. Almkvist O., Wahlund L. O., Andersson Lundman G., Basun H. and Backman L. (1992) White-matter hyperintensity and neuropsychological functions in dementia and healthy aging. *Archs Neurol.* **49,** 626–632.
3. Boiten J. and Lodder J. (1991) Lacunar infarcts. Pathogenesis and validity of the clinical syndromes. *Stroke* **22,** 1374–1378.
4. Choi D. W. and Rothman S. M. (1990) The role of glutamate neurotoxicity in hypoxic-ischemic neuronal death. *A. Rev. Neurosci.* **13,** 171–182.
5. Crumrine R. C., Bergstrand K., Cooper A. T., Faison W. L. and Cooper B. R. (1997) Lamotrigine protects hippocampal CA1 neurons from ischemic damage after cardiac arrest. *Stroke* **28,** 2230–2236.
6. De Juan J., Cuenca N., Iniguez C. and Fernandez E. (1992) Axon types classified by morphometric and multivariate analysis in the rat optic nerve. *Brain Res.* **585,** 431–434.
7. De Juan J., Iniguez C. and Carreres J. (1978) Number, diameter and distribution of the rat optic nerve fibers. *Acta anat. basel* **102,** 294–299.
8. Eriksson A. S., Hoppu K., Nergardh A. and Boreus L. (1996) Pharmacokinetic interactions between lamotrigine and other antiepileptic drugs in children with intractable epilepsy. *Epilepsia* **37,** 769–773.
9. Fehlings M. G., Tator C. H. and Linden R. D. (1989) The relationships among the severity of spinal cord injury, motor and somatosensory evoked potentials and spinal cord blood flow. *Electroenceph. clin. Neurophysiol.* **74,** 241–259.
10. Fern R., Davis P., Waxman S. G. and Ransom B. R. (1998) Axon conduction and survival in CNS white matter during energy deprivation: a developmental study. *J. Neurophysiol.* **79,** 95–105.
11. Fern R., Ransom B. R., Stys P. K. and Waxman S. G. (1993) Pharmacological protection of CNS white matter during anoxia: actions of phenytoin, carbamazepine and diazepam. *J. Pharmac. exp. Ther.* **266,** 1549–1555.
12. Fern R., Ransom B. R. and Waxman S. G. (1995) Voltage-gated calcium channels in CNS white matter: role in anoxic injury. *J. Neurophysiol.* **74,** 369–377.
13. Fisher C. M. (1982) Lacunar strokes and infarcts: a review. *Neurology* **32,** 871–876.
14. Follis F., Scremin O. U., Blisard K. S., Scremin A. M., Pett S. B., Scott W. J., Kessler R. M. and Wernly J. A. (1993) Selective vulnerability of white matter during spinal cord ischemia. *J. cerebr. Blood Flow Metab.* **13,** 170–178.
15. Forrester J. and Peters A. (1967) Nerve fibres in optic nerve of rat. *Nature* **214,** 245–247.
16. Garthwaite G., Goodwin D. A. and Garthwaite J. (1999) Nitric oxide stimulates cGMP formation in rat optic nerve axons, providing a specific marker of axon viability. *Eur. J. Neurosci.* (in press).
17. Garthwaite J. and Batchelor A. M. (1996) A biplanar slice preparation for studying cerebellar synaptic transmission. *J. Neurosci. Meth.* **64,** 189–197.
18. Gaspary H. L., Simon R. P. and Graham S. H. (1994) BW1003C87 and NBQX but not CGS19755 reduce glutamate release and cerebral ischemic necrosis. *Eur. J. Pharmac.* **262,** 197–203.
19. Graham S. H., Chen J., Lan J., Leach M. J. and Simon R. P. (1994) Neuroprotective effects of a use-dependent blocker of voltage-dependent sodium channels, BW619C89, in rat middle cerebral artery occlusion. *J. Pharmac. exp. Ther.* **269,** 854–859.
20. Graham S. H., Chen J., Sharp F. R. and Simon R. P. (1993) Limiting ischemic injury by inhibition of excitatory amino acid release. *J. cerebr. Blood Flow Metab.* **13,** 88–97.
21. Grunze H., Greene R. W., Moller H. J., Meyer T. and Walden J. (1998) Lamotrigine may limit pathological excitation in the hippocampus by modulating a transient potassium outward current. *Brain Res.* **791,** 330–334.
22. Hammarström A. K. M. and Gage P. W. (1998) Inhibition of oxidative metabolism increases persistent sodium current in rat CA1 hippocampal neurons. *J. Physiol., Lond.* **510.3,** 735–741.
23. Ju Y. K., Saint D. A. and Gage P. W. (1996) Hypoxia increases persistent sodium current in rat ventricular myocytes. *J. Physiol., Lond.* **497,** 337–347.
24. Kawaguchi K. and Graham S. H. (1997) Neuroprotective effects of the glutamate release inhibitor 619C89 in temporary middle cerebral artery occlusion. *Brain Res.* **749,** 131–134.
25. Leach M. J., Swan J. H., Eisenthal D., Dopson M. and Nobbs M. (1993) BW619C89, a glutamate release inhibitor, protects against focal cerebral ischemic damage. *Stroke* **24,** 1063–1067.
26. Leppanen L. and Stys P. K. (1997) Ion transport and membrane potential in CNS myelinated axons. I. Normoxic conditions. *J. Neurophysiol.* **78,** 2086–2094.
27. Leppanen L. and Stys P. K. (1997) Ion transport and membrane potential in CNS myelinated axons. II. Effects of metabolic inhibition. *J. Neurophysiol.* **78,** 2095–2107.
28. Ma J. Y., Catterall W. A. and Scheuer T. (1997) Persistent sodium currents through brain sodium channels induced by G protein βγ subunits. *Neuron* **19,** 443–452.
29. Marcoux F. W., Morawetz R. B., Crowell R. M., DeGirolami U. and Halsey J. H. Jr (1982) Differential regional vulnerability in transient focal cerebral ischemia. *Stroke* **13,** 339–346.
30. McNaughton N. C., Leach M. J., Hainsworth A. H. and Randall A. D. (1997) Inhibition of human N-type voltage-gated Ca^{2+} channels by the neuroprotective agent BW619C89. *Neuropharmacology* **36,** 1795–1798.
31. Meldrum B. and Garthwaite J. (1990) Excitatory amino acid neurotoxicity and neurodegenerative disease. *Trends pharmac. Sci.* **11,** 379–387.
32. Meldrum B. S., Swan J. H., Leach M. J., Millan M. H., Gwinn R., Kadota K., Graham S. H., Chen J. and Simon R. P. (1992) Reduction of glutamate release and protection against ischemic brain damage by BW 1003C87. *Brain Res.* **593,** 1–6.
33. Morimoto K., Sato H., Sato K., Sato S. and Yamada N. (1997) BW1003C87, phenytoin and carbamazepine elevate seizure threshold in the rat amygdala-kindling model of epilepsy. *Eur. J. Pharmac.* **339,** 11–15.
34. Muir K. W., Hamilton S. J., Lunnon M. W., Hobbiger S. and Lees K. R. (1998) Safety and tolerability of 619C89 after acute stroke. *Cerebrovasc. Dis.* **8,** 31–37.

35. Pantoni L. and Garcia J. H. (1997) Pathogenesis of leukoaraiosis: a review. *Stroke* **28**, 652–659.
36. Pantoni L., Garcia J. H. and Gutierrez J. A. (1996) Cerebral white matter is highly vulnerable to ischemia. *Stroke* **27**, 1641–1646.
37. Ragsdale D. S., McPhee J. C., Scheuer T. and Catterall W. A. (1996) Common molecular determinants of local anesthetic, antiarrhythmic, and anticonvulsant block of voltage-gated Na^+ channels. *Proc. natn. Acad. Sci. U.S.A.* **93**, 9270–9275.
38. Ramsay R. E. (1998) Use of the new antiepileptic drugs in monotherapy. *Neurologist* **4**, S11–S15.
39. Ransom B. R., Waxman S. G. and Davis P. K. (1990) Anoxic injury of CNS white matter: protective effect of ketamine. *Neurology* **40**, 1399–1403.
40. Rees B. E. (1987) The distribution of axons according to diameter in the optic nerve and optic tract of the rat. *Neuroscience* **22**, 1015–1024.
41. Requena J. and Mullins L. J. (1979) Calcium movement in nerve fibres. *Q. Rev. Biophys.* **12**, 371–460.
42. Siegel J. M., Nienhuis R., Gulyani S., Ouyang S., Wu M. F., Mignot E., Switzer R. C., McMurry G. and Cornford M. (1999) Neuronal degeneration in canine narcolepsy. *J. Neurosci.* **19**, 248–257.
43. Siesjo B. K. (1981) Cell damage in the brain: a speculative synthesis. *J. cerebr. Blood Flow Metab.* **1**, 155–185.
44. Smith S. E., al Zubaidy Z. A., Chapman A. G. and Meldrum B. S. (1993) Excitatory amino acid antagonists, lamotrigine and BW 1003C87 as anticonvulsants in the genetically epilepsy-prone rat. *Epilepsy Res.* **15**, 101–111.
45. Smith S. E., Hodges H., Sowinski P., Man C. M., Leach M. J., Sinden J. D., Gray J. A. and Meldrum B. S. (1997) Long-term beneficial effects of BW619C89 on neurological deficit, cognitive deficit and brain damage after middle cerebral artery occlusion in the rat. *Neuroscience* **77**, 1123–1135.
46. Smith S. E., Lekieffre D., Sowinski P. and Meldrum B. S. (1993) Cerebroprotective effect of BW619C89 after focal or global cerebral ischaemia in the rat. *NeuroReport* **4**, 1339–1342.
47. Smith S. E. and Meldrum B. S. (1995) Cerebroprotective effect of lamotrigine after focal ischemia in rats. *Stroke* **26**, 117–121.
48. Stefani A., Spadoni F., Siniscalchi A. and Bernardi G. (1996) Lamotrigine inhibits Ca^{2+} currents in cortical neurons: functional implications. *Eur. J. Pharmac.* **307**, 113–116.
49. Steffensen I., Waxman S. G., Mills L. and Stys P. K. (1997) Immunolocalization of the Na^+–Ca^{2+} exchanger in mammalian myelinated axons. *Brain Res.* **776**, 1–9.
50. Stys P. K. (1995) Protective effects of antiarrhythmic agents against anoxic injury in CNS white matter. *J. cerebr. Blood Flow Metab.* **15**, 425–432.
51. Stys P. K. (1998) Anoxic and ischemic injury of myelinated axons in CNS white matter: from mechanistic concepts to therapeutics. *J. cerebr. Blood Flow Metab.* **18**, 2–25.
52. Stys P. K., Hubatsch D. A. and Leppanen L. L. (1998) Effects of K^+ channel blockers on the anoxic response of CNS myelinated axons. *NeuroReport* **9**, 447–453.
53. Stys P. K. and Lopachin R. M. Jr (1996) Elemental composition and water content of rat optic nerve myelinated axons during *in vitro* post-anoxia reoxygenation. *Neuroscience* **73**, 1081–1090.
54. Stys P. K. and Lopachin R. M. (1998) Mechanisms of calcium and sodium fluxes in anoxic myelinated central nervous system axons. *Neuroscience* **82**, 21–32.
55. Stys P. K., Ransom B. R. and Waxman S. G. (1990) Effects of polyvalent cations and dihydropyridine calcium channel blockers on recovery of CNS white matter from anoxia. *Neurosci. Lett.* **115**, 293–299.
56. Stys P. K., Ransom B. R. and Waxman S. G. (1991) Compound action potential of nerve recorded by suction electrode: a theoretical and experimental analysis. *Brain Res.* **546**, 18–32.
57. Stys P. K., Ransom B. R. and Waxman S. G. (1992) Tertiary and quaternary local anesthetics protect CNS white matter from anoxic injury at concentrations that do not block excitability. *J. Neurophysiol.* **67**, 236–240.
58. Stys P. K., Ransom B. R., Waxman S. G. and Davis P. K. (1990) Role of extracellular calcium in anoxic injury of mammalian central white matter. *Proc. natn. Acad. Sci. U.S.A.* **87**, 4212–4216.
59. Stys P. K., Sontheimer H., Ransom B. R. and Waxman S. G. (1993) Noninactivating, tetrodotoxin-sensitive Na^+ conductance in rat optic nerve axons. *Proc. natn. Acad. Sci. U.S.A.* **90**, 6976–6980.
60. Stys P. K., Waxman S. G. and Ransom B. R. (1992) Ionic mechanisms of anoxic injury in mammalian CNS white matter: role of Na^+ channels and Na^+–Ca^{2+} exchanger. *J. Neurosci.* **12**, 430–439.
61. Sun F. Y. and Faden A. I. (1995) Neuroprotective effects of 619C89, a use-dependent sodium channel blocker, in rat traumatic brain injury. *Brain Res.* **673**, 133–140.
62. Taylor C. P. and Meldrum B. S. (1995) Na^+ channels as targets for neuroprotective drugs. *Trends pharmac. Sci.* **16**, 309–316.
63. Teng Y. D. and Wrathall J. R. (1997) Local blockade of sodium channels by tetrodotoxin ameliorates tissue loss and long-term functional deficits resulting from experimental spinal cord injury. *J. Neurosci.* **17**, 4359–4366.
64. Tsuchida E., Harms J. F., Woodward J. J. and Bullock R. (1996) A use-dependent sodium channel antagonist, 619C89, in reduction of ischemic brain damage and glutamate release after acute subdural hematoma in the rat. *J. Neurosurg.* **85**, 104–111.
65. Urenjak J. and Obrenovitch T. P. (1996) Pharmacological modulation of voltage-gated Na^+ channels: a rational and effective strategy against ischemic brain damage. *Pharmac. Rev.* **48**, 21–67.
66. Wang S. J., Huang C. C., Hsu K. S., Tsai J. J. and Gean P. W. (1996) Inhibition of N-type calcium currents by lamotrigine in rat amygdalar neurones. *NeuroReport* **7**, 3037–3040.
67. Waxman S. G., Black J. A., Stys P. K. and Ransom B. R. (1992) Ultrastructural concomitants of anoxic injury and early post-anoxic recovery in rat optic nerve. *Brain Res.* **574**, 105–119.
68. Waxman S. G. and Ritchie J. M. (1993) Molecular dissection of the myelinated axon. *Ann. Neurol.* **33**, 121–136.
69. Wiard R. P., Dickerson M. C., Beek O., Norton R. and Cooper B. R. (1995) Neuroprotective properties of the novel antiepileptic lamotrigine in a gerbil model of global cerebral ischemia. *Stroke* **26**, 466–472.
70. Xie X., Lancaster B., Peakman T. and Garthwaite J. (1995) Interaction of the antiepileptic drug lamotrigine with recombinant rat brain type IIA Na^+ channels and with native Na^+ channels in rat hippocampal neurones. *Pflügers Arch.* **430**, 437–446.
71. Xie X. M. and Garthwaite J. (1996) State-dependent inhibition of Na^+ currents by the neuroprotective agent 619C89 in rat hippocampal neurons and in a mammalian cell line expressing rat brain type IIA Na^+ channels. *Neuroscience* **73**, 951–962.
72. Yamauchi H., Fukuyama H., Ogawa M., Ouchi Y. and Kimura J. (1994) Callosal atrophy in patients with lacunar infarction and extensive leukoaraiosis. An indicator of cognitive impairment. *Stroke* **25**, 1788–1793.

(*Accepted* 19 *July* 1999)

ELSEVIER

Journal of Neuroimmunology 188 (2007) 175 - 180

Journal of Neuroimmunology

www.elsevier.com/locate/jneuroim

Detection of apoptotic cells in cerebrospinal fluid of patients suffering from neurological disease

R. Goertsches [a,c,*,1], S. Knappe [b,1], E. Mix [c], U.K. Zettl [c]

[a] *Institute of Immunology, University of Rostock, Schillingallee 70, 18057 Rostock, Germany*
[b] *Department of Ophthalmology, University of Rostock, Doberaner Str. 140, 18055 Rostock, Germany*
[c] *Clinic of Neurology, University of Rostock, Gehlsheimerstr. 20, 18147 Rostock, Germany*

Received 12 February 2007; received in revised form 22 May 2007; accepted 4 June 2007

Abstract

Apoptotic elimination of pathogenic immune cells is considered one of several regulatory mechanisms in inflammatory diseases. To explore the potential relationship between detection of apoptotic cells in the cerebrospinal fluid (CSF) and different types of neurological diseases, we examined cellular apoptosis at the stage of DNA fragmentation, defined by morphological criteria and a molecular biology technique (*in situ* tailing). During a first phase, 3446 CSF samples derived from admitted patients suffering of inflammatory (IND) and non-inflammatory neurological diseases (NIND) were analysed in the course of routine clinical diagnostics. First, all specimens were inspected for cells displaying atypical morphology following established morphological criteria of intact lymphocytes or apoptosis. In a second phase, 76 additional CSF samples collected from individuals according to investigated clinical groups were analysed in parallel by means of in situ tailing, which indicates the advanced degree of apoptotic demise through labelling of controlled DNA fragmentation.

No apoptotic processes were detected by either analytical method in CSF of clinically distinct diseases, amongst others multiple sclerosis (MS). This indicates that the detection of apoptotic cells in CSF during clinical routine diagnostics does not have sufficient explanatory power for the investigated conditions. Furthermore, based on immunohistochemistry, the proportion of CSF lymphocytes expressing the pro-apoptotic receptor Fas (CD95) tended to be higher in NIND patients compared to patients with other IND and MS, but the difference was not statistically significant. In contrast, expression of the anti-apoptotic protein Bcl-2 did not differ between investigated patient groups.

Keywords: Cerebrospinal fluid; Apoptosis; *In situ* tailing; Immunohistochemistry; Fas; Bcl-2

1. Introduction

The immune surveillance of the human body is operative in the systemic immune compartments and also in so-called immunologically privileged sites such as the central nervous system (CNS). Activated immune cells patrol the CNS and can induce profound damage when they 'encounter' their specific antigen in the context of appropriate restriction molecules (Wekerle et al., 1986; Hickey, 2001). This illustrates the fact that specialized anatomic barriers, such as the blood–brain barrier and blood–CSF barrier (Engelhardt and Ransohoff, 2005), do not guarantee the absence of immune-mediated damage in the brain and spinal cord, respectively (Perry et al., 1995). Furthermore, it has become clear that T cell trafficking within the CNS can be uncoupled from the development of diseases and that under certain conditions it can be used for therapeutic approaches (Sampson et al., 1996). On the other hand, multiple mechanisms operate to ensure rapid and effective termination of inflammation, e.g. via anergy or apoptosis (programmed cell death) of (autoreactive) immune cells. The importance of apoptosis for the homeostasis of the immune system as well as for the limitation of autoimmune diseases has been reviewed

* Corresponding author. Institute of Immunology, University of Rostock, Schillingallee 70, 18057 Rostock, Germany. Tel.: +49 381 494 5891; fax: +49 381 494 5882.
E-mail address: robert.goertsches@med.uni-rostock.de (R. Goertsches).
[1] These authors contributed equally.

0165-5728/$ - see front matter © 2007 Elsevier B.V. All rights reserved.
doi:10.1016/j.jneuroim.2007.06.004

extensively (Cohen et al., 1992; Gold et al., 1997; Bellgrau and Duke, 1999; Vaux and Flavell, 2000), e.g. in neurological conditions such as the chronic inflammatory disease of the CNS multiple sclerosis (MS) (Merrill and Scolding, 1999).

The cerebrospinal fluid (CSF) is an extension of the extracellular space of the brain parenchyma, thus to some extent it reflects chemical processes taking place around neurons, glial cells and blood–brain and blood–CSF barrier structures, which may well be involved in the pathology of neurological disorders. The CSF of healthy individuals contains between 150,000 cells and 500,000 cells. During a CNS inflammation, this number increases dramatically. However, neither in the healthy individual nor in MS does the cellular composition of the CSF directly reflect that of the peripheral blood suggesting a stringent control for leucocyte entry into the CSF (Kivisakk et al., 2003). Nevertheless, the CSF is considered a CNS compartment and it is relatively easy to analyse by means of lumbar puncture, enabling the investigation of apoptosis of CSF cells.

Kerr et al. (1972) established morphological criteria, which still represent the gold standard for the definition of apoptosis as a specialized form of cell death, basically characterized by cell shrinkage and membrane blebbing (zeiosis), collapse of the nucleus, chromatin condensation and marginalisation, DNA fragmentation and final phagocytosis of apoptotic bodies. Each phase of the apoptotic cascade can be precisely monitored applying electron microscopy. However, in daily clinic routine diagnostics, identification of apoptotic cells is restricted to analysis of the mentioned morphological criteria using light microscopy.

Molecular techniques such as *in situ* tailing assays that detect biochemical events associated with oligonucleosomal DNA fragmentation in apoptotic cells are more accurate. DNA fragmentation can easily be visualized by the incorporation of labelled nucleotides into the nuclei of affected cells utilizing a tailing technique that denotes the advanced stages of cell degeneration (Gold et al., 1994).

The process of apoptosis is basically mediated by two main pathways: (i) death receptor-induced mechanisms, which include the surface receptor Fas (CD95) and other members of the tumor necrosis factor receptor family (Krammer, 2000), and (ii) mitochondria-mediated pathways, which are partly controlled by the family of Bcl-2 proteins (Rathmell and Thompson, 2002). In autoimmunity, the persistence of activated autoreactive lymphocytes in the intrathecal compartment is a common feature and it is believed that this is due to an increased resistance to apoptosis stimuli. In MS patients, defective apoptotic deletion of pathogenic myelin reactive lymphocytes was proven *in vitro* and *in vivo* (Zang et al., 1999; Comi et al., 2000; Correale et al., 2000; Huang et al., 2000; Sharief et al., 2002).

The most prominent molecules, pro-apoptotic Fas and the death antagonist Bcl-2, do not directly interact. They thereby represent two rather independent apoptosis checkpoints that could disclose valuable information about the cellular context, separately.

The present study was driven by two main questions: (i) Are apoptotic cells detectable by morphological analysis and/or by quantification of generated DNA fragments in CSF of patients suffering of neurological disorders? (ii) Can we detect via immunohistochemistry, whether there are differences in the expression of pro-apoptotic Fas and anti-apoptotic Bcl-2 molecules by CSF cells in the investigated patients?

2. Materials and methods

2.1. Patients

Patients were recruited at the Department of Neurology of Rostock University, and none of them received therapeutic medications. In line of ensuring first clinical diagnosis, CSF examinations were inquired. In a first screening stage, 3446 CSF samples were evaluated for apoptosis applying morphological standard criteria (Kerr et al., 1972). In a subsequent stage, 76 clinically appropriately chosen samples were analysed enzymatically for the degree of DNA fragmentation (*in situ* tailing) (Gold et al., 1994). Fifteen MS patients (11 with relapsing–remitting and 4 with secondary progressive MS) were diagnosed according to the revised diagnostic criteria (McDonald et al., 2001); none had received immunomodulatory therapy or steroid treatment during 2 months preceding CSF collection. Patients with relapsing remitting disease course were examined during active and inactive stages of their disease. 19 IND and 11 NIND patients were examined, some of which repeatedly at different times. The clinical diagnoses and numerical distribution of examined subjects are summarized in Table 1.

Table 1
Diagnoses of patients examined, numbers of corresponding CSF samples and mean values of counted cells that were subjected to cell morphology analysis

Diagnosis (n [a])	Number of CSF samples	Median cell count, µl (range)
Multiple sclerosis (15)	**26**	10 (4–87)
Relapsing–remitting MS (11)	19	11 [b] (6–87)
Secondary progressive MS (4)	7	6 [b] (4–14)
Inflammatory neurological disease (19)	**32**	106 (1–1280)
Encephalitis (viral) (8)	13	162 (4–593)
Myelitis (2)	6	107 (3–211)
Meningitis (bacterial) (2)	2	675 (70–1280)
Abscess of the brain (4)	7	151 (82–531)
Neuritis multiplex cranialis (1)	1	30
Neuroborreliosis (1)	1	1
Facialisparesis (viral) (1)	1	38
Non-inflammatory neurological disease (11)	**18**	15 (2–98)
Pseudomigraine (2)	5	21 (15–26)
Paranoide schizophrenia (1)	3	20
Headache with arterial hypertonus (1)	1	4
Glioblastoma multiforme (1)	1	5
Cerebral seizure (1)	1	4
Cerebral infarction (4)	7	44 (2–98)
Multifocal motor neuropathy (1)	1	29 (–)
Total of analyzed preparations	**76**	

[a] Number of individuals.
[b] No significant difference between RRMS and SPMS ($p=0.064$).

2.2. Cell preparation

10 ml of CSF was drained by lumbar puncture with standard technique and subsequently processed during 30 min. CSF samples contaminated with blood were excluded from analysis. CSF cells were collected by centrifugation for 20 min at 200×*g* and counted after resuspension in phosphate-buffered saline supplemented with 10% fetal bovine serum (FBS) manually by means of estimation of the stained fraction (toluidine blue) in a Fuchs–Rosenthal-chamber.

2.3. Cell morphology

Attained CSF cells were evaluated following Kerr et al. gold standard criteria.

2.4. In situ tailing (detection of DNA fragmentation)

The collected CSF was fixed in ice-acetone for 10 min and dried on glass slides at room temperature. CSF was incubated with protein kinase 5% for 15 min at 37 °C and subsequently in a special tailing-mix (aqua bidest, tailing-buffer, cobalt chloride, digoxigenin nucleotide, terminal transferase solution; Boehringer Mannheim, Germany) for 60 min at 37 °C, and left in 10% FBS for 15 min at room temperature. Finally, a solution of alkaline phosphatase containing anti-digoxigenin-antibodies was added onto the slides and incubated for 60 min at 37 °C. In-between washing was carried out with Tris-buffered solution (TBS). Lymphocytes (1×10^7 murine thymocytes) incubated at 37 °C for 4 h with steroids (glucocorticoid dexamethasone, 1×10^{-5} mol) served as a positive control (Gold et al., 1994). Apoptotic cells were visualized by 4-nitroblue-tetrazolium-chloride/5-bromine-4-chloride-3-indolyl-phosphate (NBT/BCIP) (Boehringer Mannheim, Germany), which produced black and brown staining, respectively.

2.5. Immunohistochemistry – detection of Fas and Bcl-2 protein

The antigens cell surface Fas and mitochondrial Bcl-2 were identified with primary polyclonal rabbit and monoclonal mouse antibodies, respectively (Dako). The binding signal was amplified by means of the alkaline phosphatase/anti-alkaline phosphatase detection system (APAAP, Dako), using secondary mouse–anti-rabbit or rabbit–anti-mouse antibodies [1:50] (Dako). After up to 15 min, the Fas and Bcl-2 reaction products were visualized by NBT/BCIP, generating the characteristic coloration.

2.6. Statistical analysis

Statistical evaluation was performed using the non-parametric Kruskal–Wallis (KW) ranking test for comparisons between groups. The level of significance was set at 0.05. Statistical analyses were performed with SPSS (ver. 12.1) for MS-windows.

3. Results

3522 CSF samples were collected and analysed morphologically, thereof the last 76 using additional *in situ* tailing methodology (Table 1). Mean counts of leucocytes corresponded to the different clinical entities with no significant difference between the clinical courses of RRMS and SPMS [MS: 15.5 cells/µl (S.D.: 20.3)]. The highest values and greatest variation were seen in the inflammatory neurological disease group [IND: 209.9 cells/µl; S.D.: 309.8). A patient suffering from bacterial meningitis revealed the maximum number (1280 cells/µl). Moderate mean counts were found in the category of non-inflammatory neurological disease [NIND: 26.3 cells/µl; S.D.: 33.0) (Table 1). So-called apoptotic bodies derived from cell pyknosis, nuclear condensation and marginalisation were not detected in any of the examined samples, neither by the mentioned morphological criteria nor by enzymatic detection of DNA fragmentation, which was successful in steroid-treated control leucocytes only.

Immunohistochemical examination of Fas and Bcl-2 expression by CSF-derived lymphocytes revealed that, with the exception of each one Fas and one Bcl-2 outlier, these apoptosis-related proteins are present in more than 80% of lymphocytes in each patients group investigated. Almost all CSF lymphocytes expressed the Fas molecule in the NIND group (99.4%, KW rank: 16.4), whereas in the MS and IND group the values were slightly lower (97.9%, KW rank: 11.4 and 94.3%, KW rank: 9.8, respectively) (Fig. 1). However, the differences were not statistically significant ($p=0.134$). The percentages of Bcl-2$^+$ lymphocytes did not differ between the analysed groups ($p=0.655$; MS: mean 95.5%, KW rank: 12.9; IND: mean

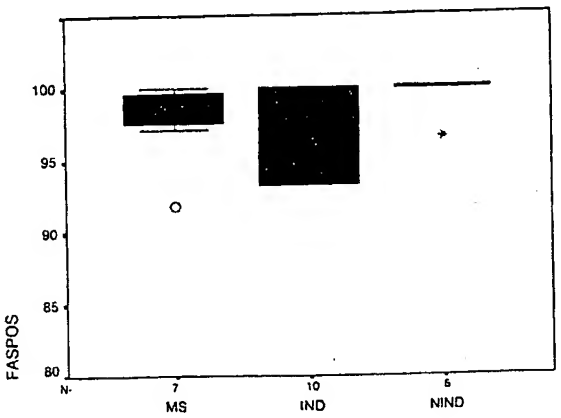

Fig. 1. Fas-expressing lymphocytes derived from CSF of different patients groups. Percentages of Fas$^+$ lymphocytes are displayed as box plots, where the boxes represent the 25th to 75th percentiles, the bars within correspond to the medians, and the lines above and below depict percentiles 10 and 90. Red crosses indicate values outside the percentiles 10 to 90. Diagnoses: multiple sclerosis (MS) ($n=1337$ cells), inflammatory diseases (IND) ($n=2171$ cells), non-inflammatory diseases (NIND) ($n=179$ cells). For statistical analysis the non-parametric Kruskal–Wallis ranking test for comparisons between groups was applied. An outlier of 67.7% in the category IND (abscess of the brain) is not shown. (For interpretation of the references to colour in this figure legend, the reader is referred to the web version of this article.)

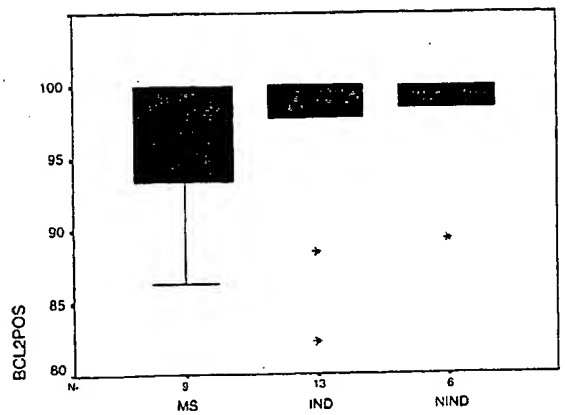

Fig. 2. Bcl-2-expressing lymphocytes derived from CSF of different patients groups. Percentages of Bcl-2$^+$ lymphocytes are displayed as box plots, where the boxes represent the 25th to 75th percentiles, the bars within correspond to the medians, and the lines above and below depict percentiles 10 and 90. Red crosses indicate values outside the percentiles 10 to 90. Diagnoses: multiple sclerosis (MS) (n=2390 cells), inflammatory diseases (IND) (n=2904 cells), non-inflammatory diseases (NIND) (n=1070 cells). For statistical analysis the non-parametric Kruskal–Wallis ranking test for comparisons between groups was applied. An outlier of 2.4% in the category IND (viral encephalitis) is not shown. (For interpretation of the references to colour in this figure legend, the reader is referred to the web version of this article.)

97.4%, KW rank: 15.9; NIND: mean 97.7, KW rank: 14.0) (Fig. 2). Accordingly, the concluding Fas/Bcl-2 ratios were not significantly different between the groups (MS=1.03; IND=0.97; NIND=1.02).

4. Discussion

CSF analysis has remained indispensable for a safe diagnosis of many neurological diseases, e.g. oligoclonal bands indicate an ongoing immune reaction in the CNS. Various studies showed that both the assessment of cell death by morphologic criteria and *in situ* tailing are useful in detecting apoptosis and DNA fragmentation (hallmark of late-stage apoptosis) in cell suspensions derived from CSF (Zettl et al., 1996; Gold et al., 1997). In our study, despite a large variation of disease etiology, providing different CSF cell counts, no apoptotic events were detectable by means of the described techniques.

There have been few studies concerning the proportion of apoptotic immune cells in the CSF of analysed individuals, some of which based on anti-Fas antibody stimulation in culture (Ichikawa et al., 1996; Sharief, 2000a) or instantaneously after freshly performed cell isolation (Ciusani et al., 1998; Okuda et al., 2006). Furthermore, different methodologies were applied to monitor the apoptotic process, such as DNA fragmentation by electrophoresis (Ichikawa et al., 1996), fragmentation of 5-bromo 2′deoxy-uracil (BrdU)-labelled DNA from cell lysates by immunoassay (Sharief, 2000a), propidium iodide (Ciusani et al., 1998) and Annexin V staining (Okuda et al., 2006), the latter two in combination with flow cytometric analysis.

Whereas Ichikawa and Sharief applied their respective methods in order to examine the characteristics of potentially impaired apoptosis in CSF lymphocytes, Ciusani et al. and Okadu et al. sought to record the actual proportion of apoptotic cells, which is comparable to our approach. Ciusani et al. reported on high proportions of apoptotic mononuclear cells, describing highest values in CSF of patients with NIND (40–95%) followed by CSF of MS patients (10–80%) and of patients with other IND (1–10%); in the peripheral blood, the values were lower (1–10%) in all three patient groups. However, Okuda et al. investigated a similar setting, in terms of intra-individual comparisons of peripheral blood vs. CSF T lymphocytes, and detected the inverse relationship, indicating less Annexin V-positive cells in the CSF. Both studies provided with fairly low numbers of mean CSF cells (Ciusani: 3 cells in MS; 325 cells in IND; 3 cells in NIND) and mean CSF cell percentages (Okadu: 2% AV$^+$ CD3$^+$ cells).

Our study design concentrated on the more advanced stages of apoptotic cell death. Here, in the second phase, applied *in situ* tailing procedure is a sensitive differentiator and indicator of the degree of internucleosomal non-random DNA fragmentation. It was chosen to confirm the previous results of phase 1, i.e. the microscopical judgement of apoptotic CSF lymphocytes. Although the sensitivity of Annexin V and propidium iodide staining analysed by flow cytometry may be slightly higher, we did not apply them as it appeared too elaborated, if implemented in routine clinical diagnostics. Due to low cell numbers in CSF, great quantities would be needed to reach the detection threshold of flow cytometry, e.g. a minimum of 30 ml. Therefore, for this analytical setting, evaluation of cell morphology by experienced personnel has to suffice. This indicates that our result of having no detected apoptotic cells in the analysed samples can, by all means, reflect the actual *in vivo* situation.

Several reports implied that abnormalities in the apoptotic stages were involved in the disease course of MS, often measured in relation to other neurological conditions and healthy control individuals. Of main interest are the pro-apoptotic molecule Fas/CD95, which is known to contribute to physiological control of the immune system through activation-induced cell death (Krammer, 2000), and the potentially counteracting anti-apoptotic protein Bcl-2 (Strasser et al., 1995; Rathmell and Thompson, 2002). *In vitro* studies demonstrated impaired apoptosis of peripheral blood-derived lymphocytes (Zipp et al., 1998; Macchi et al., 1999; Zang et al., 1999; Sharief, 2000a) and in CSF cells (Sharief, 2000b) of MS patients. Furthermore, recent studies showed that pro-apoptotic molecules such as Fas are down-regulated in lymphocytes of MS patients with ongoing inflammation (Semra et al., 2002; Sharief, 2000b; Achiron et al., 2004). So far, the Bcl-2 protein has not been examined extensively in this setting, but, in addition to peripheral blood (Macchi et al., 1999), its expression was proven in brain parenchyma (Zettl et al., 1998; Kuhlmann et al., 1999) and in CSF cells (Sharief, 2000b; Sharief et al., 2002) of MS patients.

Since co-expression of Fas and Bcl-2 proteins in lymphocytes is closely associated with apoptotic cell death in the animal models of MS (Kohji and Matsumoto, 2000), and was partially confirmed in peripheral blood mononuclear cells and CSF by studies of Sharief et al., we also examined the

relationship between cellular expression of Fas and Bcl-2 in a subset of collected CSF cell samples. In each patient group investigated, these proteins were present in more than 80% of lymphocytes, except one Bcl-2 outlier (2.4%) in an individual suffering from a viral encephalitis and a Fas outlier (Fas: 67.7%) in an individual with abscess of the brain. CSF cells have to pass through a long distance between the choroid plexus, where they most probably leave the blood stream and enter the CSF compartment (Ransohoff et al., 2003), and the lumbar sack where they are collected for analysis. Considering the estimated turnover of CSF (8 h), such prolonged presence of immune cells outside of their 'normal' environment might result in expression of apoptosis related proteins in the majority of cells irrespectively of the background disease. This may be the reason why comparisons of Fas-expressing lymphocytes in the CSF of MS, IND and NIND patients revealed no significant differences between the lower expression rate of patients suffering from inflammatory diseases and patients with MS and non-inflammatory diseases (Fig. 1), although the trend might reach significance if more samples are analysed. The lowest percentage of Bcl-2$^+$ lymphocytes were found in MS patients, whereas the corresponding values of both IND and NIND patients were higher (Fig. 2), resulting in similar Fas/Bcl-2 ratios in each clinical entity. These findings are in accordance with data of Sharief et al. (Sharief, 2000a,b; Sharief et al., 2002), who did not detect significant differences of Fas and Bcl-2 expression in cells from the intrathecal and systemic compartments nor between different clinical groups. On the other hand, they found MS patients to be hypo-responsive to Fas-independent apoptosis (Sharief, 2000a).

Ichikawa et al. and Okuda et al. measured the Fas receptor protein and attained expression rates of about 60% Fas-positive T lymphocytes in CSF cell suspensions of MS patients, which were different in a former study when compared with healthy controls and in a subsequent study between active and inactive MS. As these studies in CSF did not address respective states in other clinical settings, presented data of Fas and Bcl-2 expression rates add to the possibility of enhanced differences in-between rather than within clinical categories. Deviating results in terms of percentage rates may be due to methodological differences and different patient selection in the respective studies.

Several groups studied the cognate molecule soluble Fas (sFas) in CSF using commercially available enzyme-linked immunosorbent assay (ELISA) kits, which still led to conflicting results (Inoue et al., 1997; Ciusani et al., 1998; Sharief, 2000a,b; Mahovic et al., 2004). Whereas Inoue et al. reported on increased sFas levels both in CSF and serum of MS patients during the active stage as compared to inactive MS and other IND, Mahovic et al. did not detect differences in serum of relapsing–remitting MS patients and healthy controls, but a lower sFas expression in the CSF of MS patients compared to healthy controls. Also, many detailed analyses, e.g. monitoring apoptosis-related transcripts of individuals up to 1 (Bilinska et al., 2003) or even 10 years (Lopatinskaya et al., 2006), were performed with peripheral blood cells. The concept of a differential Fas/Bcl-2 ratio was clearly shown in a work by Julia et al. (2006) who investigated the effect of interferon-β on Fas- and Bcl-2 expression, which is known to increase apoptosis susceptibility.

The experimental design of the different studies were similar with regard to detection of pro- and/or anti-apoptotic molecules that are involved in early apoptotic stages occurring at cell membrane or in the cytosol during the apoptotic cascade in immune cells. Nevertheless, the entire ongoing of apoptosis remains speculative, as the regulatory potential of the apoptotic system can very well include the absorption of pro-apoptotic molecules and thereby regulate the activated cascade at several cell death checkpoints. This may result in the final inhibition of the release of pro-inflammatory cytoplasmic constituents. Hence, the presence of apoptotic signals may be measured, but final demise through such programmed cell death cannot be predicted and thereby render it inadequate for diagnostic purposes in examined neurologic conditions.

We can conclude that regardless of the diagnosis, no evidence for ongoing apoptotic processes are detected by means of morphological criteria and molecular techniques in this compartment of the CNS. This study may not provide information of relevance to the pathogenesis of MS, but with the exception of apoptosis as a diagnostic measure.

Acknowledgement

We are grateful to the patients who participated in this study.

References

Achiron, A., Gurevich, M., Friedman, N., Kaminski, N., Mandel, M., 2004. Blood transcriptional signatures of multiple sclerosis: unique gene expression of disease activity. Ann. Neurol. 55, 410–417.

Bellgrau, D., Duke, R.C., 1999. Apoptosis and CD95 ligand in immune privileged sites. Int. Rev. Immunol. 18, 547–562.

Bilinska, M., Frydecka, I., Podemski, R., Gruszka, E., 2003. Fas expression on T cells and sFas in relapsing–remitting multiple sclerosis. Acta Neurol. Scand. 107, 387–393.

Ciusani, E., Frigerio, S., Gelati, M., Corsini, E., Dufour, A., Nespolo, A., La Mantia, L., Milanese, C., Massa, G., Salmaggi, A., 1998. Soluble Fas (Apo-1) levels in cerebrospinal fluid of multiple sclerosis patients. J. Neuroimmunol. 82, 5–12.

Cohen, J.J., Duke, R.C., Fadok, V.A., Sellins, K.S., 1992. Apoptosis and programmed cell death in immunity. Annu. Rev. Immunol. 10, 267–293.

Comi, C., Leone, M., Bonissoni, S., DeFranco, S., Bottarel, F., Mezzatesta, C., Chiocchetti, A., Perla, F., Monaco, F., Dianzani, U., 2000. Defective T cell Fas function in patients with multiple sclerosis. Neurology 55, 921–927.

Correale, J., Gilmore, W., Li, S., Walsh, J., Bassani, M.M., Lund, B., Arias, M., Weiner, L.P., 2000. Resistance to glucocorticoid-induced apoptosis in PLP peptide-specific T cell clones from patients with progressive MS. J. Neuroimmunol. 109, 197–210.

Engelhardt, B., Ransohoff, R.M., 2005. The ins and outs of T-lymphocyte trafficking to the CNS: anatomical sites and molecular mechanisms. Trends Immunol. 26, 485–495.

Gold, R., Schmied, M., Giegerich, G., Breitschopf, H., Hartung, H.P., Toyka, K.V., Lassmann, H., 1994. Differentiation between cellular apoptosis and necrosis by the combined use of in situ tailing and nick translation techniques. Lab. Invest. 71, 219–225.

Gold, R., Hartung, H.P., Lassmann, H., 1997. T-cell apoptosis in autoimmune diseases: termination of inflammation in the nervous system and other sites with specialized immune-defense mechanisms. Trends Neurosci. 20, 399–404.

Hickey, W.F., 2001. Basic principles of immunological surveillance of the normal central nervous system. Glia 36, 118–124.
Huang, W.X., Huang, P., Gomes, A., Hillert, J., 2000. Apoptosis mediators FasL and TRAIL are upregulated in peripheral blood mononuclear cells in MS. Neurology 55, 928–934.
Ichikawa, H., Ota, K., Iwata, M., 1996. Increased Fas antigen on T cells in multiple sclerosis. J. Neuroimmunol. 71, 125–129.
Inoue, A., Koh, C.S., Sakai, T., Yamazaki, M., Yanagisawa, N., Usuku, K., Osame, M., 1997. Detection of the soluble form of the Fas molecule in patients with multiple sclerosis and human T-lymphotropic virus type I-associated myelopathy. J. Neuroimmunol. 75, 141–146.
Julia, E., Montalban, X., Al-Zayat, H., Issazadeh-Navikas, S., Goertsches, R., Martin, R., Comabella, M., 2006. Deficient Fas expression by CD4$^+$ CCR5$^+$ T cells in multiple sclerosis. J. Neuroimmunol. 180, 147–158.
Kerr, J.F., Wyllie, A.H., Currie, A.R., 1972. Apoptosis: a basic biological phenomenon with wide-ranging implications in tissue kinetics. Br. J. Cancer 26, 239–257.
Kivisakk, P., Mahad, D.J., Callahan, M.K., Trebst, C., Tucky, B., Wei, T., Wu, L., Baekkevold, E.S., Lassmann, H., Staugaitis, S.M., Campbell, J.J., Ransohoff, R.M., 2003. Human cerebrospinal fluid central memory CD4$^+$ T cells: evidence for trafficking through choroid plexus and meninges via P-selectin. Proc. Natl. Acad. Sci. U. S. A. 100, 8389–8394.
Kohji, T., Matsumoto, Y., 2000. Coexpression of Fas/FasL and Bax on brain and infiltrating T cells in the central nervous system is closely associated with apoptotic cell death during autoimmune encephalomyelitis. J. Neuroimmunol. 106, 165–171.
Krammer, P.H., 2000. CD95's deadly mission in the immune system. Nature 407, 789–795.
Kuhlmann, T., Lucchinetti, C., Zettl, U.K., Bitsch, A., Lassmann, H., Bruck, W., 1999. Bcl-2-expressing oligodendrocytes in multiple sclerosis lesions. Glia 28, 34–39.
Lopatinskaya, L., Zwemmer, J., Uitdehaag, B., Lucas, K., Polman, C., Nagelkerken, L., 2006. Mediators of apoptosis Fas and FasL predict disability progression in multiple sclerosis over a period of 10 years. Mult. Scler. 12, 704–709.
Macchi, B., Matteucci, C., Nocentini, U., Caltagirone, C., Mastino, A., 1999. Impaired apoptosis in mitogen-stimulated lymphocytes of patients with multiple sclerosis. NeuroReport 10, 399–402.
Mahovic, D., Petravic, D., Petelin, Z., Zurak, N., Horvat, G., Hajnsek, S., 2004. Level of sFas/APO 1 in serum and cerebrospinal fluid in multiple sclerosis. Clin. Neurol. Neurosurg. 106, 230–232.
McDonald, W.I., Compston, A., Edan, G., Goodkin, D., Hartung, H.-P., Lublin, F.D., McFarland, H.F., Paty, D.W., Polman, C.H., Reingold, S.C., Sandberg-Wollheim, M., Sibley, W., Thompson, A., van den Noort, S., Weinshenker, B.Y., Wolinsky, J.S., 2001. Recommended diagnostic criteria for multiple sclerosis: guidelines from the international panel on the diagnosis of multiple sclerosis. Ann. Neurol. 50, 121–127.
Merrill, J.E., Scolding, N.J., 1999. Mechanisms of damage to myelin and oligodendrocytes and their relevance to disease. Neuropathol. Appl. Neurobiol. 25, 435–458.
Okuda, Y., Apatoff, B.R., Posnett, D.N., 2006. Apoptosis of T cells in peripheral blood and cerebrospinal fluid is associated with disease activity of multiple sclerosis. J. Neuroimmunol. 171, 163–170.
Perry, V.H., Bell, M.D., Brown, H.C., Matyszak, M.K., 1995. Inflammation in the nervous system. Curr. Opin. Neurobiol. 5, 636–641.
Ransohoff, R.M., Kivisakk, P., Kidd, G., 2003. Three or more routes for leukocyte migration into the central nervous system. Nat. Rev. Immunol. 3, 569–581.
Rathmell, J.C., Thompson, C.B., 2002. Pathways of apoptosis in lymphocyte development, homeostasis, and disease. Cell 109, S97–S107.
Sampson, J.H., Archer, G.E., Ashley, D.M., Fuchs, H.E., Hale, L.P., Dranoff, G., Bigner, D.D., 1996. Subcutaneous vaccination with irradiated, cytokine-producing tumor cells stimulates CD8$^+$ cell-mediated immunity against tumors located in the "immunologically privileged" central nervous system. Proc. Natl. Acad. Sci. U. S. A. 93, 10399–10404.
Semra, Y.K., Seidi, O.A., Sharief, M.K., 2002. Disease activity in multiple sclerosis correlates with T lymphocyte expression of the inhibitor of apoptosis proteins. J. Neuroimmunol. 122, 159–166.
Sharief, M.K., 2000a. Impaired Fas-independent apoptosis of T lymphocytes in patients with multiple sclerosis. J. Neuroimmunol. 109, 236–243.
Sharief, M.K., 2000b. Increased cellular expression of the caspase inhibitor FLIP in intrathecal lymphocytes from patients with multiple sclerosis. J. Neuroimmunol. 111, 203–209.
Sharief, M.K., Douglas, M., Noori, M., Semra, Y.K., 2002. The expression of pro- and anti-apoptosis Bcl-2 family proteins in lymphocytes from patients with multiple sclerosis. J. Neuroimmunol. 125, 155–162.
Strasser, A., Harris, A.W., Huang, D.C., Krammer, P.H., Cory, S., 1995. Bcl-2 and Fas/APO-1 regulate distinct pathways to lymphocyte apoptosis. EMBO J. 14, 6136–6147.
Vaux, D.L., Flavell, R.A., 2000. Apoptosis genes and autoimmunity. Curr. Opin. Immunol. 12, 719–724.
Wekerle, H., Linington, C., Lassmann, H., Meyermann, R., 1986. Cellular immune reactivity within the CNS. Trends Neurosci. 9, 271–277.
Zang, Y.C., Kozovska, M.M., Hong, J., Li, S., Mann, S., Killian, J.M., Rivera, V.M., Zhang, J.Z., 1999. Impaired apoptotic deletion of myelin basic protein-reactive T cells in patients with multiple sclerosis. Eur. J. Immunol. 29, 1692–1700.
Zettl, U.K., Mix, E., Gold, R., Rothe, G., Hartung, H.P., 1996. Detection of oxidative burst and apoptotic cell death in cerebrospinal fluid (CSF) and blood. J. Lab. Med. 20, 176–177.
Zettl, U.K., Kuhlmann, T., Bruck, W., 1998. Bcl-2 expressing T lymphocytes in multiple sclerosis lesions. Neuropathol. Appl. Neurobiol. 24, 202–208.
Zipp, F., Otzelberger, K., Dichgans, J., Martin, R., Weller, M., 1998. Serum CD95 of relapsing remitting multiple sclerosis patients protects from CD95-mediated apoptosis. J. Neuroimmunol. 86, 151–154.

35. Kertesz A, Munoz DG. Primary progressive aphasia: a review of the neurobiology of a common presentation of Pick complex. Am J Alzheimers Dis 2002;17:30–36.
36. Benson DF, Zaias BW. Progressive aphasia: a case with postmortem correlation. Neuropsychiatry Neuropsychol Behav Neurol 1991;4:215–223.
37. Engel PA, Fleming PD. Primary progressive aphasia, left anterior atrophy, and neurofibrillary hippocampal pathology: observations in an unusual case. Neuropsychiatry Neuropsychol Behav Neurol 1997;10:213–218.
38. Li F, Iseki E, Kato M, et al. An autopsy case of Alzheimer's disease presenting with primary progressive aphasia: a clinicopathological and immunohistochemical study. Neuropathology 2000;20:239–245.
39. Turner RS, Kenyon LC, Trojanowski JQ, et al. Clinical, neuroimaging, and pathologic features of progressive nonfluent aphasia. Ann Neurol 1996;39:166–173.
40. Clark DG, Mendez MF, Farag E, Vinters HV. Clinicopathologic case report: progressive aphasia in a 77-year-old man. J Neuropsychiatry Clin Neurosci 2003;15:231–238.

Glutamate uptake by oligodendrocytes

Implications for excitotoxicity in multiple sclerosis

David Pitt, MD; Iris E. Nagelmeier; Heather C. Wilson, MD; and Cedric S. Raine, PhD

Abstract—*Background:* Excitotoxic damage is a common pathologic event in a number of neurologic diseases occurring after accumulation of excess extracellular glutamate in the CNS and subsequent overstimulation of glutamate receptors. In gray matter, astrocytes take up synaptically released glutamate and are thus key cells in maintaining glutamate homeostasis. In white matter, oligodendrocytes have been shown to express glutamate transporters, but their role in extracellular glutamate removal is unclear. *Objective:* To investigate whether cultured human fetal oligodendrocytes functionally express the main glutamate transporters EAAT-1 and EAAT-2. *Methods:* Cultures of fetal human oligodendrocytes were examined by immunocytochemistry and [^{3}H]glutamate uptake, and the findings were correlated with glutamate transporter expression in normal and multiple sclerosis (MS) CNS tissue. *Results:* Both EAAT-1 and EAAT-2 were expressed by human oligodendrocytes in vitro. Incubation of oligodendrocytes with the proinflammatory cytokine tumor necrosis factor-α (TNFα) reduced EAAT-1 expression and inhibited glutamate uptake by >75%. Furthermore, in normal human white matter, oligodendrocytes were found to be the predominant cells to express EAAT-1 and EAAT-2, both at the mRNA and at the protein level. A small number of astrocytes in white matter expressed these receptors, more so EAAT-1 than EAAT-2. In MS white matter, oligodendrocytes lost expression of EAAT-1 and EAAT-2 receptors in the lesion vicinity. *Conclusions:* Oligodendrocytes appear to be predominant cells for glutamate clearance in human white matter. Glutamate receptor expression and glutamate removal were defective in MS white matter, possibly mediated by TNFα, changes that might underlie high extracellular glutamate and an increased risk for glutamate excitotoxicity.

NEUROLOGY 2003;61:1113–1120

A common pathologic event shared by a number of neurologic conditions is extracellular accumulation of glutamate, the major excitatory neurotransmitter in the CNS.[1] High levels of free glutamate are known to lead to excessive stimulation of glutamate receptors and subsequent excitotoxic injury to both neurons and glial cells.[2,3] Therefore, maintenance of subtoxic extracellular glutamate levels is crucial in the CNS and is achieved by rapid uptake of glutamate into glial cells. This is carried out by high-affinity, sodium-dependent glutamate transporters, of which at least five have been cloned: EAAT-1, EAAT-2, EAAT-3 (corresponding to GLAST, GLT-1, and EAAC-1 in rodents), EAAT-4, and EAAT-5.[4-8]

On the basis on localization studies, it is generally believed that EAAT-1 and EAAT-2 are expressed exclusively by astrocytes in gray matter, which therefore play a key role in the clearance of free glutamate from synaptic regions.[9-12] EAAT-3 is regarded as the principal glutamate transporter in neurons,[10] whereas EAAT-4 and EAAT-5 are expressed in Purkinje cells[13] and retina,[8] respectively. This distribution pattern has been revised recently by the observation that GLT-1 can be expressed by different types of neurons in the rat and the macaque monkey.[14,15] Moreover, in CNS white matter, glutamate transporters have been reported to be present also on oligodendrocytes.[16] Recent studies have acknowledged the presence of GLAST, GLT-1, and EAAC-1 mRNA[17] and protein[16] on cultured rat oligodendrocytes. This is in accord with studies on glutamate uptake by oligodendrocytes in vitro,[16,18] where gluta-

From the Departments of Neurology (Drs. Pitt and Raine), Pathology (Drs. Pitt, Wilson, and Raine, I.E. Nagelmeier), and Neuroscience (Dr. Raine), Albert Einstein College of Medicine, Bronx, NY.

Supported in part by Health and Human Services grants NS 08952, NS 11920, and NS 07098 and National Multiple Sclerosis Society grant RG 1001-J-10. H.C.W. was supported by the Patrick Berthoud Trust (University of Cambridge, UK), and C.S.R. is the Wollowick Professor for Multiple Sclerosis Research at this institution.

Received May 8, 2003. Accepted in final form July 2, 2003.

Address correspondence and reprint requests to Dr. D. Pitt, Department of Neurology, Albert Einstein College of Medicine, 1300 Morris Park Ave., F-140, Bronx, NY 10461; e-mail: dfpitt@yahoo.com

mate transport was suggested to be mediated primarily by GLT-1 in oligodendrocytes and by GLAST in astrocytes.[16] In the same study, however, immunohistochemical examination of rat optic nerve showed oligodendrocytes to express primarily GLAST and astrocytes to express GLT-1. Thus, the relative contributions of astroglial vs oligodendroglial cells in glutamate uptake in white matter are not clear.

In a recent study on human white matter, we found that key enzymes of glutamate metabolism and glutamate transporters were present predominantly on oligodendrocytes and to a much lesser extent on astrocytes, implying a major role for oligodendrocytes in the maintenance of glutamate homeostasis in white matter.[19] Moreover, a significant paucity of glutamate-metabolizing enzymes and glutamate transporters in white matter of patients with MS suggested reduced intracellular glutamate processing and, by extrapolation, accumulation of extracellular glutamate and potentially excitotoxic consequences. Previous studies had demonstrated that excitotoxic mechanisms play a role in white matter pathology in a mouse model for MS, experimental autoimmune encephalomyelitis, where administration of glutamate receptor blockers reduced disease severity as well as damage to oligodendroglia and axons,[20] potential targets for excitotoxicity in white matter.

Here, we substantiate our previous proposal that oligodendrocytes are key in glutamate removal. In parallel with white matter, we examined glutamate transport in an in vitro system, cultured human fetal oligodendrocytes, where glutamate uptake and transporter expression could readily be demonstrated. Glutamate transport was facilitated primarily by EAAT-2. Both EAAT-2 expression and glutamate transport were suppressed by exposure to the proinflammatory cytokine tumor necrosis factor-α (TNFα). The latter findings offer evidence for a mechanism underlying the reported glutamate transporter down-regulation in MS.

Materials and methods. *Human tissue.* Human CNS tissue was obtained at autopsy according to an institutional review board–approved protocol. Brain and spinal cord were stored frozen or fixed for histologic examination. Postmortem intervals were between 2 and 6 hours for MS and 2 and 8 hours for control CNS tissue. MS CNS tissue was from six subjects. Three had primary progressive MS displaying early active (acute), chronic active, and chronic silent lesions: Patient 1 was a 31-year-old woman with 4-year disease duration; Patient 2 was a 37-year-old woman with 17-year disease duration; and Patient 3 was a 32-year-old woman with 4-year disease duration. Three had secondary progressive MS and displayed chronic silent lesions only: Patient 4 was a 55-year-old woman with 20-year disease duration; Patient 5 was a 69-year-old man with 10-year disease duration; and Patient 6 was a 60-year-old woman with 15-year disease duration. Non-MS CNS tissue was from four patients dying from nonneurologic causes (myocardial infarction [three cases] and acute myeloblastic leukemia [one case]) and two cases of noninflammatory other neurological diseases (olivopontocerebellar atrophy and adult polyglucosan body disease). Fresh-frozen blocks of CNS tissue were embedded in optimum cooling temperature medium using an acetone/dry ice bath and stored at −80 °C until used.

Lesion classification. MS lesions were classified histopathologically following hematoxylin/eosin, Luxol fast blue, and Bodian staining.[19] Inflammation, infiltration, demyelination, and the profile of immune cells were used to classify the lesions. Early active lesions were characterized by intense inflammation, demyelination, hypercellularity, edema, and astroglial hypertrophy but no obvious fibrous astrogliosis. Chronic active lesions were areas of long-term demyelination and gliosis with recent inflammatory activity, astroglial hypertrophy, and ongoing demyelination at the margins. Chronic silent lesions consisted of areas of long-term demyelination and gliosis but no inflammation.

Immunostaining. Frozen sections, 10 μm thick, from human CNS tissue blocks were air dried, acetone fixed, and quenched with H_2O_2 for 10 minutes each. After blocking with normal serum, sections were incubated with anti-GLAST/EAAT-1 (1:1,000) and anti-GLT-1/EAAT-2 (1:500) primary antibodies (both from Alpha Diagnostics, San Antonio, TX), overnight at 4 °C. Secondary antibodies were applied for 2 hours at room temperature, followed by incubation with Vectastain ABC reagent and reaction with diaminobenzidine tetrahydrochloride as chromogen (Vector Laboratories, Burlingame, CA). For immunofluorescent staining, cultured glial cells were fixed with 2% paraformaldehyde (PFA) in phosphate-buffered saline (PBS) or ice-cold methanol, washed in PBS, and incubated with anti-GLAST and anti-GLT-1 antibody at a dilution of 1:50 overnight, a concentration giving optimal staining as determined from a gradient of 1:50 to 1:500. Fluorescein isothiocyanate– or Texas Red–labeled secondary antibodies were applied for 30 minutes at 37 °C, followed by nuclear counterstaining with Hoechst Nuclear Stain (Roche Molecular Biochemicals, Indianapolis, IN) for 5 minutes at room temperature. Specificity for EAAT-1 and EAAT-2 immunoreactivity was tested by specific absorption with the respective antigens.

In situ hybridization. cDNA probes were generated by digoxigenin-labeling reverse transcription (RT) PCR product (EAAT-1 [515 to 928] and EAAT-2 [41 to 486]) from human whole-brain mRNA utilizing the DIG-Nick-Translation Mix (Roche Molecular Biochemicals). Probes were used according to the procedures of Komminoth et al.[21] In brief, 10-μm frozen sections of human CNS were air dried, fixed with 4% PFA, and de- and rehydrated through graded ethyl alcohol to water. After rinsing with diethylpyrocarbonate (DEPC)/PBS, sections were treated with proteinase K in Tris-ethylenediaminetetra-acetic acid buffer (1 μg/mL, 15 minutes at 37 °C), briefly rinsed in DEPC/H_2O and DEPC/PBS, and fixed again in 4% PFA for 5 minutes. Sections were preincubated for 1 hour at 37 °C with hybridization mix (50% formamide, 5× saline–sodium citrate [SSC], 1× Denhardt's solution, 10% dextran sulfate, and 200 μg/ml baker's yeast tRNA/salmon sperm DNA) in a wet chamber. Subsequently, purified probes were denatured for 5 minutes and applied at a concentration of 0.3 ng/mL in hybridization solution. Incubation was carried out in a wet chamber at 43 °C for 18 hours. Following hybridization, sections were rinsed in 4× SSC and 2× SSC both for 45 minutes at 50 °C. Hybridized probes were immunodetected with alkaline phosphatase-labeled antibodies to digoxigenin (Roche) in catalyzing nitroblue tetrazolium/5-bromo-4-chloro-3-inodolylphosphate substrate (Sigma, St. Louis, MO).

Human fetal oligodendrocytes. Primary dissociated oligodendrocyte cultures from spinal cords from human fetuses at 19 to 24 weeks' gestation were prepared as described elsewhere (H.C. Wilson et al., submitted). In brief, spinal cords were cleared of meninges and vessels, mechanically disrupted, and enzymatically digested with enzyme solutions containing trypsin, collagenase III, DNase, and papain (Sigma). After centrifugation in 20 mL of Dulbecco's modified Eagle medium (DMEM) containing 10% fetal calf serum, the pellet was resuspended in N2B3 medium (DMEM supplemented with 0.5 g/mL insulin, 0.1 g/mL transferrin, 2 m*M* glutamine, 0.002% ovine serum albumin, 14.5 g/mL putrescine, 360 ng/mL thyroxine, 300 ng/mL tri-iodothyronine, 56 ng/mL progesterone, and 35 ng/mL sodium selenite), and the solution was incubated at 37 °C in a culture flask overnight. The next day, the supernate was removed and centrifuged and the pellet resuspended in N2B3 medium. Cells were seeded onto poly-L-lysine-coated glass coverslips in 24-well plates. One spinal cord yielded an average 20 to 24 coverslips, each containing 2,000 to 3,000 cells. Medium was changed initially after 2 days and afterward every 4 days. Platelet-derived growth factor-AA (10 ng/mL; Sigma) was added daily until day 5. The established cultures consisted of 75 to 95% oligodendrocytes, depending on the preparation, and were used between days 8 and 10.

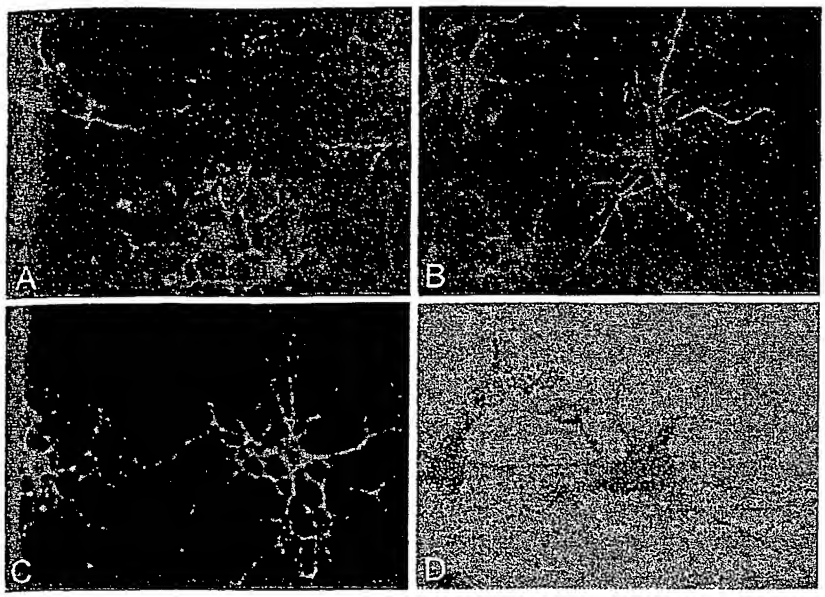

Figure 1. (A and B) Immunofluorescent staining of human fetal oligodendrocyte cultures with EAAT-1 (A) and EAAT-2 (B) antibodies. (C) Staining with the phenotypic oligodendrocyte marker 2',3'-cyclic nucleotide 3'-phosphohydrolase (CNPase) for cell type identification. Counterstaining with Hoechst Nuclear Stain (blue). (D) Autoradiograph of [^{3}H]glutamate uptake in oligodendrocyte cultures. Oligodendrocytes with labeled perikarya and labeled branched processes are seen after 20 minutes of incubation with [^{3}H]glutamate. Counterstaining with hematoxylin/eosin. ×750 (A to C); ×800 (D).

Western blotting. Oligodendrocyte cultures were lysed in hot (95 °C) Laemmli buffer. For sodium dodecyl sulfate–polyacrylamide gel electrophoresis (SDS-PAGE), lysates of five to eight coverslips were pooled and run on a 7.5% acrylamide gel. After electroblotting onto polyvinylidene difluoride membrane for 16 to 18 hours, blots were rinsed briefly and blocked with 5% nonfat dry milk for 1 hour at room temperature. Primary antibodies were applied at a concentration of 1:5,000 (anti-GLAST/EAAT-1; Alpha Diagnostics, San Antonio, TX) and 1:10,000 (anti-GLT-1/EAAT-2; Chemicon, Temecula, CA) in 5% nonfat dry milk. Subsequently, blots were washed and incubated with the respective peroxidase-labeled secondary antibodies for 90 minutes. After washing, proteins were visualized with enhanced chemoluminescence (Amersham, UK) or Super Signal West Femto (Pierce, Rockford, IL). Blots were stripped and reprobed for β-tubulin (1:1,000; Sigma) for control purposes. Western blots were carried out at least three times.

Viability assay. Viability of oligodendrocytes after TNFα treatment was assessed by three different methods: trypan blue dye exclusion and quantitation of lactate dehydrogenase (LDH) activity in cell medium (cytotoxicity and cell lysis) and of cytoplasmic histone-associated DNA fragments (apoptosis). Trypan blue was added to the oligodendrocyte cultures and the ratio of stained vs unstained cells evaluated under the light microscope. For the quantification of LDH activity and histone-associated mono- and oligonucleosomes, a Cytotoxicity Detection and Cell Death Detection $ELISA_{PLUS}$ Kit was used according to the manufacturer's instructions (both from Roche). Respective data were derived from five different experiments performed in triplicate cultures.

Glutamate uptake studies. Uptake experiments were carried out as described previously.[22-24] In short, oligodendrocyte cultures were equilibrated at 37 °C for 10 minutes in 5 mmol KH_2PO_4-K_2HPO_4 buffer (pH 7.4), adjusted to 330 mOsmol with sodium chloride or choline chloride for determination of total uptake or background values, respectively. Incubation was continued for between 5 and 40 minutes after [^{3}H]glutamate was added to the respective buffer for a concentration of 10 n*M* [^{3}H]glutamate and 1 μ*M* cold glutamate (approximately 0.1 μCi/well) based on published techniques.[23] Subsequently, cells were washed three times with ice-cold KH_2PO_4-K_2HPO_4 buffer containing choline chloride and excess nonradioactive glutamate (1 m*M*). Cells were lysed with hot (95 °C) Laemmli buffer and additional sonication, and cell-associated radioactivity was measured by liquid scintillography. Values were adjusted to the β-tubulin content of each sample, which was determined by SDS-PAGE and western blotting.

Autoradiography. Cultures incubated with [^{3}H]glutamate were fixed in 2% PFA/PBS for 5 minutes, rinsed, and air dried. Coverslips were mounted on microscope slides and covered with NTB-2 emulsion (Eastman Kodak, Rochester, NY). Coverslips were exposed for approximately 4 weeks at 4 °C, developed with D-19 developer, and fixed with general-purpose fixer (both Kodak).

Results. *Glutamate transporter expression and glutamate uptake in cultured human oligodendrocytes.* To determine the functionality of glutamate transporter expression in oligodendrocytes, glutamate transporters and glutamate transport were examined in cultured human fetal oligodendrocytes. Antibodies against EAAT-1 and EAAT-2 were used, and high levels of immunoreactivity for both glutamate transporters were detected on the cell bodies and processes of virtually 100% of mature, 2',3'-cyclic nucleotide 3'-phosphohydrolase (CNPase)–positive oligodendrocytes (day 7 to 12 in culture) (figure 1). The specificity of the antisera to EAAT-1 and EAAT-2 was tested by specific absorption with antigen that was found to abolish the immunoreactivity. EAAT-1 and EAAT-2 immunostaining of contaminating astrocytes was also noted (not shown).

Having established glutamate transporter expression, we then examined glutamate uptake in cultured human oligodendrocytes. In preliminary studies, we found [^{3}H]glutamate uptake to be almost linear in a range between 1 and 40 n*M* (figure 2A). A steady state in glutamate uptake was reached after approximately 30 minutes (see figure 2B). On average, 97% of the measured radioactivity was determined to be cell associated and 3% to be nonspecific.

Glutamate incorporation in vitro was visualized by autoradiography of [^{3}H]glutamate-incubated cells. After a 30-minute incubation period with [^{3}H]glutamate, two populations of surface phase-dark cells appeared to be labeled. Cells with an oligodendrocyte morphology represented the majority of mature cells and were labeled over the cell soma and over numerous intercalated processes (see figure 1D). Pronounced labeling was also seen in large astrocytes (not shown): Bipolar, immature oligodendrocytes displayed minimal labeling. The morphology and frequency of the labeled surface dark-phase oligodendrocytes

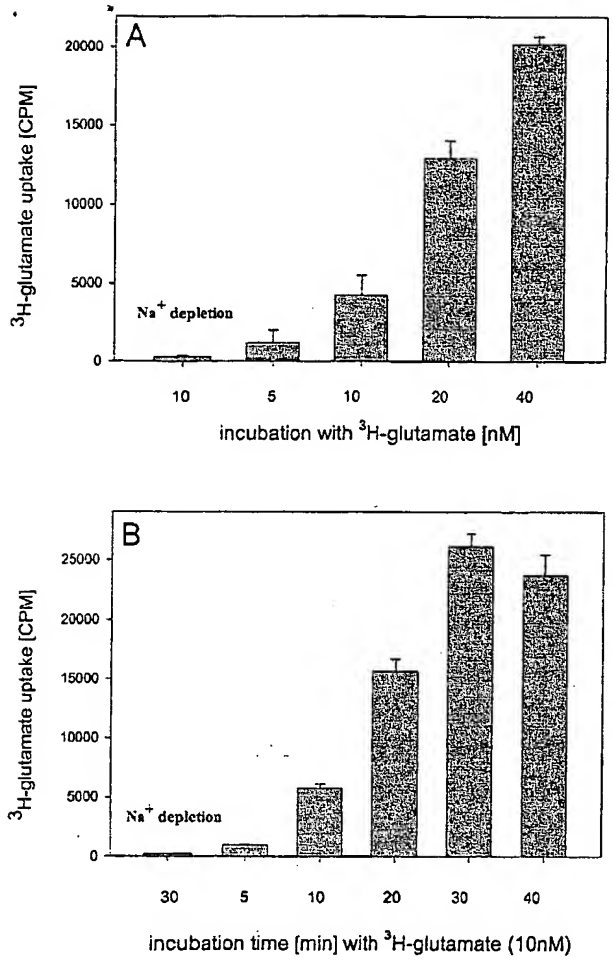

Figure 2. (A) [^{3}H]Glutamate uptake calculated as counts per minute per coverslip of human fetal oligodendrocytes. [^{3}H]Glutamate uptake was found to be near linear between 5 and 40 nM [^{3}H]glutamate. The incubation time was 20 minutes. Cell-associated radioactivity was found to be <96%. (B) [^{3}H]Glutamate uptake was linear between 5 and 30 minutes of incubation time with [^{3}H]glutamate and was saturated after incubation for >30 minutes. The [^{3}H]glutamate concentration used in these experiments was 10 nM. Data are obtained from three different sets of experiments, each carried out in triplicate.

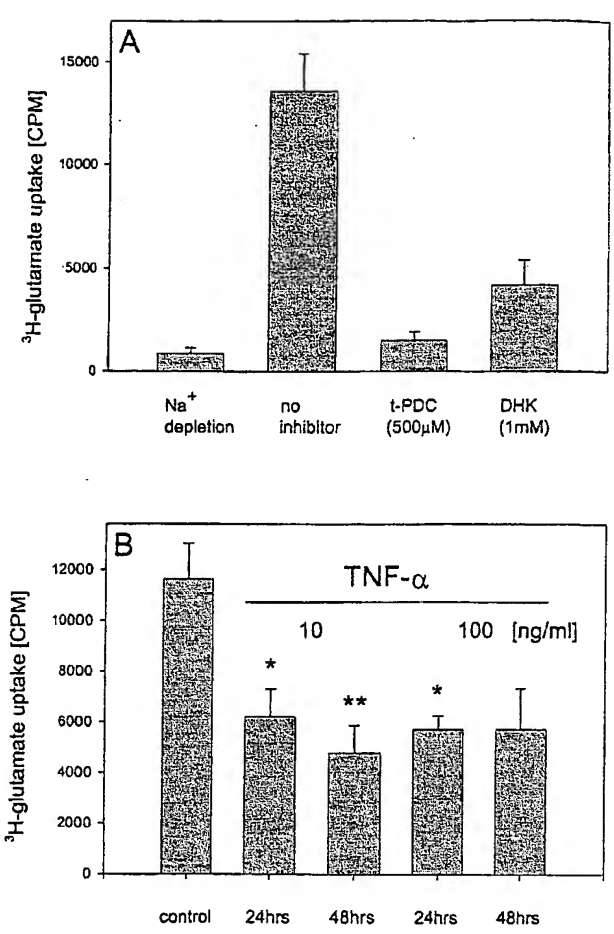

Figure 3. (A) [^{3}H]Glutamate uptake in oligodendroglial cultures in the presence of L-trans-pyrrolidine-2,4-dicarboxylate (t-PDC) and dihydrokainate (DHK). Cell-associated radioactivity was decreased by approximately 94% after incubation with 500 μM t-PDC. Cell-associated [^{3}H]glutamate was reduced by 71% with the EAAT-2-specific blocker DHK (1 mM). Data represent four different sets of experiments, each carried out in triplicate. (B) Tumor necrosis factor-α (TNFα)–mediated inhibition of glutamate uptake. Oligodendrocyte cultures were exposed for 24 and 48 hours to 10 and 100 ng/mL TNFα. Data are from a single representative experiment (n = 3). This experiment was repeated three times with similar results.

and astrocytes correlated with their CNPase and glial fibrillary acidic protein (GFAP) positivity, respectively. Increase of the final [^{3}H]glutamate concentration resulted in increased labeling intensity but did not change the distribution of the labeling.

Glutamate uptake is mediated by both EAAT-2 and EAAT-1. To examine the relative contributions of EAAT-1 and EAAT-2 to glutamate uptake into oligodendrocytes, we employed the general glutamate transporter inhibitor L-*trans*-pyrrolidine-2,4-dicarboxylate (*t*-PDC) and the EAAT-2-specific inhibitor dihydrokainate (DHK). The efficacy of the respective inhibitors and the ionic dependence of glutamate uptake were compared with overall glutamate uptake (figure 3A). As reported above, the substitution of sodium with choline in the incubation buffer resulted in blockage of all sodium-driven glutamate transport and in the reduction of [^{3}H]glutamate incorporation to approximately 3 to 4%. Similarly, incubation with *t*-PDC (500 μ*M*) blocked 94% of cell-associated radioactivity, indicating that the gross glutamate influx took place via transporter-mediated mechanisms. Incubation with DHK (1 m*M*) inhibited total incorporation by 71% and transporter-mediated glutamate uptake by 78%, thus indicating that EAAT-2-mediated uptake accounts for approximately three-quarters of the glutamate transport into oligodendrocytes.

Glutamate uptake is reduced by TNFα. Next, we investigated the effect of the proinflammatory cytokine TNFα on glutamate uptake in oligodendrocyte cultures. As

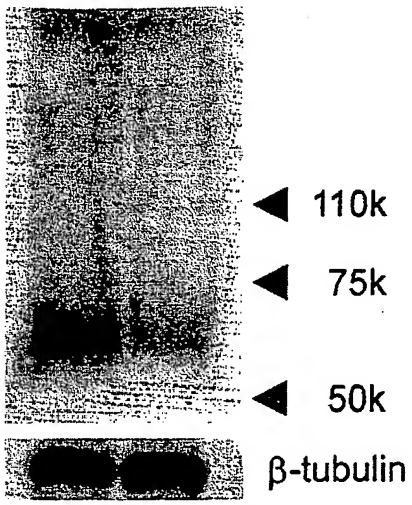

Figure 4. Western blot analysis showing immunoreactivity to EAAT-2/GLT-1 in human oligodendrocyte cultures treated with phosphate-buffered saline (control) or 10 nM tumor necrosis factor-α (TNFα) for 48 hours prior to harvesting. Blots were standardized by immunodetection of β-tubulin and were carried out in quadruplicate.

shown in figure 3B, exposure to TNFα (10 ng/mL) reduced glutamate uptake to 53 and 41% after 24 and 48 hours, respectively. Interestingly, exposure to 100 ng/mL TNFα for 48 hours, the highest and longest exposure tested, had no significant effect on glutamate uptake. These alterations in glutamate uptake were not due to TNFα-induced apoptosis or cytotoxicity as the addition of TNFα (10 ng/mL) did not result in any detectable decline in cell viability, as determined by nucleosome enrichment assay (apoptosis) and LDH activity assay (necrosis [data not shown]). Only incubation with 100 ng/mL TNFα for 48 hours resulted in a statistically nonsignificant increase in LDH activity.

We have no explanation for the lack of effect of high-dose TNFα treatment for 48 hours.

Immunoblot analysis of oligodendrocyte culture homogenates confirmed the presence of the glutamate transporters EAAT-1 and EAAT-2. A marked reduction in expression of the main glutamate transporter, EAAT-2, in oligodendrocyte cultures was observed after treatment with 10 ng/mL TNFα (48 hours) (figure 4).

Glutamate transporter mRNA and protein expression in normal human and MS tissue. Expression of the glutamate transporters EAAT-1 and EAAT-2 was confirmed at both the protein and the message level in normal human and MS white matter. As reported previously,[19] staining for both glutamate transporters in normal white matter was observed predominantly on oligodendrocytes (figure 5, A through C). Only a few of the stained cells were astrocytes, and these tended to be localized to subcortical layers. However, the astrocytic component was higher after staining for EAAT-1 than after EAAT-2 (figure 6). These results were compared with data obtained from a different approach: in situ hybridization of digoxigenin-labeled cDNA probes for EAAT-1 (515 to 928) and EAAT-2 (41 to 486) with human white matter. In situ hybridization revealed a pattern of cellular EAAT-1 and EAAT-2 mRNA distribution identical to the respective expression of protein, that is, prominent staining of oligodendrocytes and weak staining of scattered astrocytes and microglia (see figure 5, D and E).

MS white matter displaying chronic active lesions (see figure 5F) was also examined by immunohistochemistry. In the center of active lesions, from which oligodendrocytes had been depleted, staining for both EAAT-1 and EAAT-2 was markedly diminished (see figure 5,G and H). In early active lesions, reduction of EAAT-2 but not EAAT-1 extended into normal-appearing white matter adjacent to lesions (see figure 5, I and J). In contrast, in both older chronic active lesions and chronic silent lesions, the area of reduced EAAT-1 and EAAT-2 expression was restricted to the immediate lesion perimeter (not shown).

Discussion. In the current report, with the aid of human oligodendrocyte cultures, we have established that oligodendrocytes play a role in the removal of extracellular glutamate, a proposal stemming from a previous study on MS tissue.[19] As has been shown herein, cultured human fetal oligodendrocytes robustly expressed the major glutamate transporters EAAT-1 and EAAT-2. The functionality of the transporters was demonstrated by glutamate uptake studies in these cells, and EAAT-2 was found to facilitate the majority of glutamate transport. In human white matter, oligodendrocytes were the principal cells expressing glutamate transporters as demonstrated by both immunohistochemistry and in situ hybridization.

The current work is in accordance with reports where glutamate transporters were observed in rat optic nerve oligodendrocytes both in situ and in vitro[16,17] but is at variance with earlier studies, mostly on rat brain, which attributed GLAST and GLT-1 (EAAT-1 and EAAT-2) expression exclusively to astrocytes[9,10] or to astrocytes and neurons.[11,14,15,25] These studies focused primarily on gray matter where high levels of astroglial immunolabeling were found, with most intense labeling in areas of highest glutamatergic transmission, suggesting a role for astrocytes as the principal retrievers of synaptically released glutamate.[12] In contrast to gray matter, glutamate release in white matter probably takes place at a much lower level, requiring in turn less glutamate uptake capacity. Correspondingly, glutamate transporter expression was reported to be largely absent in white matter.[10,25] Thus, comparatively low transporter levels, although functionally significant in its environment, might not have been previously appreciated.

The relative lack of glutamate transporters, especially EAAT-2, in astrocytes in white matter (except for some low-level expression seen in subcortical layers, more so of EAAT-1 than EAAT-2), places oligodendrocytes in a key position for maintaining glutamate homeostasis. Sources of possible glutamate release in white matter include axons following

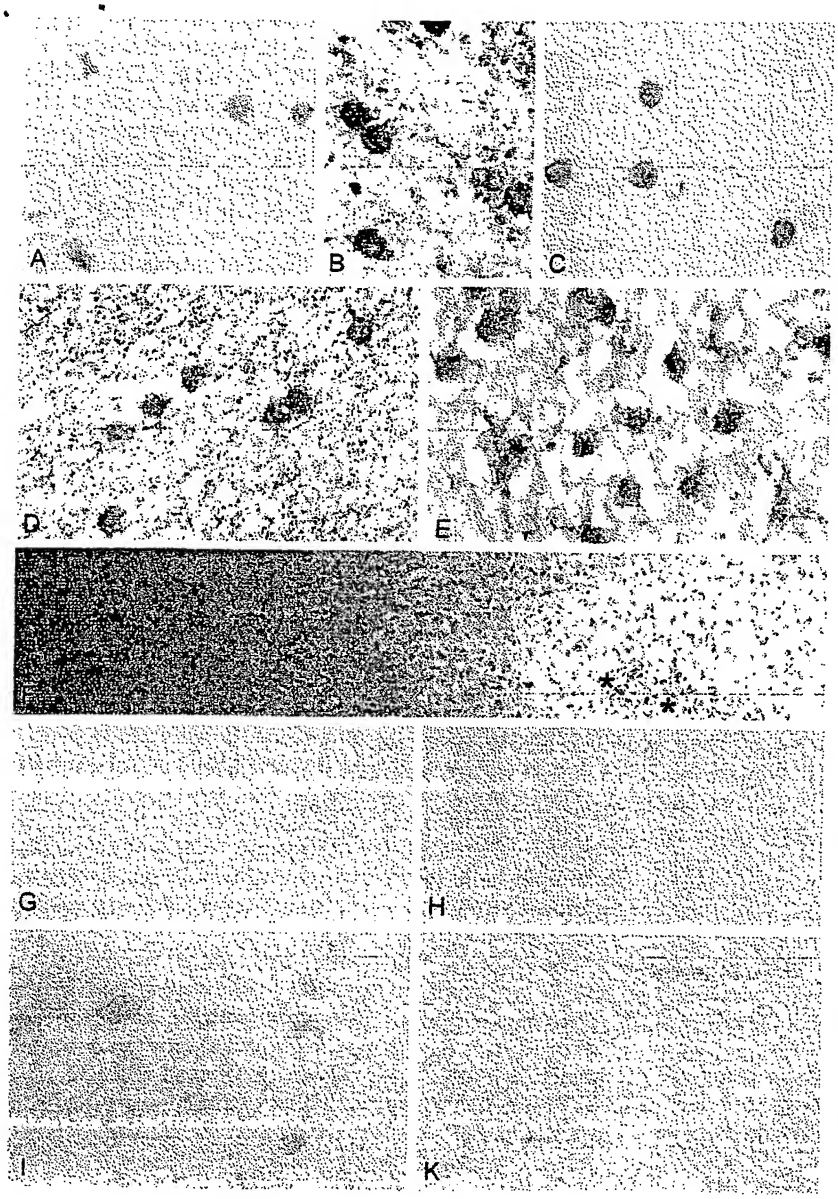

Figure 5. Glutamate transporter expression in human white matter. (A and C) Immunohistochemical staining of normal human white matter with EAAT-1 (A) and EAAT-2 (C) reactivity. Transporters were localized predominantly on oligodendrocytes. Astrocytic staining was limited and more commonly seen with EAAT-1 immunolabeling. (B) The identity of the respective cell types was confirmed by double labeling with the oligodendrocyte phenotypic marker (2',3'-cyclic nucleotide 3'-phosphohydrolase) and EAAT-2. (D and D) In situ hybridization using digoxigenin-labeled cDNA probe to show mRNA expression for EAAT-1 (D) and EAAT-2 (E). As with immunostaining of glutamate transporter protein, oligodendrocytes were identified as the most prevalent in situ hybridization–reactive cell type. (F) Hematoxylin/eosin staining of the active multiple sclerosis (MS) lesion on which the immunohistochemical staining (below) was performed. From left to right: normal-appearing white matter, lesion edge, and active lesion center containing infiltrates (asterisk). (G and H) Immunostaining of the center of an early active MS lesion with EAAT-1 (G) and EAAT-2 (H). Both EAAT-1 and EAAT-2 reactivity is minimal, occurring on astroglial cells. (I and J) White matter adjacent to early active MS lesion is labeled with EAAT-1 (I) and EAAT-2 (J) antibodies. EAAT-1 immunoreactivity is largely preserved and is seen on oligodendrocytes (right) and astrocytes (center left). In contrast, expression of EAAT-2 is faint and markedly downregulated on oligodendrocytes. ×750 (A to E); ×160 (F); ×750 (G to K).

electrical activity[26] and astrocytes through a controlled Ca^{2+}-dependent process.[27] In addition, in conditions such as brain hypoxia and hypoglycemia, astroglial release of glutamate, due to either cellular swelling[28] or altered ion gradients (i.e., reversed transport),[29] has been observed. Moreover, in inflammatory diseases of white matter such as MS, excessive glutamate release can occur from activated macrophages and microglia.[19,30]

In MS white matter, where axons and oligodendrocytes are thought to be major targets of glutamate excitotoxicity,[19,31] we have found that glutamate transporters were virtually absent from the center of active MS lesions from which oligodendrocytes had been depleted. Interestingly, the loss of oligodendroglial EAAT-2 extended far into normal-appearing white matter where oligodendrocytes remained viable. This selective loss of EAAT-2 may have a significant impact on glutamate clearance. In oligodendrocyte cultures, glutamate transport was substantially blocked by a selective EAAT-2 inhibitor, DHK, suggesting that glutamate uptake in oligodendrocytes was largely facilitated by EAAT-2. Thus, these findings underscore the likelihood of a glutamate imbalance at the periphery of MS lesions where EAAT-2 was selectively reduced.

The degree of reduction in EAAT-2 expression appeared proportionate to lesion inflammation, thus implicating a diffusible mediator. Studies in vitro showed TNFα to reduce both EAAT-2 expression and glutamate uptake. The effect of TNFα was not the result of cytotoxicity as this same cytokine was found to have no detectable effect on cell viability at the concentration used. Similar studies on astrocytes

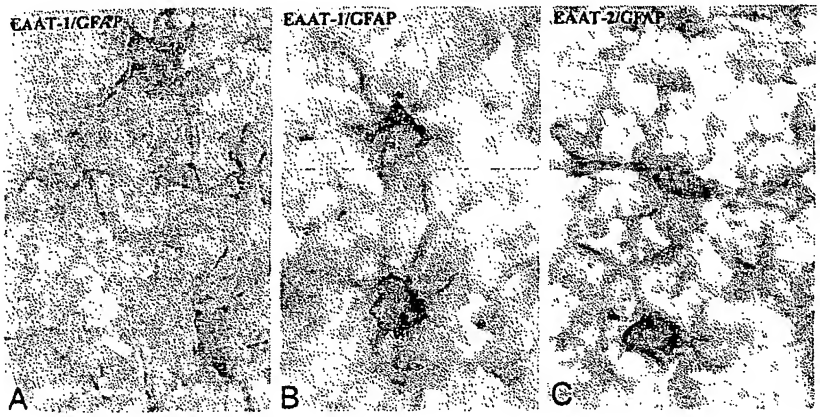

Figure 6. Glutamate transporter expression on astrocytes in white matter. (A) Immunocytochemical staining for glial fibrillary acidic protein (GFAP; brown) and EAAT-1 (blue) in deep white matter reveals astrocytes to be GFAP-positive only. The tissue is taken from a chronic active multiple sclerosis (MS) lesion. (B) In the same case of MS, two astrocytes in the superficial layers of the subcortical white matter display double staining for GFAP (brown) and EAAT-1 (blue). (C) In a section adjacent to that used in (B), double staining in a similar area of subcortical white matter is seen for GFAP and EAAT-2 on astrocytes. The frequency of EAAT-2-positive astrocytes was less than that for EAAT-1. ×750.

have demonstrated an inhibition of glutamate uptake after incubation with TNFα.[23,32] This effect was suggested to be mediated by a mechanism involving nitric oxide.[33] However, TNFα was not found to interfere with glutamate transporters directly as their expression after TNFα treatment remained unaltered. This discrepancy might be due to different regulatory mechanisms for glutamate transporters in oligodendrocytes and astrocytes.

As TNFα is a major proinflammatory cytokine in the active MS lesion,[34] its presence may set the stage for its interference in glutamate transporter expression, leading to reduced glutamate uptake. The existence of a gradient in the reduction of EAAT-2 as one moves out of the lesion area corresponded with the pattern of TNFα reactivity that is maximal at the growing edge of the lesion. Thus, we propose that one of the pathogenic activities of TNFα in MS may be via its induction of glutamate excitotoxicity by reducing glial uptake of glutamate.

Together with our previous work,[19] the results are consistent with the notion that oligodendrocytes are important players in glutamate uptake in human white matter. In MS, we speculate that TNFα may cause oligodendrocytes to lose this function within the environment of the lesion. It is apparent that the observed glutamate excitotoxicity in MS may be open to manipulation at least at two levels, that is, at the level of a down-regulator of glutamate retrieval (e.g., TNFα) and at the level of the glutamate receptor, where blockage has been shown to ameliorate CNS disease.[20] The addition of a key role for glutamate transporters in the pathogenesis of the MS lesion provides yet another important avenue for therapeutic exploration.

Acknowledgment

The authors thank Drs. Barbara Cannella, Steffi Gaupp, Susanna Weerth, Kakuri Omari, and Herbert H. Schaumburg for helpful discussion, Miriam Pakingan and Everett Swanson for technical assistance, and Patricia Cobban-Bond for administrative assistance.

References

1. Lipton SA, Rosenberg PA. Excitatory amino acids as a final common pathway for neurologic disorders. N Engl J Med 1994;330:613–622.
2. Choi DW. Excitotoxic cell death. J Neurobiol. 1992;9:1261–1276.
3. McDonald JW, Althomsons SP, Hyrc KL, Choi DW, Goldberg MP. Oligodendrocytes from forebrain are highly vulnerable to AMPA/kainate receptor-mediated excitotoxicity. Nat Med 1998;3:291–297.
4. Storck T, Schulte S, Hofmann K, Stoffel W. Structure, expression, and functional analysis of a Na(+)-dependent glutamate/aspartate transporter from rat brain. Proc Natl Acad Sci USA 1992;89:10955–10959.
5. Pines G, Danbolt NC, Bjoras M et al. Cloning and expression of a rat brain L-glutamate transporter. Nature 1992;360:464–467.
6. Kanai Y, Hediger MA. Primary structure and functional characterization of a high-affinity glutamate transporter. Nature 1992;360:467–471.
7. Fairman WA, Vandenberg RJ, Arriza JL, Kavanaugh MP, Amara SG. An excitatory amino-acid transporter with properties of a ligand-gated chloride channel. Nature 1995;375:599–603.
8. Arriza JL, Eliasof S, Kavanaugh MP, Amara SG. Excitatory amino acid transporter 5, a retinal glutamate transporter coupled to a chloride conductance. Proc Natl Acad Sci USA 1997;94:4155–4160.
9. Lehre KP, Levy LM, Ottersen OP, Storm-Mathisen J, Danbolt NC. Differential expression of two glial glutamate transporters in the rat brain: quantitative and immunocytochemical observations. J Neurosci 1995;15:1835–1853.
10. Rothstein JD, Martin L, Levey AI, et al. Localization of neuronal and glial glutamate transporters. Neuron 1994;13:713–725.
11. Schmitt A, Asan E, Puschel B, Jons T, Kugler P. Expression of the glutamate transporter GLT-1 in neural cells of the rat central nervous system: non-radioactive in situ hybridization and comparative immunocytochemistry. Neuroscience 1996;71:989–1004.
12. Schousboe A, Hertz L. Role of astroglial cells in glutamate homeostasis. Adv Biochem Psychopharmacol 1981;27:103–113.
13. Furuta A, Martin LJ, Lin CL, Dykes-Hoberg M, Rothstein JD. Cellular and synaptic localization of the neuronal glutamate transporters excitatory amino acid transporter 3 and 4. Neuroscience 1997;81:1031–1042.
14. Mennerick S, Dhond RP, Benz A, et al. Neuronal expression of the glutamate transporter GLT-1 in hippocampal microcultures. J Neurosci 1998;18:4490–4499.
15. Grunert U, Martin PR, Wassle H. Immunocytochemical analysis of bipolar cells in the macaque monkey retina. J Comp Neurol 1994;348: 607–627.
16. Domercq M, Sanchez-Gomez MV, Areso P, Matute C. Expression of glutamate transporters in rat optic nerve oligodendrocytes. Eur J Neurosci 1999;11:2226–2236.
17. Kondo K, Hashimoto H, Kitanaka J, et al. Expression of glutamate transporters in cultured glial cells. Neurosci Lett 1995;188:140–142.
18. Reynolds R, Herschkowitz N. Uptake of [^{3}H]GABA by oligodendrocytes in dissociated brain cell culture: a combined autoradiographic and immunocytochemical study. Brain Res 1984;322:17–31.
19. Werner P, Pitt D, Raine CS. Multiple sclerosis: altered glutamate homeostasis in lesions correlates with oligodendrocyte and axonal damage. Ann Neurol 2001;50:169–180.
20. Pitt D, Werner P, Raine CS. Glutamate excitotoxicity in a model of multiple sclerosis. Nat Med 2000;6:67–70.
21. Komminoth P, Merk FB, Leav I, Wolfe HJ, Roth J. Comparison of ^{35}S- and digoxigenin-labeled RNA and oligonucleotide probes for in situ hybridization. Expression of mRNA of the seminal vesicle secretion

protein II and androgen receptor genes in the rat prostate. Histochemistry 1992;98:217–228.
22. Volterra A, Trotti D, Cassutti P, et al. High sensitivity of glutamate uptake to extracellular free arachidonic acid levels in rat cortical synaptosomes and astrocytes. J Neurochem 1992;59:600–606.
23. Fine SM, Angel RA, Perry SW, et al. Tumor necrosis factor alpha inhibits glutamate uptake by primary human astrocytes. J Biol Chem 1996;271:15303–15306.
24. Reynolds R, Herschkowitz N. Selective uptake of neuroactive amino acids by both oligodendrocytes and astrocytes in primary dissociated culture: a possible role for oligodendrocytes in neurotransmitter metabolism. Brain Res 1986;371:253–266.
25. Torp R, Danbolt NC, Babaie E, et al. Differential expression of two glial glutamate transporters in the rat brain: an in situ hybridization study. Eur J Neurosci 1994;6:936–942.
26. Kriegler S, Chiu SY. Calcium signaling of glial cells along mammalian axons. J Neurosci 1993;13:4229–4245.
27. Bezzi P, Volterra A. A neuron–glia signalling network in the active brain. Curr Opin Neurobiol 2001;11:387–394.
28. Kimelberg HK, Goderie SK, Higman S, Pang S, Waniewski RA. Swelling-induced release of glutamate, aspartate and taurine from astrocyte cultures. J Neurosci 1990;10:1583–1591.
29. Szatkowski M, Barbour B, Attwell D. Nonvesicular release of glutamate from glial cells by reversed electrogenic glutamate uptake. Nature 1990;348:443–446.
30. Piani D, Frei K, Do KQ, Cuenod M, Fontana A. Murine brain macrophages induced NMDA receptor mediated neurotoxicity in vitro by secreting glutamate. Neurosci Lett. 1991;133:159–162.
31. McDonald JW, Althomsons SP, Hyrc KL, Choi DW, Goldberg MP. Oligodendrocytes from forebrain are highly vulnerable to AMPA/kainate receptor-mediated excitotoxicity. Nat Med 1998;4:291–297.
32. Chao CC, Hu S. Tumor necrosis factor-alpha potentiates glutamate neurotoxicity in human fetal brain cell cultures. Dev Neurosci. 1994;16:172–179.
33. Hu S, Sheng WS, Ehrlich LC, Peterson PK, Chao CC. Cytokine effects on glutamate uptake by human astrocytes. Neuroimmunomodulation 2000;7:153–159.
34. Raine CS. The Norton Lecture. A review of the oligodendrocyte in the multiple sclerosis lesion. J Neuroimmunol 1997;77:135–152.

0026-895X/07/7206-1508–1521$20.00
MOLECULAR PHARMACOLOGY

Mol Pharmacol 72:1508–1521, 2007

Vol. 72, No. 6
3898/3277936
Printed in U.S.A.

Resveratrol (*trans*-3,5,4′-Trihydroxystilbene) Ameliorates Experimental Allergic Encephalomyelitis, Primarily via Induction of Apoptosis in T Cells Involving Activation of Aryl Hydrocarbon Receptor and Estrogen Receptor

Narendra P. Singh, Venkatesh L. Hegde, Lorne J. Hofseth, Mitzi Nagarkatti, and Prakash Nagarkatti

Department of Pathology, Microbiology & Immunology, University of South Carolina School of Medicine (N.P.S., V.L.H., M.N., P.N.); and Department of Basic Pharmaceutical Sciences, South Carolina College of Pharmacy (L.J.H.), University of South Carolina, Columbia, South Carolina

Received June 12, 2007; accepted September 13, 2007

ABSTRACT

Resveratrol (*trans*-3,5,4′-trihydroxystilbene), a polyphenolic compound found in plant products, including red grapes, exhibits anticancer, antioxidant, and anti-inflammatory properties. Using an animal model of multiple sclerosis (MS), we investigated the use of resveratrol for the treatment of autoimmune diseases. We observed that resveratrol treatment decreased the clinical symptoms and inflammatory responses in experimental allergic encephalomyelitis (EAE)-induced mice. Furthermore, we observed significant apoptosis in inflammatory cells in spinal cord of EAE-induced mice treated with resveratrol compared with the control mice. Resveratrol administration also led to significant down-regulation of certain cytokines and chemokines in EAE-induced mice including tumor necrosis factor-α, interferon-γ, interleukin (IL)-2, IL-9, IL-12, IL-17, macrophage inflammatory protein-1α (MIP-1α), monocyte chemoattractant protein-1 (MCP-1), regulated on activation normal T-cell expressed and secreted (RANTES), and Eotaxin. In vitro studies on the mechanism of action revealed that resveratrol triggered high levels of apoptosis in activated T cells and to a lesser extent in unactivated T cells. Moreover, resveratrol-induced apoptosis was mediated through activation of aryl hydrocarbon receptor (AhR) and estrogen receptor (ER) and correlated with up-regulation of AhR, Fas, and FasL expression. In addition, resveratrol-induced apoptosis in primary T cells correlated with cleavage of caspase-8, caspase-9, caspase-3, poly(ADP-ribose) polymerase, and release of cytochrome *c*. Data from the present study demonstrate, for the first time, the ability of resveratrol to trigger apoptosis in activated T cells and its potential use in the treatment of inflammatory and autoimmune diseases including, MS.

Resveratrol (*trans*-3,5,4′-trihydroxystilbene), a nonflavinoid polyphenolic compound found in a large number of plant products including mulberries, peanuts, and red grapes (Jang et al., 1997), is a member of the class of plant antibiotic compounds produced as a part of a plant's defense system against fungal infection (Soleas et al., 1997). In recent years, it got attention not only for its usefulness in "French Paradox" as a phytoestrogen agent (Kopp, 1998) but also for its anticancer (Clément et al., 1998; Bernhard et al., 2000; Dörrie et al., 2001; Delmas et al., 2003; Atten et al., 2005), antioxidant (Kim et al., 2006b; Notas et al., 2006; Ovesn á et al., 2006), and an anti-inflammatory properties (Donnelly et al., 2004; de la Lastra and Villegas, 2005; Cignarella et al., 2006; Notas et al., 2006). Resveratrol is also an essential

This work was funded in part by National Institutes of Health grants P01-AT003961, R01-ES09098, R01-DA016545, R01-AI053703, R01-HL058641, R21-DA014885, and F31-ES11562, by A. D. Williams Trust Funds (to N.P.S.), and by an American Cancer Society Institutional Grant (to N.P.S.).
Article, publication date, and citation information can be found at http://molpharm.aspetjournals.org.
doi:10.1124/mol.107.038984.

ABBREVIATIONS: resveratrol, *trans*-3,5,4′-trihydroxystilbene; AP-1, activator protein-1; AhR, aryl hydrocarbon receptor; ER, estrogen receptor; ConA, concanavalin A; mAb, monoclonal antibody; TNF-α, tumor necrosis factor-α; INF-γ, interferon-γ; IL, interleukin; RANTES, regulated on activation normal T-cell expressed and secreted; MIP, macrophage inflammatory protein; MCP, monocyte chemoattractant protein; Z-, *N*-benzyloxycarbonyl-; FMK, fluoromethyl ketone; PARP, poly(ADP-ribose) polymerase; HRP, horseradish peroxidase; Ab, antibody; TUNEL, terminal deoxynucleotidyl transferase dUTP nick-end labeling; ANF, α-naphthoflavone; DMSO, dimethyl sulfoxide; TCDD, 2,3,7,8-tetrachlorodibenzo-*p*-dioxin; MOG, myelin oligodendrocyte glycoprotein; PCR, polymerase chain reaction; ELISA, enzyme-linked immunosorbent assay; BSA, bovine serum albumin; DC, dendritic cell; bp, base pair(s); TAM, tamoxifen; $DiOC_6$, 3,3′-dihexyloxacarbocyanine iodide; PI, propidium iodide; KO, knockout; $\Delta\psi_m$, mitochondrial membrane potential.

component of Ko-jo-kon, an oriental medicine used to treat diseases of the blood vessels, heart (Celotti et al., 1996; Soleas et al., 1997), and liver (Soleas et al., 1997).

Resveratrol has been the focus of recent studies of its pharmacological and beneficial properties on a wide range of diseases, including neurological, hepatic, cardiovascular, and autoimmune (Baur and Sinclair, 2006). Resveratrol has been shown to exhibit anti-inflammatory properties, and the possible mechanisms include inhibition of synthesis and release of pro-inflammatory mediators, modification of eicosanoid synthesis, and/or blockade of inducible nitric-oxide synthase and cyclo-oxygenase-2 pathways via its inhibitory effects on nuclear factor-κB or activator protein-1 (AP-1) (de la Lastra and Villegas, 2005). Resveratrol has been shown to improve health and survival of mice on a high-calorie diet and was found to mediate its effects through insulin sensitivity, reduced insulin-like growth factor-1 levels, increased AMP-activated protein kinase and peroxisome proliferator-activated receptor-γ coactivator 1α activity, increased mitochondrial number, and improved motor function (Baur et al., 2006). The beneficial effects of resveratrol have led to introduction of resveratrol as a nutritional supplement in the market and its extensive use.

Several reports demonstrate that resveratrol induces apoptosis in various cancer cells (Clément et al., 1998; Bernhard et al., 2000; Dörrie et al., 2001; Delmas et al., 2003; Atten et al., 2005). Although resveratrol has been shown to induce apoptosis in various cancer cells, the precise mechanisms and pathways involved in apoptosis of cancer cells are not similar. There are reports demonstrating that resveratrol acts as a ligand for aryl hydrocarbon receptor (AhR) and promotes translocation of AhR from cytosol to the nucleus and binding to DNA at dioxin-responsive elements of various genes (Casper et al., 1999). Resveratrol has also been shown to interact with estrogen receptors (ER) and acts as a mixed agonist-antagonist for ER (Gehm et al., 1997; Bowers et al., 2000). In addition, resveratrol has been shown to trigger CD95 signaling-dependent apoptosis in human tumor cells (Clément et al., 1998; Delmas et al., 2003). Dörrie et al. (2001) have shown that resveratrol induces apoptosis by depolarizing mitochondrial membrane and activating caspase-9 in acute lymphoblastic leukemia cells. Resveratrol may also induce FasL-related apoptosis through Cdc42 activation of ASK1/c-Jun NH_2-terminal kinase-dependent signaling pathway in human leukemia HL-60 cells (Su et al., 2005).

In the current study, we demonstrate for the first time that the anti-inflammatory properties of resveratrol can be attributed, at least in part, to its ability to induce apoptosis in activated T cells. Furthermore, using a murine model of MS, we demonstrate that resveratrol can ameliorate the inflammation and clinical disease of EAE.

Materials and Methods

Mice. We purchased C57BL/6 (H-2^b), AhR KO on C57BL/6 background, B6.129P2Esr1 (ER-α KO), and B6.129P2Esr2 (ER-β KO) mice from The Jackson Laboratory (Bar Harbor, ME). OT II.2a (C57BL/6-TgN (OT-II.2a)-RAG1^{tm1Mom}) mice were purchased from Taconic Farms (Garmantown, NY). The animals were housed in University of South Carolina Animal facility. Care and maintenance of the animals were in accordance with the declaration of Helsinki and according to guide for the care and use of laboratory animals as adopted by Institutional and National Institutes of Health guidelines.

Cell Line. EL4 (mouse T lymphoma cell line) cells, maintained in complete RPMI 1640 medium supplemented with 10% heat-inactivated fetal bovine serum, 10 mM L-glutamine, 10 mM HEPES, and 100 μg/ml penicillin/streptomycin at 37°C and 5% CO_2, were used in this study.

Reagents and Antibodies. RPMI 1640, L-glutamine, HEPES, Gentamicin, Dulbecco's modified Eagle's medium, phosphate-buffered saline (PBS), and fetal bovine serum, were purchased from Invitrogen (Carlsbad, CA). ConA was purchased from Sigma-Aldrich (St. Louis, MO). The following mAbs were purchased from BD Pharmingen (San Diego, CA): anti-mouse IgG-PE, FcBlock, CD3-PE (chain) purified anti-FasL (k-10), anti-FasL-PE (Kay-10), and anti-Fas-PE (Jo2). Inhibitors against caspase 3 (Z-DEVD), caspase 8 (Z-IETD-FMK), and caspase 9 (Z-LEHD-FMK) were purchased from R & D Systems (Minneapolis, MN). The primary Abs caspase-2, caspase-3, caspase-8, caspase-9, cytochrome *c*, PARP, Bax, Bad, Bcl-xl, c-FLIP (all from Cell Signaling Technologies, Danvers, MA), Bid (R & D Systems), and β-actin (Sigma-Aldrich) for Western blots were used. HRP-conjugated secondary Ab was purchased from Cell Signaling Technologies (Danvers, MA). RNeasy Mini kit and iScript cDNA synthesis kit were purchased from QIAGEN (Valencia, CA). Epicenter's PCR premix F and Platinum *Taq* Polymerase kits were purchased from Invitrogen. TUNEL kits were purchased from Roche (Indianapolis, IN). α-Naphthoflavone (ANF), an antagonist for AhR, and tamoxifen, an antagonist for ER, were purchased from Sigma-Aldrich. Resveratrol was purchased from Sigma-Aldrich. Resveratrol suspended in DMSO was used in the in vitro studies. 2,3,7,8-Tetrachlorodibenzo-*p*-dioxin (TCDD) was a generous gift from Dr. K Chae (National Institute of Environmental Health Sciences, Research Triangle Park, NC). TCDD dissolved in DMSO was used in the in vitro studies.

Effect of Resveratrol on Experimental Autoimmune Encephalomyelitis (EAE) in Mice. EAE was induced in C57BL/6 mice (8–10 weeks old) by subcutaneous immunization with 100 μl of 20 mg or 150 mg of myelin oligodendrocyte glycoprotein (MOG_{35-55}) peptide emulsified in complete Freund's adjuvant (Difco, Detroit, MI) containing 4 mg/ml killed *Mycobacterium tuberculosis* (strain H37Ra; Difco). After immunization, 400 ng of pertussis toxin (Sigma-Aldrich) was i.p. injected into mice on Days 0 and 2. Next, the mice received resveratrol (100 mg/kg of body weight) on a daily basis after day 2. Resveratrol was administered as a suspension in water (0.2 ml) by oral gavage. Body weight and clinical score (0, no symptoms; 1, limp tail; 2, partial paralysis of hind limbs; 3, complete paralysis of hind limbs or partial hind and front limb paralysis; 4, tetraparalysis; 5, moribund; 6, death) were recorded on daily basis. The mean clinical score was calculated for each group every day.

Histopathological Examination of EAE. Spinal cords from control or resveratrol treated mice were collected 25 days after immunization. The spinal cord was fixed, paraffin blocks were prepared, microtome sections were generated, and tissue sections were stained using hematoxylin and eosin. The sections were examined for inflammatory cell infiltrates under a microscope.

In Situ Apoptosis in Spinal Cord of EAE Mice. Spinal cords from control or resveratrol-treated mice were collected 25 days after immunization. The spinal cord was fixed, paraffin blocks were prepared, microtome sections were generated, and in situ TUNEL assays were performed (DeadEnd Colorometric TUNEL System, Promega, Madison, WI) on tissue sections. The sections were examined for apoptosis in inflammatory cell infiltrates under a microscope.

Detection of Foxp3 Expression by RT-PCR. Total RNAs from spleen harvested from EAE mice treated with vehicle or resveratrol were prepared using the RNeasy minikit (QIAGEN, Germantown, MD). First-strand cDNA synthesis was performed in a 20-μl reaction mix containing 2 μg total RNA using iScript Kit and following the protocol of the manufacturer (Bio-Rad Laboratories, Hercules, CA). After first-strand synthesis, 2 μl (10% of the reaction volume) was

used as a template for PCR amplification. To detect the expression of Foxp3, forward (5′-GGG GAA GCC ATG GCA ATA GTT-3′) and reverse (5′-TGA AGT AGG CGA ACA TGC GAG TAA-3′) primers specific to mouse Foxp3 were used. PCR was performed for 35 cycles using the following conditions: 30 s at 95°C (denaturing temperature), 40 s at 56.7°C (annealing temperature), and 60 s at 72°C (extension temperature), with a final incubation at 72°C for 10 min. The PCR products, generated from mouse Foxp3 primer pairs, were normalized against PCR products generated from β-actin (427 bp) forward (5′-AAG GCC AAC CGT GAA AAG ATG ACC-3′) and reverse (5′-ACC GCT CGT TGC CAA TAG TGA TGA-3′) primers after electrophoresis on 1.5% agarose gel and visualization with UV light. The band intensity of PCR products was determined using Bio-Rad image analysis system (Bio-Rad Laboratories).

Determination of Various Cytokines/Chemokines in Serum. Blood was collected on day 25 from vehicle or resveratrol-treated EAE mice. Various cytokines/chemokines present in blood serum were determined using Bio-Plex cytokine assay kit and according to the protocol of the company (Bio-Rad).

Determination of Anti-MOG Antibody in Serum. Blood samples were collected on day 25 from control (MOG) and resveratrol-treated (MOG + resveratrol) mice and anti-MOG antibody in blood sera was determined by performing ELISA. In brief, ELISA was performed in 96-well ELISA plates (BD Biosciences, San Jose, CA). The wells were coated with MOG peptide (1 mg/ml, 50 ml/well) in coating buffer (50 mM carbonate-bicarbonate buffer, pH 9.6) for 2 h at room temperature followed by overnight at 4°C. Blocking was done using 2% BSA in PBS for 1 h at room temperature. Wells were washed three times using wash buffer (PBS/0.05% Tween 20) followed by incubation with "serum" diluted in wash buffer containing 1% BSA for 2 h at room temperature. After washing, wells were further incubated together with secondary antibody (goat anti-mouse IgG-peroxidase conjugate) diluted 1:20,000 in wash buffer containing 1% BSA. After washing, ABTS substrate solution was added for color development and the plate was read at 405 nm using a microplate reader. Values are represented after appropriate blank corrections.

Detection of Resveratrol-Induced Apoptosis in Primary T Cells. To determine resveratrol-induced apoptosis in primary T cells, T cells from C57BL/6 mice were purified from the spleens using nylon wool column (Polysciences, Inc., Warrington, PA) followed by depletion of B cells and macrophages. The purity of T cells was more than 90% as determined by flow cytometry (Cytomics FC 500; Beckman Coulter). T cells, unactivated or activated with ConA (2.5 μg/ml) for 24 h, were treated with vehicle (DMSO) or different concentrations (1–100 μM) of resveratrol for 12 to 24 h. Apoptosis in unactivated or activated T cells after resveratrol exposure was determined by performing TUNEL assays (fluorescein isothiocyanate-dUTP nick-end labeling) using In situ Cell-Death Detection kit (Roche, Indianapolis, IN) as described previously (Camacho et al., 2004; Camacho et al., 2005) and/or using fluorescein isothiocyanate-labeled Annexin V and PI kit and following the company's protocol (BD Pharmingen). In some experiments, purified T cells were cultured in the absence or presence of ConA and mature syngeneic dendritic cells (DCs), generated from bone marrow of C57BL/6 mice as described previously (Inaba et al., 1992) for 24 h, and apoptosis was determined 24 h after vehicle or resveratrol treatment. Furthermore, we also examined resveratrol-induced apoptosis in antigen-specific activated T cells. For analysis of ovalbumin peptide (Ova323–339: ISQAVHAAHAEINEAGR)-specific activated T cells, we used purified T cells from OT.II.2a mice and cultured them in the absence or presence of mature syngeneic DCs pulsed with agonist ovalbumin peptide for 2 days followed by treatment with vehicle or resveratrol for 24 h and analyzed for proliferation and apoptosis. To investigate the effect of resveratrol on MOG-specific activated T cells, mice were immunized into the footpads with MOG (150 μg/mice) + Freund's complete adjuvant. Seven days after immunization, popliteal-draining lymph nodes were harvested, single-cell suspensions were prepared, and the cells (5×10^5/well) were cultured in the presence of MOG (10 μg/ml) + various doses (10–50 μM) of resveratrol or vehicle for 3 days in vitro. Proliferation was determined by incorporation of [^{3}H]thymidine.

Reverse Transcriptase PCR to Determine the Expression of AhR, Fas, and FasL in T Cells. Total RNA was isolated from unactivated or ConA-activated primary T cells treated with vehicle (DMSO) or resveratrol using RNeasy Mini Kit and following the protocol of the company (QIAGEN). First-strand cDNA synthesis was performed in a 20-μl reaction mix containing 2 μg of total RNA using iScript Kit and following the protocol of the manufacturer (Bio-Rad Laboratories). After first-strand synthesis, 2 μl (10% of the reaction volume) was used as a template for PCR amplification. To detect the expression of mouse-specific AhR (482 bp), FasL (435 bp), and Fas (486 bp), the protocols described previously (Singh et al., 2007) were followed. The PCR products, generated from mouse AhR, Fas, and FasL primer pairs, were normalized against PCR products generated from mouse 18S forward (5′-GCC CGA GCC GCC TGG ATA C-3′) and reverse (5′-CCG GCG GGT CAT GGG AAT AAC-3′) primers after electrophoresis on 1.5% agarose gel and visualization with UV light. The band intensity of PCR products was determined using Bio-Rad Laboratories image analysis system.

Determination of the Role of AhR in Resveratrol-Induced T-Cell Apoptosis. To determine the role of AhR in resveratrol-mediated early signaling, we performed a series of in vitro assays using T cells from wild-type (C57BL/6) and AhR knock out (AhR KO) mice. In brief, purified T cells from wild-type or AhR KO mice were not activated or activated with ConA (2.5 μg) for 24 h and then treated with vehicle (DMSO) or resveratrol (5–50 μM). Apoptosis in T cells 12 and/or 24 h after resveratrol treatments was determined by performing TUNEL assays and using flow cytometry as described previously (Camacho et al., 2004, 2005). Furthermore, 1 μM/ml ANF, an antagonist for AhR, was added in the culture of wild-type T cells 1 h before resveratrol treatment. The role of AhR in resveratrol-mediated early signaling was further determined by performing luciferase assays in the presence mouse Fas or FasL promoter in an expression vector (pGL-3) as described previously (Singh et al., 2007). Luciferase expression was also determined in the absence or presence of ANF, an antagonist for AhR, in the culture. Data from three to four independent experiments were depicted as mean fluorescence units ± S.E.M.

Determine the Role of ER in Resveratrol-Induced T-Cell Apoptosis. To determine the role of ER in resveratrol-mediated early signaling, we performed a series of in vitro assays using T cells from wild-type (C57BL/6) and ER-α and ER-β knockout mice. In brief, purified T cells from wild-type and ER-α and ER-β knockout mice, unactivated or activated with ConA (2.5 μg) for 24 h, were treated with vehicle (DMSO) or resveratrol (5–50 μM). Apoptosis in T cells was determined by performing TUNEL assays and using flow cytometry 24 h after resveratrol treatments. Furthermore, 1 μM tamoxifen (TAM), an antagonist for ER, was added in the culture of wild-type T cells 1 h before resveratrol treatment and apoptosis was determined. The role of ER in resveratrol-mediated signaling was further determined by performing luciferase assays in the presence mouse Fas or FasL promoter in an expression vector (pGL-3) as described previously (Singh et al., 2007). Luciferase expression was also determined in the absence or presence of TAM. Data from three to four independent experiments were depicted as mean fluorescence units ± S.E.M.

Role of FasL in Resveratrol-Induced T-Cell Apoptosis. Primary T cells from C57BL/6 mice were cultured in the absence or presence of antibody against mouse FasL (5 μg/ml) 1 h before resveratrol treatment. Apoptosis in T cells 24 h after resveratrol treatments was determined by performing TUNEL assays as described previously (Camacho et al., 2004, 2005). At least three independent experiments were performed and the data shown represent one representative experiment. Data from three to four independent experiments were also depicted as mean fluorescence units ± S.E.M.

Analysis of Caspase 3/7, Caspase 8, and Caspase 9 Activity. Caspases 3/7, 8, and 9 were measured in T cells exposed to resveratrol using the Apo-ONE Homogeneous Caspase-3/7, caspase-8, and caspase-9 Assays according to manufacturer's instructions (Promega, Madison, WI). In brief, ConA-activated T cells were treated with various concentrations (5–50 μM) of resveratrol or vehicle (DMSO) for 24 h at 37°C, 5% CO_2. The following day, the cells were collected and used for caspase assays. A Wallac 1420 multilabel counter, Victor^2 (PerkinElmer Life and Analytical Sciences, Waltham, MA) was used to measure the relative fluorescence units of

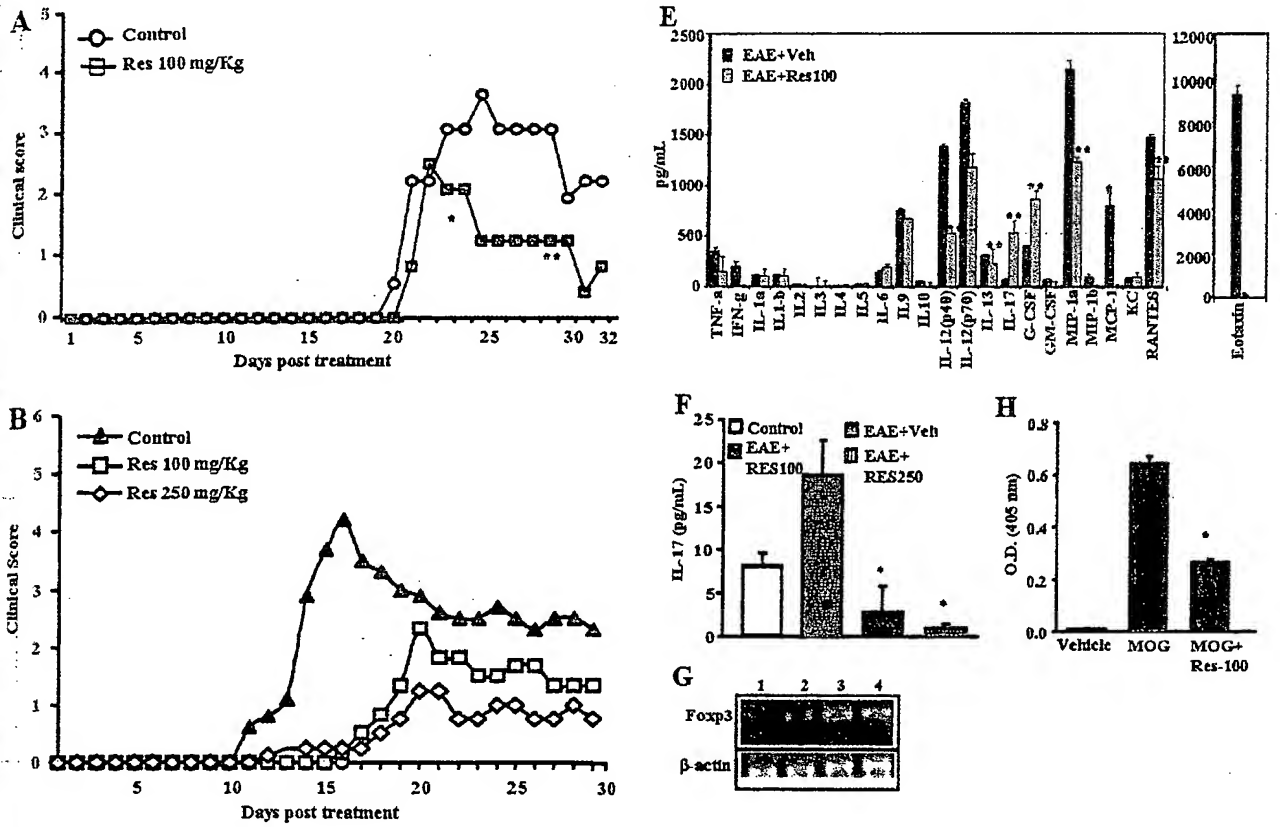

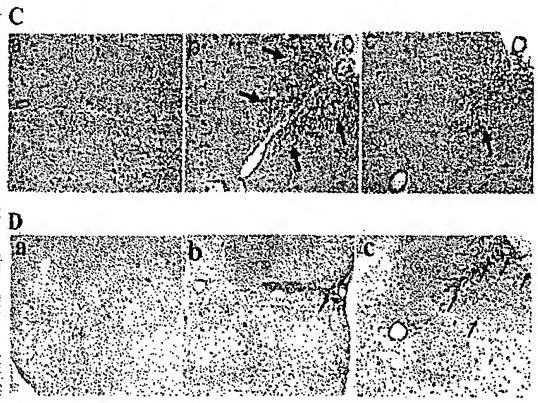

Fig. 1. Resveratrol treatment diminishes clinical symptoms of EAE. A and B, C57BL/6 mice were immunized with 20 μg (A) or 150 μg (B) of MOG_{35-55} peptide emulsified in complete Freund's adjuvant and 400 ng of pertussis toxin. These immunized mice received 100 mg/kg (A and B) or 250 mg/kg (B) of resveratrol daily from day 2 until the termination of the experiment. C, images from immunohistopathological examination of spinal cord of EAE-induced mice. Spinal cords were collected from: a, normal mice; b, EAE-induced vehicle-treated mice; c, EAE-induced resveratrol-treated mice. Arrows indicate infiltration of polymorphonuclear cells. D, in situ TUNEL assays for apoptosis in spinal cord of EAE-induced mice. Spinal cords from normal mice (a), EAE-induced vehicle-treated mice (b), EAE-induced resveratrol-treated mice (c) were collected and in situ apoptosis was determined using DeadEnd colometric TUNEL system. E, expression of various cytokines and chemokines in serum of EAE-induced mice on day 25 after immunization that were treated with vehicle or resveratrol. F, expression of cytokine IL-17 in serum of EAE-induced mice on day 9. G, expression of Foxp3 in splenocytes harvested from EAE induced mice (C57BL/6) treated with vehicle or resveratrol on day 25 after immunization. Lane 1, normal spleen; lane 2, MOG + Vehicle; lane 3, MOG + resveratrol (100 mg/kg), and lane 4: MOG + resveratrol (500 mg/kg). β-Actin was used as a positive control. H, presence of anti-MOG antibody in the sera of EAE induced mice (C57BL/6) treated with vehicle or resveratrol on day 25 after immunization. Data represent mean ± S.E.M. of six animals and asterisks (*) represent significant differences between resveratrol-treated groups compared with vehicle controls.

each sample at an excitation wavelength of 485 nm and at an emission wavelength of 535 nm. Luminescence of caspase-8 and caspase-9 was measured using Wallac 1420 multilabel counter, Victor^2 (PerkinElmer Life and Analytical Sciences). Data from three to four independent experiments were depicted as mean fluorescence units ± S.E.M.

Caspase Blocking Assays to Determine the Role of Various Caspases in Resveratrol-Induced T-Cell Apoptosis. To investigate the role and participation of caspases in resveratrol-induced apoptosis in primary T cells, we performed in vitro assays as described above (under *Detection of Resveratrol-Induced Apoptosis in Primary T Cells*) with inhibitors specific to mouse caspase-3 (Z-DEVD), caspase-8 (Z-IETD-FMK), and caspase-9 (Z-LEHD-FMK) at a concentration of 20 μM. The cells were incubated with various caspase inhibitors for at least 1 h before resveratrol treatment. T cells were harvested 24 h after vehicle or resveratrol treatment, and TUNEL assays were performed to determine apoptosis as described previously (Camacho et al., 2004, 2005). At least three independent experiments were performed and the data shown represent one of the experiments.

Immunoblot Analysis. Immunoblotting was performed as described previously (Camacho et al., 2005). The source of antibodies was as follows (all from Cell Signaling Technologies unless otherwise specified): caspase-2 (1:1000; Alexis Laboratories, San Diego, CA), caspase-3, caspase-8, and caspase-9 (1:2000), Bid, (1:1000; R & D Systems), cytochrome *c* (1:2000), PARP (1:2000), Bax (1:2000), Bad (1:2000; Cell Signaling), Bcl-xl (1:2000), Smac (1:2000), c-FLIP (1:2000), and β-actin (1:50,000; Sigma-Aldrich). HRP-conjugated secondary Ab was used at 1:4000 dilution (Cell Signaling Technologies). Lysates from resveratrol-treated cells were prepared by freezing and thawing, and the protein concentration was measured using standard Bradford assay (Bio-Rad Laboratories). The proteins were fractionated in SDS-polyacrylamide gel electrophoresis and transferred onto polyvinylidene difluoride membranes using a dry-blot apparatus (Bio-Rad Laboratories). The membrane was incubated in blocking buffer for 1 h at room temperature, followed by incubation in primary antibody at 4°C overnight. The membrane was then washed three times (10–15 min) with washing buffer (PBS + 0.2% Tween 20) and incubated for 1 h in HRP-conjugated secondary antibody (Cell Signaling Technology) in blocking buffer. The membranes were then washed several times and incubated in developing solution (equal volume of solution A and B; ECL Western blotting detection reagents; GE Healthcare, Chalfont St. Giles, Buckinghamshire, UK) and signal was detected using ChemiDoc System (Bio-Rad Laboratories). Densitometric analyses of the Western blots were performed using ChemiDoc software (Bio-Rad Laboratories).

Analysis of Mitochondrial Membrane Potential. Mitochondrial membrane potential ($\Delta\psi_m$) of T cells after vehicle (DMSO) or resveratrol treatment was determined using 3,3′-dihexyloxacarbocyanine iodide ($DiOC_6$) dye as described previously (Camacho et al., 2004, 2005). Propidium iodide (PI) was used to differentiate the dead cells. At least three independent experiments were performed.

Statistical Analysis. Results presented here represent at least three independent experiments and are presented as the mean ± S.E.M. Statistical analyses were performed using Student's *t* test or two-factor ANOVA as appropriate, with a *P* value of ≤ .05 considered to be statistically significant. For EAE, significant difference between control and experimental groups was determined using the Mann-Whitney *U* test (*, $p < 0.01$).

Results

Resveratrol Suppressed the Development of EAE in Mice. Resveratrol is known to exhibit anti-inflammatory properties. In the current study, therefore, we investigated whether resveratrol would be effective in the tretament of EAE, a model for human multiple sclerosis. To this end, EAE was induced in C57BL/6 mice (8–10 weeks of age) by subcutaneous immunization with 100 μl of 20 μg MOG_{35-55} peptide emulsified in complete Freund's adjuvant containing 4 mg/ml killed *M. tuberculosis*. Next, mice were injected i.p. with 400 ng of pertussis toxin on days 0 and 2. These mice received

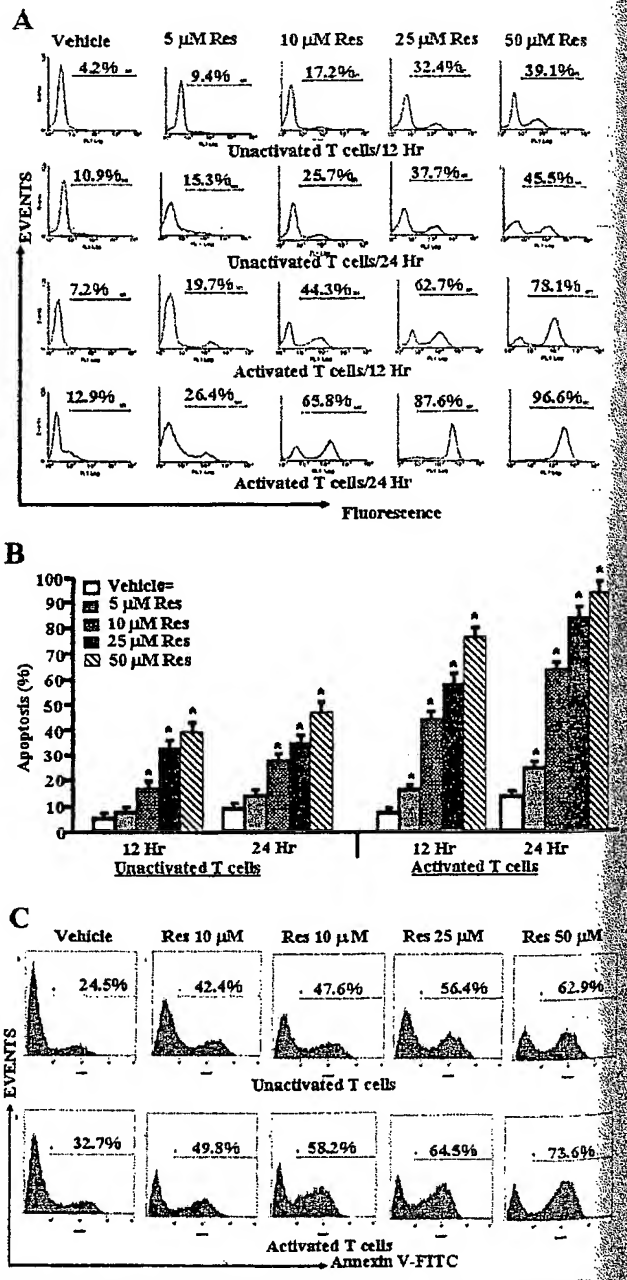

Fig. 2. Resveratrol triggers apoptosis in primary T cells. Purified primary T cells from C57BL/6 mice were activated or not with ConA for 24 h followed by treatment with resveratrol or vehicle for 12 to 24 h (A–C). cells were analyzed for apoptosis by TUNEL assays (A and B) and Annexin V/PI (C). A demonstrates representative experiment for apoptosis and B shows mean ± S.E.M. of four independent experiments. C demonstrates representative experiment on apoptosis determined using Annexin V/PI. Cells stained for Annexin but negative for PI alone have been depicted. We observed 5 to 6% dead (PI-positive) cells (data not shown). Asterisks (*) indicate statistically significant difference between resveratrol-treated groups compared with vehicle controls.

resveratrol (100 mg/kg) daily from day 2 until the termination of experiment. Clinical scores of disease were recorded daily. A mean clinical score was calculated for each group for each day. As seen from Fig. 1A, with 20 μg of MOG, the symptoms started to develop around day 19 and resveratrol at 100 mg/kg caused significant suppression of clinical symptoms of EAE ($p < 0.001$; by Mann-Whitney U test). For example, in resveratrol-treated mice, the clinical scores never reached above 2, whereas in control mice, the score reached a peak of 4. The clinical score correlated well with histopathological data showing that there was a dose-dependent decrease in inflammatory response seen in the spinal cord of EAE-induced mice that were administered resveratrol (Fig. 1C). Next, we tested whether resveratrol would be effective against EAE induced with a higher dose of MOG, which triggers an early onset of clinical disease. To this end, we repeated experiments described above except that we injected a higher dose of MOG (150 μg) and tested the effect of resveratrol at two doses (100 and 250 mg/kg body weight). In these experiments we noted that the vehicle-treated mice showed symptoms of paralysis much earlier, by day 10 (Fig. 1B). It is noteworthy that when similar groups of MOG-injected mice were treated with resveratrol, there was not only a delay in the onset of the symptoms (> 6 days) but also a dramatic, dose-dependent reduction in the clinical disease (Fig. 1B; $p = 0.0094$ by Mann-Whitney U test). Resveratrol was more effective in delaying the onset of clinical disease when EAE was induced using a higher dose of MOG. This might be because the anti-inflammatory properties of res-

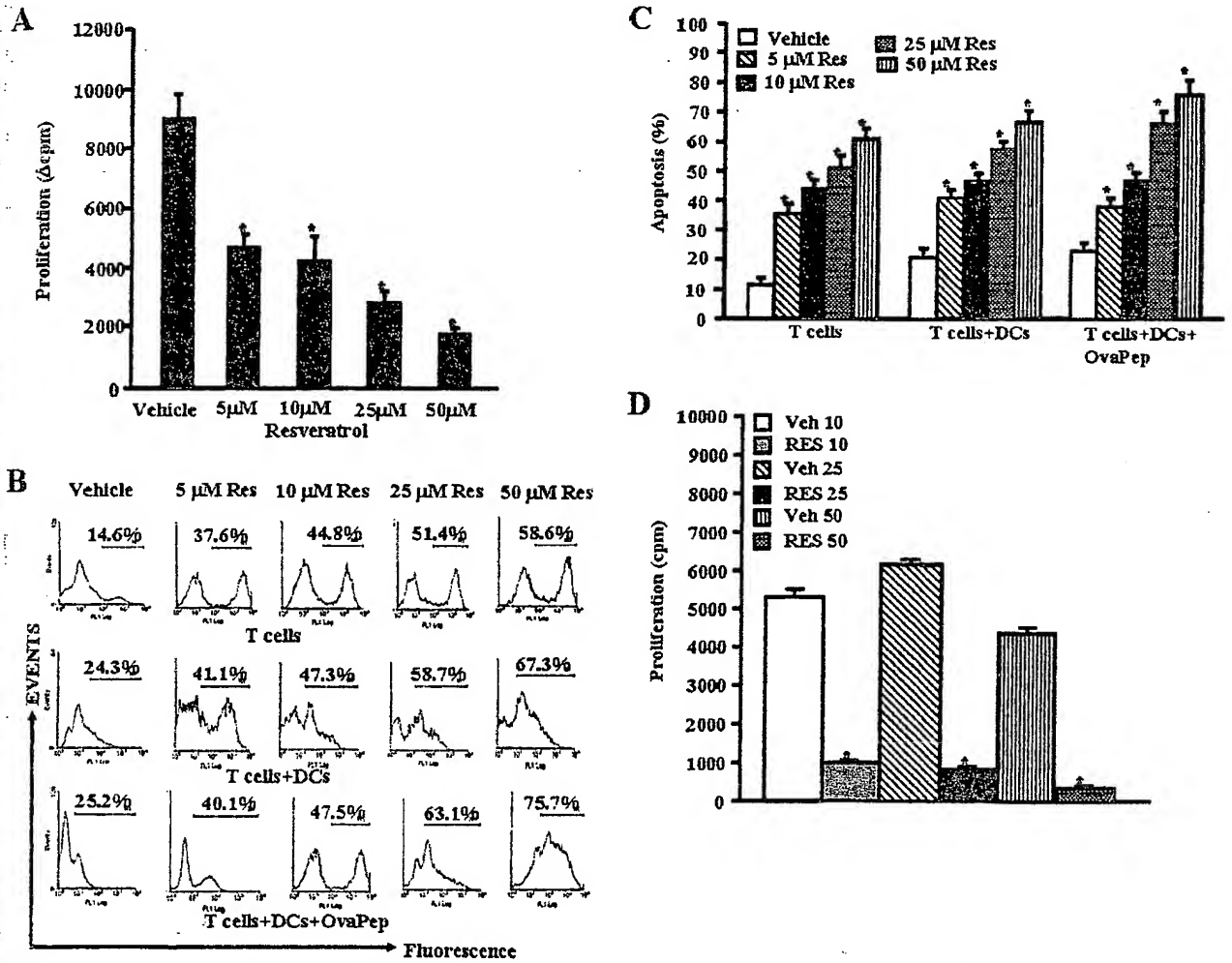

Fig. 3. Resveratrol causes apoptosis in antigen-specific activated T cells in vitro. Purified primary T cells from OT.II.2a mice were activated with ovalbumin-specific peptide (ISQAVHAAHAEINEAGR) by coculturing T cells and peptide-pulsed mature DCs for 2 days and then treated with various doses of resveratrol (5–50 μM; A–C). Proliferation of T cells was determined by [^{3}H]thymidine incorporation (A) 24 h after resveratrol or vehicle exposure and apoptosis as determined by TUNEL assays (B and C). A represents mean ± S.E.M. of triplicate cultures and data were expressed as change in counts per minute. Asterisks (*) represent significant difference in proliferation of antigen-specific (ova-peptides) activated OT.II.2a T cells treated with resveratrol compared with vehicle controls. B is a representative of three independent TUNEL assays, and C represents mean ± S.E.M. of three independent TUNEL experiments and asterisks (*) represent significant difference in apoptosis between resveratrol-treated groups compared with vehicle controls. D, popliteal draining lymph nodes were harvested from mice immunized with MOG (150 μg/mice) on day 7 and cultured in the presence of MOG (10 μg/ml) and vehicle or resveratrol (10–50 μM) for 3 days. Proliferation of lymph node cells was determined by [^{3}H]thymidine incorporation (D). D represents mean ± S.E.M. of triplicate cultures. Asterisks (*) represent significant difference in proliferation of MOG-specific activated lymph node cells treated with resveratrol compared with vehicle controls.

veratrol may be more effective at early stages of administration, an aspect that needs further investigation.

Resveratrol-Mediated Apoptosis Reduced Inflammatory Cells in Spinal Cord. Histological studies revealed that resveratrol treatment significantly inhibited the inflammation induced by MOG (Fig. 1C, compare b and c). Next, we performed in situ TUNEL assays to determine apoptosis in migrating inflammatory cells in spinal cord as described under *Materials and Methods*. When we counted the number of apoptotic cells at sites of inflammation at 20 different fields using a microscope, we noted six apoptotic cells in untreated mice, 17 in MOG + vehicle-treated mice and 49 in MOG + resveratrol-injected mice (Fig. 1D). These data suggested that presence of less inflammation in spinal cord of resveratrol-treated EAE mice compared with vehicle-treated EAE mice might result from resveratrol-mediated apoptosis in inflammatory cells.

Effect of Resveratrol on Cytokine/Chemokine Profile and Foxp3 Expression in EAE-Induced Mice. Next, we examined the presence of various cytokines in the sera of EAE-induced mice and observed significant reduction in certain cytokines [tumor necrosis factor-α (TNF-α), interferon-γ (INF-γ), interleukin (IL)-2, IL-9, IL-12, IL-17, macrophage inflammatory protein-1α (MIP-1α), monocyte chemoattractant protein-1 (MCP-1), regulated on activation normal T-cell expressed and secreted (RANTES)] and a modest increase in other cytokines (IL-6, IL-17, and granulocyte cell-stimulating factor) in the serum of mice treated with resveratrol (Fig. 1E), compared with vehicle-treated mice with EAE, demonstrating that resveratrol treatment decreased the induction of a majority of cytokines screened. Of particular interest was the demonstration that vehicle-treated mice with EAE exhibited very high levels of eotaxin, which was dramatically decreased after resveratrol treatment. Recent studies have shown that IL-17 plays a critical role in EAE. Thus, we were surprised at the low levels of IL-17 seen during EAE in the serum and the fact that resveratrol did not decrease the levels. This may be because the serum was analyzed for cytokines on day 25 of EAE. It is noteworthy that when we measured the levels of IL-17 on day 9 of EAE, we found that IL-17 levels were increased in vehicle-treated EAE mice and that resveratrol treatment caused a significant decrease in IL-17 levels (Fig. 1F). Furthermore, we also examined the effect of resveratrol on induction of Foxp3, an important

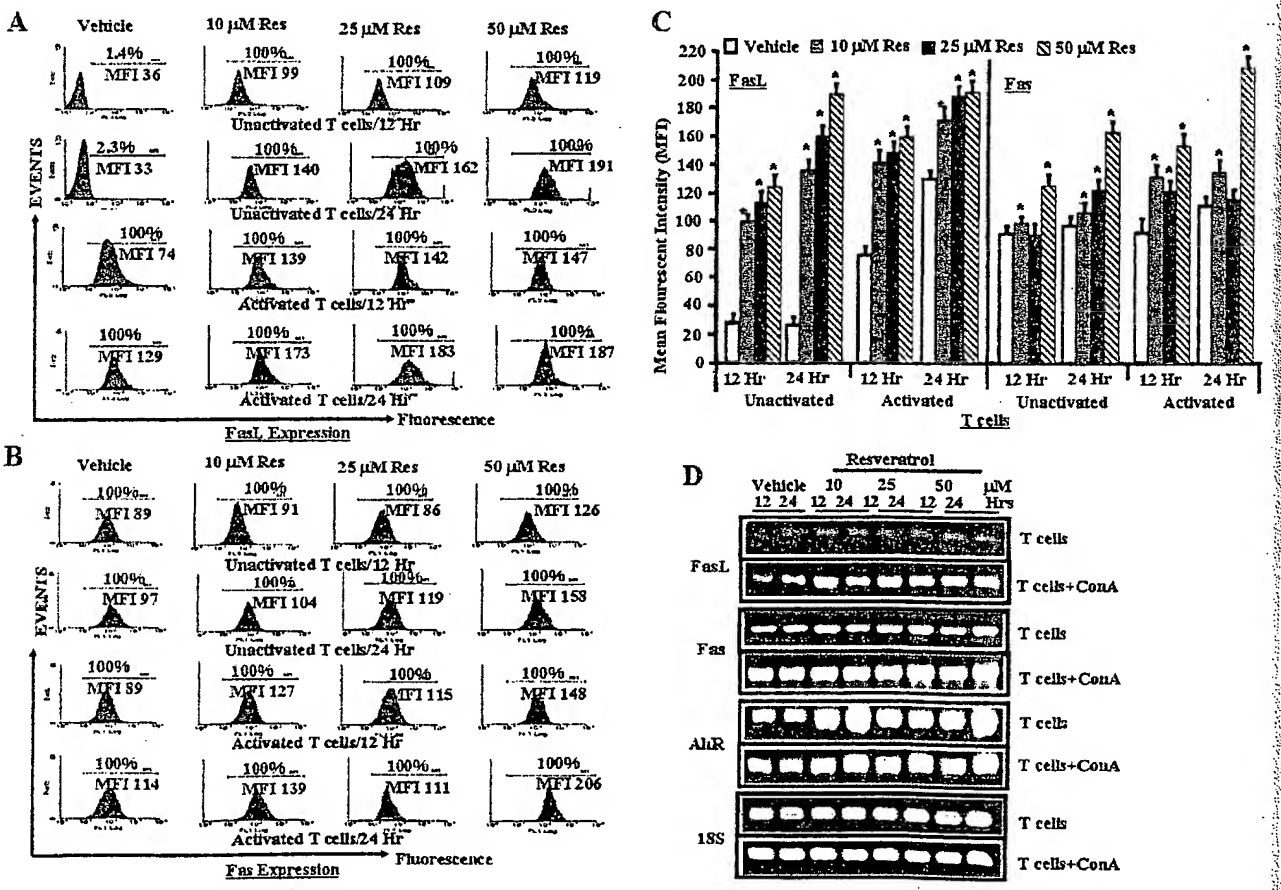

Fig. 4. Role of Fas and FasL in resveratrol-mediated apoptosis in T cells. Expression of Fas and FasL in unactivated or ConA-activated T cells was determined by staining the cells with anti-mouse Fas-PE and anti-mouse FasL-PE antibodies and analyzed by Flow cytometry and RT-PCR. A, expression of FasL in unactivated or ConA-activated T cells 12 and 24 h after resveratrol or vehicle treatment (flow cytometry). B, expression of Fas in unactivated or ConA-activated T cells 12 and 24 h after resveratrol or vehicle treatment. C, mean fluorescent intensity of FasL and Fas expression after resveratrol or vehicle treatment. C represents mean ± S.E.M. of three independent experiments and asterisks (*) represent significant difference between resveratrol-treated groups compared with vehicle controls. D, expression of AhR, Fas, and FasL in unactivated T cells and activated T cells (T cells + ConA) using RT-PCR. 18S, a housekeeping gene, was used as a positive control.

transcription factor of Treg cells during EAE development. We observed significant up-regulation of Foxp3 gene in splenocytes of mice treated with resveratrol, compared with control mice (Fig. 1G).

Effect of Resveratrol on Production of Anti-MOG Antibody in EAE Mice. We determined whether resveratrol had any effect on the production of antibody against MOG peptides in EAE-developing mice. Upon analysis of anti-MOG antibody production, we observed significantly less production of anti-MOG antibody in resveratrol-treated EAE mice compared with vehicle-treated EAE mice (Fig. 1H). These data demonstrated that resveratrol effectively blocked the production of anti-MOG antibody in EAE mice.

Effect of Resveratrol on Unactivated and Activated Primary T Cells. We next performed in-depth analysis of the mode of action of resveratrol using in vitro assays. To this end, purified T cells from C57BL/6 mice were either unactivated or activated with ConA for 24 h and treated with various concentrations of resveratrol (5–100 μM). These concentrations were selected based on pilot studies in which we noted that resveratrol at <5 μM concentrations did not induce significant apoptosis in T cells. First, we determined the survival of primary T cells after resveratrol or vehicle treatments using trypan blue dye and observing the cells under an inverted phase contrast microscope. We observed a statistically significant effect of resveratrol on survival of T cells (data not shown); the total number of viable unactivated or ConA-activated primary T cells was reduced in a dose-dependent manner. However, we observed significantly higher reduction in survival of ConA-activated primary T cells after resveratrol treatment at all doses (data not shown). The data obtained from TUNEL assays demonstrated that primary T cells unactivated or activated with ConA and cultured in the presence of resveratrol underwent apoptosis in a dose-dependent fashion (Fig. 2, A and B). The induction of apoptosis by resveratrol was also confirmed using Annexin V/PI staining (Fig. 2C). We observed 5 to 6% necrotic (PI positive) cells (data not shown). These data demonstrated that resveratrol can induce apoptosis in primary T cells and that activated T cells are more sensitive to resveratrol-induced apoptosis compared with unactivated T cells.

Resveratrol Induced Apoptosis in Antigen-Specific Activated T Cells. Next, we investigated whether resveratrol would induce apoptosis in antigen-specific T cells activated by DCs. To this end, we used purified T cells from OT.II.2a mice, which recognize specific ovalbumin peptides, cultured them alone or in the presence of syngeneic mature DCs or DCs pulsed with agonist ovalbumin peptides (Ova323–339: ISQAVHAAHAEINEAGR) for 3 days and then treated with various concentrations (5–50 μM) of resveratrol for 24 h. The T cell proliferation was measured by thymidine (^{3}H) incorporation and apoptosis in T cells was determined by gating CD3 positive T cells and detecting TUNEL positive T cells. We noted a dose-dependent decrease in antigen-specific T cell proliferation upon resveratrol treatment (Fig. 3A). Using TUNEL analysis, we noted dose-dependent apoptosis in unactivated T cells and in T cells cultured with DCs. Moreover, significant apoptosis was also noted in T cells cultured with DCs + ovalbumin peptide (Fig. 3, B and C). We noted that the levels of apoptosis, particularly at higher concentrations of resveratrol, were slightly higher in cultures consisting of T + DCs + ova compared with T cells alone. However, these differences in susceptibility of antigen-activated T cells versus unactivated T cells were less dramatic than ConA-activated T cells. This may be because in the ova experiments, the T cells had been cultured in vitro for 2 days before resveratrol treatment. Furthermore, upon examination of the effect of resveratrol on MOG-specific activated T cells, we observed significant reduction in proliferation of MOG-specific activated T cells in the presence of resveratrol, compared with vehicle treatment (Fig. 3D). Together, these data demonstrated that antigen-specific activated T cells became more susceptible to resveratrol-induced apoptosis.

Resveratrol Up-Regulated AhR, Fas, and FasL Expression in T Cells. Next, we determined whether resveratrol regulated the expression of AhR, Fas, and FasL in T cells in vitro by staining the cells with mouse-specific anti-Fas and FasL antibodies, respectively, and performing RT-PCR. Vehicle-exposed activated but not unactivated T cells expressed significant levels of FasL (Figs. 4A and C). Furthermore, resveratrol treatment caused significant and dose-dependent increase in FasL in both unactivated and activated T cells (Fig. 4, A and C). We also observed a significant increase in expression of Fas in both unactivated and activated upon resveratrol treatment (Fig. 4, B and C). Data obtained from RT-PCRs for the expression of Fas, and FasL in T cells after reseveratrol/vehicle treatments corroborated flow cytometry

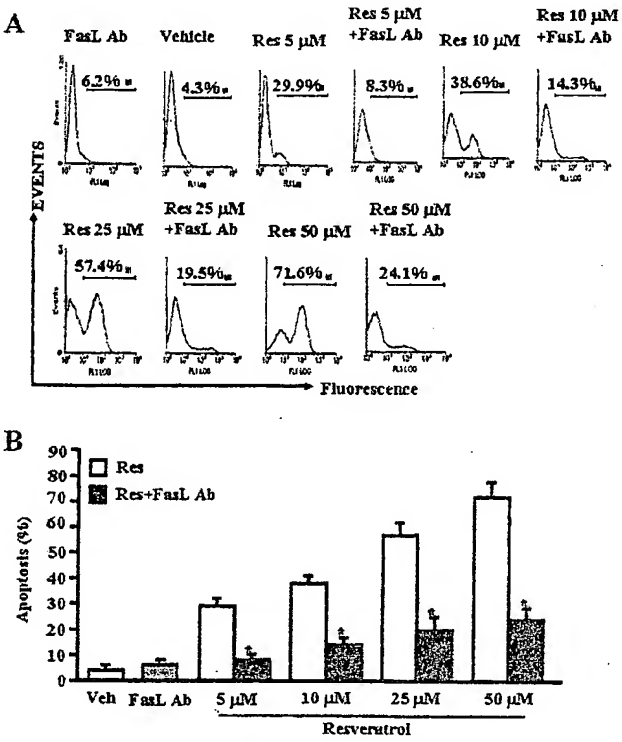

Fig. 5. FasL plays critical role in induction of death-receptor pathway of apoptosis by resveratrol. T cells purified from C57BL/6 (wild-type) mice were activated with ConA and cultured in the presence of vehicle or resveratrol (5–50 μM) and incubated in the absence or presence of mouse-specific anti-FasL Ab. Apoptosis in T cells was determined by TUNEL assays. The data presented in A are representative of three independent experiments. B represents mean of three independent experiments, and asterisks (*) represent significant reduction in resveratrol-induced apoptosis of T cells cultured in the presence of FasL Ab compared with the controls.

data (Fig. 4D). In addition, resveratrol treatment caused a significant increase in expression of AhR in both unactivated and activated T cells, compared with vehicle (DMSO)-treated T cells as determined by RT-PCR (Fig. 4D). We observed similar 18S (a house keeping gene) expression between resveratrol- and vehicle-treated T cells (Fig. 4D).

FasL Played a Significant Role in Initiating Death-Receptor Pathway during Resveratrol-Induced T-Cell Apoptosis. To test the role of FasL in resveratrol-induced apoptosis in T cells, we performed in vitro assays using primary T cells from C57BL/6 mice. Purified T cells were activated with ConA for 24 h followed by culture in the absence or presence of anti-mouse FasL mAb (5 μg/ml). We observed significant reduction in resveratrol-induced T-cell apoptosis when Abs against FasL mAb was added to the culture (Figs. 5A and B). Addition of isotype control Abs failed to exhibit any significant effect on resveratrol-induced apoptosis (data not shown). The data suggested a role for FasL in initiating resveratrol-mediated death-receptor pathway.

Role of AhR In Resveratrol-Induced Apoptosis in T Cells. We tested the role of AhR in resveratrol-induced apoptosis in T cells. To this end, we performed a series of in vitro assays using primary T cells from wild-type (C57BL/6) or AhR KO mice. We observed significantly less resveratrol-induced apoptosis in T cells from AhR KO mice compared with AhR wild-type mice at all resveratrol doses tested (Fig. 6, A and B). Likewise, we observed significant reduction in resveratrol-induced apoptosis in T cells from wild-type mice in the presence of ANF, an antagonist for AhR compared with T cells that were cultured in the absence of ANF (Fig. 5C). These data together demonstrated that AhR plays an important role in initiating early signals leading to resveratrol-induced T-cell apoptosis. Furthermore, upon examination of luciferase expression under the control of mouse Fas or FasL promoter after resveratrol treatments, we observed up-regulation of luciferase expression under the control of Fas or FasL promoter (Fig. 6D), but the expression of luciferase was significantly reduced in the presence of ANF (Fig. 6D) thereby suggesting that AhR activation may regulate the

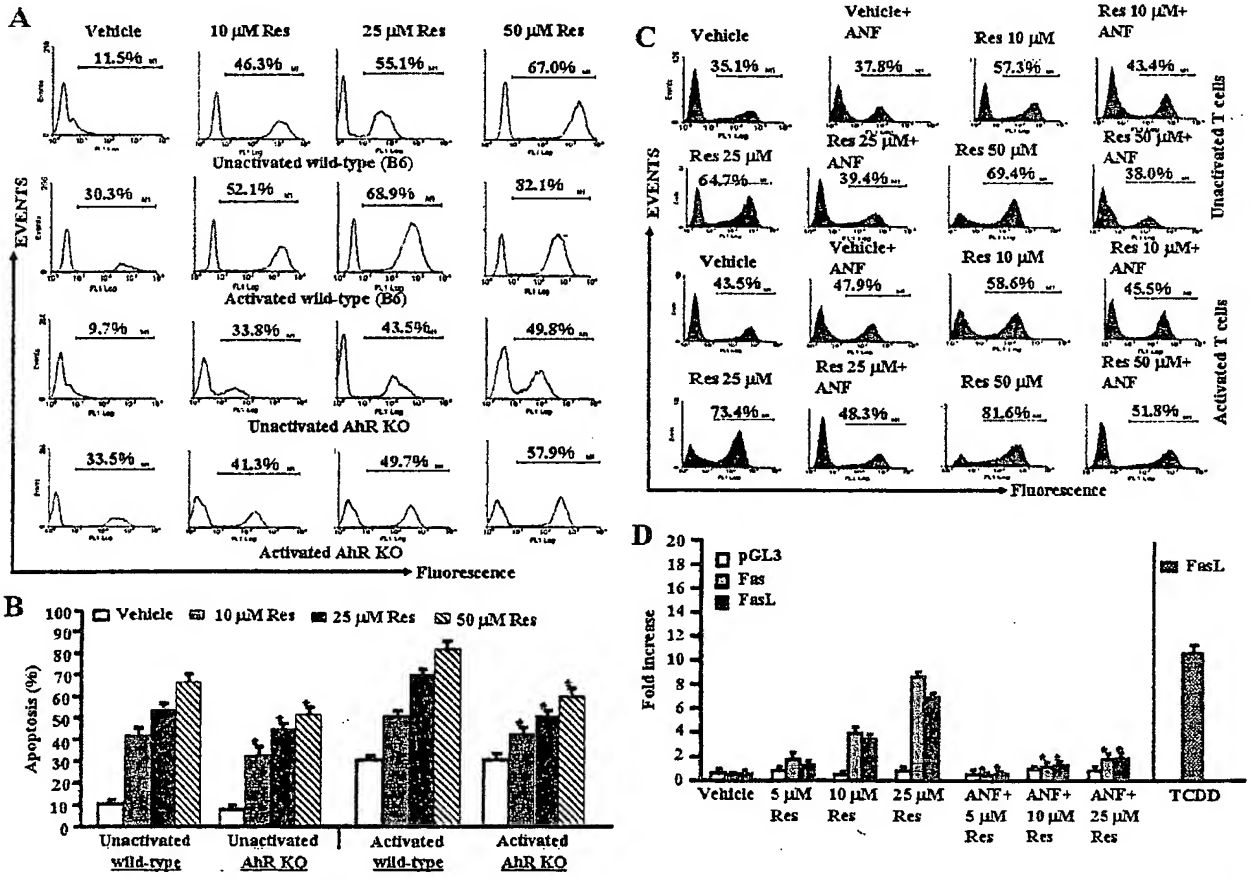

Fig. 6. Role of AhR in resveratrol-induced apoptosis in T cells. A, unactivated or ConA-activated purified T cells from AhR wild-type or AhR KO mice were treated with vehicle or resveratrol, and apoptosis was determined by performing TUNEL assays as described in Fig. 2. B, mean ± S.E.M. of three independent experiments; asterisks (*) represent significant difference of resveratrol-induced apoptosis in AhR KO T cells compared with wild-type T cells. C, unactivated or ConA-activated T cells were cultured with resveratrol (10–50 μM) or vehicle (DMSO) for 24 h in the absence or presence of ANF in the culture and TUNEL assays were performed. The data presented are representative for 3 independent assays. D, ConA-activated EL4 cells were transfected with pGL-3-Fas or pGL-3-FasL promoter, cultured in the presence of resveratrol (5–25 μM) or vehicle for 24 h in the absence or presence of ANF in the culture, and luciferase assays were performed. Data represent mean of three independent experiments, and asterisks (*) indicate significant down-regulation of luciferase expression in the presence of ANF compared with cultures that did not receive ANF. Expression of luciferase in the presence of FasL promoter and treated with TCDD represents positive control.

expression of Fas and FasL by resveratrol. In these experiments, we used TCDD as a positive control because our previous studies demonstrated that it up-regulates FasL expression (Singh et al., 2007). It should be noted that T cells from AhR KO mice did exhibit decreased apoptosis at all doses of resveratrol (Fig. 6, A and B), and ANF was only partially able to block resveratrol-induced apoptosis. These data suggested that in addition to AhR, other molecules might also play a role in initiating resveratrol-induced apoptosis.

Resveratrol Also Used Estrogen Receptor (ER) to Initiate Early Signaling Leading to Apoptosis. To examine the role of ER in resveratrol-induced early signaling, we purified T cells from wild-type (C57BL/6), ER-α, and ER-β KO mice and cultured them in the absence or presence of TAM and treated the cells with vehicle or various concentrations (5–50 μM) of resveratrol. We observed significantly lower resveratrol-induced apoptosis in T cells from ER-α KO, compared with wild-type mice (Figs. 7, A and B). However, we observed no difference in resveratrol-induced apoptosis in T cells from wild-type (Fig. 7A) and ER-β KO mice (Fig. 7B). These data demonstrated that ER-α plays an important role in resveratrol-induced apoptosis. Furthermore, when T cells from wild-type mice were cultured in the presence of TAM and treated the cells with vehicle or various concentrations of resveratrol (10–50 μM), we observed significant reduction in T-cell apoptosis in the presence of TAM (Fig. 7C), further demonstrating the role of ER in resveratrol-induced apoptosis. Because addition of ANF (Fig. 6C) or TAM (Fig. 7C) separately to cultures had partially blocked resveratrol-induced apoptosis, we further investigated the effect of a combination of ANF + TAM (Fig. 7C). The data demonstrated that combination treatment with TAM + ANF completely reversed the resveratrol-induced apoptosis in T cells and brought the apoptosis to the level seen with the vehicle-treated groups. Upon examination of luciferase expression under the control of mouse Fas or FasL promoter after resveratrol treatments, we observed up-regulation of luciferase expression under the control of Fas or FasL promoter (Fig. 7D), but the expression of luciferase was significantly re-

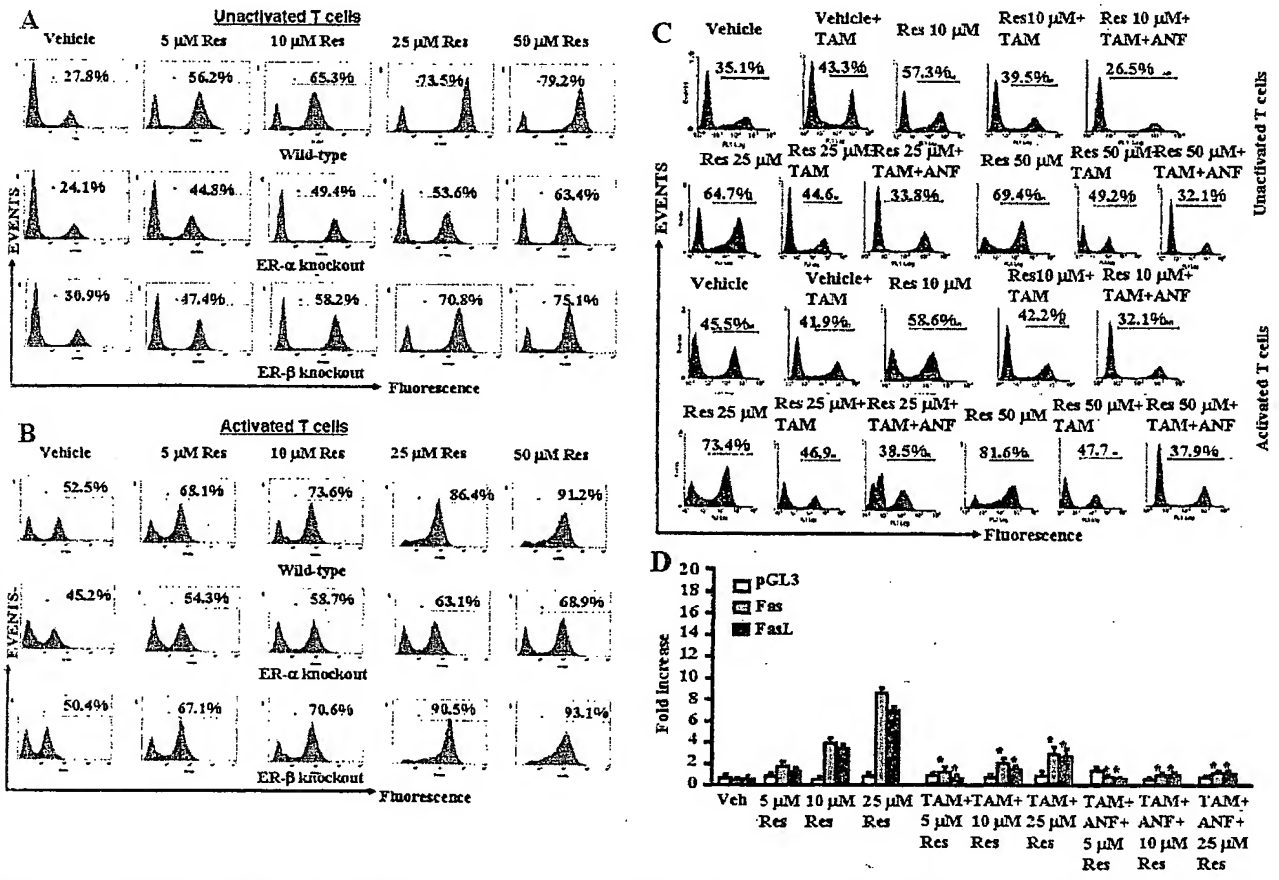

Fig. 7. Role of ER in resveratrol-induced apoptosis in T cells. A, unactivated T cells from wild-type (C57BL/6), ER-α knockout, ER-β knockout mice were cultured in the presence of various concentration (5–50 μM) of resveratrol (Res) or vehicle (DMSO) for 24 h, and TUNEL assays were performed 24 h after treatment. The data presented are representative of three independent assays. B, ConA-activated T cells from wild-type (C57BL/6), ER-α knockout, and ER-β knockout mice were cultured in the presence of various concentration (5–50 μM) of resveratrol (Res) or vehicle (DMSO) for 24 h, and TUNEL assays were performed 24 h after treatment. The data presented are representative of three independent assays. C, unactivated or ConA-activated T cells were cultured with resveratrol (10–50 μM) or vehicle (DMSO) for 24 h in the absence or presence of TAM alone or in combination with ANF (TAM+ANF) in the culture and TUNEL assays were performed. The data presented are representative for three independent assays. D, ConA-activated EL4 cells were transfected with pGL-3-Fas or pGL-3-FasL promoter, cultured in the presence of resveratrol (5–25 μM) or vehicle for 24 h in the absence or presence of TAM alone or in combination of ANF (TAM+ANF) in the culture, and luciferase assays were performed. D, mean ± S.E.M. of three independent experiments; asterisks (*) represent significant down-regulation of luciferase expression compared with controls.

duced in the presence of TAM (Fig. 7D) demonstrating the role of ER in activation of Fas and FasL. Furthermore, a combination of TAM + ANF (Fig. 7D) was further able to decrease the luciferase activity, thereby corroborating the involvement of both ER and AhR in the regulation Fas and FasL by resveratrol.

Resveratrol Triggered Both Death-Receptor (Extrinsic) and Mitochondrial (Intrinsic) Pathways to Cause Apoptosis in T Cells. To investigate the role of various apoptotic pathways in resveratrol-induced T-cell apoptosis, we determined the role of various caspases (caspase-3/7, caspase-8, and caspase-9). Standard enzymatic assays using caspase assays reagents from Promega and following the company's protocols were performed after vehicle or resveratrol exposure of T cells for 24 h. We observed significantly increased caspase enzymatic activities for all three caspases examined in ConA-activated, resveratrol-treated T cells compared with vehicle-treated T cells (Fig. 8A). The role of various caspases was further confirmed by blocking caspase activity using various caspase inhibitors (caspase-3, Z-DEVD; caspase-8, Z-IETD-FMK; and caspase-9; Z-LEHD-FMK). TUNEL assays performed on ConA-activated T cells that were cultured in the presence of various caspase inhibitors and treated with reveratrol (10–50 μM) demonstrated almost complete blocking (~90%) of resveratrol-induced T-cell apoptosis in the presence of caspase-3 inhibitor (Fig. 8B), significant blocking (~65%) in the presence of caspase-8 inhibitor (Fig. 8B), and partial blocking (~50%) in the presence of caspase-9 inhibitor (Fig. 8B). These data demonstrated that resveratrol-induced apoptosis in T cells was caspase-dependent and that caspases-3, -8, and -9 participated in resveratrol-induced T-cell apoptosis.

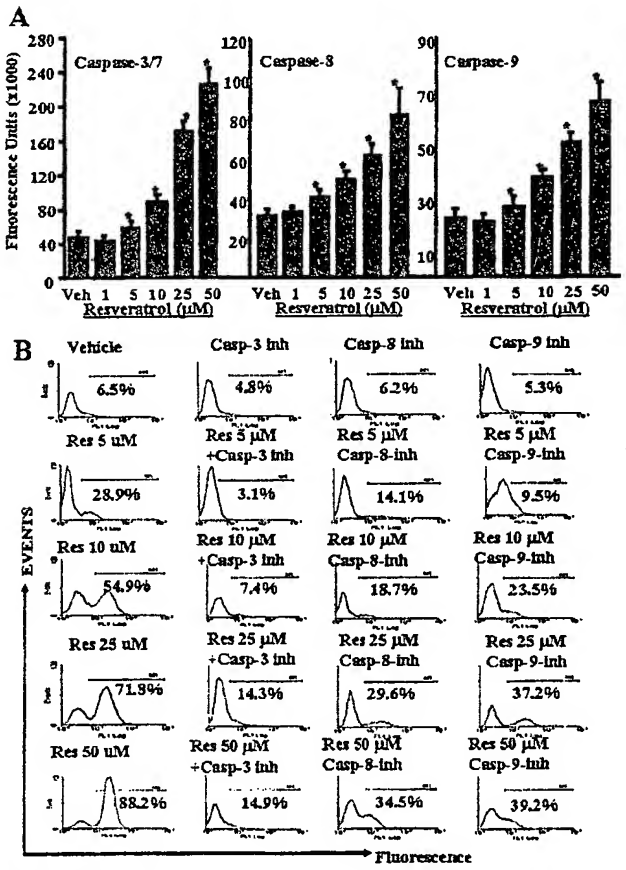

Fig. 8. Resveratrol activates and cleaves various caspases to cause apoptosis in primary T cells. Enzymatic activities of caspase-3/7, -8, and -9 were determined in ConA-activated primary T cells 24 h after resveratrol treatment. A, caspase-3/7, -8, and -9 activities, and the data represent mean of three independent experiments. Vertical bars represent S.E. of three experiments. Asterisks (*) represent statistically significant ($p < 0.02$) increase in enzymatic activities of caspase-3, -8, and -9 in resveratrol-treated groups compared with vehicle-treated T cells. B, ConA-activated T cells were cultured with vehicle or resveratrol in the presence or absence of inhibitors of caspase-3, -8, and -9. The data presented are representative of three independent experiments.

We also examined the expression of BAD, Bcl-xl, and Smac in resveratrol-treated activated T cells and observed significant reductions after resveratrol exposure. These data demonstrated that resveratrol caused decrease in expression of antiapoptotic genes such as Bcl-xl and Smac and thus allowed apoptosis in T cells. As shown in Fig. 9C, cytochrome c was released from mitochondria to cytoplasm in resveratrol-treated T cells, thus demonstrating the role of the mitochondrial pathway in resveratrol-induced T cell apoptosis.

To further corroborate the role of mitochondrial pathway, we examined mitochondrial membrane potential loss ($\Delta\psi_m$) using $DiOC_6$ dye after resveratrol or vehicle treatment. We observed significant reduction in $\Delta\psi_m$ in resveratrol-treated T cells compared with vehicle-treated T cells (Fig. 9D). However even at a high dose of 50 μM resveratrol, we noted moderate levels of reduction in $\Delta\psi_m$ (in ~24% cells), suggesting that mitochondrial pathway plays only a partial role in resveratrol-mediated apoptosis.

Discussion

Multiple sclerosis is an autoimmune disease that affects the central nervous systems of patients and is triggered by myelin-specific T cells that cause inflammation, resulting in demyelinated plaques and neurological symptoms (Sospedra and Martin, 2005). In the current study, we investigated the effect of resveratrol on EAE by triggering the clinical disease in C57BL/6 mice through injection of MOG. We noted that resveratrol treatment had the following beneficial effects on EAE compared with vehicle-treated control mice: 1) Significant decrease in severity and delayed onset of clinical disease (Fig. 1, A and B), 2) presence of less number of inflammatory cells in the spinal cord (Fig. 1C), 3) increased numbers of apoptotic inflammatory cells in the spinal cord (Fig. 1D), 4) down-regulation of a majority of cytokines tested (Fig. 1E) and IL-17 (Fig. 1F), 5) up-regulation of Foxp3 (Fig. 1G), and 6) Reduced anti-MOG antibody production (Fig. 1H). The presence of fewer inflammatory cells in spinal cords of resveratrol-treated EAE-induced mice correlated with increased apoptosis, thereby suggesting that resveratrol may act in vivo through induction of apoptosis in activated T cells. Up-regulation of Foxp3 in resveratrol-treated mice demonstrates an increase in the regulatory T cell activity, which has been shown to play important role in immunosuppression (Hum-

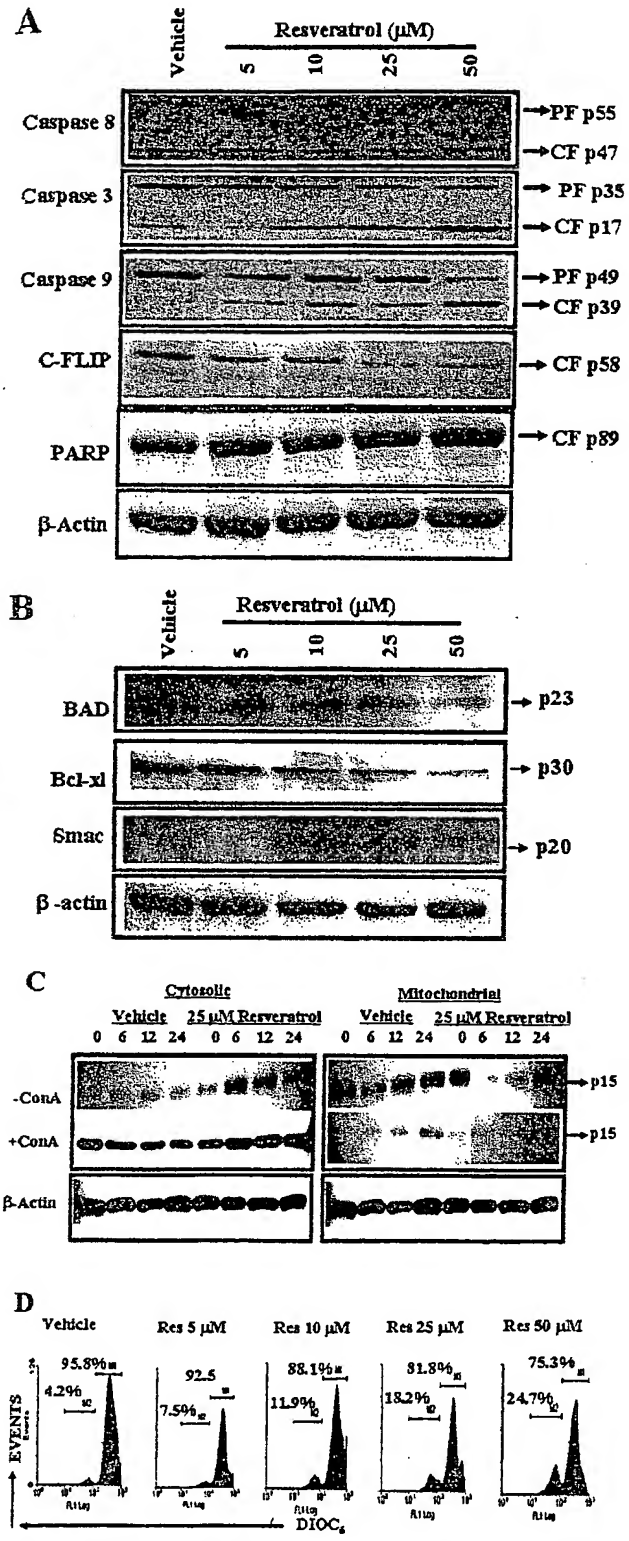

Fig. 9. Resveratrol activates members of death-receptor and mitochondrial pathways. Cell lysates prepared from resveratrol-treated (24 h) unactivated primary T cells (A and B) and unactivated (−ConA) or activated primary T cells (+ConA) (C) were resolved by SDS-polyacrylamide gel electrophoresis and probed with primary Abs against various appropriate molecules. A and B, cell lysates prepared from unactivated and resveratrol-treated T cells were probed with caspase-8, caspase-3, caspase-9, caspase-2, c-FLIP, PARP (A), Bad, Bcl-xl, and Smac (B) antibodies. C, cell lysates prepared from unactivated and ConA-activated and resveratrol-treated T cells were probed with cytochrome c antibodies. β-Actin was used as a control. D, effect of resveratrol on $\Delta\psi_m$ in primary T cells. Unactivated primary T cells were treated with vehicle (DMSO) or resveratrol (5–50 μM) and stained with $DIOC_6$ to evaluate $\Delta\psi_m$. Results are representative of at least three independent experiments.

rich and Riemekasten, 2006; Jiang et al., 2006a,b; Kim et al., 2006a; Seo et al., 2007).

We noted significant reduction in certain cytokines (TNF, IFN-γ, IL-2, IL-9, IL-12, MIP-1α, MCP-1, and RANTES) and a modest increase in other cytokines (IL-6, IL-17, and granulocyte cell-stimulating factor) in serum of EAE-induced mice treated with resveratrol (Fig. 1E). These data are consistent with reports demonstrating resveratrol-mediated suppression of various cytokines such as IFN-γ (Wirleitner et al., 2005), TNF-α, IL-1β, IL-2, and IL-6 (Marier et al., 2005; Schroecksnadel et al., 2005; Wirleitner et al., 2005). Recent studies have shown that IL-17 plays a critical role in induction of EAE (Lock et al., 2002; Iwakura and Ishigame, 2006). It is noteworthy that EAE-bearing mice had low levels of IL-17 and, in fact, resveratrol treatment caused a modest increase in IL-17. This may be because we measured IL-17 much later in the disease course. When we measured the levels of IL-17 on day 9 of EAE, we found that IL-17 levels were increased in vehicle-treated EAE mice and resveratrol treatment caused a significant decrease in IL-17 levels (Fig. 1F). In the central nervous systems of EAE mice, mRNAs for RANTES, eotaxin, MIP-1α, MIP-1β, MIP-2, inducible protein-10, and MCP-1 were detected at disease onset, increased as disease progressed, and fell as clinical signs improved (Rajan et al., 2000). The decrease in cytokines may result from inhibitory effects on nuclear factor-κB and AP-1 (de la Lastra and Villegas, 2005) or induction of apoptosis in T cells, as seen in the current study. Eotaxin, a recently described chemotactic factor belonging to the CC chemokine family, has been implicated in animal and human eosinophilic inflammatory states (Rothenberg et al., 1996; Fukuyama et al., 2000). In the present study, we observed a robust induction of eotaxin in animals exhibiting EAE and a dramatic reduction of eotaxin upon resveratrol treatment (Fig. 1D). At present, we do not know the precise role played by eotaxin in the development of EAE in mice; additional studies are clearly necessary.

Resveratrol has been previously identified as an AhR mixed agonist/antagonist (de Medina et al., 2005). In addition, we have earlier shown that activation of AhR induces Fas and FasL expression and consequent apoptosis in T cells (Camacho et al., 2005). Resveratrol treatment caused significant and dose-dependent increase in FasL in both unactivated and activated T cells (Fig. 4, A and C). We also observed a significant increase in expression of Fas in both unactivated and activated T cells upon resveratrol treatment (Fig. 4, B and C). Data obtained from RT-PCR for the expression of FasL and Fas in T cells after reseveratrol/vehicle treatment corroborated flow cytometry data (Fig. 4D). In addition, resveratrol treatment caused a significant increase in expression of AhR in both unactivated and activated T cells, compared with vehicle-treated T cells as determined by RT-PCR (Fig. 4D). Next, we tested whether up-regulation of Fas and FasL was directly involved in resveratrol-induced

apoptosis. We observed significant reduction in resveratrol-induced apoptosis in T cells in the presence of Abs against FasL (Fig. 5, A and B), whereas isotype control Abs failed to mediate an effect. The data suggested a role for FasL in initiating resveratrol-mediated death-receptor pathway of apoptosis.

In the current study, we noted that AhR played a significant role in resveratrol-induced apoptosis in T cells. However, it should be noted that T cells from AhR KO mice did exhibit decreased apoptosis at all doses of resveratrol (Fig. 6, A and B), and ANF was able to block resveratrol-induced apoptosis only partially, suggesting that other molecules in addition to AhR might also be involved in initiating resveratrol-induced apoptosis.

Resveratrol is a phytoestrogen that exhibits variable degrees of estrogen receptor agonism in different test systems (Gehm et al., 1997). We therefore examined the role of ER in resveratrol-induced apoptosis using T cells from wild-type, ER-α, and ER-β KO mice in the absence or presence of TAM, an ER antagonist. We observed significantly lower resveratrol-induced apoptosis in T cells from ER-α KO compared with wild-type mice (Fig. 7, A–C). However, we observed no significant difference in resveratrol-induced apoptosis in T cells from wild-type and ER-β KO mice (Fig. 7C). These data demonstrated that ER-α plays an important role in resveratrol-induced apoptosis.

Mor et al. (2003) showed that estrogen treatment increased FasL expression in monocytes through the binding of ER to the estrogen responsive elements and AP-1 motifs present on FasL promoter. To test whether resveratrol regulated Fas and FasL promoter activity through AhR and/or ER, we performed luciferase assays in the presence mouse Fas or FasL promoter in an expression vector (pGL-3). We observed that resveratrol induced luciferase expression under the control of Fas or FasL promoter (Figs. 6D and 7D), and the expression of luciferase was significantly reduced in the presence of ANF (Fig. 6D) and TAM (Fig. 7D). In these experiments, we used TCDD, a potent AhR agonist as a positive control shown to up-regulate FasL expression (Singh et al., 2007). Furthermore, a combination of TAM + ANF (Fig. 7D) was further able to decrease the luciferase activity, thereby corroborating the involvement of both AhR and ER in the regulation Fas and FasL by resveratrol.

Upon examination of apoptotic pathways, we noted that both death-receptor (Fas/FasL-mediated) and mitochondrial pathways are involved in resveratrol-induced T-cell apoptosis. However, only a small proportion of apoptotic cells showed loss of mitochondrial membrane potential, and Abs against FasL could almost completely block resveratrol-mediated apoptosis in T cells, both of which suggest that the death receptor pathway may play more critical role and that the mitochondrial pathway may be activated through cross-talk via Bid.

In the current study, we used resveratrol dosed of 10, 100, and 500 mg/kg administered by oral gavage, similar to the doses used in other studies (Gao et al., 2002). Previous in vivo studies to treat cancer suggested that low doses such as 40 mg/kg are not effective, whereas higher doses, such as 80 mg/kg were partially effective (Gao et al., 2002). In another study, resveratrol was shown to inhibit tumor growth in BALB/c mice at 500, 1000 and 1500 mg/kg in a dose-dependent manner when administered for 10 days (Liu et al., 2003). In addition, in a rat model, 100 mg/kg of resveratrol was very effective in delaying tumorigenesis (Bhat et al., 2001). It is feasible to achieve in vivo 25 to 50 μM, a dose that we found to be effective in vitro. Thus, in vivo, doses greater than 100 mg/kg may be necessary to study the efficacy of resveratrol. In addition, in humans, a dose of 1 g of resveratrol has been tested (Zhou et al., 2005).

Use of resveratrol to treat inflammatory and anti-immune diseases may hold significant promise because resveratrol was more effective in inducing apoptosis in activated T cells. Thus, resveratrol may be less toxic to normal immune cells. Data from the current study demonstrate that the anti-inflammatory properties of resveratrol can be attributed, at least in part, to its ability to trigger apoptosis in activated T cells. The current study demonstrates that resveratrol may serve as a novel therapeutic agent against multiple sclerosis.

Acknowledgments

We thank Daniel Sisco and Shweta Hegde for technical help.

References

Atten MJ, Godoy-Romero E, Attar BM, Milson T, Zopel M, and Holian O (2005) Resveratrol regulates cellular PKC alpha and delta to inhibit growth and induce apoptosis in gastric cancer cells. *Invest New Drugs* 23:111–119.

Baur JA, Pearson KJ, Price NL, Jamieson HA, Lerin C, Kalra A, Prabhu VV, Allard JS, Lopez-Lluch G, Lewis K, et al. (2006) Resveratrol improves health and survival of mice on a high-calorie diet. *Nature* 444:337–342.

Baur JA and Sinclair DA (2006) Therapeutic potential of resveratrol: the in vivo evidence. *Nat Rev Drug Discov* 5:493–506.

Bernhard D, Tinhofer I, Tonko M, Hubl H, Ausserlechner MJ, Greil R, Kofler R, and Csordas A (2000) Resveratrol causes arrest in the S-phase prior to Fas-independent apoptosis in CEM-C7H2 acute leukemia cells. *Cell Death Differ* 7:834–842.

Bhat KP, Lantvit D, Christov K, Mehta RG, Moon RC, and Pezzuto JM (2001) Estrogenic and antiestrogenic properties of resveratrol in mammary tumor models. *Cancer Res* 61:7456–7463.

Bowers JL, Tyulmenkov VV, Jernigan SC, and Klinge CM (2000) Resveratrol acts as a mixed agonist/antagonist for estrogen receptors alpha and beta. *Endocrinology* 141:3657–3667.

Camacho IA, Nagarkatti M, and Nagarkatti PS (2004) Evidence for induction of apoptosis in T cells from murine fetal thymus following perinatal exposure to 2,3,7,8-tetrachlorodibenzo-*p*-dioxin (TCDD). *Toxicol Sci* 78:96–106.

Camacho IA, Singh N, Hegde VL, Nagarkatti M, and Nagarkatti PS (2005) Treatment of mice with 2,3,7,8-tetrachlorodibenzo-p-dioxin leads to aryl hydrocarbon receptor-dependent nuclear translocation of NF-kappaB and expression of fas ligand in thymic stromal cells and consequent apoptosis in T cells. *J Immunol* 175:90–103.

Casper RF, Quesne M, Rogers IM, Shirota T, Jolivet A, Milgrom E, and Savouret JF (1999) Resveratrol has antagonist activity on the aryl hydrocarbon receptor: implications for prevention of dioxin toxicity. *Mol Pharmacol* 56:784–790.

Celotti E, Ferrarini R, Zironi R, and Conte LS (1996) Resveratrol content of some wines obtained from dried Valpolicella grapes: Recioto and Amarone. *J Chromatogr A* 730:47–52.

Cignarella A, Minici C, Bolego C, Pinna C, Sanvito P, Gaion RM, and Puglisi L (2006) Potential pro-inflammatory action of resveratrol in vascular smooth muscle cells from normal and diabetic rats. *Nutr Metab Cardiovasc Dis* 16:322–329.

Clément MV, Hirpara JL, Chawdhury SH, and Pervaiz S (1998) Chemopreventive agent resveratrol, a natural product derived from grapes, triggers CD95 signaling-dependent apoptosis in human tumor cells. *Blood* 92:996–1002.

de la Lastra CA and Villegas I (2005) Resveratrol as an anti-inflammatory and anti-aging agent: mechanisms and clinical implications. *Mol Nutr Food Res* 49: 405–430.

de Medina P, Casper R, Savouret JF, and Poirot M (2005) Synthesis and biological properties of new stilbene derivatives of resveratrol as new selective aryl hydrocarbon modulators. *J Med Chem* 48:287–291.

Delmas D, Rebe C, Lacour S, Filomenko R, Athias A, Gambert P, Cherkaoui-Malki M, Jannin B, Dubrez-Daloz L, Latruffe N, et al. (2003) Resveratrol-induced apoptosis is associated with Fas redistribution in the rafts and the formation of a death-inducing signaling complex in colon cancer cells. *J Biol Chem* 278:41482–41490.

Donnelly LE, Newton R, Kennedy GE, Fenwick PS, Leung RH, Ito K, Russell RE, and Barnes PJ (2004) Anti-inflammatory effects of resveratrol in lung epithelial cells: molecular mechanisms. *Am J Physiol Lung Cell Mol Physiol* 287:L774–L783.

Dörrie J, Gerauer H, Wachter Y, and Zunino SJ (2001) Resveratrol induces extensive apoptosis by depolarizing mitochondrial membranes and activating caspase-9 in acute lymphoblastic leukemia cells. *Cancer Res* 61:4731–4739.

Fukuyama S, Inoue H, Aizawa H, Oike M, Kitaura M, Yoshie O, and Hara N (2000) Effect of eotaxin and platelet-activating factor on airway inflammation and hyperresponsiveness in guinea pigs in vivo. *Am J Respir Crit Care Med* 161:1844–1849.

Gao X, Xu YX, Divine G, Janakiraman N, Chapman RA, and Gautam SC (2002)

Disparate in vitro and in vivo antileukemic effects of resveratrol, a natural polyphenolic compound found in grapes. *J Nutr* 132:2076–2081.
Gehm BD, McAndrews JM, Chien PY, and Jameson JL (1997) Resveratrol, a polyphenolic compound found in grapes and wine, is an agonist for the estrogen receptor. *Proc Natl Acad Sci U S A* 94:14138–14143.
Humrich J and Riemekasten G (2006) [Regulatory T cells in rheumatic diseases]. *Dtsch Med Wochenschr* 131:2288–2291.
Inaba K, Inaba M, Romani N, Aya H, Deguchi M, Ikehara S, Muramatsu S, and Steinman RM (1992) Generation of large numbers of dendritic cells from mouse bone marrow cultures supplemented with granulocyte/macrophage colony-stimulating factor. *J Exp Med* 176:1693–1702.
Iwakura Y and Ishigame H (2006) The IL-23/IL-17 axis in inflammation. *J Clin Invest* 116:1218–1222.
Jang M, Cai L, Udeani GO, Slowing KV, Thomas CF, Beecher CW, Fong HH, Farnsworth NR, Kinghorn AD, Mehta RG, et al. (1997) Cancer chemopreventive activity of resveratrol, a natural product derived from grapes. *Science* 275:218–220.
Jiang S, Lechler RI, He XS, and Huang JF (2006a) CD4+CD25+ regulatory T cell therapy for the induction of donor-specific clinical transplantation tolerance. *Expert Opin Biol Ther* 6:1003–1009.
Jiang S, Lechler RI, He XS, and Huang JF (2006b) Regulatory T cells and transplantation tolerance. *Hum Immunol* 67:765–776.
Kim R, Emi M, and Tanabe K (2006a) Cancer immunosuppression and autoimmune disease: beyond immunosuppressive networks for tumour immunity. *Immunology* 119:254–264.
Kim YA, Lim SY, Rhee SH, Park KY, Kim CH, Choi BT, Lee SJ, Park YM, and Choi YH (2006b) Resveratrol inhibits inducible nitric oxide synthase and cyclooxygenase-2 expression in beta-amyloid-treated C6 glioma cells. *Int J Mol Med* 17:1069–1075.
Kopp P (1998) Resveratrol, a phytoestrogen found in red wine. A possible explanation for the conundrum of the 'French paradox'? *Eur J Endocrinol* 138:619–620.
Liu HS, Pan CE, Yang W, and Liu XM (2003) Antitumor and immunomodulatory activity of resveratrol on experimentally implanted tumor of H22 in Balb/c mice. *World J Gastroenterol* 9:1474–1476.
Lock C, Hermans G, Pedotti R, Brendolan A, Schadt E, Garren H, Langer-Gould A, Strober S, Cannella B, Allard J, et al. (2002) Gene-microarray analysis of multiple sclerosis lesions yields new targets validated in autoimmune encephalomyelitis. *Nat Med* 8:500–508.
Marier JF, Chen K, Prince P, Scott G, del Castillo JR, and Vachon P (2005) Production of ex vivo lipopolysaccharide-induced tumor necrosis factor-alpha, interleukin-1beta, and interleukin-6 is suppressed by trans-resveratrol in a concentration-dependent manner. *Can J Vet Res* 69:151–154.
Mor G, Sapi E, Abrahams VM, Rutherford T, Song J, Hao XY, Muzaffar S, and Kohen F (2003) Interaction of the estrogen receptors with the Fas ligand promoter in human monocytes. *J Immunol* 170:114–122.
Notas G, Nifli AP, Kampa M, Vercauteren J, Kouroumalis E, and Castanas E (2006) Resveratrol exerts its antiproliferative effect on HepG2 hepatocellular carcinoma cells, by inducing cell cycle arrest, and NOS activation. *Biochim Biophys Acta* 1760:1657–1666.
Ovesn á Z, Kozics K, Bader Y, Saiko P, Handler N, Erker T, and Szekeres T (2006) Antioxidant activity of resveratrol, piceatannol and 3,3',4,4',5,5'-hexahydroxy-trans-stilbene in three leukemia cell lines. *Oncol Rep* 16:617–624.
Rajan AJ, Asensio VC, Campbell IL, and Brosnan CF (2000) Experimental autoimmune encephalomyelitis on the SJL mouse: effect of gamma delta T cell depletion on chemokine and chemokine receptor expression in the central nervous system. *J Immunol* 164:2120–2130.
Rothenberg ME, Ownbey R, Mehlhop PD, Loiselle PM, van de Rijn M, Bonventre JV, Oettgen HC, Leder P, and Luster AD (1996) Eotaxin triggers eosinophil-selective chemotaxis and calcium flux via a distinct receptor and induces pulmonary eosinophilia in the presence of interleukin 5 in mice. *Mol Med* 2:334–348.
Schroecksnadel K, Winkler C, Wirleitner B, Schennach H, Weiss G, and Fuchs D (2005) Anti-inflammatory compound resveratrol suppresses homocysteine formation in stimulated human peripheral blood mononuclear cells in vitro. *Clin Chem Lab Med* 43:1084–1088.
Seo KS, Lee SU, Park YH, Davis WC, Fox LK, and Bohach GA (2007) Long-term staphylococcal enterotoxin C1 exposure induces soluble factor mediated immunosuppression by bovine CD4+ and CD8+ T cells. *Infect Immun* 75:260–269.
Singh NP, Nagarkatti M, and Nagarkatti PS (2007) Role of dioxin response element and nuclear factor-κB motifs in 2,3,7,8-tetrachlorodibenzo-*p*-dioxin-mediated regulation of Fas and Fas ligand expression. *Mol Pharmacol* 71:145–157.
Soleas GJ, Diamandis EP, and Goldberg DM (1997) Wine as a biological fluid: history, production, and role in disease prevention. *J Clin Lab Anal* 11:287–313.
Sospedra M and Martin R (2005) Immunology of multiple sclerosis. *Annu Rev Immunol* 23:683–747.
Su JL, Lin MT, Hong CC, Chang CC, Shiah SG, Wu CW, Chen ST, Chau YP, and Kuo ML (2005) Resveratrol induces FasL-related apoptosis through Cdc42 activation of ASK1/JNK-dependent signaling pathway in human leukemia HL-60 cells. *Carcinogenesis* 26:1–10.
Wirleitner B, Schroecksnadel K, Winkler C, Schennach H, and Fuchs D (2005) Resveratrol suppresses interferon-gamma-induced biochemical pathways in human peripheral blood mononuclear cells in vitro. *Immunol Lett* 100:159–163.
Zhou HB, Chen JJ, Wang WX, Cai JT, and Du Q (2005) Anticancer activity of resveratrol on implanted human primary gastric carcinoma cells in nude mice. *World J Gastroenterol* 11:280–284.

Address correspondence to: Dr. Prakash S. Nagarkatti, Department of Pathology, Microbiology, and Immunology, University of South Carolina School of Medicine, Columbia, SC 29208. E-mail: pnagark@gw.med.sc.edu

Neuroprotective Properties of the Novel Antiepileptic Lamotrigine in a Gerbil Model of Global Cerebral Ischemia

Robert P. Wiard, BS; Mary Carroll Dickerson, BS; Otto Beek, BS; Ronald Norton, BS; Barrett R. Cooper, PhD

Background and Purpose Elevated glutamate levels are thought to be a primary cause of neuronal death after global cerebral ischemia. The purpose of this study was to investigate the potential neuroprotective effects of lamotrigine, a novel anticpileptic drug that inhibits the release of glutamate in vitro, with both behavioral and histological measures of global ischemia in gerbils.

Methods The common carotid arteries of gerbils were occluded for either 5, 10, or 15 minutes. Twenty-one days after reperfusion, gerbils were tested for impairments in a spatial memory task (Morris water maze). After water maze testing the animals were killed, and damage to hippocampal pyramidal cells was assessed. The effect of lamotrigine on the behavioral and histological outcome of either 5 or 15 minutes of global ischemia was evaluated.

Results Bilateral occlusion of the common carotid arteries for 5 minutes resulted in severe degeneration of hippocampal CA1 and CA2 pyramidal cells. Lamotrigine significantly prevented loss of hippocampal CA1 neurons when administered acutely (100 mg/kg PO) immediately after reperfusion or when administered in two equal doses of 30 or 50 mg/kg 2 hours before and immediately after reperfusion. Gerbils subjected to 5 minutes of ischemic insult were not impaired in their ability to solve a spatial memory task 21 days after cerebral ischemia. However, gerbils subjected to 10 and 15 minutes of carotid artery occlusion showed significant impairment in their ability to solve a water maze task. Lamotrigine significantly protected against the cognitive deficits associated with 15 minutes of cerebral ischemia. Histologically, increased durations of cerebral ischemia resulted in a progressive loss of CA1, CA2, and CA3 pyramidal cells. Lamotrigine completely protected gerbils exposed to 15 minutes of cerebral ischemia against CA3 cell loss and greatly reduced damage to the CA1 and CA2 cell tracts of the hippocampus. Lamotrigine also reduced the mortality associated with 15 minutes of ischemia.

Conclusions Lamotrigine had neuroprotective effects in a gerbil model of global cerebral ischemia. Lamotrigine protected gerbils against behavioral deficits resulting from 15 minutes of carotid occlusion and also prevented histological damage resulting from 5 and 15 minutes of global cerebral ischemia. (*Stroke*. 1995;26:466-472.)

Key Words • behavior, animal • cerebral ischemia • neuroprotection • gerbils

Surgical procedures that involve the reduction or interruption of blood supply to the brain as well as events such as stroke, cardiac arrest, and traumatic brain injury are often accompanied by memory loss and other neuropsychiatric signs that persist for several months during recovery.[1-6] These changes are thought to be related to global cerebral ischemia. In animals, 5-minute or longer periods of global cerebral ischemia result in cell death, especially in the hippocampus.[7-9] The development of mazes to study spatial learning and memory has provided a way to study the protective effects of drugs on both the behavioral consequences and the neurological damage to the hippocampus and other areas involved in the neurotoxic effects of ischemia.

Glutamate has been the focus of recent investigations into the neurochemical events leading to neuronal cell death in cerebral ischemia. During cerebral ischemia, synaptic glutamate release coupled with the failure of uptake systems leads to large increases of extracellular glutamate.[10-12] Elevated glutamate levels are thought to be a primary cause of neuronal death after ischemia.[13-15] Studies that support this theory demonstrate that *N*-methyl-D-aspartate antagonists have neuroprotective properties in animal models of ischemia.[16-20]

See Editorial Comment, page 472

Lamotrigine [3,5-diamino-6-(2,3-dichlorophenyl)-1,2,4-triazine] is a novel antiepileptic drug that inhibits use-dependent sodium ion channels and reduces the synaptic release of glutamate in vitro.[21-23] Recent studies[24,25] indicate that lamotrigine and its analogue 1003C87 reduce infarct size after middle cerebral artery occlusion in the rat. The postulated role of glutamate release in the neurotoxic effects of ischemia led us to investigate the potential neuroprotective properties of lamotrigine in gerbils using behavioral and histological measures of global ischemic damage.

Materials and Methods

Materials

Male Mongolian gerbils (Tumblebrook Farm, West Brookfield, Mass) weighing 60 to 70 g were used for these studies. Gerbils

Received July 18, 1994; final revision received October 11, 1994; accepted November 30, 1994.

From the Division of Pharmacology, Burroughs Wellcome Co, Research Triangle Park, NC 27709.

Correspondence to Barrett R. Cooper, PhD, Division of Pharmacology, Burroughs Wellcome Co, 3030 Cornwallis Rd, Research Triangle Park, NC 27709.

were housed four per cage and were maintained on a 12-h/12-h light/dark cycle (lights on at 6 AM) at a temperature of 21°C throughout the study. Food and water were available ad libitum. The procedures used in these studies were conducted in accordance with the US Health Service, National Institutes of Health guidelines for the care and use of laboratory animals.

Surgical Procedures

Cerebral ischemia was induced by the method of Ito et al[7] as modified by Carroll and Beck.[26] Gerbils were anesthetized with a mixture of halothane gas (3%) and room air. An incision was made along the midline in the ventral neck, and both common carotid arteries were occluded for either 5, 10, or 15 minutes by means of microaneurysm clips. After clip removal, the incision was closed and the anesthesia discontinued. Body temperature was maintained throughout the surgery. Animals used in behavioral studies were allowed to recover for at least 3 weeks before testing began. Sham-operated animals received the same surgical procedure except that the carotid arteries were not occluded.

Drug Administration

Lamotrigine (Lamictal; Burroughs Wellcome Co) was suspended in a 0.5% methyl cellulose solution and administered orally in a volume of 0.01 mL/g body wt. For behavioral studies, two doses of lamotrigine (50 mg/kg) or vehicle were administered. The first dose was given 2 hours before ischemia, and the second was administered immediately after reperfusion.

Plasma and Brain Determinations

Gerbils were anesthetized with CO_2 before the collection of blood in evacuated tubes (15% ethylenediaminetetraacetic acid) via cardiac puncture. The blood was centrifuged at 2900*g* for 5 minutes to obtain plasma. Plasma levels of lamotrigine were determined by reversed-phase high-performance liquid chromatography with UV detection at 210 nm. One-milliliter aliquots of plasma were made basic to pH 10.0 by the addition of 10 μL 10N NaOH before extracting twice with 3 mL methyl-*t*-butyl ether (MTBE). The combined organic phases were dried under nitrogen. The samples were reconstituted to 100 μL in a mobile phase and applied to a 15-cm×4.6-mm C-18 base deactivated column. Lamotrigine was eluted with the use of a mobile phase consisting of 20 mmol/L glacial acetic acid and 20 mmol/L triethylamine containing 20% CH_3CN.

For brain determinations, gerbils were anesthetized with CO_2 before decapitation. The whole brain was weighed and then homogenized in 4 mL of carbonate buffer (0.6 mol/L, pH 9.5). One milliliter of this homogenate was extracted by mixing it with a total of 6 mL (2×3 mL) of 1.5% isoamyl alcohol in *n*-heptane. The organic layer was transferred into tubes containing 1 mL of 0.1N HCl. After mixing and centrifuging to separate phases (2900*g* for 2 minutes), the isoamyl alcohol layer was discarded. One half milliliter of carbonate buffer and two drops of 1N NaOH were added to the HCl layer, which was extracted with a total of 6 mL (2×3 mL) of MTBE. The final organic phase was dried in tubes containing 10 μL of 0.1N HCl with the use of a Speed Vac Sample Concentrator. Samples were reconstituted, and lamotrigine concentrations were determined by the methods described above for plasma.

Histological Procedures

Animals were killed 4 days after surgery except for gerbils used in behavioral studies, which were killed after water maze testing. Gerbils were decapitated under halothane anesthesia, and their brains were removed and fixed for at least 3 days in 10% buffered formalin. The brains were processed for paraffin sectioning, and a 10-μm coronal section of the anterior hippocampus was obtained. The sections were stained with cresyl violet and microscopically evaluated for hippocampal damage. Damage to CA1 and CA3 cells was quantified by counting the viable cells in four 0.4-mm lengths (two samples from each hemisphere) of each respective pyramidal cell tract of the hippocampus. CA2 cell damage was assessed in a similar manner, except that cells were counted in two 0.4-mm lengths of the CA2 cell tract.

Behavioral Testing

Training in a modified Morris water maze[27] was carried out 3 weeks after cerebral ischemia. The apparatus consisted of a circular galvanized steel tank 79 cm in diameter and 58 cm high, which was filled with water (27°C) to a depth of 13 cm. (The water depth on the first day of training was 6 cm to allow the animals to acclimate to the test conditions.) Powdered milk was added to the water to make it opaque. Three different visual cues were placed around the inside wall of the tank at a level that would be visible to the gerbils. A circular platform 7 cm in diameter remained in a fixed location 20 cm from the apparatus wall and was 1 cm below the surface of the water.

Each animal was given three daily trials with a 5-minute intertrial interval for 9 days. Each gerbil was individually placed in the apparatus at one of three preselected locations and allowed 1 minute to escape to the hidden platform. Animals not finding the platform after 1 minute were guided to it by the experimenter. Animals were allowed to remain on the platform for 15 seconds and were then returned to their holding cage until the next trial. After 9 days of testing in the Morris water maze the animals were killed and their brains examined for hippocampal damage.

Statistical Analysis

All histological data were analyzed with a one-way ANOVA. Behavioral data were analyzed with a two-way ANOVA (treatment×trial). Post hoc comparisons between independent groups were made with the Tukey test. Animal mortality data were analyzed with a χ^2 test. In all cases, the acceptable level for statistical significance was $P<.05$.

Results

Effects of Different Durations of Occlusion on Water Maze Performance

Fig 1 shows a direct correlation between performance in the Morris water maze and duration of cerebral ischemia. While there were no significant differences in performance of gerbils after 5 minutes of occlusion when compared with control, 10 and 15 minutes of occlusion resulted in significant impairments in acquisition of the spatial task (ANOVA: $F_{1,38}=9.527$, $P<.01$ and $F_{1,11}=22.182$, $P<.001$, respectively). No gross motor abnormalities were noted at the time of testing, which was a minimum of 3 weeks after the induction of global ischemia.

Fig 2 shows a representation of the histological damage produced by each duration of carotid occlusion, and Table 1 summarizes the degree of damage to each hippocampal cell field. Significant group differences were observed for all pyramidal cell fields measured (ANOVA: $F_{3,70}=676.02$, $P<.001$; $F_{3,70}=383.98$, $P<.001$; and $F_{3,70}=15.68$, $P<.001$ for CA1, CA2, and CA3 pyramidal cells, respectively). Animals subjected to 5 minutes of occlusion demonstrated significant cell loss to CA1 and CA2 pyramidal cells, but cells in the CA3 region remained intact. Occlusion of the common carotid arteries for 10 or 15 minutes resulted in a significant reduction in the number of pyramidal cells in all regions measured. CA3 cell loss was significantly greater in animals exposed to 15 minutes of carotid occlusion when compared with those occluded for 5 or 10 minutes.

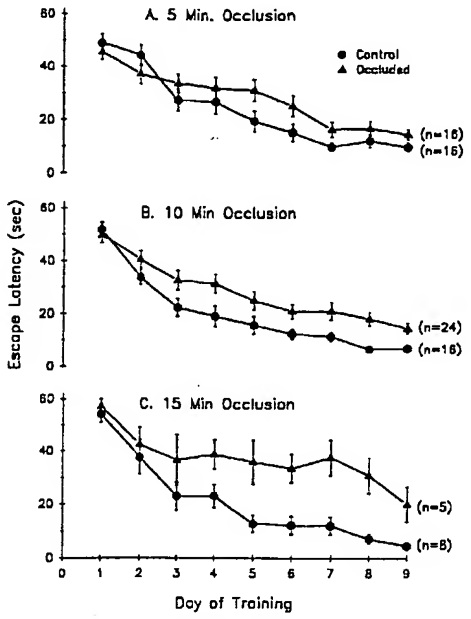

FIG 1. Line graphs show Morris water maze performance of gerbils 21 days after either 5 (A), 10 (B), or 15 (C) minutes of bilateral carotid occlusion. Values are mean±SEM. See text for statistical analysis.

Effect of Lamotrigine on Reperfusion-Induced Cell Death

Histological analysis of the brains of untreated gerbils examined 4 days after 5 minutes of bilateral occlusion of the common carotid arteries showed an almost complete loss of hippocampal CA1 pyramidal cells. Lamotrigine, when administered in two equal doses of 30 mg/kg or 50 mg/kg 2 hours before and immediately after occlusion, significantly prevented hippocampal CA1 cell loss (Fig 3A; ANOVA: $F_{4,51}=61.04$, $P>.001$). To a lesser degree, treating gerbils acutely with lamotrigine (100 mg/kg) immediately after reperfusion also afforded significant protection to CA1 pyramidal cells (Fig 3B; ANOVA: $F_{3,28}=8.25$, $P<.001$). This protection, however, was limited to treatment within 1 hour after reperfusion. When administered at times greater than 1 hour after reperfusion, lamotrigine failed to show significant protection of CA1 cells when compared with untreated controls (Fig 3C).

Effects of Lamotrigine on Water Maze Performance

Fig 4 shows that treatment with lamotrigine significantly protected against the deficits in gerbil performance in the Morris water maze produced by 15 minutes of bilateral carotid occlusion (ANOVA: $F_{2,43}=8.666$, $P<.001$). The performance of treated animals was not different from that of nonoccluded controls.

Histological examination revealed that animals exposed to 15 minutes of cerebral ischemia without any drug treatment experienced a significant loss of neurons in the CA1, CA2, and CA3 regions of the hippocampus (Table 2; ANOVA: $F_{2,36}=39.19$, $P<.001$; $F_{2,36}=29.66$, $P<.001$; and $F_{2,36}=10.91$, $P<.001$ for CA1, CA2, and CA3 pyramidal cells, respectively). However, treatment with lamotrigine afforded complete protection to the CA3 region of the hippocampus and greatly reduced cell loss in the CA1 and CA2 cell regions.

Lamotrigine also protected against mortality resulting from 15 minutes of cerebral ischemia. Untreated animals subjected to 15 minutes of bilateral carotid occlusion had a mortality rate of 66% compared with 23% mortality observed in lamotrigine-treated animals ($\chi^2=10.774$, $P<.005$).

Plasma and Brain Levels of Lamotrigine at Doses That Protect Against the Behavioral and Histological Consequences of Global Ischemia

Table 3 shows the plasma and brain levels of lamotrigine in gerbils after two 30-mg/kg doses of lamotrigine given orally 2 hours apart or a single dose

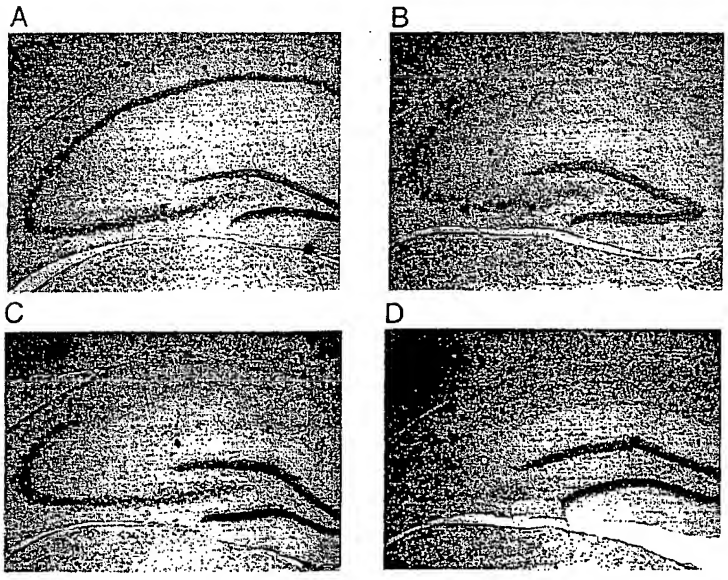

FIG 2. Photomicrographs of 10-μm-thick sections of gerbil hippocampus mounted in paraffin and stained with cresyl violet. Shown are normal nonoccluded controls (A) and 5 weeks after 5 (B), 10 (C), or 15 minutes (D) of occlusion followed by reperfusion.

TABLE 1. Number of Hippocampal Cells Remaining in Gerbils After Various Durations of Carotid Occlusion

Group	n	Sector of Hippocampus		
		CA1	CA2	CA3
Sham controls	21	371±4.6	197±3.7	218±4.7
Occlusion, min				
5	15	42±15.2*	34±9.1*	189±10.0
10	23	27±2.3*	22±2.5*	175±7.1*
15	15	16±2.1*†	17±2.7*†	134±13.5*†‡

Values are mean±SEM.
*$P<.05$ vs controls.
†$P<.05$ vs 5-minute group.
‡$P<.05$ vs 10-minute group.

of 100 mg/kg given orally. In both experiments the plasma and brain levels of lamotrigine rose rapidly, and peak levels occurred within 30 minutes of dosing. The levels of lamotrigine decreased slowly and only slightly during a 6-hour period. In the 100-mg/kg single-dose study, significant levels were observed up to 24 hours after dosing.

Discussion

Patients suffering from stroke, cardiac arrest, or traumatic brain injury, as well as patients undergoing cardiac and cardiopulmonary bypass surgery, commonly experience persistent neuropsychological dysfunction.[1-6] Postmortem analyses of the brains of patients who have suffered cerebral ischemia or trauma reveal extensive neuronal damage to the CA1 pyramidal cells of the hippocampus,[28,29] a region that is thought to play a critical role in learning and memory. This hippocampal damage has been related to memory impairments often suffered by these patients.[28,29]

The histological and behavioral effects of global cerebral ischemia in animals are similar to those observed in humans. In several rodent species, occlusion of the carotid arteries results in selective hippocampal damage, particularly to CA1 pyramidal cells. In rats, hippocampal damage associated with cerebral ischemia also is accompanied by impairments in tests measuring learning and memory.[30-32] Although the gerbil has been extensively used as a model of global cerebral ischemia, the association between hippocampal cell damage and impairments in learning and memory in this species remains unclear. Gerbils exposed to 5 minutes of bilateral carotid occlusion fail to show impairment in the discrete lever-press avoidance and the discrete shuttle avoidance paradigms, despite complete degeneration of CA1 pyramidal neurons.[33,34] Similarly, Corbett et al[35] failed to find any lasting impairments in a Morris water maze task 21 days after 5 minutes of cerebral ischemia in the gerbil.

At the histological level, lamotrigine protected gerbils in our study from damage to hippocampal CA1 pyramidal cells resulting from 5 minutes of occlusion of the common carotid arteries. The drug was most effective when administered both before and immediately after occlusion. How-

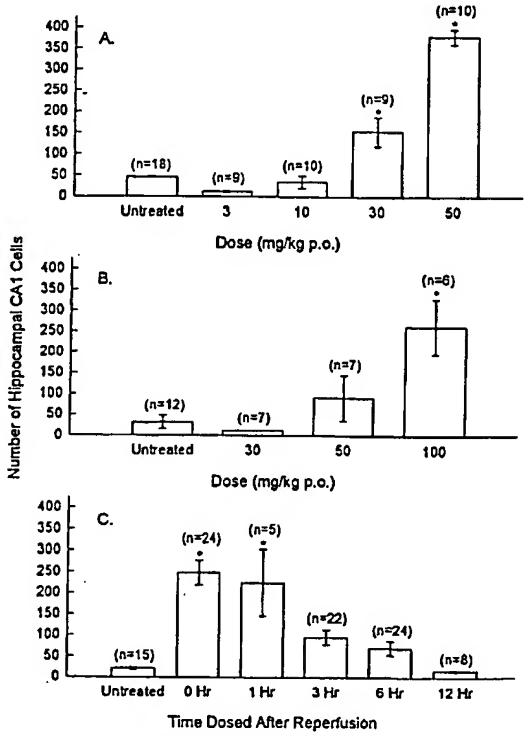

FIG 3. Bar graphs show the effect of lamotrigine on ischemia-induced CA1 cell death in gerbils (A) administered in equal doses 2 hours before and immediately after bilateral occlusion of the common carotid arteries; (B) administered immediately after bilateral occlusion; or (C) administered at a dose of 100 mg/kg PO at various times after occlusion of the common carotid arteries. Values are mean±SEM. *$P<.05$ vs untreated group.

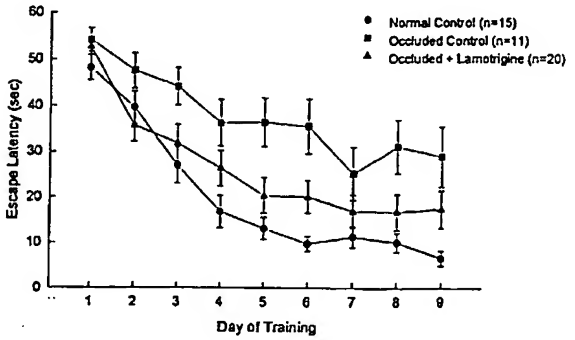

FIG 4. Line graph shows the effect of lamotrigine on Morris water maze performance of gerbils exposed to 15 minutes of bilateral carotid occlusion. Values are mean±SEM. See text for statistical analysis.

TABLE 2. Number of Hippocampal Cells Remaining in Gerbils Subjected to 15 Minutes of Carotid Occlusion

Group	n	Sector of Hippocampus		
		CA1	CA2	CA3
Sham controls	8	360±8.4	184±5.3	208±5.6
Untreated	11	16±2.9*	18±3.4*	138±17.7*
Lamotrigine	20	164±25.5*	92±14.1*	193±7.1†

Values are mean±SEM.
*$P<.05$ vs controls.
†$P<.05$ vs untreated group.

ever, lamotrigine still afforded significant protection when administered acutely up to 1 hour after reperfusion.

The behavioral results from our study were consistent with the literature[33-35] showing that 5 minutes of bilateral carotid occlusion in the gerbil fail to produce a deficit in a test of spatial memory 21 days after an ischemic insult. However, increasing the duration of bilateral carotid occlusion to 10 and 15 minutes resulted in increased deficits in water maze performance. Since damage to the CA1 pyramidal cells was complete with the ineffective 5-minute occlusion, these cognitive deficits are more likely correlated with cell loss elsewhere in the brain. We quantified such loss for the CA2 and CA3 sectors of the hippocampus. Our findings indicate that deficits observed in Morris water maze behavior in gerbils are not dependent on the degeneration of the CA1 cells of the hippocampus; they are more likely related to damage to other areas of the brain, possibly the CA2 and CA3 cells of the hippocampus.

Nevertheless, lamotrigine was effective in protecting against the cognitive deficit observed with 15 minutes of cerebral ischemia. After 15 minutes of ischemia, lamotrigine completely protected cells of the CA3 region of the hippocampus against the neurotoxic effects of ischemia. Approximately half of the CA1 and CA2 hippocampal cells remained intact in lamotrigine-treated gerbils undergoing this long interruption of blood supply. It is unlikely that this partial protection of CA1 pyramidal cells is responsible for the observed improvement in water maze behavior, since animals with complete destruction of CA1 cells show no deficits in this task. In addition to increasing cell survival, lamotrigine enhanced the survival rate of animals exposed to 15 minutes of bilateral carotid occlusion: lamotrigine-treated animals had a survival rate two times greater than that of untreated animals.

Lamotrigine does not cause a large reduction in body temperature, and artificial warming was used to maintain body temperature in our study. Nevertheless, it is possible that lamotrigine and anesthesia may have cooled gerbils more than anesthesia alone. This was not determined. For animals used in behavioral testing, cell counts were taken from brains harvested 45 days after carotid occlusion. This is important because hypothermia antagonizes CA1 cell death when cell counts are made on day 4 or 5 after reperfusion. Dietrich et al[36] recently showed that hypothermia merely delays cell death. The 45-day period between occlusion and decapitation is sufficiently long to allow for completion of any cell death delayed by hypothermia.

The gerbil model of cerebral ischemia is not without other problems as well. Gerbils are susceptible to seizures in response to a variety of stimuli, such as handling or exposure to a novel environment.[37,38] Prolonged seizure activity results in degeneration of hippocampal pyramidal neurons.[39] For this reason, it would not be surprising for an antiepileptic drug to prevent cell loss during ischemia because of its anticonvulsant activity. Although seizure activity was not directly monitored in the present study, indications are that the neuroprotective effect of lamotrigine in this model was not owing to its ability to prevent seizures. The ED_{50} of lamotrigine for protecting against maximal electroshock-evoked hind limb extension in mice and rats is 2.6 mg/kg PO and 1.9 mg/kg PO, respectively.[40] Doses in this range were ineffective in preventing ischemia-induced cell loss in our study. Also, several studies have suggested that seizure activity does not play a role in cell loss in gerbils during cerebral ischemia. Chon[41] found that convulsive activity did not originate from the ischemic brain in gerbils. Also, postischemic measurment of CA1 cell activity in gerbils showed an increase in cell firing but not

TABLE 3. Concentration of Lamotrigine in Plasma and Brain of Gerbils After Two Doses of 30 mg/kg or a Single Dose of 100 mg/kg PO

Time After Dosing, h	Plasma Levels, μg/mL		Brain Levels, μg/g	
	2×30 mg/kg	1×100 mg/kg	2×30 mg/kg	1×100 mg/kg
0.25	27.2±1.3	17.9±2.5	36.2±1.9	20.4±3.6
0.5	24.8±1.2	27.5±2.3	36.3±2.6	50.5±3.6
0.75	...	23.2±4.5	...	36.5±3.7
1	22.5±0.8	24.9±2.4	36.8±1.3	47.9±4.5
2	21.5±1.2	24.0±2.2	35.6±2.0	41.7±2.0
4	19.2±0.7	22.7±2.3	32.8±0.6	45.1±2.8
6	18.1±0.9	20.2±1.7	25.1±0.5	33.7±3.9
24	...	19.4±0.7	...	33.2±1.1

Values are mean±SEM. Sample times for 2×30 mg/kg dose are hours after second dose. Means are based on 3 to 5 replications per time point.

in convulsant activity.[42] In a study by Suzuki et al,[43] no signs of seizure activity were observed in gerbils exposed to 5 minutes of carotid occlusion.

The gerbils' responsiveness to novel environments and stimuli prompted us to make several modifications to the Morris water maze. For the first day of training, the water depth in the test apparatus was set at a level that permitted the gerbils to easily support themselves on the apparatus floor. Water depth on subsequent training days was adjusted, making the apparatus floor just out of reach of the gerbils when floating. These modifications allowed gerbils to readily acclimate to the novel test conditions, resulting in proficient ability of the animals to perform in the Morris water maze.

The antiepileptic effect of lamotrigine is believed to result from its ability to inhibit glutamate release.[22,23] Lamotrigine significantly protects against kainic acid–induced neurotoxicity in rats, which is dependent on neuronally released glutamate.[44] Leach et al[22,23] found that lamotrigine specifically inhibits veratrine- but not K^+-induced glutamate release, indicating the inhibition of voltage-sensitive sodium channels as the probable mechanism of action. The importance of sodium channels was shown by Lang et al,[21] who demonstrated that lamotrigine inhibits use-dependent sodium channels in mouse neuroblastoma cells. Since glutamate appears to play a major role in the neuropathology observed in ischemia, the ability of lamotrigine to inhibit glutamate release by blocking voltage-sensitive sodium channels could also be the primary mechanism of action for its neuroprotective properties observed in the present study. However, inhibition of glutamate release cannot fully explain the neuroprotective effects observed with lamotrigine. Several studies indicate that extracellular glutamate levels peak during the ischemic period and return to normal levels within 30 minutes after reperfusion.[10,45] Lamotrigine protected against ischemia-induced cell loss when administered 1 hour after reperfusion, well after peak extracellular glutamate levels are reached. This result suggests that lamotrigine activity in the present model cannot be explained solely by inhibition of glutamate release and that other mechanisms of action, perhaps its effect on use-dependent sodium channels,[21] are involved.

Experience with lamotrigine use in the treatment of epilepsy indicates that plasma levels of 10 to 15 μg/mL are achieved in monotherapy patients.[46] Results from the present study suggest that peak plasma levels of 27 μg/mL lamotrigine provide protection against cell damage produced by global ischemia in gerbils. These levels have not been reported during antiepileptic therapy in patients, and it is not clear if they would be achievable with acceptable side effects.

References

1. Shaw PJ, Bates D, Cartlidge NE, Heaviside D, French JM, Julian DG, Shaw DA. Neurologic and neuropsychological morbidity following major surgery: comparison of coronary artery bypass and peripheral vascular surgery. *Stroke*. 1987;18:700-707.
2. Townes BD, Bashein G, Hornbein TF, Coppel DB, Goldstein DE, Davis KB, Nessly ML, Bledsoe SW, Veith RC, Ivey TD, Cohen MA. Neurobehavioral outcomes in cardiac operations. *J Thorac Cardiovasc Surg*. 1989;98:774-782.
3. Brooks DN. Memory and head injury. *J Nerv Ment Dis*. 1972;155:350-355.
4. Victor M, Angevine JB, Mancall EL, Fisher CM. Memory loss with lesions of hippocampal formation. *Arch Neurol*. 1961;5:244-263.
5. Ott BR, Saver JL. Unilateral amnesic stroke: six new cases and a review of the literature. *Stroke*. 1993;24:1033-1042.
6. Volpe BT, Petito CK. Dementia with bilateral medial temporal lobe ischemia. *Neurology*. 1985;35:1793-1797.
7. Ito U, Spatz M, Walker JT Jr, Klatzo I. Experimental cerebral ischemia in mongolian gerbils, I: light microscopic observations. *Acta Neuropathol (Berl)*. 1975;32:209-223.
8. Pulsinelli WA, Brierley JB, Plum F. Temporal profile of neuronal damage in a model of transient forebrain ischemia. *Ann Neurol*. 1982;11:491-498.
9. Kirino T. Delayed neuronal death in the gerbil hippocampus following ischemia. *Brain Res*. 1982;239:57-69.
10. Benveniste H, Drejer J, Schousboe A, Diemer NH. Elevation of the extracellular concentrations of glutamate and aspartate in rat hippocampus during transient cerebral ischemia monitored by intracerebral microdialysis. *J Neurochem*. 1984;43:1369-1374.
11. Hagberg H, Lehmann A, Sandberg M, Nyström B, Jacobson I, Hamberger A. Ischemia-induced shift of inhibitory and excitatory amino acids from intra- to extracellular compartments. *J Cereb Blood Flow Metab*. 1985;5:413-419.
12. Silverstein FS, Buchanan K, Johnston MV. Perinatal hypoxia-ischemia disrupts striatal high-affinity [3H] glutamate uptake into synaptosomes. *J Neurochem*. 1986;47:1614-1619.
13. Rothman SM, Olney JW. Glutamate and the pathophysiology of hypoxic-ischemic brain damage. *Ann Neurol*. 1986;19:105-111.
14. Rothman S. Synaptic release of excitatory amino acid neurotransmitter mediates anoxic neuronal death. *J Neurosci*. 1984;4:1884-1891.
15. Choi DW, Rothman SM. The role of glutamate neurotoxicity in hypoxic-ischemic neuronal death. *Annu Rev Neurosci*. 1990;13:171-182.
16. Simon RP, Swan JH, Griffiths T, Meldrum BS. Blockade of N-methyl-D-aspartate receptors may protect against ischemic damage in the brain. *Science*. 1984;226:850-852.
17. Gill R, Foster AC, Woodruff GN. Systemic administration of MK-801 protects against ischemia-induced hippocampal neurodegeneration in the gerbil. *J Neurosci*. 1987;7:3343-3349.
18. Ozyurt E, Graham DI, Woodruff GN, McCulloch J. Protective effect of the glutamate antagonist, MK-801 in focal cerebral ischemia in the cat. *J Cereb Blood Flow Metab*. 1988;8:138-143.
19. Park CK, Nehls DG, Graham DI, Teasdale GM, McCulloch J. The glutamate antagonist MK-801 reduces focal ischemic brain damage in the rat. *Ann Neurol*. 1988;24:543-551.
20. Simon R, Shiraishi K. N-Methyl-D-aspartate antagonist reduces stroke size and regional glucose metabolism. *Ann Neurol*. 1990;27:606-611.
21. Lang DG, Wang CM, Cooper BR. Lamotrigine, phenytoin and carbamazepine interactions on the sodium current present in N4TG1 mouse neuroblastoma cells. *J Pharmacol Exp Ther*. 1993;266:829-835.
22. Leach MJ, Marden CM, Miller AA. Pharmacological studies on lamotrigine, a novel potential antiepileptic drug, II: neurochemical studies on the mechanism of action. *Epilepsia*. 1986;27:490-497.
23. Leach MJ, Baxter MG, Critchley MAE. Neurochemical and behavioral aspects of lamotrigine. *Epilepsia*. 1991;32:S4-S8.
24. Meldrum BS, Swan JH, Leach MJ, Millan MH, Gwinn R, Kadota K, Graham SH, Chen J, Simon RP. Reduction of glutamate release and protection against ischemic brain damage by BW1003C87. *Brain Res*. 1992;593:1-6.
25. Smith SE, Meldrum BS. Cerebroprotective effect of lamotrigine after focal cerebral ischemia in the rat. *Br J Pharmacol*. 1994;111(suppl):91P. Abstract.
26. Carroll M, Beek O. Protection against hippocampal CA1 cell loss by post-ischemic hypothermia is dependent on delay of initiation and duration. *Metab Brain Dis*. 1992;7:45-50.
27. Morris R. Developments of a water-maze procedure for studying spatial learning in the rat. *J Neurosci Methods*. 1984;11:47-60.
28. Zola-Morgan S, Squire LR, Amaral DG. Human amnesia and the medial temporal region: enduring memory impairment following a bilateral lesion limited to field CA1 of the hippocampus. *J Neurosci*. 1986;6:2950-2967.

29. Victor M, Agamanolis D. Amnesia due to lesions confined to the hippocampus: a clinical-pathologic study. *J Cognitive Neurosci.* 1990;2:246-257.
30. Volpe BT, Pulsinelli WA, Tribuna J, Davis HP. Behavioral performance of rats following transient forebrain ischemia. *Stroke.* 1984;15:558-562.
31. Jaspers RMA, Block F, Heim C, Sontag K-H. Spatial learning is affected by transient occlusion of common carotid arteries (2VO): comparison of behavioural and histopathological changes after '2VO' and 'four-vessel-occlusion' in rats. *Neurosci Lett.* 1990;117:149-153.
32. Volpe BT, Davis HP, Towle A, Dunlap WP. Loss of hippocampal CA1 pyramidal neurons correlates with memory impairment in rats with ischemic or neurotoxin lesions. *Behav Neurosci.* 1992;106:457-464.
33. Kuribara H, Tadokoro S. Aspects of animal experiments for evaluation of cognitive enhancers: in particular, the behavioral characteristics of Mongolian gerbils. *Prog Neuropsychopharmacol Biol Psychiatry.* 1992;16:389-396.
34. Umezu T, Kuribara H, Hirate K, Saito T, Tadokoro S. A brief brain ischemia produces morphological damage of hippocampal CA1 pyramidal cells without affecting the sensitivities to psychoactive drugs in two types of discrete avoidance tasks in Mongolian gerbils. *Jpn J Pharmacol.* 1989;50:63-69.
35. Corbett D, Evans SJ, Nurse SM. Impaired acquisition of the Morris water maze following global ischemic damage in the gerbil. *Neuroreport.* 1992;3:204-206.
36. Dietrich WD, Busto R, Alonso O, Globus MY-T, Ginsberg MD. Intraischemic but not postischemic brain hypothermia protects chronically following global forebrain ischemia in rats. *J Cereb Blood Flow Metab.* 1993;13:541-549.
37. Cox B, Lomax P. Brain amines and spontaneous epileptic seizures in the Mongolian gerbil. *Pharmacol Biochem Behav.* 1976;4:263-267.
38. Thiessen DD, Lindzey G, Friend HC. Spontaneous seizures in the Mongolian gerbil *(Meriones unguiculatus). Psychonomic Sci.* 1968;11:227-228.
39. Corsellis JAN, Meldrum BS. Epilepsy. In: Blackwood W, Corsellis JAN, eds. *Greenfield's Neuropathology.* London, England: Edward Arnold Publishers Ltd; 1976:771-795.
40. Miller AA, Wheatley P, Sawyer DA, Baxter MG, Roth B. Pharmacological studies on lamotrigine, a novel potential antiepileptic drug, I: anticonvulsant profile in mice and rats. *Epilepsia.* 1986;27:483-489.
41. Chon R. Convulsive activity in gerbils subjected to cerebral ischemia. *Exp Neurol.* 1979;65:391-397.
42. Suzuki R, Yamaguchi T, Li C-L, Klatzo I. The effects of 5-minute ischemia in Mongolian gerbils, II: changes of spontaneous neuronal activity in cerebral cortex and CA1 sector of hippocampus. *Acta Neuropathol (Berl).* 1983;60:217-222.
43. Suzuki R, Yamaguchi T, Kirino T, Orzi F, Klatzo I. The effects of 5-minute ischemia in Mongolian gerbils, I: blood-brain barrier, cerebral blood flow, and local cerebral glucose utilization changes. *Acta Neuropathol (Berl).* 1983;60:207-216.
44. McGeer EG, Zhu SG. Lamotrigine protects against kainate but not ibotenate lesions in rat striatum. *Neurosci Lett.* 1990;112:348-351.
45. Globus MY-T, Busto R, Dietrich WD, Martinez E, Valdes I, Ginsberg MD. Effect of ischemia on the *in vivo* release of striatal dopamine, glutamate, and γ-aminobutyric acid studied by intracerebral microdialysis. *J Neurochem.* 1988;51:1455-1464.
46. Faught E, Leroy RF, Messenheimer JA, Matsuo F, Bergen D, Dren AT, Keaney PA. Clinical experience with lamotrigine (Lamictal®) monotherapy for partial seizures in adult outpatients. Presented at the 1992 Annual Meeting of the American Epilepsy Society; December 4-10, 1992; Seattle, Wash.

Editorial Comment

The hallmark of the delayed and selectively vulnerable hippocampal neurons in gerbils after global cerebral ischemia and reperfusion has prompted many investigators to use this model to study the neuroprotective effects of a drug and its underlying cellular mechanisms. Several major criteria need to be fulfilled for a drug that is claimed to be therapeutically valuable: (1) lack of toxic side effects; (2) well-defined and known normal physiological functions (ie, mean arterial blood pressure) and pharmacokinetics (ie, half-life); (3) ability to pass the blood-brain barrier; (4) effectiveness in neuronal protection when applied after ischemia; and (5) improvement in neurological deficits and behavioral outcomes.

The antiepileptic drug lamotrigine, used by Wiard and colleagues in this study, appears to fulfill these preclinical criteria. A question remaining is the unclear cellular mechanism underlying its protective effect against ischemic hippocampal neurons. As suggested by the authors, caution must be taken to attribute the neuroprotective effects to its in vitro functions as an inhibitor of presynaptic glutamate release since disparity in time occurred between the early release of glutamate and the delayed treatment of the drug. Obviously, the blockage of use-dependent sodium channels as a neuroprotective mechanism needs to be further elucidated.

Pak H. Chan, PhD, *Guest Editor*
Department of Neurosurgery and Neurology
CNS Injury and Edema Research Center
University of California
School of Medicine
San Francisco, Calif

Reference

1. Kirino T. Delayed neuronal death in the gerbil hippocampus following ischemia. *Brain Res.* 1982;239:57-69.